Phosphodiesterase 10A Pet Imaging in Early Parkinson's Disease

Pagano, Gennaro

Awarding institution:
King's College London

PHOSPHODIESTERASE 10A PET IMAGING IN EARLY PARKINSON'S DISEASE

Department of Basic & Clinical Neuroscience

Institute of Psychiatry, Psychology and Neuroscience

King's College London

This dissertation is submitted to King's College London for the degree of Doctor of Philosophy

July 2018

by

Dr. Gennaro Pagano

Dissertation for the degree of PhD in Clinical Neuroscience

DECLARATION

This dissertation is the result of my own work and that all the material has not been written for me, in whole or in part, by any other person. I also undertake that any quotation or paraphrase from the published or unpublished work of another person has been duly acknowledged in the work which I present for examination. This dissertation has not been previously submitted, in part or whole, to any university or institution for any degree, diploma, or other qualification.

This is to certify that I have carried out the studies embodied in this thesis under the supervision of Professor Marios Politis and Professor Mitul Metha.

Signed: 

Date: 31st July 2018

Dr. Gennaro Pagano, MSc, MD

King's College London

ABSTRACT

Recent work has shown loss of phosphodiesterase 10A (PDE10A) expression in middle-stage and advanced treated patients with Parkinson's disease, which was associated with motor symptom severity. In this thesis, I used molecular imaging to evaluate whether the reduction of PDE10A expression is characteristic of the early stages of the Parkinson's disease and is related to disease severity and other markers of Parkinson's disease pathology *via* the following objectives:

1) By using [^{11}C]IMA107 PET imaging to assess the integrity of PDE10A enzyme *in vivo* in early *de novo* and early levodopa-treated patients with Parkinson's disease compared to age- and sex-matched healthy control subjects (*Project 1*)

2) Compare and investigate the associations between the expression of PDE10A with known molecular markers of dopaminergic dysfunction in Parkinson's patients such as loss of dopamine transporters, as quantified with [^{11}C]PE2I PET and [^{123}I]FP-CIT SPECT molecular imaging (*Project 2*)

3) Explore the associations between the expression of PDE10A with MRI markers of Parkinson's pathology such as iron depositions (assessed with susceptibility-weighted MR imaging), neuromelanin loss (assessed with neuromelanin sensitive MR imaging) and changes in structural volumetric (assessed with T1 MR imaging) and connectivity (assessed with diffusion tensor MR imaging) (*Project 3*)

4) Investigate for associations between the expression of PDE10A and non-motor symptoms considered pre-motor (sleep problems, autonomic dysfunction, mood disorders etc).

Overall, the findings of this thesis indicate that loss of PDE10A expression is a very early phenomenon during Parkinson's disease and is associated with the disease duration and gradual increase of motor symptom burden in different disease stages. PDE10A PET was not associated with non-motor symptoms. PDE10A PET shows a diagnostic power similar to DAT PET and DAT SPECT, but greater than any MRI imaging modalities. This suggests PDE10A imaging as a robust alternative worth exploring further for use in clinical practice.

TABLE OF CONTENTS

DECLARATION OF AUTHORSHIP **1**

ABSTRACT **2**

TABLE OF CONTENTS **3**

LIST OF FIGURES **5**

LIST OF TABLES **6**

PEER-REVIEWED PUBLICATIONS RELATED TO THIS PHD **7**

ACKNOWLEDGEMENTS **8**

ABBREVIATIONS **9**

CHAPTER 1. INTRODUCTION **13**

1.1 PARKINSON'S DISEASE **14**

1.2 PDE10A IN PARKINSON'S DISEASE **18**

1.3 NEUROIMAGING TECHNIQUES IN PARKINSON'S DISEASE **32**

1.3.1 SPECT AND PET MOLECULAR IMAGING **32**

1.3.2 MRI **46**

1.4 HYPOTHESIS AND AIMS **66**

CHAPTER 2. METHODS **68**

2.1 STUDY PLANNED **69**

2.2 POPULATION **70**

2.2.1 INCLUSION CRITERIA **70**

2.2.2 RECRUITMENT **73**

2.3 CLINICAL ASSESSMENTS **74**

2.3.1 MOTOR SCALES **76**

2.3.2 NON-MOTOR SCALES **77**

2.3.3 QUALITY OF LIFE **81**

2.3.4 NEUROPSYCHOLGICAL BATTERY **81**

2.4 MOLECULAR IMAGING **83**

2.4.1 SPECT DAT SCAN **83**

2.4.1.1 SCANNING DETAILS **83**

2.4.1.2 IMAGING ANALYSES **84**

2.4.2 PET DAT PE2I 84
2.4.2.1 SCANNING DETAILS 84
2.4.2.2 IMAGING ANALYSES 85
2.4.3 PET PDE10A IMA107 88
2.4.3.1 SCANNING DETAILS 88
2.4.3.2 IMAGING ANALYSES 88
2.5 MRI IMAGING 90
2.5.1 STRUCTRAL VOLUMETRIC T1 90
2.5.1.1 SCANNING DETAILS 90
2.5.1.2 IMAGING ANALYSES 91
2.5.2 STRUCTRAL CONNECTIVITY DTI 94
2.5.2.1 SCANNING DETAILS 94
2.5.2.2 IMAGING ANALYSES 94
2.5.3 NEUROMELANIN 96
2.5.3.1 SCANNING DETAILS 96
2.5.3.2 IMAGING ANALYSES 96
2.5.4 SUSCEPTIBILITY-WEIGHTED IMAGING 98
2.5.4.1 SCANNING DETAILS 98
2.5.4.2 IMAGING ANALYSES 98
2.6 STATISTICAL ANALYSES 99
CHAPTER 3. PDE10A IN PARKINSON'S DISEASE 100
3.1 CLINICAL CHARACTERISTICS OF THE POPULATIONS 101
3.2 PDE10A AND EARLY PARKINSON'S DISEASE 103
CHAPTER 4. DAT SPECT AND PET IN PARKINSON'S DISEASE 119
CHAPTER 5. MRI MARKERS IN PARKINSON'S DISEASE 144
CHAPTER 6. DISCUSSION 170
CHAPTER 7. FUTURE DIRECTIONS 186
CHAPTER 8. REFERENCES 189

LIST OF FIGURES

Figure 1. Roles of PDE10A in the control of basal ganglia–thalamocortical circuitry. 20

Figure 2. PDE10A expression in Parkinson's disease. 27

Figure 3. Chemical structure of potential PET ligand for in vivo imaging of PDE10A. 40

Figure 4. MIAKAT™ Pipeline 86

Figure 5. ROIs for Substantia nigra and Locus coeruleus. 97

Figure 6. PDE10A expression in the groups of PD patients and healthy controls. 111

Figure 7. Altered PDE10A expression in anatomically defined brain regions of PD patients. 112

Figure 8. Correlations between PDE10A and disease duration in PD patients 113

Figure 9. Correlations between PDE10A to motor symptoms in PD patients. 114

Figure 10. DAT SPECT (A) and PET (B) expression in the groups of Parkinson's disease patients and healthy controls 128

Figure 11. Altered DAT and PDE10A expression in anatomically defined brain regions of Parkinson's disease patients 130

Figure 12. Correlations between DAT and disease duration in PD patients 131

Figure 13. Correlations between DAT and motor symptoms in PD patients. 133

Figure 14. Correlations between PDE10A and DAT imaging in PD patients 137

Figure 15. SWI MRI markers in the groups of PD patients and healthy controls 154

Figure 16. NM MRI markers in the groups of PD patients and healthy controls. 155

Figure 17. DTI MRI markers in the groups of PD patients and healthy controls 156

Figure 18. Altered SWI and NM markers in the substantia nigra of PD patients 157

Figure 19. Correlations between MRI and motor symptoms in PD patients 160

Figure 20. Correlations between PDE10A and MRI imaging in PD patients. 163

LIST OF TABLES

TABLE 1. Demographic and clinical characteristics of cohorts of early *de novo* and early treated patients with idiopathic Parkinson's disease and healthy controls 102

TABLE 2. [^{11}C]IMA107 BP_{ND} in early *de novo* and early treated patients with idiopathic Parkinson's disease compared to healthy controls 110

TABLE 3. [^{11}C]PE2I BP_{ND} and [^{123}I]FP-CIT SBR in early *de novo* and early treated patients with idiopathic Parkinson's disease compared to healthy controls..... 127

TABLE 4. Freesurfer volumes, microstructural DTI, SWI iron depositions and NM changes in subcortical areas and substantia nigra of early *de novo* and early treated idiopathic Parkinson's disease patients compared to healthy controls 153

,

PEER-REVIEW PUBLICATIONS RELATED TO THIS PHD

*co-first authorship

1. Pagano G, Yousaf T, Wilson H, Niccolini F, and Politis M. The Role of Phosphodiesterase 10A in Neurodegenerative Disorders. *in preparation*
2. Pagano G, Niccolini F, Wilson H, Yousaf T, Khan NL, Martino D, Plisson C, Gunn R, Rabiner EA, Foltynie T and Politis M. Comparison of PDE10A and DAT expression as markers of disease burden in early Parkinson's disease. *in preparation*
3. Pagano G, Yousaf T, Niccolini F, Wilson H, Corcoran B, Vivian G, Metha M, Khan NL, Martino D, Gunn R, Rabiner EA, and Politis M. Comparison between [^{11}C]PE2I PET and [^{123}I]FP-CIT SPECT as markers of DAT expression in early Parkinson's disease. *in preparation*
4. Pagano G, Yousaf T, Wilson H, Niccolini F, Metha M, Gunn R, Rabiner EA, and Politis M. Imaging Parkinson's disease pathology: A comparison between neuromelanin-sensitive MRI, susceptibility weighted imaging, diffusion tensor imaging and [^{11}C]PE2I DAT PET. *in preparation*
5. Pagano G, Wilson H, Valkimadi P, Niccolini F, Searle G, Gunn R, Rabiner EA, Foltynie T and Politis M. Loss of phosphodiesterase 10A in the hippocampus and episodic memory deficits in Parkinson's disease. *in preparation*
6. Wilson H, Niccolini F, Haider S, Marques T, Pagano G, Coello C, Natesan S, Kapur S, Rabiner EA, Gunn R, Tabrizi S, Politis M Loss of extra-striatal phosphodiesterase 10A expression in early premanifest Huntington's disease gene carriers *Journal of the Neurological Sciences 2016 15 Sept;368:243–248.*
7. Schulz J, Pagano G*, Bonfante J, Wilson H, Politis M. Nucleus basalis of Meynert degeneration precedes and predicts cognitive impairment in Parkinson's disease. *Brain. 2018 May 1;141(5):1501-1516. doi: 10.1093/brain/awy072.*
8. Pagano G, Yousaf T, Politis M. PET Molecular Imaging Research of Levodopa-Induced Dyskinesias in Parkinson's Disease. *Curr Neurol Neurosci Rep. 2017 Oct 3;17(11):90. doi: 10.1007/s11910-017-0794-2.*
9. Pagano G, Niccolini F, Politis M. The serotonergic system in Parkinson's patients with dyskinesia: evidence from imaging studies. *J Neural Transm (Vienna). 2017 Dec 20. doi: 10.1007/s00702-017-1823-7.*
10. Pagano G, Niccolini F, Fusar-Poli P, Politis M. Serotonin transporter in Parkinson's disease: A meta-analysis of positron emission tomography studies. *Ann Neurol. 2017 Feb;81(2):171-180. doi: 10.1002/ana.24859. Review.*
11. Pagano G, Niccolini F, Politis M. Imaging in Parkinson's disease. *Clin Med (Lond). 2016 Aug;16(4):371-5.*

Acknowledgments

I would like to express my sincere gratitude to my first supervisor Professor Marios Politis for his unwavering support during my PhD research. His guidance has been a constant help throughout my time of intellectual growth and allowed me to think as a truly independent research scientist. His advice on both research studies as well as on my career path has been priceless. I could not have imagined having a better advisor and mentor for my PhD study.

I would like to thank my second supervisor Professor Mitul Metha. His brilliant comments and suggestions have made the journey lighter and I am incredibly grateful for all his input during the past three years.

I thank all my colleagues at the Neurodegeneration Imaging Group for all the stimulating discussions, all the time spent working together before deadlines and for all the fun we have had in the last three years:

Heather Wilson, Tayyabah Yousaf, George Dervenoulas, Sotirios Polychronis, Beniamino Giordano, Flavia Niccolini, Konstantinos Diamantopoulos, Jonathan Schulz, Antonio Carotenuto, Silvia Caminiti, Edoardo de Natale, Avinash (Avi) Chandra, Zachary Chappell, Giacomo Tondo, Chloe Farrell, Polytimi-Eleni Valkimadi, Christina Belogianni, Ioanna Palamidous, Juan Bonfante, Gundega Gulbe, Alessia Oneri and Ishpal Moonga.

I would like to thank my wonderful Emanuela and my 2-year-old son Gabriele for their continuous support during the nights spent to write this thesis, for all their love and encouragement. I would also like to thank my parents, Luigi and Fiorella who raised me with a love for science and physically, mentally and financially supported me in all my pursuits. Thank you for inspiring me to follow my dreams. My brother, Raffaele has always believed in me and wanted the best for me.

My family is the most important people in my world and I dedicate this thesis to them.

Thank you.

London, 31st July 2018

ABBREVIATIONS

Abbreviation	Definition
6-OHDA	6-hydroxydopamine
AC	Adenylate cyclase
AADC	Aromatic L-Amino Acid Decarboxylase
AD	Alzheimer's Disease
ADi	Axial diffusivity
ADC	Apparent diffusion coefficient
AMPA	2-Amino-3-(5-Methyl-3-Oxo-1,2-Oxazol-4-Yl) Propanoic Acid
BBB	Blood-Brain Barrier
BDI-II	Beck Depression Inventory II
BP_{ND}	Nondisplaceable Binding Potential
cAMP	Cyclic adenosine monophosphate
CBD	Corticobasal degeneration
cGMP	cyclic guanine monophosphate
CIT (FP)	Ioflupane, ligand for DAT
CREB	cAMP response element-binding protein
CSF	Cerebrospinal Fluid
CT	Computed Tomography
DAT	Dopamine Transporter
DJ-1	Deglicase 1 Gene
DLB	Dementia with Lewy bodies
DNA	Deoxyribonucleic Acid
DTI	Diffusion Tensor Imaging
DSI	Diffusion spectrum imaging
EDS	Excessive Daytime Sleepiness
ESS	Epworth Sleepiness Scale
ET	Essential tremor
FA	Fractional Anisotropy
GDS	Geriatric Depression Scale

H&Y	Hoehn & Yahr
IMA107	PET ligand for PDE10A
KCL	King's College London
L-DOPA	Levodopa
LIDs	Levodopa-induced dyskinesias
LRRK2	Leucine-Rich Repeat Kinase 2
MAO-B	Monoamine oxidase B
MBq	Megabecquerel
MCI	Mild Cognitive Impairment
MD	Mean diffusivity
MDS-UPDRS	Movement Disorder Society Unified Parkinson's Disease Rating Scale
MMSE	Mini-Mental State Examination
MoCA	Montreal Cognitive Assessment
MPRAGE	Magnetization Prepared Rapid Acquisition Gradient Echo
MR	Magnetic Resonance
MRI	Magnetic Resonance Imaging
mRNA	messenger RNA
MSA	Multiple system atrophy
mSv	Millisievert
NET	Noradrenaline transporter
NHS	National Health Service
NIG	Neurodegeneration Imaging Group
NMDA	N-Methyl-D-Aspartate
NMSS	Non-Motor Symptom Scale
NM-MRI	Neuromelanin-sensitive MRI
PARK2	Parkin Gene
PD	Parkinson's Disease
PDE	Phosphodiesterase
PDE10A	Phosphodiesterase 10A
PDQ-39	Parkinson's Disease Questionnaire
PDSS	Parkinson Disease Sleep Scale

PE2I	Ligand for DAT
PET	Positron Emission Tomography
PINK1	PTEN Induced Putative Kinase 1 Gene
PKA	cAMP-dependent protein kinase
PP-1	protein phosphatase-1
PSP	Progressive Supranuclear Palsy
QSM	Quantitative susceptibility mapping
RBD	REM Sleep Behaviour Disorder
RBSQ	REM Sleep Behaviour Sleep Disorder Questionnaire
RCT	Randomized Controlled Trial
RD	Radial diffusivity
RF	Radio Frequency
ROI	Region-of-interest
SCOPA-AUT	Scales for Outcomes in PD-Autonomic dysfunction
SERT	Serotonin transporter
SN	Substantia Nigra
SNpc	Substantia nigra pars compacta
SNCA	Synuclein Gene
SNP	Single Nucleotide Polymorphism
SNR	Signal-to-Noise Ratio
SPECT	DAT single-photon emission computed tomography
SRTM	Simplified Reference Tissue Model
STEP	Striatal-enriched tyrosine phosphatase
SYNJ1	Synaptojanin 1 Gene
SWI	Susceptibility-weighted imaging
T1	Longitudinal Relaxation Time
T2	Transverse Relaxation Time
TBSS	Tract-based spatial statistic
TE	Time Echo
TR	Time Repetition
UK	United Kingdom

UPSIT	University of Pennsylvania Smell Identification Test
VBM	Voxel-Based Morphometry
VCF	Variant Call Format
VMAT2	Vesicular Monoamine Transporter 2
WM	White Matter

Chapter 1. Introduction

This chapter introduces the background of the major topics that are discussed in greater detail throughout this thesis. Recent *post-mortem* and imaging evidence of Parkinson's disease pathology are reviewed and described underlying the role of phosphodiesterase 10A (PDE10A) in Parkinson's disease. Emphasis has been given on: why current imaging techniques, such as DAT single-photon emission computed tomography (SPECT) or DAT positron emission tomography (PET), are not appropriate to entirely define Parkinson's disease; the rationale of using both PET, SPECT and magnetic resonance imaging (MRI) in comparison with PDE10A; and why imaging markers have been compared with non-motor symptoms. Our hypothesis and aims are described at the end of the Introduction.

1.1 Parkinson's disease

Through precisely detailing the pathognomonic symptoms of six patients in his medical chef-d'oeuvre *'An Essay of the Shaking Palsy'*, in 1817 James Parkinson highlighted a clinical entity which had only insubstantially been comprehended before that date (Parkinson, 2002). Parkinson's disease is now recognized as the second most common neurodegenerative disease, with a prevalence steadily rising with age across all regions of the world (Pringsheim *et al.*, 2014). This chronic neurodegenerative movement disorder typically transpires insidiously in the sixth decade, progressing slowly over a duration of 10 – 30 years (Pavese and Brooks, 2009).

Parkinson's disease is characterized by cardinal motor features, including a combination of bradykinesia, rest tremor (4 – 6 Hz), muscle rigidity, postural instability and gait disturbance (Lees *et al.*, 2009). Although a clinical diagnosis rests exclusively on the appearance of these motor manifestations, non-motor symptoms including depression, chronic fatigue, sleep disorders, autonomic dysfunction and cognitive impairment are equally debilitating, disproving James Parkinson's original notion claiming that 'the sense and intellect remain uninjured' (Korczyn and Gurevich, 2010).

The aetiology of Parkinson's disease is poorly understood. The prevailing model suggests that the disease develops through a complex interplay between genetics and environmental factors (Kalia and Lang, 2015). A recent meta-analysis by Noyce *et al.* (2012) of 30 potential environmental factors affecting Parkinson's disease onset identified 11 significant environmental factors. From the highest to the lowest, the three most significant factors which increased the risk of Parkinson's disease were pesticide exposure, prior head injury, and rural living. From highest to lowest again, the three most significant factors which reduced the risk of Parkinson's disease were tobacco smoking, coffee drinking, and non-steroidal anti-inflammatory drug use. However, the link between the environment and the onset of Parkinson's disease is still unclear (Kalia and Lang, 2015).

The quintessential neuropathological hallmark of Parkinson's disease is the selective atrophy of neuromelanin-containing dopaminergic neurons within the substantia nigra *pars compacta* (SNpc) and the subsequent dopaminergic denervation of forebrain areas, predominantly the striatum (Marsden, 1982). Although neuronal neuropathological changes are pronounced in SNpc, non-dopaminergic systems including the serotonergic (Politis *et al.*, 2010a), glutamatergic (Hallett *et al.*, 2005), noradrenergic and cholinergic (Zheng *et al.*, 2011) systems are also affected.

Parkinson's disease is also characterized by abnormal aggregates in surviving neurons called Lewy bodies, mainly composed by α-synuclein (Gelb *et al.*, 1999; Davie, 2008; Kalia and Lang, 2015). This results in damage to neurons which leads to a dopamine deficiency in the basal ganglia and visible motor symptoms. Braak *et al.* (2003) have staged Parkinson's disease progression by mapping the distribution of Lewy bodies. In addition to the SNpc, the Lewy Bodies accumulation also occurs in the raphe nuclei, locus coeruleus, nucleus basalis of Meynert, amygdala, hypothalamus, and other cortical and subcortical regions (Dickson, 2012). According to Braak's staging, the pathological process in Parkinson's disease occurs in a gradual ascending fashion, starting from the olfactory nucleus and the medulla in premotor stages and spreading to the pons and midbrain later (Braak *et al.*, 2003). Braak, by examining *post-mortem* tissue, has described six stages of Parkinson's disease pathology of which three take places before motor symptoms become evident and a clinical diagnosis can be made (Braak *et al.*, 2007). The early premotor Braak stages are characterized by Lewy bodies and neurites lesions within the median raphe nuclei containing serotonergic neurons (Braak *et al.*, 2003). Some non-motor symptoms, such as constipation, depression, rapid eye movement sleep behaviour disorder (RBD) and anosmia, have been associated with the development of Parkinson's disease (Gagnon *et al.*, 2006) and are currently considered pre-motor symptoms. Subjects with these pre-motor symptoms, who might be considered as having prodromal idiopathic Parkinson's disease, provide limited possibilities to study premotor pathology because not all people at risk will eventually

develop Parkinson's disease, and observation of such individuals needs long follow-up periods, while the mechanisms underlying neurodegeneration remain obscure.

Familial forms of Parkinson's disease without manifest disease, though accounting only for 5-10% of the total Parkinson's disease population (Crosiers *et al.*, 2011), represent an ideal model to study premotor stages to not only elucidate disease pathophysiology, but enable the identification of biomarkers with the capacity to detect persons at risk for Parkinson's disease. A separate meta-analysis by Nalls *et al.* (2014) investigated the genetic contribution to Parkinson's disease onset and concluded that 24 loci have a clinically significant association with increased risk. To date, more than 25 mutated genes have been associated with familial forms of parkinsonism; monogenic causes include dominantly (*SNCA, LRRK2, VPS35, EIF4G1*) and recessively (*PARK2, PINK1, DJ-1*) inherited mutations. *SNCA* was the first gene to be associated with Parkinson's disease and codes for α-synuclein, the main component of Lewy bodies, and α-synuclein (SNCA) mutation carriers with manifest Parkinson's disease have similar clinical and pathologic findings of idiopathic Parkinson's disease, including a good response to levodopa and the presence of Lewy bodies (Gasser, 2001).

Currently, there is no cure for Parkinson's disease and only therapies which ease symptoms. The most widely used medications for motor symptoms enhance the dopamine concentration or stimulate dopamine receptors. These include levodopa, dopamine agonists, and monoamine oxidase B (MAO-B) inhibitors. In addition to adverse drug reactions, such as nausea, long-term dopaminergic treatment by Levodopa and dopamine agonists can cause drug-induced motor and non-motor complications (Thanvi and Lo, 2004). Alongside these medications, a wide range of drugs targeting the individual non-motor symptoms are used, such as antidepressants for Parkinson's disease associated depression. Today, no therapy is able to slow down or halt the neurodegenerative process, and a major goal of Parkinson's disease research is the potential development of a disease-modifying drug (Mesulam *et al.*, 1983; Kalia and Lang, 2015).

Use of Biomarkers to measure disease progression

Identifying patients with Parkinson's disease in the initial stage would be desirable to unravel the earliest mechanism underlying Parkinson's disease and, eventually, to develop specific disease-modifying therapy preventing the disease progression or complications. In this scenario, the role of neuroimaging biomarkers needs to be confirmed before these imaging measures could reliably be endorsed in the current guidelines for clinical use. Biomarkers are expected to reflect distinct aspects of Parkinson's disease pathology, either detecting preclinical and initial stages of Parkinson's disease or correlating with the progression of the disease. Molecular imaging techniques are able to identify subtle alterations at the nano-molecular level and this represents a prerequisite to quantify *in vivo* the brain activity in humans. SPECT and PET molecular probes bind a target, such as a receptor, a transporter or an enzyme, with high specificity and power of resolution (Politis, 2014). To date, PET and SPECT have been used in clinical setting to directly visualize the loss of dopaminergic terminals to confirm the diagnosis of Parkinson's disease (Pagano *et al.*, 2016b). The evaluation at the molecular level of biomarkers associated with the neuronal survival might be the cornerstone for the development of the cure for Parkinson's disease. Over the past decades, also MRI has been gaining ground as an attractive alternative diagnostic tool. In fact, in comparison with radiotracer methods, MRI has a diversity of possible contrasts and it is more readily available, less expensive, and above all avoids the ionizing radiation of radiotracers, employed in both PET and SPECT (Tuite, 2017).

1.2 PDE10A in Parkinson's disease

The survival of the organism is based on a correct signal transduction between cells that can adjust themselves in relation to changes in the environment. Activation of receptors on the plasma membrane represents the main mechanism of signal transduction that produces a downstream reaction inside the cell. Despite the thousands of "first messengers" (molecules that activate the receptors) and receptors expressed on a cell at any one time, the number of second messengers is quite limited.

Cyclic adenosine monophosphate (cAMP) and cyclic guanine monophosphate (cGMP) are the main second messengers identified and finely regulate the cell differentiation, proliferation, apoptosis, learning and memory (Shaulsky *et al.*, 1998; Richards, 2001; Insel *et al.*, 2012). The levels of intracellular cAMP and cGMP are tightly regulated by their synthesis by adenylyl and guanylyl cyclase, respectively, and their degradation by phosphodiesterase (PDEs).

In the recent years, the role of PDEs in the cellular homeostasis has been extensively studied. PDEs are intracellular enzymes that modulates the second messenger effect induced by the activation of G-protein-coupled receptors through the hydrolysis of cAMP and cGMP. They play a pivotal role in cell signals transduction (Fujishige *et al.*, 1999), with cAMP that activates the cAMP-dependent protein kinase (PKA) and cAMP response element-binding protein (CREB), which induce protein phosphorylation or gene expression and cGMP that modulates long-term changes in synaptic activity (Jones *et al.*, 2015). In the brain, intracellular levels of cAMP and cGMP regulate the mechanisms underlying neuroplasticity, such as long-term potentiation (Houslay and Milligan, 1997). These signaling cascades are negatively controlled by PDEs that breakdown cAMP and/or cGMP and turn off the cAMP and/or cGMP signaling pathways. PDEs cleave the phosphodiester bond of the cAMP and/or cGMP to generate inactive 5'-nucleotide metabolites.

PDEs are commonly divided into two classes: class 1 with low-affinity and class 2 with high-affinity for cAMP and/or cGMP. Human PDEs are mainly class 1 and are linked to 21 identified genes, which

give rise to 11 families of PDEs (PDE1–PDE11). They have approximately 270 conserved amino acids in the C-terminal catalytic domain, and around 35-50% sequence identity (Richter, 2002). Individual PDEs display sequence homology, the presence of certain regulatory domains, tissue specificity, sensitivity to specific inhibitors and whether they hydrolyze cAMP, cGMP or both. cAMP is selectively hydrolyzed by PDE4, 7 and 8, cGMP by PDE5, 6, and 9 while the other PDEs, such as PDE10, hydrolyze both cAMP and cGMP (Soderling and Beavo, 2000). The PDE10 family consists of only one gene, which express only one PDE10 called PDE10A. PDE10A is expressed almost exclusively in the striatum and subcortical areas (Seeger *et al.*, 2003; Coskran *et al.*, 2006; Lakics *et al.*, 2010), primarily in medium spiny neurons (MSNs), where it is thought to integrate dopaminergic and glutamatergic signals (Xie *et al.*, 2006; Nishi *et al.*, 2008; Nishi *et al.*, 2011) and to modulate the activity of dopamine D1 *direct* and dopamine D2 *indirect* pathways (Coskran *et al.*, 2006; Xie *et al.*, 2006). Dopamine regulates cAMP synthesis *via* D1-related activation or D2-mediated inhibition of adenylate cyclase (AC) (Garau *et al.*, 1978; Kebabian, 1978), and cGMP synthesis through modulation of the NO–GC pathway (Sammut *et al.*, 2007). PDE10A regulates cAMP and cGMP downstream signaling cascades, such as cAMP/PKA/DARPP32 signaling cascade (Greengard *et al.*, 1999), which primarily controls the activity and phosphorylation state of various physiological effectors including CREB and ERK, alongside several neurotransmitter receptors and voltage-gated ion channels through inhibition of protein phosphatase-1 (PP-1) (Girault, 2012). Thus, the inhibition of PDE10A is expected to increase cAMP and/or cGMP levels improving the cAMP/PKA/DARPP32 signaling cascade (Siuciak *et al.*, 2006; Strick *et al.*, 2010) (Figure 1).

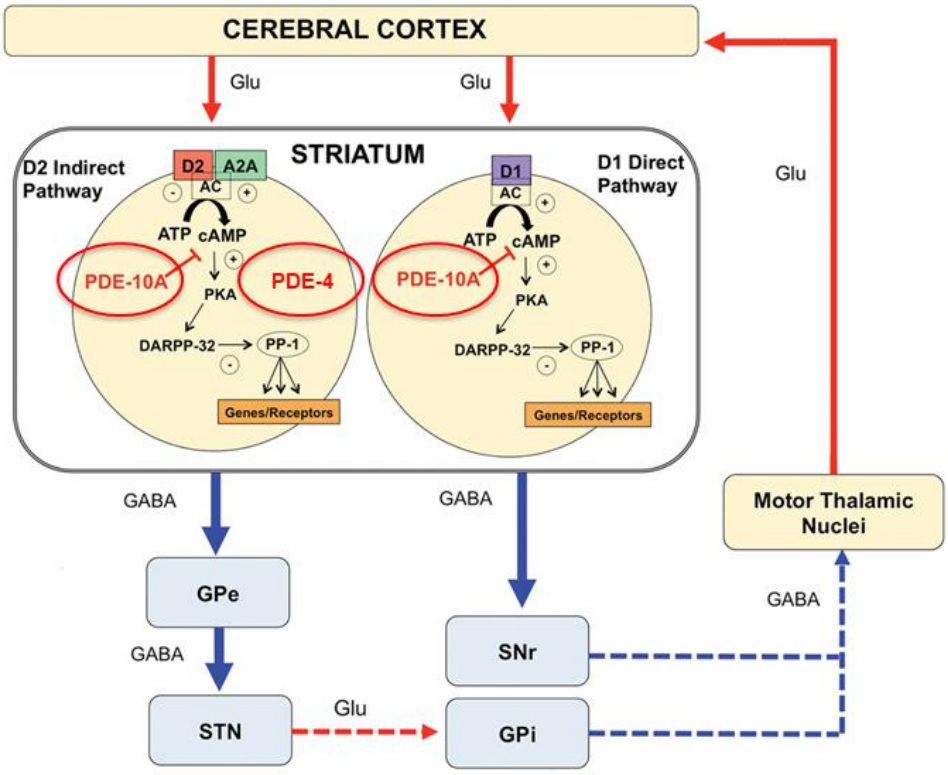

Figure 1. Roles of PDE10A in the control of basal ganglia–thalamocortical circuitry. *Output neurons in the striatum are medium spiny neurons (MSNs), which consist of striatonigral/direct pathway and striatopallidal/indirect pathway neurons. Direct pathway neurons are GABAergic, and inhibit tonically active neurons in globus pallidus interna (GPi)/substantia nigra pars reticulata (SNpr). Indirect pathway neurons are also GABAergic, and activate neurons in GPi/SNpr via inhibition of globus pallidus externa (GPe) GABAergic neurons and activation of subthalamic nucleus (STN) glutamatergic neurons. Direct and indirect pathway neurons induce opposing effects on the output neurons in GPi/SNpr, resulting in dis-inhibition and pro-inhibition of output, respectively, to motor areas of the thalamus and cortex. The inhibition of PDEs increases cAMP/PKA signaling in both direct and indirect pathway neurons. PDE inhibitors that predominantly act in direct pathway neurons work like dopamine D1 receptor agonists and activate motor function, whereas PDE inhibitors that predominantly act in indirect pathway neurons work like dopamine D2 receptor antagonists and inhibit motor function. Inhibition of PDE10A by papaverine activated cAMP/PKA signaling in both striatonigral and striatopallidal neurons, resulting in potentiation of dopamine D1 receptor signaling and inhibition of dopamine D2 receptor signaling. SNpc, substantia nigra pars compacta. Adapted from Nishi 2011 (Nishi et al., 2011).*

Preclinical studies

The role of PDE10A in the control of movements is mediated by the second messengers cAMP and cGMP, which appears to play a prominent part in regulating dopaminergic signaling and neuroplasticity. The role of PDE10A in the control of movements has been tested in animal models of Parkinson's disease and preclinical studies have also suggested an early role for PDE10A in the development of Parkinson's disease. (Sancesario *et al.*, 2004; Giorgi *et al.*, 2008; Nishi *et al.*, 2008). In fact, although Parkinson's disease is caused by specific pathological events such as loss of dopamine-producing cells in the substantia nigra, it is primarily classified as a movement disorder resulting from basal ganglia dysfunction and clinically characterized by hypokinetic manifestations. Therefore, dysregulation of PDE10A might be cardinal for its involvement in the regulation of both the striatonigral (direct) and striatopallidal (indirect) output pathways (Jones *et al.*, 2015). In these experimental models of Parkinson's disease, it has been shown that nigrostriatal deafferentation increased cAMP and decreased cGMP levels in the ipsilateral striatum compared to the contralateral side (Sancesario *et al.*, 2004; Giorgi *et al.*, 2008). Reduced cGMP levels may be the result of reduced NO-mediated cGMP synthesis as well as increased degradation of cGMP by an up-regulation of PDEs activity (Sancesario *et al.*, 2004).

A lesion of the nigrostriatal dopaminergic projections with 6-hydroxydopamine (6-OHDA) increased cAMP levels in the caudate and putamen of rats (Hossain and Weiner, 1993). In 6-OHDA lesioned rats, PDE10A protein levels and mRNA levels were reduced in the caudate-putamen and striatal projections (Giorgi *et al.*, 2011). Increased PDE10A protein and activity, despite unchanged PDE10A mRNA levels, was observed within the nucleus accumbens. PDE10A has distinct roles in modulating cAMP signaling in the striatonigral and striatopallidal postsynaptic pathways. In striatonigral neurons, dopamine loss leads to a reduced synthesis of D1 receptor-stimulated cAMP (Herve *et al.*, 2001); the inhibition of PDE10A expression will, therefore, increase cAMP levels and could in part compensate for the reduced cAMP signaling. In striatopallidal neurons, dopamine loss decreases the

inhibitory effect of D2 receptor on cAMP synthesis (Stoof and Kebabian, 1981). Thus, loss of PDE10A levels may further increase cAMP levels by enhancing the negative consequences of dopamine loss on D2 receptor signaling and potentiate adenosine A2A receptor signaling (Svenningsson *et al.*, 1998), which may result in functional imbalance between striatonigral and striatopallidal dopaminergic pathways, contributing to the development of motor symptoms in Parkinson's disease.

Based on these preclinical studies, it is also possible to hypothesize that the failure of dopamine to activate properly post-synaptic striatal neurons (which is associated with the development of motor symptoms) might be also due to a primary dysregulation of PDE10A expression, with a reduction below the physiological levels. This would be associated with an increased level of cAMP which mimics the condition induced by the 6-OHDA in animal models and could potentially be a pathogenic mechanism fundamental to the dysfunction of second messenger signaling associated with the development of motor symptoms typical of Parkinson's disease.

Preclinical studies have suggested that PDE10A could be involved in the development of Parkinson's disease motor complications. In dyskinetic rodent, Parkinson's disease models, cAMP, and cGMP levels in the cortical-striatal-pallidal pathway were significantly lowered at the peak of dyskinesias compared to eukinetic animals (Giorgi *et al.*, 2008). When dyskinetic animals were pre-treated with the non-selective PDE inhibitor, zaprinast, before levodopa administration, the severity of dyskinesias was effectively reduced and prevented the decline in cyclic nucleotide levels (Giorgi *et al.*, 2008). A more recent study discovered an inverse correlation between cAMP/cGMP and the time course of dyskinesias in dyskinetic animals, where cellular levels of cAMP/cGMP were lower during the surge of dyskinesias (at 60 minutes after levodopa administration), but were upregulated during depletion and extinction of dyskinesias (from 90 to 150 minutes after levodopa) (Sancesario *et al.*, 2014). Thus, this data suggests that changes in cyclic nucleotide levels are implicated in the appearance and regression of levodopa-induced dyskinesias (LIDs). The equilibrium between dopamine-induced

synthesis and PDE-related catabolism is fundamental to the regulation of cyclic nucleotides. Studies have previously demonstrated that Parkinson's disease patients with LIDs have prominently higher striatal synaptic dopamine levels following levodopa administration compared to stable responders (de la Fuente-Fernandez *et al.*, 2001). Therefore, altered cAMP/cGMP levels due to dopamine-induced synthesis and PDE catabolism may contribute to the development of LIDs (Sancesario *et al.*, 2014).

Although PDE10A knockout mice demonstrated a reduction in spontaneous locomotor activity, the inhibition of PDE10A decreased spontaneous and stimulant-induced behavior, inhibits conditioned behavior and also reverses stimulant-induced sensory gating deficits (Megens *et al.*, 2014). These effects resemble the therapeutic profile of D2 receptor blockers and are consistent with the amplified output of the indirect pathway (Megens *et al.*, 2014). Studies have confirmed, however, that PDE10A inhibitors activate both dopamine D1 receptor and dopamine D2 receptor- pathways, thus combining functional characteristics of D1 agonists and D2 antagonists (Nishi *et al.*, 2008; Strick *et al.*, 2010). A recent study revealed that PDE10A inhibitors were effective only when dopaminergic neurotransmission was reduced with D1 antagonist SCH-23390 but not with D2 antagonist haloperidol, which indicates that stimulation/inhibition of motor behavior is conditional to the relative activation state of the direct and indirect striatal output pathways. In the reserpine model of Parkinson's disease, PDE10A inhibitors showed an anti-cataleptic effect, which suggests a therapeutic perspective in Parkinson's disease (Megens *et al.*, 2014) (Figure 1).

Preclinical studies have also shown an association between PDE10A and neuronal survival. In the striatal pathways, cAMP regulates a diverse array of neural functions ranging from ion conductance to synaptic plasticity through activation of PKA (Meinkoth *et al.*, 1993; Girault, 2012). The cAMP/PKA signaling cascade targets the DARPP-32 (Greengard *et al.*, 1999; Svenningsson *et al.*, 2004). DARPP-32 is phosphorylated by PKA and inhibits a wide-spectrum of proteins such as the PP-1. Inhibition of PP-1 by DARPP-32 controls the phosphorylation state and activity of many

downstream physiological effectors including gene transcription factors (CREB protein and Elk-1) and various neurotransmitter receptors (AMPA and NMDA receptors) and voltage-gated ion channels, indicating an essential role for the cAMP/PKA/ DARPP-32 in DA-ergic signalling (Fienberg *et al.*, 1998; Girault, 2012). Phosphorylation of DARPP-32 inhibits the PP1-induced striatal-enriched tyrosine phosphatase (STEP), which play a critical role in the dephosphorylation of ERK (Paul *et al.*, 2003). ERK phosphorylates the nuclear kinase MSK, which appears to play a prominent role in phosphorylation of histone H3 and CREB protein. This leads to the expression of genes such as cFos, which are particularly important for neuron survival (Girault, 2012). Thus, by enhancing the activity of DARPP-32, reduced expression of PDE10A may lead to decreased gene expression and subsequently to neuronal degeneration in the striatum. DARPP-32 enhances phosphorylation of histone H3 (Stipanovich *et al.*, 2008) and through inhibition of PP1 increases multiple posttranslational modifications of histones, including acetylation of H2B, H3K14, and H4K5, as well as trimethylation of H3K36 (Koshibu *et al.*, 2009). PDE10A by regulating DARPP-32 levels may lead to the activation of a complex network of protein kinases and phosphatases converging on the nucleus and contribute to epigenetic regulations (Koshibu *et al.*, 2009).

Genetic studies

Positive evidence on the role of PDE10A in neurodegenerative disorders come from recent genetic studies on PDE10A gene mutations (Diggle *et al.*, 2016; Mencacci *et al.*, 2016). An early-onset hyperkinetic movement disorder was identified in eight subjects with loss of striatal PDE10A due to homozygous mutations (c.320A>G - p.Tyr107Cys and c.346G>C - p.Ala116Pro) of PDE10A gene (Diggle *et al.*, 2016). Both mutations lead to a reduction in PDE10A levels in recombinant cellular systems. PET imaging with [^{11}C]IMA107, a selective PDE10A ligand, confirmed that striatal PDE10A levels are also decreased in one subject with p.Tyr107Cys variant (Diggle *et al.*, 2016).

Other *de novo* heterozygous mutations in PDE10A gene were found in three subjects (c.898T>C [p.Phe300Leu] in two individuals and c.1000T>C[p.Phe334Leu] in one individual) (Mencacci *et al.*, 2016). These mutations caused a unique movement disorder characterized by benign childhood-onset chorea that was followed by adult-onset levodopa-responsive parkinsonism (Mencacci *et al.*, 2016). All these mutations caused a loss of function of the PDE10A gene and the three young subjects showed atrophy of caudate nuclei at MRI imaging, of the same extent seen in Huntington's disease patients, and, for the older subject, who developed levodopa-responsive parkinsonism, it was seen a bilateral abnormality of striatal dopamine reuptake transporters consistent with nigrostriatal degeneration. However, it was not clear whether the observation of parkinsonism with nigrostriatal degeneration in that subject was accidental or whether individuals with *de novo* PDE10A mutations are also at an increased risk of developing degeneration of nigral neurons. These genetic studies confirm the potential involvement of PDE10A in the development of movement disorders, such as Parkinson's disease and Huntington's disease, and gave us further evidence to investigate PDE10A in a cohort of Parkinson's disease patients.

Another very interesting fact is that the gene encoding PDE10A has been identified in 6q26-27 (OMIM 610652) (Fujishige *et al.*, 1999). Many loci have been identified in chromosome 6 but one locus of interest has been identified in 6q25.2-q27 (OMIM 602544) (Matsumine *et al.*, 1997), which is the gene responsible for the parkin familial form of Parkinson's disease (PARK 2). Both PDE10A signaling and parkin mutated protein are expressed in the striatum and are involved in striatal neuronal function, thus making the possibility of genetic linkage between these two intriguing. In idiopathic Parkinson's disease, epigenetic processes such as DNA methylation, histone modifications, and small RNA-mediated mechanisms may regulate the expression of Parkinson's disease-related genes and contribute to disease pathogenesis (Urdinguio *et al.*, 2009; Masliah *et al.*, 2013). Several genes including parkin have been shown vulnerable to epigenetic regulation in Parkinson's disease, and therefore supporting the role of epigenetic alterations as a molecular mechanism in nigrostriatal

degeneration (Asikainen *et al.*, 2010; Masliah *et al.*, 2013). The relationship between PDE10A and parkin have not been investigated either in preclinical nor in clinical studies.

Human studies

Post-mortem studies in humans have shown that PDE10A is expressed in the caudate, putamen, ventral striatum, globus pallidus, SNpc and thalamus (Lakics *et al.*, 2010).

In humans, PDE10A expression can be measured with high selectivity ligands, such as [^{11}C]IMA107, [^{18}F]JNJ42259152, [^{18}F]MNI-659 (Ahmad *et al.*, 2014; Russell *et al.*, 2014; Niccolini *et al.*, 2015a; Niccolini *et al.*, 2015b; Russell *et al.*, 2016).

One study has been performed in Parkinson's disease patients, investigating PDE10A expression by using [^{11}C]IMA107 PET imaging in 24 moderate-advanced Parkinson's disease patients (Niccolini *et al.*, 2015a). Parkinson's disease patients showed lower [^{11}C]IMA107 binding in the caudate, putamen and globus pallidus compared to healthy controls. Longer Parkinson's disease duration and higher Unified Parkinson's Disease Rating Scale part-III motor scores correlated with lower [^{11}C]IMA107 binding in the caudate, putamen, and globus pallidus. Higher Unified Dyskinesia Rating Scale scores in those Parkinson's disease with levodopa-induced dyskinesias correlated with lower [^{11}C]IMA107 binding in the caudate and putamen. This provides evidence for the role of PDE10A within the striatum in the development of cardinal motor symptoms in Parkinson's disease. Interestingly, a decline in PDE10A expression within the globus pallidus correlated with worse axial signs including the freezing of gait, falls and imbalance (Niccolini *et al.*, 2015a) (Figure 2).

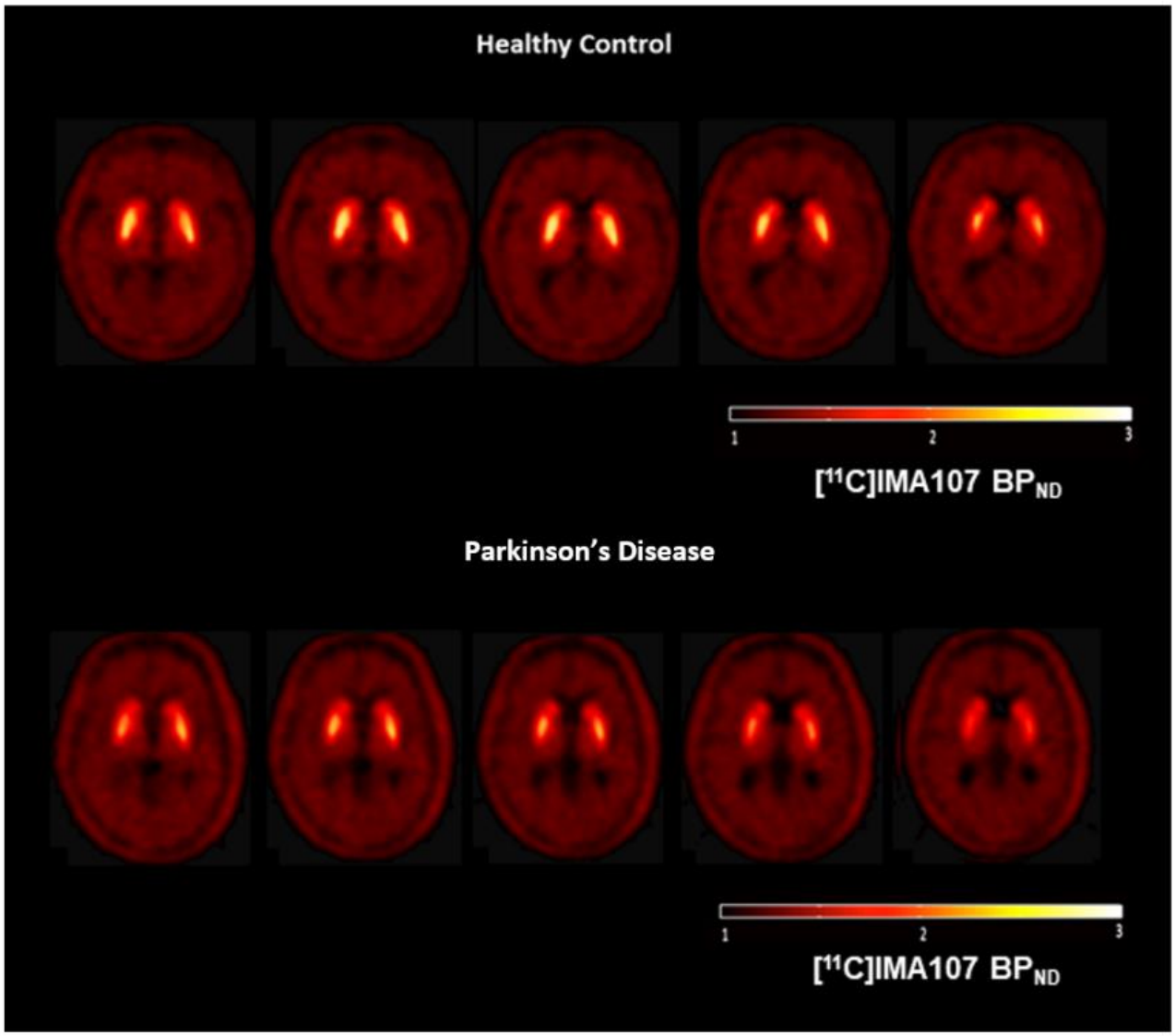

Figure 2. PDE10A expression in Parkinson's disease. *Parametric images of [^{11}C]IMA107 PET imaging in a healthy control and in a patient with Parkinson's disease.*

In summary, PDE10A is localized almost exclusively within the axons of striatal MSNs modifying cAMP/cGMP downstream signaling cascades in both striatonigral and striatopallidal neurons, *via* cAMP and cGMP hydrolysis, playing a fundamental role in regulating the direct and indirect striatal output pathways, respectively. Therefore, alterations in cyclic nucleotide availability can result in dysregulation of striatopallidal and striatonigral downstream signaling cascades, leading

to an imbalance of striatal output (Siuciak *et al.*, 2006). This consequently results in the abnormal thalamocortical input, which can precipitate or exacerbate motor and cognitive symptoms that are typical of Parkinson's disease (Andre *et al.*, 2010).

Evidence links PDE10A to both Parkinson's disease and Huntington's disease showing that a deletion of PDE10A is associated with hyperkinetic motor symptoms in early ages but hypokinetic motor symptoms in older ages (Diggle *et al.*, 2016). This is in line with the pharmacological data indicate that PDE10A might regulate differentially direct and indirect pathways, in which pharmacological inhibition of PDE10A with papaverine or TP-10 is consistent with the preferential activation of the indirect pathway (Threlfell *et al.*, 2009). A genetic loss of PDE10A would then preferential affect the function of the indirect pathway, thus, induces a hyperkinetic movement disorder. With the progression of the pathology, in older age, the direct pathway would also be affected, with the onset of motor symptoms typical of Parkinson's disease (Diggle *et al.*, 2016; Niccolini *et al.*, 2018). In the population of patients with genetic loss of PDE10A that showed motor Parkinson's disease symptoms, PDE10A PET imaging with [^{11}C]IMA107 was correlated with DAT [^{123}I]FP-CIT SPECT imaging and MRI markers of Parkinson's disease pathology (NM-MRI and DTI) (Niccolini *et al.*, 2018).

PDE10A function is critical for the control of movements and for neuronal survival, thus, understanding whether PDE10A is abnormally expressed will provide a major step towards understanding the mechanisms underlying neurodegenerative processes. PDE10A could serve as a novel therapeutic target for manipulation with pharmacotherapy in the neuropathological salient circuits, which promote neuronal survival and control of movements, cognitive and mood functions.

We hypothesized that the failure of dopamine to activate properly post-synaptic striatal neurons (which is associated with the development of motor symptoms in Parkinson's disease) might not be due only to a deficit of dopamine release (consequence of SNpc cell loss) but also due to a primary dysregulation of PDE10A expression, with a reduction below the physiological levels. This would be associated with an increased level of cAMP, which mimics the condition induced by the 6-OHDA in animal models of Parkinson's disease, and could potentially be a pathogenic mechanism fundamental to the dysfunction of second messenger signaling associated with the development of motor symptoms typical of Parkinson's disease. Thus, loss of PDE10A expression could be one of the earliest pathophysiological events in the course of Parkinson's disease, even earlier that DAT terminal loss.

Previous PET imaging studies have shown that changes in the molecular binding profile of selected brain targets may serve as promising markers of disease burden and progression, drug target identification and treatment response in therapeutic trials in patients with Parkinson's disease (Politis, 2014). Loss of DAT signal in Parkinson's disease patients reflects loss of nigrostriatal dopamine neurons and is typically associated with dopaminergic pathology in the putamen and the motor features of bradykinesia and rigidity (Pirker, 2003). However, molecular imaging of DAT cannot be considered an ideal biomarker for Parkinson's disease due to several limitations, including a lack of specificity for Parkinson's compared to atypical parkinsonism, and the fact that dopaminergic supplementation may modulate DAT levels, limiting its use as biomarker for clinical trials testing disease-modification drugs (Fahn *et al.*, 2004; Schapira, 2013). Recent work with PET molecular imaging has demonstrated loss of PDE10A expression in moderate to advanced levodopa-treated patients with Parkinson's disease, which was associated with motor symptoms and complications (Niccolini *et al.*, 2015a). Therefore, PDE10A, as an enzyme regulating striatal output and dopaminergic signalling, shows promise to serve as a marker of disease burden in

patients with early Parkinson's disease. However, it is unknown whether PDE10A is implicated at the earlier stages of the disease and how its biomarker value compares with the gold standard DAT molecular imaging.

DAT can be measured with different tracers and we decided here to use two different tracers, [^{11}C]PE2I which is more specific of DAT, and [^{123}I]FP-CIT, which binds also SERT but it is widely used in clinical practice. We could not use both PET PE2I and PET FP-CIT due to the limited amount of funding (SPECT is approximately 7 times cheaper than PET) but we compared [^{11}C]PE2I PET versus [^{123}I]FP-CIT SPECT to confirm that both were correlated with Parkinson's disease symptoms.

Using molecular imaging, we aimed to investigate the role of PDE10A in the early stages of the Parkinson's disease with the main hypothesis that a reduction of PDE10A expression is an early phenomenon in the course of Parkinson's disease, and that PDE10A expression decreases further as Parkinson's disease progress (in term of duration and clinical severity). We have investigated this in the Project 1, in which, by using [^{11}C]IMA107 PET imaging, we assessed *in vivo* the integrity of PDE10A enzyme in early *de novo* and in a population of early levodopa-treated patients with three-year longer Parkinson's disease duration in relation to a group of age- and sex-matched healthy controls.

We also hypothesize that PDE10A expression might be affected earlier on in the course of the disease, investigating the associations between PDE10A and non-motor symptoms considered pre-motor (sleep problems, autonomic dysfunction, mood disorders etc).

We also hypothesize that PDE10A expression was correlated with dopaminergic pathology, which can be measured either with PET or SPECT. We have investigated this in the Project 2, in which we compared the expression of PDE10A, measured with [^{11}C]IMA107 PET imaging, with the best known molecular markers of dopaminergic dysfunction in Parkinson's patients, the [^{11}C]PE2I PET

imaging, and the clinical validated [^{123}I]FP-CIT SPECT imaging. In this Project, we also compared [^{11}C]PE2I PET versus [^{123}I]FP-CIT SPECT because the two tracers have a different affinity for the DAT ([^{11}C]PE2I is more specific of DAT where [^{123}I]FP-CIT binds both DAT and SERT). This would give us a greater understanding of the relationship between PDE10A expression and dopaminergic and non-dopaminergic pathology.

We also hypothesize that PDE10A expression was correlated with other markers of Parkinson's disease pathology, such as iron depositions, neuromelanin loss, and changes in structural and microstructural changes in the substantia nigra and in the striatum. We have investigated this in the Project 3, in which we compared the expression of PDE10A, measured with [^{11}C]IMA107 PET imaging, with MRI markers of Parkinson's pathology such as iron depositions (assessed with susceptibility-weighted MR imaging), neuromelanin loss (assessed with neuromelanin sensitive MR imaging) and changes in structural volumetric (assessed with T1 MR imaging) and microstructural connectivity (assessed with diffusion tensor MR imaging).

1.3 Neuroimaging techniques in Parkinson's disease

In this section, SPECT and PET molecular and MRI imaging are described from a methodological point of view and previous application in Parkinson's disease are discussed in detail. Differences in molecular imaging of DAT with different tracers and with SPECT and PET imaging, PDE10A PET molecular imaging and novel MRI markers of Parkinson's disease, such as SWI iron deposition, NM density and structural and microstructural DTI imaging are also described in detail.

1.3.1 SPECT and PET molecular imaging

1.3.1.1 Methodological consideration

Molecular imaging techniques are able to identify subtle alterations at the nano-molecular level and this represents a prerequisite to evaluate *in vivo* the brain activity in humans. SPECT and PET molecular probes bind a target, such as a receptor, a transporter or an enzyme, with high specificity and power of resolution (Politis, 2014).

MRI is a diagnostic tool that provide very high structural information of the tissue, giving a better soft tissue contrast compared to SPECT or PET. The relative weaknesses and strengths that exist among imaging techniques are important to be understood (Khalil *et al.*, 2011). The spatial resolution of MRI and Computed Tomography (CT) is significantly higher than that of SPECT and PET, however, the detection sensitivity of SPECT and PET is significantly higher than those given by structural modalities and moreover can detect tracer concentration in the picomolar or nanomolar range. Both approaches use the tracer principal to detect physiological abnormality or disturbed biochemical process. The key elements in radionuclide imaging are a biomarker and an imaging device. The first should have high specificity, as well as sensitive characteristics to optimally study a molecular or cellular phenomenon. The imaging device is a radiation detector with specific performance to localize activity distribution within the human body or the animal. The most commonly used instrument in SPECT imaging is the conventional gamma camera that was invented

in the middle of the last century (Khalil *et al.*, 2011). In clinical practice, almost all nuclear medicine procedures that use single photon emission tracers rely on the use of the gamma camera. It is a gamma ray position sensitive detector that typically consists of a large slab of scintillator crystal with position circuitry and energy determination. To localize the emission site of the released photons, a multihole collimator is mounted on the front face of the system to provide a spatial correlation of the detected events. The gamma camera is able to localize an activity distribution of an administered radionuclide. However, for detection of coincidence events and localization of PET-administered compounds, a PET scanner is normally used. Both imaging devices have witnessed a notable change in the last decade in terms of performance characteristics as well as diagnostic quality.

Spatial resolution and detection sensitivity are two important performance characteristics that play a key role in molecular imaging research using SPECT and PET tracers. The clinical gamma camera provides a tomographic resolution of about 10 mm for SPECT scans compared to 4-5 mm of common PET and 2.5 mm of High-Resolution Research Tomograph PET scans. These resolution differences are mainly due to the fact that PET systems are not affected by some physical and fundamental limits that hinder the SPECT camera to reach sub-millimeter ranges. Many factors serve to impact the final reconstructed images of data acquired from a PET scanner. These are crystal size, positron range, photon acollinearity, inter-crystal interaction and scatter, depth of interaction and the reconstruction algorithm. In preclinical PET machines, positron range appears to be the most important challenge that needs to be tackled to improve the spatial resolution of the PET images. However, the current generation of clinical PET scanners is slightly affected by the positron range, but correction of the phenomenon was shown to be effective in positron emitters of high maximum kinetic energy (Sanchez-Crespo *et al.*, 2004). These issues are obviously absent in clinical as well as preclinical SPECT systems. The gamma camera relies on hardware collimators to determine the trajectory of the photon and hence able to localize the emission site by analyzing the electronic signal detected by the imaging detector. This hardware collimation plays a significant role in reducing the overall system

sensitivity as well as the spatial resolution. The intrinsic resolution of the gamma camera is about 3-4 mm and tomographic SPECT acquisition reveals a spatial resolution, as mentioned above, not better than 10 mm.

SPECT degrading factors have been extensively studied in the literature and, namely, include attenuation, scatter and resolution effects, in addition to motion artifacts. Apart from the later, most of these physical issues can be resolved in great part using SPECT/CT systems. Nevertheless, correction for photon attenuation, scatter and partial volume would collectively improve the detection and estimation task (Khalil *et al.*, 2011). This is particularly important for small structures and in small energy radionuclides such as I-125 (Hwang *et al.*, 2008).

Unlike PET, single photon emitting radiopharmaceuticals have several features in the context of molecular imaging such as cost and wide availability of the radioligands as well as relative ease of labeling. Small animal imaging using preclinical scanners and PET radiopharmaceuticals showed better capability in tracer kinetic studies when compared to its SPECT counterparts. PET compounds have been extensively used in compartmental modeling and kinetic analysis.

1.3.1.2 Dopaminergic molecular imaging in Parkinson's disease

SPECT and PET molecular imaging targeting presynaptic and postsynaptic dopaminergic markers has been extensively employed to aid with the early diagnosis of Parkinson's disease, track disease progression, and investigate motor and non-motor symptoms of Parkinson's disease (Politis, 2014).

The integrity of the presynaptic nigrostriatal dopaminergic system can be studied with radiotracers targeting the Dopamine Transporter (DAT), the Aromatic L-Amino Acid Decarboxylase (AADC) and the Vesicular Monoamine Transporter 2 (VMAT2). AADC and VMAT2 however are not specific of dopaminergic neurons.

DAT is a symporter expressed on the presynaptic end-terminal of dopaminergic neurons, which clears the synapses from released dopamine by re-uptaking it in the presynaptic terminals and, thus, stopping its transmission. The expression of DAT declines with aging (van Dyck *et al.*, 2002; Kaasinen *et al.*, 2015).

Several PET and SPECT radiotracers targeting the DAT have been developed. These radioligands are mostly cocaine or tropane analogs and bind to DAT with nanomolar affinity. Most of these tracers show high affinity for other monoaminergic transporters such as Serotonin (SERT) and Noradrenaline (NET); however, the concentration of DAT in the basal ganglia highly exceeds that of the other transporters so that its measure in striatal regions is not significantly affected. By contrast, the study of extra-striatal regions with these tracers may be less reliable. [^{123}I]β-CIT has better sensitivity and specificity than [^{99}Tc]TRODAT-1 in the detection of DAT density reductions (Van Laere *et al.*, 2004), but presents protracted periods of striatal uptake and long wash-out. [^{123}I]PE2I shows higher selectivity for DAT compared to SERT and NET in extra-striatal areas (Emond *et al.*, 1997). [^{123}I]FP-CIT (also named [^{123}I]FP-CIT or DaTSCAN) has been approved in 2000 by the European Medicine Agency for the clinical use in the differential diagnosis of clinically uncertain Parkinsonism. [^{123}I]FP-

CIT has lower selectivity for DAT compared to [^{123}I]PE2I and has been shown that is able to bind also SERT in brain area rich of SERT terminals, such as raphe nuclei (Qamhawi *et al.*, 2015).

All SPECT tracers can distinguish patients with degenerative parkinsonism from healthy controls with high sensitivity and specificity evidencing reductions up to 81% of tracer uptake in the posterior putamen contralateral to the clinically most affected side (Schwarz *et al.*, 2000; Huang *et al.*, 2001; Chou *et al.*, 2004; Weng *et al.*, 2004; Filippi *et al.*, 2005; Eshuis *et al.*, 2009). PET imaging with radioligands binding to DAT has yielded comparable results: a consistent and severe decrease of DAT activity can be detected in the putamen contralateral to the clinically most affected side of Parkinson's disease patients. Guttman and colleagues studied 11 *de novo* Parkinson's disease patients using [^{11}C]RTI-32 PET, and showed that, contralaterally to motor symptoms, the posterior putamen displayed a 56% decrease in radioligand uptake, and 28% decrease in the anterior putamen, demonstrating a gradient of dopamine transporter changes within this region (Guttman *et al.*, 1997). The putamen is more affected than the caudate and this pattern is highly preserved during disease course (Marek *et al.*, 1996; Guttman *et al.*, 1997; Mozley *et al.*, 2000). However, other studies, demonstrated higher decreases in the caudate rather than putamen (Rinne *et al.*, 1999a; Rinne *et al.*, 1999b). DAT-SPECT studies have also demonstrated a significant reduction of tracer uptake to an extent up to 44% in the striatum ipsilateral to the clinically most affected side of *de novo* Parkinson's disease patients, implying, therefore, that DAT-SPECT imaging is able to detect subclinical presynaptic dopaminergic degeneration (Schwarz *et al.*, 2000; Weng *et al.*, 2004; Filippi *et al.*, 2005).

The extent of DAT decline is inversely correlated with the severity of motor symptoms as assessed with the Unified Parkinson's disease Rating Scale – Motor Part III (Rinne *et al.*, 1999b; Huang *et al.*, 2001; Moccia *et al.*, 2014). Interestingly, in all these studies, a correlation was found with bradykinesia and rigidity subscores, but not with tremor. This implies that tremor in Parkinson's disease may have a different pathophysiology, not primarily driven by dopaminergic dysfunction,

such as SERT deficit, seems to have a prominent role (Politis *et al.*, 2010b; Politis *et al.*, 2011; Loane *et al.*, 2013; Pagano *et al.*, 2017).

The degree of progression of dopaminergic degeneration in Parkinson's disease has been assessed by longitudinal studies. PET and SPECT imaging have yielded comparable results. Using [^{18}F]CFT PET, Nurmi and colleagues found that the annual rate of decline of DAT in a two-year follow-up was 13.1% in the putamen and 12.5% in the caudate, compared to 2.1% and 2.9%, respectively, for controls (Nurmi *et al.*, 2000). Marek and colleagues investigated 32 Parkinson's disease patients in a one-to-four-year period with [^{123}I]β-CIT and showed that in Parkinson's disease patients the annual decline of striatal DAT density was of 11.2% compared to 0.8% of controls (Marek *et al.*, 2001), which corresponds to a functional decline. In another study, 21 Parkinson's disease patients were studied over a time span of five years in which they performed three SPECT scans with [^{123}I]β-CIT (Pirker *et al.*, 2003). It was found that the absolute rate of striatal decline was of 7.5% between scan one and two, and 5.6% decline between scan two and three, suggesting that the progression of DAT degeneration in Parkinson's disease is not linear and slows over time. Moreover, during follow-up, 11 patients also developed levodopa (L-DOPA)-related motor complications. These patients did not display any specific progression in DAT decline, probably because they initial levels were so low to induce the so-called "floor effect" (Pirker *et al.*, 2003). In patients with long-standing disease, the rate of degeneration of dopaminergic terminals slows down and reaches a plateau (Hely *et al.*, 2005; Hely *et al.*, 2008), whereas it appears to progress significantly only in concomitance with the presence of dementia (Colloby *et al.*, 2005). Parkinson's disease patients with mean disease duration of 20.6 years still show some uptake of [^{123}I]FP-CIT with preservation of the putamen greater than the caudate and asymmetry in radiotracer uptake (Djaldetti *et al.*, 2011).

The prognostic implications of low striatal levels of DAT density have been additionally studied. Low striatal [^{123}I]β-CIT SPECT uptake is independently associated with higher risk of motor-related disability and falls. Moreover, Parkinson's disease patients with the lowest levels of striatal uptake at

baseline were at higher risk of developing cognitive impairment and psychosis at a 22-month follow-up (Ravina *et al.*, 2012). Recently, changes in DAT density over time have been studied as a possible marker of disease progression. Li and colleagues demonstrated in 33 Parkinson's disease patients that, after a mean follow-up of 18.8 months, striatal [^{11}C]PE2I uptakes were more predictive of worse motor symptom severity than striatal [^{18}F]DOPA uptakes (Li *et al.*, 2018). This result has been explained by the different compensatory adjustments that DAT and AADC undergo during Parkinson's disease natural history (Li *et al.*, 2018). It can be therefore concluded that low levels of striatal DAT activity in Parkinson's disease patients represent a negative prognostic factor.

SPECT imaging is widely used in the diagnostic workup of patients in which clinical examination is ambiguous. [^{123}I]FP-CIT facilitates the diagnosis in patients with isolated tremor symptoms not fulfilling Parkinson's disease or essential tremor (ET) criteria, as well as in functional, and drug-induced parkinsonism (Scherfler *et al.*, 2007; Huertas-Fernandez *et al.*, 2015). In patients with clinically uncertain parkinsonism, lower striatal [^{99}Tc]TRODAT-1 uptake identified who, when followed up for up to 2 years, clinically converted to Parkinson's disease with 100% sensitivity and 70% specificity (Felicio *et al.*, 2010). Patients with vascular parkinsonism usually display normal DAT SPECT scans (Antonini *et al.*, 2012), although in a recent large survey, abnormal [^{123}I]FP-CIT uptake levels could be detected in up to 67.5% of 106 vascular parkinsonian patients (Benitez-Rivero *et al.*, 2013). Atypical Parkinsonism, such as Multiple System Atrophy (MSA) or Progressive Supranuclear Palsy (PSP), typically display reduced DAT striatal activity. Attempts have been done to distinguish between Parkinson's disease and atypical syndromes, by means of DAT imaging. It has been found that the striatal DAT reduction in MSA and PSP was more uniform than in Parkinson's disease (Kim *et al.*, 2002; Im *et al.*, 2006); moreover, the ratio DAT/D2 uptake was significantly higher in PSP than in MSA (Knudsen *et al.*, 2004).

In summary, SPECT and PET molecular imaging of DAT are able to measure in vivo the pathognomonic loss dopaminergic terminals of Parkinson's disease. PET have higher definition

than SPECT but also higher costs. Different tracers have different affinity to DAT, SERT and NET. We decided to use the [^{11}C]PE2I PET as considered the most specific DAT tracer, and [^{123}I]FP-CIT SPECT as considered the most validated Parkinson's disease *in vivo* marker in clinical practice and with a degree of affinity also to SERT. This would allowed us to compare PDE10A expression with both dopaminergic (DAT - [^{11}C]PE2I PET) and non-dopaminergic (DAT and SERT - [^{123}I]FP-CIT SPECT) pathology. We did not use FP-CIT PET due to funding constrains.

1.3.1.3 PDE10A molecular imaging in Parkinson's disease

Multiple PET radiotracers targeting the PDE10A have provided promising results in preclinical studies and allow assessment of target engagement in the human brain (Figure 3). These radioligands are mostly based on incorporation of radioisotopes onto PDE10A inhibitors (Barret *et al.*, 2014; Fan *et al.*, 2014; Hwang *et al.*, 2014; Kehler *et al.*, 2014; Li *et al.*, 2015; Liu *et al.*, 2016; Boscutti *et al.*, 2018).

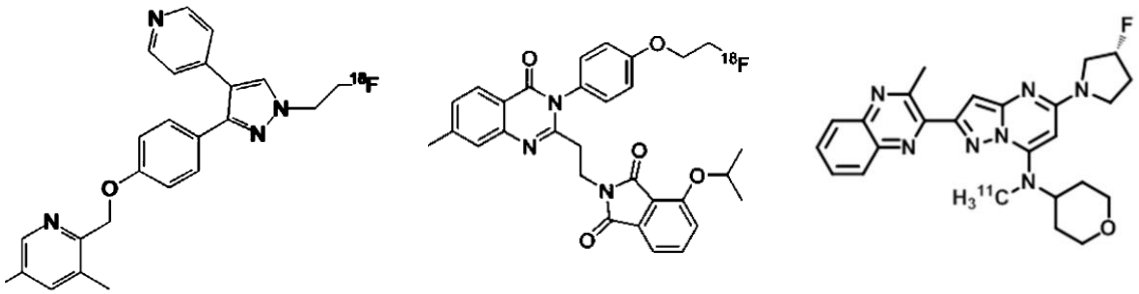

[^{18}F]JNJ42259152 **[^{18}F]MNI659** **[^{11}C]IMA107**

Figure 3. Chemical structure of potential PET ligand for in vivo imaging of PDE10A. *Adapted by Bosciutti et al. 2018 (Boscutti et al., 2018)*

For an ideal brain PET radiotracer, there are several generally required properties, including small molecular weight, appropriate lipophilicity, high binding affinity, good target selectivity, favourable *in vivo* kinetics and metabolism. The first attempts to develop a PDE10A PET tracer has been performed by Pfizer with the incorporation of [^{11}C] onto MP-10 (2-[(4-(1-methyl-4-pyridin-4-yl-1H-pyrazol-3-yl)phenoxymethyl]quinoline) (Tu *et al.*, 2011). [^{11}C]MP-10 showed a slow kinetic, high non-displaceable binding, and the potential to generate metabolites able to cross the blood-brain-barrier (Lin *et al.*, 2015). In parallel, [^{11}C]LuAE92686 (Kehler *et al.*, 2014) and [^{11}C]AMG7980 (Hwang *et al.*, 2014; Hu *et al.*, 2016) were developed but shared the same limitation of [^{11}C]MP-10, suggesting that both tracers are not ideal for quantification of PDE10A. A second attempt was done by Merck that developed [^{11}C]MK-8193, a PDE10A PET tracer derived from a high through put

screening hit. *In vitro* experiments showed that [^{11}C]MK-8193 binds to PDE10A catalytic core suggesting its potential role as PDE10A PET tracer (Cox *et al.*, 2015). PET studies with [^{11}C]MK-8193 were conducted in rats and rhesus monkeys showing that [^{11}C]MK-8193 has rapid kinetics, low test-retest variability, and a large specific signal that is displaced by a structurally multiple PDE10A inhibitors, enabling the determination of pharmacokinetic/enzyme occupancy relationships (Hostetler *et al.*, 2016). No studies have been performed with [^{11}C]MK-8193 in humans yet.

[^{18}F]JNJ42259152 provides a PDE10A-specific signal in the striatum with good pharmacokinetic properties, showing specific retention in the PDE10A-rich striatum, and fast wash-out, with a good contrast to non-specific binding, in other brain regions (Celen *et al.*, 2013). Pre-treatment in rats with the selective PDE10A inhibitor MP-10 showed that tracer binding was specific and reversible. Absence of specific binding in PDE10A knock-out (KO) mice further confirmed PDE10A specificity. *In vivo* radiometabolite analysis using high performance liquid chromatography showed presence of polar radiometabolites in rat plasma and brain. *In vivo* imaging in rat and monkey further showed faster brain kinetics, and high striatum-to cerebellum ratio for [^{18}F]JNJ42259152. The arterial input function corrected for radiometabolites was determined in rats and basic kinetic modeling was established. For a 60-min acquisition time interval, striatal binding potential of the intact tracer referenced to the cerebellum showed good correlation with corresponding binding potential values of a Simplified Reference Tissue Model and referenced Logan Plot, the latter using a population averaged reference tissue-to-plasma clearance rate and offering the possibility to generate representative parametric binding potential images (Celen *et al.*, 2013). [^{18}F]JNJ42259152 was tested in humans and kinetic modeling showed that PDE10A activity can be reliably quantified with a simplified tissue model using the frontal cortex as reference and a 60-min acquisition period (Van Laere *et al.*, 2013b). In a human dosimetry study, [^{18}F]JNJ42259152 was readily taken up by the brain and showed exclusive retention in the brain, especially in the striatum with good washout starting after 20 min. The tracer was cleared through both the hepatobiliary and the urinary routes. No

defluorination was observed. Organ absorbed doses were largest for the gallbladder (239 μSv/MBq) and upper large intestine (138 μSv/MBq). The mean effective dose was 24.9 ± 4.1 μSv/MBq. No adverse events were encountered. Therefore, the tracer has been considered suitable for further human studies (Van Laere *et al.*, 2013a). Thus, [^{18}F]JNJ42259152 PET imaging has been performed in five manifest Huntington's disease patients showing a reduction in the expression of PDE10A in the caudate and in the putamen, with no correlations with clinical scales (Ahmad *et al.*, 2014).

Recently, [^{11}C]TZ1964B and [^{18}F]MNI-659 have been also developed and showed high binding potency and good selectivity to PDE10A (Li *et al.*, 2013). Rat biodistribution and autoradiography studies revealed that [^{11}C]TZ1964B had high accumulation in the striatal region and rapid clearance from non-target brain regions (Fan *et al.*, 2014; Li *et al.*, 2015) while MNI659 has sub-nanomolar binding potency for PDE10A (0.097 nM) (Barret *et al.*, 2014). TZ1964B and MNI659 have similar lipophilicity and potent *in vitro* binding affinity for PDE10A, but the radiotracers differ in terms of *in vivo* kinetics. [^{11}C]TZ1964B has higher striatal retention, so it could provide better measurements for static scan acquisition, for steady-state analysis methods, or for displacement studies. [^{18}F]MNI659 shows higher initial tracer uptake, and could be preferred for short-term dynamic scans or for measurement of dissociation rates (Liu *et al.*, 2016). Considering its good properties as PDE10A PET tracer, [^{18}F]MNI659 has also been evaluated in healthy human brains, showing a regional brain uptake consistent with *post-mortem* PDE10A distribution: highest in striatal regions and lowest in cerebellum (Barret *et al.*, 2014). [^{18}F]MNI659 has been used in humans to examine the expression of PDE10A in relation with ageing. PDE10A showed a significant age-related decline that was larger compared to the age-related decline of volumes measured with MRI (Fazio *et al.*, 2017).

No studies have been performed in Parkinson's disease patients with [^{18}F]MNI659 PET imaging but interesting data have been generated in Huntington's disease. A decrease in striatal and pallidal [^{18}F]MNI659 binding was found in eight patients with early manifest Huntington's disease, with lower striatal [^{18}F]MNI659 binding associated with worse UHDRS motor scores, disease burden of

pathology and regional atrophy (Russell *et al.*, 2014). On follow-up scans, [^{18}F]MNI659 uptake declined in the putamen and caudate nucleus in all eight participants. The mean annualized rates of decline in signal in the caudate, putamen, and globus pallidus and the putamen were 16.6%, 6.9%, and 5.8%, respectively. In healthy controls, the annualized reduction in signal in striatal regions was less than 1%. Longitudinal data in this small cohort of participants with early Huntington's disease support [^{18}F]MNI659 PET imaging of PDE10 as a useful biomarker to track Huntington's disease disease progression (Russell *et al.*, 2016).

However, although [^{18}F]JNJ42259152 and [^{18}F]MNI659 are good PET ligand for the imaging of PDE10A in humans *in vivo*, they are [^{18}F]labeled tracers with the limitations associated with that. Because of their longer half-life, [^{18}F]labeled ligands offer significant advantages over [^{11}C]labeled ones, both in terms of the reduced radiation exposure to study participants and in the facilitation of multiple scanning sessions in the same individual on the same day. The ability to conduct multiple PET scans in the same day is critical in drug development when performing time–course occupancy studies required to evaluate the relationship between plasma and brain pharmacokinetics. In addition, [^{11}C]labeled ligands allow multiple daily syntheses on the same platform, providing optimization of imaging infrastructure. The first [^{11}C]labeled PDE10A radioligands developed for human studies is [^{11}C]IMA107, that was reported as having suitable tracer kinetics in pig, baboon, and human brain. [^{11}C]IMA107 showed a regional distribution of radioactivity in the human brain consistent with the distribution previously observed in the pig and baboons. The tracer kinetics were also reversible, indicating a good translation of the tracer behavior between all species studied. [^{11}C]IMA107 showed a good signal to noise, with suitably fast kinetics and consistent good kinetics model fits and can be quantified using a simplified reference tissue model with a 90-minutes acquisition (Plisson *et al.*, 2014b).

[^{11}C]IMA107 has also been tested previously in humans, in patients with Parkinson's disease. PDE10A expression was investigated in 24 moderate-advanced Parkinson's disease patients by using [^{11}C]IMA107 PET imaging (Niccolini *et al.*, 2015a). Parkinson's disease patients showed lower [^{11}C]IMA107 binding in the caudate, putamen and globus pallidus compared to healthy controls. Longer Parkinson's disease duration and higher Unified Parkinson's Disease Rating Scale part-III motor scores correlated with lower [^{11}C]IMA107 binding in the caudate, putamen, and globus pallidus. Higher Unified Dyskinesia Rating Scale scores in those Parkinson's disease with levodopa-induced dyskinesias correlated with lower [^{11}C]IMA107 binding in the caudate and putamen. This provides evidence for the role of PDE10A within the striatum in the development of cardinal motor symptoms in Parkinson's disease. Interestingly, a decline in PDE10A expression within the globus pallidus correlated with worse axial signs including the freezing of gait, falls and imbalance (Niccolini *et al.*, 2015a).

In summary, [^{11}C]IMA107 PET molecular imaging is able to measure loss of PDE10A expression, as shown in moderate to advanced levodopa-treated patients with Parkinson's disease (Niccolini *et al.*, 2015a), but is unknown whether PDE10A is implicated at the earlier stages of the disease and how its biomarker value compares with the gold standard DAT molecular imaging.

Using [^{11}C]IMA107 PET molecular imaging, we aimed to investigate the role of PDE10A in the early stages of the Parkinson's disease with the main hypothesis that a reduction of PDE10A expression is an early phenomenon in the course of Parkinson's disease, and that PDE10A expression decreases further as Parkinson's disease progress (in term of duration and clinical severity). By using [^{11}C]IMA107 PET imaging, we assessed *in vivo* the integrity of PDE10A enzyme in early *de novo* and in a population of early levodopa-treated patients with three-year longer Parkinson's disease duration in relation to a group of age- and sex-matched healthy controls. We also hypothesize that

PDE10A expression might be affected earlier on in the course of the disease, investigating the associations between PDE10A and non-motor symptoms considered pre-motor (sleep problems, autonomic dysfunction, mood disorders etc).

1.3.2 MRI

1.3.2.1 Structural MRI

MRI techniques do not rely on ionizing radiation, and thus, it is one of the features that characterize magnetic resonance procedures over SPECT and PET. However, the MRI alone is not able to characterize the brain at the molecular level. Over the last decade, there has been a large interest to combine more than one or two modalities into one imaging system able to morphologically and molecular address pathophysiologic questions.

1.3.2.1.1 Methodological consideration

Structural MRI may capture "macroscopic" changes associated with Parkinson's disease and is based on the ubiquitous presence of water in body tissues and the spin of the hydrogen atom proton, which works as a small magnetic dipole (Seppi and Poewe, 2010). A powerful, uniform, external magnetic field is employed to align the protons that are normally randomly oriented within the water nuclei of the tissue being examined. This alignment (or magnetization) is next perturbed or disrupted by introduction of an external Radio Frequency (RF) energy. The nuclei return to their resting alignment through various relaxation processes and in so doing emit RF energy. After a certain period following the initial RF, the emitted signals are measured. Fourier transformation is used to convert the frequency information contained in the signal from each location in the imaged plane to corresponding intensity levels, which are then displayed as shades of gray in a matrix arrangement of pixels. By varying the sequence of RF pulses applied & collected, different types of images are created. Repetition Time (TR) is the amount of time between successive pulse sequences applied to the same slice. Time to Echo (TE) is the time between the delivery of the RF pulse and the receipt of the echo signal (Brooks and Pavese, 2011). Tissue can be characterized by two different relaxation times – T1 and T2. T1 (longitudinal relaxation time) is the time constant which determines the rate at which excited protons return to equilibrium. It is a measure of the time taken for spinning protons to realign with the external magnetic field. T2 (transverse relaxation time) is the time constant which

determines the rate at which excited protons reach equilibrium or go out of phase with each other. It is a measure of the time taken for spinning protons to lose phase coherence among the nuclei spinning perpendicular to the main field.

T1-weighted sequences are produced by using short TE and TR times. The contrast and brightness of the image are predominately determined by T1 properties of tissue. Conversely, T2-weighted images are produced by using longer TE and TR times. In these images, the contrast and brightness are predominately determined by the T2 properties of tissue. In general, T1- and T2-weighted images can be easily differentiated by looking the CSF. CSF is dark on T1-weighted imaging and bright on T2-weighted imaging.

T2-weighted sequences are sensitive to tissue properties, including tissue damage, astroglial reaction, microglial proliferation and neurodegenerative processes, such as iron deposition. MRI visualizes non-heme iron in the brain, stored as ferritin, hemosiderin and neuromelanin, due to a selective shortening of the T2 relaxation time, thus leading to signal hypointensity on T2-weighted and minimal intensity change on T1 images (Seppi and Poewe, 2010). Standard T1-weighted sequences are important for anatomical details since present high grey/white matter contrast for cortex and basal ganglia structures, although the contrast is lower in other regions of interest in Parkinson's disease, such as the substantia nigra, subthalamic nucleus, globus pallidus and red nucleus. In fact, unlike the layered structure of the cortex, basal ganglia and thalamic nuclei are connected by complex and intertwined axonal tracts, below the resolution limits of conventional T1-weighted imaging ($\sim$ 1 mm), reducing contrast by partial volume averaging. In addition, the high iron content of the major midbrain nuclei (SNpc, red and subthalamic nuclei, pallidum and putamen) further shortens T1 (Helms *et al.,* 2008). These structures thus exhibit reduced contrast from white matter on conventional MRI sequences and are often misclassified by segmentation algorithms (Helms *et al.,* 2008).

Various attempts have been made to enhance the contrast of T1-weighted images. Firstly, by using an inversion pulse, a three-dimensional magnetization prepared rapid acquisition with gradient echo (MPRAGE) sequence has been obtained and quality image, as well as contrast, have been proved to be superior with this imaging compared to T1-weighted spin echo (SE) imaging. Subsequently, distinct Inversion Recovery Sequences were used which respectively suppress grey matter and white matter. The obtained ratio image depends only on T1 so that signal values could be recast in the form of a T1 map. A newer semi-automated segmentation analysis has also enabled to display the substantia nigra as an isolated structure, which allows for a more accurate assessment of the gross abnormalities. In particular, Segmented Inversion Recovery Ratio Imaging (SIRRIM), has shown a lateral-to-medial gradient for structural changes of the substantia nigra, consistent with neuronal loss pattern as know from *post-mortem* studies on Parkinson's disease. Lastly, Magnetization Transfer Imaging (MTI) relies on the transfer of energy between highly bound protons within structures such as myelin and cell membranes, and mobile protons in free water. The new contrast in MTI is induced by the application of radiofrequency pulses that selectively saturate the magnetization of rotationally immobilized macromolecules. This process leads in turn to a decrease of free water signal, probably as cross-relaxation or chemical exchange between mobile and bound protons increases. MT ratios, obtained by calculating the differences between signal intensity with and without MT, hence represent surrogate parameters for macromolecular density, which is clearly reduced in demyelinated lesions and neurodegeneration (Seppi and Poewe, 2010). However, MTI ratios are not absolute measures, as they show a residual dependence on T1 relaxation; thus, a semi-quantitative parameter, namely MT saturation, has been calculated to correct MT maps for confounding influences of proton density and T1 relaxation changes. As an additional benefit of MT maps, they resulted more suitable than T1-weighted images for automated segmentation, which enables automatic correction of inhomogeneities in the transmit and receive radio-frequency (B1) fields. By this method, more accurate anatomical delineation has been demonstrated for subcortical regions, including SNpc,

putamen, pallidum and thalamus, which are involved in the pathogenesis of many neurological diseases, such as Parkinson's disease and atypical parkinsonism (Helms *et al.*, 2008).

To improve the delineation of subcortical nuclei, an innovative approach defined Fast Grey Matter Acquisition T1 Inversion Recovery (FGATIR) has been implemented. The FGATIR provides significantly better high-resolution thin (1mm) slice visualization of substantia nigra globus pallidus internal and external than does either standard 3T T1 or T2-weighted imaging, with sharper delineation of these structures. This was achieved was achieved by using a shorter value of inversion time than the inversion time typically employed in the standard MPRAGE (400 in FGATIR *vs.* 900 msec in MPRAGE, which nulls the signal of Cerebrospinal Fluid (CSF)). Shortening of the TI resulted in nulling the signal of white matter while preserving most of the signal of grey matter and CSF (Sudhyadhom *et al.*, 2009). The FGATIR also revealed features not visible on other scan types: the internal lamina of the globus pallidus internal, fiber bundles from the internal capsule piercing the striatum, and the boundaries of the subthalamic nuclei (Tanner *et al.*, 2012).

1.3.2.1.2 Structural MRI in Parkinson's disease

Standard MRI is normal in early Parkinson's disease but brain atrophy, mainly in the prefrontal cortex, is sometimes evident in the advanced stages (Hotter *et al.*, 2009). At 1.5T, T2-weighted sequences may also show abnormalities of the substantia nigra, including a signal increase on images or smudging of the hypointensity toward the red nucleus in both patients with advanced Parkinson's disease and atypical parkinsonism (Seppi and Poewe, 2010) . Still, visual assessment of conventional MRI takes a leading role at first clinical presentation, as it can address neurologists in the differential diagnosis. In fact, it can help either in excluding pathologies such as vascular lesions, brain tumours, multiple sclerosis and normal pressure hydrocephalus, as possible secondary causes of parkinsonism, or in pointing toward neurological disorders other than Parkinson's disease, if characteristic abnormalities of atypical parkinsonism are seen. To date, several findings suggestive of MSA have been described at 1.5T, including pontine atrophy, "hot cross bun" sign of the pons, visible on axial T2-weighted images, atrophy of the cerebellum and hyperintensity in the middle cerebellar peduncle. While putaminal atrophy also appears to discriminate MSA from Parkinson's disease, T2-putaminal hypointensity, and a putaminal hyperintense rim may also occur in Parkinson's disease, possibly the latter sign being a nonspecific, normal finding (Seppi and Poewe, 2010). Specific MRI findings associated with PSP comprise midbrain atrophy with enlargement of the third ventricle and tegmental atrophy, signal increase in the midbrain and in the inferior olives, as well as frontotemporal lobe atrophy. A specific indirect sign of midbrain atrophy is the "penguin silhouette" or "hummingbird sign", with the midbrain tegmentum and the pons respectively resembling the bird's head and body on midsagittal T1-weighted images (Seppi and Poewe, 2010). Lastly, in patients with CBD, structural MRI tends to show cortical, especially frontoparietal, atrophy, which tends to be asymmetric and contralateral to clinical symptoms. Other specific T2-weighted imaging abnormalities have been suggested, but none of them seems to be of diagnostic relevance for CBD. Overall, specificity of structural MRI for identifying different atypical Parkinsonism is inefficient, but visual assessment of

conventional T1 and T2-weighted sequences has been proved able in discriminating atypical parkinsonism from Parkinson's disease and controls with good accuracy (Seppi and Poewe, 2010).

The growing interest in finding simple measures of regional brain atrophy to help the differential diagnosis of neurological disorders has led to the development of various MRI semi-automatic segmentation techniques based on a Region of Interest (ROI) approach. More recently, interest for Voxel-Based Morphometry (VBM) is spreading due to its potential use for detecting cerebral volume loss in an automated and operator-independent manner, contrary to previous methods (Seppi and Poewe, 2010). VBM involves spatially normalizing all the subjects' brain data to an equal stereotactic space, which is achieved by co-registering each of the T1-weighted MPRAGE sequences with the same template image. A segmentation into grey matter, white matter, CSF and other nonbrain partitions is performed afterward for all the spatially normalized images, using a mixture model cluster analysis technique. In the last step of VBM, the grey matter images are smoothed by convolving with an isotropic Gaussian kernel. This makes the subsequent voxel-by-voxel statistical analysis comparable to an ROI approach, because each voxel in the smoothed images contains the mean concentration of grey matter from around the voxel. Corrections for multiple comparisons are made using the theory of Gaussian random fields (Ashburner and Friston, 2000). Whereas most of the ROI-based MRI studies were not able to detect any volume difference between Parkinson's disease patients and controls, several VBM studies have revealed grey matter loss of frontal cortical areas, including motor areas, especially in advanced Parkinson's disease (Seppi and Poewe, 2010). In patients with MSA compared to those with Parkinson's disease, VBM showed a typical atrophy progression pattern for the first group, with early degeneration of the basal ganglia, including striatum, followed by increasing atrophy in the cortical areas and cerebellar hemispheres. Grey matter loss in frontotemporal cortex has been confirmed for patients with PSP by applying VBM. Of note, a further VBM-based MRI study achieved high specificity and sensitivity in discriminating "PSP" from "non-PSP" (i.e. patients with Parkinson's disease and controls), based on the presence of grey and

white matter loss in the subthalamic nucleus, midbrain and cerebral peduncles (Price *et al.*, 2004). Lastly, from the comparison between patients with PSP and CBD, midbrain structures were more atrophied in the first, while dorsal frontal and parietal cortices were more affected in the latter (Seppi and Poewe, 2010).

Another approach to evaluating brain atrophy is the quantification of cortical thickness, with automated software such as FreeSurfer. However, past studies have yielded inconsistent results regarding the presence of cortical thinning at various stages of Parkinson's disease. In cognitively normal and early Parkinson's disease subjects, past studies have reported minimal or no evidence suggesting cortical thinning (Jubault *et al.*, 2011; Pagonabarraga *et al.*, 2013; Zarei *et al.*, 2013; Segura *et al.*, 2014). One small study of 16 Parkinson's disease and 15 control subjects, however, did report fast rates of cortical thinning in early Parkinson's disease, but still no differences in cortical thickness between Parkinson's disease and control subjects (Ibarretxe-Bilbao *et al.*, 2012). There is more substantial evidence, however, to suggest that lower cortical thickness may be related to cognitive decline or impairment (Hwang *et al.*, 2013; Pagonabarraga *et al.*, 2013; Zarei *et al.*, 2013; Pereira *et al.*, 2014; Segura *et al.*, 2014; Zhang *et al.*, 2015), worsening motor scores (Lyoo *et al.*, 2011; Hwang *et al.*, 2013), and visual hallucinations in Parkinson's disease (Hwang *et al.*, 2013).

1.3.2.2 Diffusion Tensor Imaging (DTI) MRI

1.3.2.2.1 Methodological consideration

Measuring the translational displacement of water molecules in response to an applied magnetic field is another way to evaluate brain structural anatomy at a microstructural level. This diffusion-based imaging method, namely diffusion tensor imaging (DTI), is hence capable to detect changes in white matter (Tessitore *et al.*, 2016). Several parameters are used in DTI, the most common of which are fractional anisotropy (FA) and mean diffusivity (MD). FA is related to the directionality of water molecules' motion that is restricted by the normal architecture of glial tissue and fiber tracts. Indeed, rapidity of diffusion was found to be greater longitudinal to the axons than perpendicular to them and FA can be calculated from the difference between these two motions (Tessitore *et al.*, 2016). As opposite to FA, MD depends on the overall movement of water molecules and thus it is more sensitive to tissue density than to its organization (Tessitore *et al.*, 2016). This index is quantified by applying diffusion-sensitizing gradients of different degrees in three orthogonal directions and thus calculating the apparent diffusion coefficient (ADC) for each direction. Since ADC is dependent on the orientation of the gradients applied, diffusion in each direction is averaged, obtaining the averaged ADC (ADCave), also called MD. Both FA and MD can provide insight into myelin and axon integrity, and therefore their alteration (i.e. decreased FA and increased MD) can be observed in neurodegenerative diseases, due to neuronal loss and gliosis disrupting nervous system architecture (Seppi and Poewe, 2010; Tessitore *et al.*, 2016) . Apart from quantification of MD and FA, axial diffusivity (ADi) and radial diffusivity (RD), referring to the main directions of diffusion, longitudinal and perpendicular to the axon, have also shown high specificity to underlying axonal and myelin alterations. Because DTI is sensitive to a broad spectrum of microscopic changes in brain tissue, an interpretation of its parameters variations in terms of underlying microstructural origins is not always easy. In general, however, an increased in RD has been associated with myelin damage and demyelination whereas an increase in ADi is thought to primarily indicate axonal deterioration and

neuronal loss. Tensor-derived measures can be extracted either locally in predefined regions using an ROI-based analytic approach or globally into the brain using VBM (Tessitore *et al.*, 2016).

MRI tractography is not a distinct imaging method, but a method of analyzing diffusion data. In particular, Tract-based spatial statistic (TBSS) is an example of automated voxel-based analysis at a microstructural level to assess connections between brain structures and to derive indices of connectivity that can be used to compare groups. For each seed voxel within a connectivity distribution territory, an index of voxel connectivity is calculated using probabilistic tractography. This connectivity index represents the probability of this voxel being connected to target voxels in other regions and is defined as the number of the most probable fibers at each voxel. Further resampling of the tract fibers data into volumetric data with a voxel size smaller than the original diffusion-weighted scan has allowed developing a new method to explore connectivity, referred to as "super-resolution" track-weighted imaging. Indeed, one limitation of MRI tractography within the framework of DTI is related to the intricate and complex nervous system architecture, such that each small region may contain multiple fiber orientations and fiber crossings. To resolve the consequent heterogeneity of intravoxel diffusion signal, DT model-free methods have also been suggested, such as diffusion spectrum imaging (DSI). DSI is a 6D imaging technique that has the capacity to unravel structural information from brain tissue architecture by measuring its diffusion density spectra estimator and without the need for *a priori* information or *ad hoc* models.

1.3.2.2.2 DTI in Parkinson's disease

Divergent and sometimes conflicting DTI results have been published on Parkinson's disease to date (Tessitore *et al.*, 2016). An ROI-based DTI study on early *de novo* Parkinson's disease patients has revealed that reduction of FA in the caudal region of the substantia nigra can distinguish between Parkinson's disease patients and healthy controls with a reported 100% sensitivity and specificity (Vaillancourt *et al.*, 2009). More recently, TBSS and diffusion connectometry in newly diagnosed, untreated Parkinson's disease patients showed greater FA and decreased MD and RD in callosal

projection and association fibers than controls. Accordingly, motor severity (assessed with UPDRS-III score) was inversely correlated with FA and positively associated with MD and RD in Parkinson's disease patients. Since the alterations of DTI indexes only exhibited in the group of Parkinson's disease patients with Hoehn & Yahr (H&Y) stage 1, the increase of FA together with the decrease of MD and RD may suggest neural compensations for the loss of dopaminergic input from the substantia nigra in the very early disease stage. Using an ROI-based approach, a reduction in nigral FA was correlated with the clinical severity in middle-stage Parkinson's disease patients (Atkinson-Clement *et al.*, 2017). However, in a recent meta-analysis on Parkinson's disease-related nigral DTI changes at 3T, no changes in FA values were shown, with either an ROI- or voxel-based approach, questioning the stability and validity of this measure as a Parkinson's disease biomarker (Atkinson-Clement *et al.*, 2017). On the other hand, at ROI-analysis was found a regional MD increase in the substantia nigra of Parkinson's disease patients compared to healthy controls, but no significant difference in any areas using a voxel-based approach (Atkinson-Clement *et al.*, 2017). Higher regional MD in the putamen and reduced regional FA in the motor, premotor and supplementary motor cortex have also been reported, consistent with widespread microstructural degradation primarily involving the movement control circuit in Parkinson's disease (Atkinson-Clement *et al.*, 2017). Interestingly, increased FA within the postcentral gyrus at the level of somatosensory cortex was positively correlated with UPDRS-III score in Parkinson's disease patient, reflecting a potential compensatory mechanism in response to disease-related motor deficits (Atkinson-Clement *et al.*, 2017). Lastly, the involvement of the olfactory system is well known in Parkinson's disease, with olfactory dysfunction being present even in the earliest stages, before the onset of overt motor symptoms. Several studies have accordingly reported decreased FA and increased MD values in the olfactory tract in early Parkinson's disease (Tessitore *et al.*, 2016) and, remarkably, also a significant correlation between University of Pennsylvania Smell Identification Test (UPSIT) scores and FA of white matter adjacent

to primarily olfactory cortex and right gyrus rectus also detected in one study (Ibarretxe-Bilbao *et al.*, 2010).

Whereas at baseline Parkinson's disease patients did not consistently differ from controls with regards to diffusion measures, as the disease progresses a significant decrease of nigral FA and an increase of nigral MD become apparent, both in comparison with the controls and longitudinally (Parkinson's disease baseline *vs.* Parkinson's disease follow-up) (Loane *et al.*, 2016). DTI reports of striatal diffusion over time in Parkinson's disease are not concordant (Loane *et al.*, 2016), although, according to Braak's staging of Parkinson's disease, the loss of dopamine neurons in the substantia nigra and the midbrain further leads to a degeneration of the nigrostriatal and basal ganglia-thalamocortical pathways, potentially suggesting a relationship of cause-effect. At later disease stages IV to VI, Lewy Body pathology affects the thalamus and progress to mesocortex and neocortices (Zhang *et al.*, 2016). In keeping with this neuropathological hypothesis on Parkinson's disease progression, Zhang et al. indeed found the highest rates of diffusion measures changes involving the substantia nigra and the thalamus. In line with this hypothesis, reduced FA and increased diffusivity (MD, ADi, and RD) in the substantia nigra respectively correlated with increasing putaminal DAT deficiency and declining CSF alpha-synuclein and total tau, whereas increased diffusivity in the thalamus correlated with a progressive decline in global cognition (Zhang *et al.*, 2016). These findings overall demonstrate that nigral DTI alteration is a valuable biomarker of Parkinson's disease progression and that microstructural DTI changes in the thalamus might be an indicator of a cognitive decline in Parkinson's disease (Zhang *et al.*, 2016). Other studies have been conducted to investigate the relationship between DTI changes and cognitive impairment in Parkinson's disease and to identify those white matter alterations, which may predict the development of Parkinson's disease dementia. A recent study from our team has demonstrated that structural and DTI microstructural changes in the nucleus basalis of Meynert are associated with and predictive of cognitive impairment in Parkinson's disease. Cross-sectional analysis revealed that in patients with Parkinson's disease,

cognitive impairment was associated with reduced grey matter volume and increased MD in the nucleus basalis of Meynert. A longitudinal analysis of MRI data, collected over 36 months from patients with Parkinson's disease who were cognitively healthy at baseline, showed that changes in the nucleus basalis of Meynert predicted cognitive decline (Schulz *et al.*, 2018).

In another DTI study, reduced FA values in bilateral parietal white matter significantly showed a correlation with MMSE scores in patients with MCI-Parkinson's disease, Parkinson's disease dementia and dementia with Lewy bodies (DLB), but not in patients who were cognitively normal. Patients with Parkinson's disease dementia and DLB also exhibited diffuse grey matter atrophy on T1-weighted MRI scans. Besides diffusion and structural data, the functional status of the cortex was evaluated by using SPECT, which revealed occipital and posterior parietal hypoperfusion in all patients' groups. Taken together, current results suggest that cognitive impairment in Parkinson's disease progresses with a functional alteration (hypoperfusion) followed by a structural alteration in which white matter damage precedes grey matter atrophy (Hattori *et al.*, 2012).

In summary, DTI imaging can be used to measure microstructural changes in the brain of patients with Parkinson's disease. These changes might be related to the reduction of PDE10A and we tested this hypothesis in our project 3.

1.3.2.3 Neuromelanin-MRI

1.3.2.3.1 Methodological consideration

Neuromelanin has paramagnetic properties resulting in a high signal on specific T1-weighted MRI, which allows its *in vivo* visualization. A magnetic resonance field at 3T has succeeded in enhancing neuromelanin-generated contrast thanks to the higher signal-to-noise ratio and prolonged T1 relaxation time of brain tissue. Moreover, multi-slice 2D fast spin-echo sequence, using refocusing pulses, induces off-resonance magnetization transfer (MT) effects, which also suppress the background brain noise. This is of critical importance to increase contrast in NM-sensitive sequences since MT effect is reduced in neuromelanin (Nakane *et al.*, 2008). Also, of relevance to detect substantia nigra and locus coeruleus signal is slice positioning: acquisition must be oriented perpendicular to the fourth ventricle floor, covering from the posterior commissure to the inferior border of the pons. Different post-processing methods have subsequently been used in several studies, to analyze the so obtained images. These extend from simple visual inspection and width measurements of the substantia nigra and locus coeruleus areas to the manual tracing of ROI- or semi-automated analysis of high-intensity areas (Reimao *et al.*, 2016).

1.3.2.3.2 Neuromelanin-MRI in Parkinson's disease

Neuromelanin is a substance related to skin melanin and originates from dopamine and noradrenaline metabolism. Projecting neurons from the dopaminergic SNpc and noradrenergic locus coeruleus contain neuromelanin depositions, a dark-colored pigment that gives the characteristic color to these areas. Neuronal loss is associated with a depigmentation of these areas, which represents the principal pathological feature of Parkinson's disease (Reimao *et al.*, 2016). Alpha-synuclein accumulation in Lewy bodies, the other key pathological component of Parkinson's disease, has a role in the regulation of the levels of neuromelanin with changes of its function (Reimao *et al.*, 2016). Initially, alpha-synuclein accumulation causes a compensatory activation of the tyrosine hydroxylase enzyme, which results in an increased cytosolic retention of dopamine, with a reduction of dopamine release in

dopaminergic neurons. Subsequently, this process induces an inhibition of tyrosinase, leading to a decrease of neuromelanin synthesis, mitochondrial damage and cell death (Reimao *et al.*, 2016). The association of alpha-synuclein neurotoxicity with neuromelanin concentration changes needs further research to be confirmed, but the finding of an increased incidence of melanoma in Parkinson's disease patients, in agreement with alpha-synuclein-induced melanin reduction, has been described in several studies (Reimao *et al.*, 2016). Furthermore, subjects with a family history of melanoma also have more than a double risk of developing Parkinson's disease, indicating an increased vulnerability to the disease, associated with reduced skin melanin concentration. Notably, the well-documented phenomenon of smoker's melanosis seems to be a protective factor for Parkinson's disease, thus supporting a negative association between higher skin melanin concentration and Parkinson's disease (Reimao *et al.*, 2016).

A loss of neuromelanin-containing neurons is expected to be detected by these specific MRI-sensitive sequences even in preclinical stages since a substantial part of dopaminergic neurons of the substantia nigra is generally already lost when clinical symptoms become apparent (Reimao *et al.*, 2015). One study found that measurements on these sequences, such as the area and the maximal length of the substantia nigra T1 high signal region, were reduced in the *de novo* Parkinson's disease patients compared with healthy controls. Moreover, the difference was statistically significant with both measurements, as they were able to separate the two groups with high sensitivity and specificity (Reimao *et al.*, 2015). This finding is consistent with previous results from transcranial sonography studies in Parkinson's disease, according to which reduced ultrasound signal, reflecting neuromelanin decrease, does not seem to correlate with disease duration, progression and clinical severity (Reimao *et al.*, 2015). Conversely, Miyoshi and colleagues demonstrated on the base of a visual assessment of NM-MRI that neuromelanin reduction gradually and stage-dependently extends from lateral to medial SNpc, which corresponds to the pathological lesions as demonstrated on autopsied brains (Miyoshi *et al.*, 2013). In addition, they identified a more intense NM-MRI signal reduction in the

locus coeruleus of patients with late Parkinson's disease, suggesting relative spare of noradrenergic neurons in the early stage as a potential compensatory mechanism for the substantia nigra dopaminergic neuronal loss (Miyoshi *et al.,* 2013). In another very recent study, NM-MRI measures of the substantia nigra volume and contrast-to-noise ratio correlated significantly with dopaminergic striatal innervation loss as measured by SPECT and, notably, both findings also correlated with the severity of Parkinson's disease-related motor signs, as defined on the base of the UPDRS score (Isaias *et al.,* 2016).

Only a few studies have been conducted using NM-MRI for the differential diagnosis of Parkinson's disease and atypical Parkinsonism. A recent one found signal attenuation in the SNpc but less severe attenuation in the locus coeruleus in patients with MSA, and no apparent signal changes in patients with PSP, when compared with healthy controls (Ohtsuka *et al.*, 2014). NM-MRI was also used to study rapid eye movement sleep behavior in Parkinson's disease. The authors reported reduced signal intensity in the locus coeruleus/subcoeruleus complex of these patients compared to patients without these movements (Garcia-Lorenzo *et al.*, 2013). A more recent study confirmed that this complex is affected in idiopathic rapid eye movement sleep behavior to the same degree as it is affected in Parkinson's disease, thus suggesting NM-MRI as an early biomarker of non-dopaminergic alpha-synucleinopathy (Ehrminger *et al.*, 2016). Finally, NM-MRI did not show the same substantia nigra signal attenuation in patients with ET, with respect to tremor-dominant Parkinson's disease patients, presenting itself as an important early diagnostic tool for Parkinson's disease (Reimao *et al.*, 2015).

In the present days, part of the research also aims to investigate the relation between neuromelanin reduction and increasing iron content in the substantia nigra of Parkinson's disease patients. Some researchers believe that a localized higher iron level is caused by the iron-chelated extracellular neuromelanin, which is released from dead neurons injured by alpha-synuclein aggregation, as mentioned above. Conversely, according to others, iron level increases primarily, and then extracellular neuromelanin, as a compensatory mechanism to chelate the excess iron (Reimao *et al.*,

2016). In fact, it is known by *post-mortem* studies that the amount of substantia nigra and locus coeruleus iron, normally sequestered in NM granules (20% bonded to neuromelanin in its ferric form and the remainder stored as ferritin and hemosiderin), progressively increases in Parkinson's disease (Reimao *et al.*, 2016). Neuromelanin exhibits paramagnetic properties when bound to iron that results in the acceleration of T1 relaxation and thus its bond with iron enhances neuromelanin-related contrast on NM-sensitive MRI sequences (Reimao *et al.*, 2015). However, early loss of nigral neurons in Parkinson's disease results in a general decrease in the number of NM granules, with iron being less bound to neuromelanin and with a possible increase of the proportion of iron stored as ferritin, hemosiderin and in Lewy Bodies (Reimao *et al.*, 2016). This might explain the observed lack of correlation between the substantia nigra NM-MRI signal reduction and substantia nigra iron content, as detected with T2* relaxometry in a group of early-stage Parkinson's disease patients. Indeed, while as expected substantia nigra neuromelanin was significantly decreased in patients compared to controls, substantia nigra T2* values of controls tended to be higher than those of the patients for all the examined substantia nigra segments (Reimao *et al.*, 2016). Other explanations for this finding might relate either to the still unclear pathophysiology of substantia nigra neurodegeneration, with neuromelanin loss and iron accumulation possibly being two independent pathological processes, or to methodology limitations.

1.3.2.4 SWI-MRI

1.3.2.4.1 Methodological consideration

Susceptibility-weighted imaging (SWI) exploits the different response i.e. susceptibility of tissues when placed in a high-intensity magnetic field, such as 3T and 7T, to develop an enhanced contrast MRI image. To this aim, a gradient-recalled echo sequence with a relatively long echo time is applied. This allows the multiplication of magnetic susceptibility information, recorded several times in the so filtered phase image, to the structure of the brain, described by a T2-weighted magnitude image. Inhomogeneity of local magnetic field and subsequent image phase variations are influenced by the macroscopic or geometric effect, which reflects the configuration of tissues, and by the microscopic effect, that depends on substance-specific magnetic characteristics. For instance, grey matter and deep brain nuclei are generally classified as paramagnetic, because of the high iron content, while white matter is diamagnetic, because of the myelin. As the mechanism of SWI, the signal intensity is increased when diamagnetic substances accumulate, and, at the opposite, it is reduced in the presence of brain high content of paramagnetic substances, such as iron (Wang *et al.*, 2016).

Recently, a new sophisticated post-processing technique, referred to as quantitative susceptibility mapping (QSM), has been developed to solve the SWI ill-posed inverse effect-to-source problem, considering the magnetic susceptibility as an intrinsic property of the tissue. In other words, by this method it is possible to quantify, rather than visualize, the iron content of specific cerebral areas by measuring the local magnitude susceptibility directly, obtaining values which are isotropic. Thus, QSM potentially address the limitations of SWI, such as magnetic field perturbation being non-local, i.e. affected by the surrounding areas, and anisotropic, i.e. depending on its orientation with respect to the main magnetic field (Schweser *et al.*, 2011). In addition, QSM can overcome another big limit of SWI, which is the difficulty to distinguish iron paramagnetic susceptibility from calcium diamagnetic susceptibility, due to the convoluting effect of the dipole fields. This is of major

importance since it allows avoiding confounders between brain calcifications and iron deposition (Liu *et al.*, 2015).

Several studies have been conducted to compare QSM with T2* relaxometry and its inverse R2*, previously considered the gold standard for the evaluation of the iron content in the brain. According to a recent publication, QSM measurements have high reproducibility in the basal ganglia of healthy controls and can be used as a replacement of R2* imaging in iron-rich cerebral regions (Santin *et al.*, 2017). Another study concludes that QSM is the most sensitive quantitative technique for detecting an increase of iron in the brain of patients with Parkinson's disease. Notably, the findings suggest that the phase contrast can be influenced by diamagnetic myelin. In effect, myelin correction significantly improved the linear dependence between magnetic susceptibilities and published iron values from *post-mortem* studies. Moreover, in agreement with most of the literature (Wang *et al.*, 2016), the highest significant difference with healthy controls was found in the SNpc, using the QSM method (Barbosa *et al.*, 2015).

1.3.2.4.2 SWI-MRI in Parkinson's disease

To date brain iron accumulation has been proved to be associated with the pathogenesis of Parkinson's disease in both pathological and MRI studies, comparing patients with healthy controls (Wang *et al.*, 2016). Furthermore, iron levels are uneven in different cerebral regions even in the same patient, with the substantia nigra being the most relevant area for iron deposition, according to a large body of evidence (Wang *et al.*, 2016). The specific reason for this localized phenomenon is still unclear, but iron metabolism dysregulation may relate with various aspects of Parkinson's disease pathology, such as inflammation state with permeability changes of the blood-brain barrier (BBB), or with other acquired and genetic factors affecting iron storage and transport protein function. To date, however, it is still debatable whether the defect in iron metabolism is a cause, a consequence or just an epiphenomenon of neurodegeneration. Notably, in Parkinson's disease there is not only an increase of free non-hemin iron, the iron form believed to be involved in normal aging and

neurodegenerative parkinsonism, but also in the ratio ferric state (Fe3+) / ferrous state (Fe2+). This is in line with Parkinson's disease pathology as in Fenton reaction iron in the Fe2+ is oxidized to the Fe3+, the latter highly correlating with the aggregation of alpha-synuclein (Wang *et al.*, 2016). In addition, the result of the reaction hydrogen peroxide H_2O_2 might damage proteins, nucleic acids and cell membranes by producing high-toxic free radicals, eventually leading to substantia nigra cells death (Zhang *et al.*, 2010; Chen *et al.*, 2012).

Regarding the other basal ganglia, there are contradictions between a possible iron content increase or decrease (Rossi *et al.*, 2014). To systematically explore different brain regions, a structure by structure analysis was made on Parkinson's disease patients, comparing local iron levels obtained by SWI, R2* and *post-mortem* studies. From the results of this meta-analysis, it appears that both R2* and SWI do not completely match the *post-mortem* observations. Iron accumulation is detected by SWI in the globus pallidus and caudate, but these findings are inconsistent with both R2* and *post-mortem* values. Such iron overload is also suggested by the current study in the putamen (by *post-mortem* and SWI, but not R2*) and red nucleus (by R2* and SWI; no data by *post-mortem*) (Wang *et al.*, 2016).

More recently, using QSM method, Guan et al. have reported a regionally progressive brain iron accumulation as the disease advances. According to this distinct progression pattern, iron deposit spreads from the SNpc, already affected in the early stages of the disease, to the substantia nigra reticulata, red nucleus and globus pallidus, especially in the internal segment, in the latter. Thus, this finding could explain the discrepancy between confirmed *post-mortem* neuropathology and MRI techniques, as well as provide preliminary evidence of the iron-related progression in Parkinson's disease (Wang *et al.*, 2016). A previous 2-year follow up study was also conducted, using both SWI and R2*, with the aim of evaluating a correlation of iron level progressive variation with Parkinson's disease duration and clinical evolution. The data indicate a slight grow of putative iron content over time in the medial part of the substantia nigra, anterior globus pallidus, and caudate nucleus. The rate

of this increase, however, was not predictable knowing the Parkinson's disease duration, while it seems to correlate with individual characteristics, such as age at disease onset or cognitive decline (Rossi *et al.*, 2014). This is in line with previous literature, according to which no reliable correlation exists between an increase in brain iron concentration and Parkinson's disease duration, the first reflecting instead clinical parameters, such as UPDRS motor scores (Zhang *et al.*, 2010). Nevertheless, one study found greater iron accumulation, as indicated by both R2* and SWI values, to correlate with longer disease duration, even accounting for age, and regardless of disease severity or dopaminergic drugs use (Isaias *et al.*, 2016).

Still, little research has been conducted about the application of QSM for the differential diagnosis of Parkinsonism. By SWI, the high iron level of the putamen is likely the most reliable biomarker for the differential diagnosis of Parkinson's disease and atypical Parkinsonism, since a different deposition pattern in this area has also been confirmed by autopsy (Wang *et al.*, 2016). In particular, sub-dividing the putamen into 4 regions (lower inner, lower outer, upper inner, upper outer), the lower inner part performed the best to distinguish MSA from Parkinson's disease (Wang *et al.*, 2012), while the lower outer part was more valuable in differentiating MSA from PSP, being in the latter an overall iron deposit in the putamen the predominant feature. In addition, Han et al. proved that hypointensity SWI signals in the globus pallidus and thalamus are the most accurate biomarkers to distinguish atypical Parkinsonism from Parkinson's disease, as the neuronal loss in these regions is spared in the latter, according to neuropathological studies (Wang *et al.*, 2016).

In summary, NM and SWI imaging can be used to measure neuromelanin density and iron deposition in the brain of patients with Parkinson's disease. These changes might be related to the reduction of PDE10A and we tested this hypothesis in our project 3.

1.4 Hypothesis and Aims

The overarching aim of these studies is to investigate the role of PDE10A in the early stages of the Parkinson's disease with the main hypothesis that a reduction of PDE10A expression is an early phenomenon in the course of Parkinson's disease, and that PDE10A expression decreases further as Parkinson's disease progress (in term of duration and clinical severity). We have investigated this in the Project 1, in which, by using [^{11}C]IMA107 PET imaging, we assessed *in vivo* the integrity of PDE10A enzyme in early *de novo* and early levodopa-treated patients with Parkinson's disease compared to age- and sex-matched healthy control subjects.

We aim to test this hypothesis comparing the expression of PDE10A (measured by using [^{11}C]IMA107 PET imaging) in early *de novo* and early levodopa-treated patients with Parkinson's disease versus age- and sex-matched healthy control subjects (*Project 1 Aim*).

We also hypothesize that PDE10A expression might be affected earlier on in the course of the disease investigating the associations between PDE10A and non-motor symptoms considered pre-motor (sleep problems, autonomic dysfunction, mood disorders etc). We aim to test this hypothesis checking for correlations between the expression of PDE10A and non-motor symptoms considered pre-motor (sleep problems, autonomic dysfunction, mood disorders etc).

We also hypothesize that PDE10A expression was correlated with dopaminergic pathology, which can be measured either with PET or SPECT. We have investigated this in the Project 2, in which we compared the expression of PDE10A, measured with [^{11}C]IMA107 PET imaging, with the best known molecular markers of dopaminergic dysfunction in Parkinson's patients, the [^{11}C]PE2I PET imaging, and the clinical validated [^{123}I]FP-CIT SPECT imaging. We aim to test this hypothesis checking for correlations between the expression of PDE10A and the expression of dopamine transporters (measured by using [^{11}C]PE2I PET and [^{123}I]FP-CIT SPECT molecular imaging) (*Project 2 Aim*). In this Project, we also compared [^{11}C]PE2I PET versus [^{123}I]FP-CIT SPECT

because the two tracers have a different affinity for the DAT ([^{11}C]PE2I is more specific of DAT where [^{123}I]FP-CIT binds both DAT and SERT). This would give us a greater understanding of the relationship between PDE10A expression and dopaminergic and non-dopaminergic pathology.

We also hypothesize that PDE10A expression was correlated with other markers of Parkinson's disease pathology, such as iron depositions, neuromelanin loss, and changes in structural and microstructural changes in the substantia nigra and in the striatum. We have investigated this in the Project 3, in which we compared the expression of PDE10A, measured with [^{11}C]IMA107 PET imaging, with MRI markers of Parkinson's pathology such as iron depositions (assessed with susceptibility-weighted MR imaging), neuromelanin loss (assessed with neuromelanin sensitive MR imaging) and changes in structural volumetric (assessed with T1 MR imaging) and microstructural connectivity (assessed with diffusion tensor MR imaging). We aim to test this hypothesis checking for correlations between the expression of PDE10A and MRI markers of Parkinson's pathology such as iron depositions (assessed with susceptibility-weighted MR imaging), neuromelanin loss (assessed with neuromelanin sensitive MR imaging) and changes in structural volumetric (assessed with T1 MR imaging) and microstructural connectivity (assessed with diffusion tensor MR imaging) (*Project 3 Aim*).

Chapter 2. Methods

This chapter introduces the thesis methods and provides a detailed description of the study planned, the population included in the studies, the clinical and imaging methods and the statistical analyses used in this thesis. The population included in this thesis is composed of early idiopathic Parkinson's disease patients and healthy controls. The clinical assessments performed on these subjects involved evaluation of motor and non-motor symptoms, and neuropsychological batteries. The imaging methods used in this thesis are MRI, SPECT and PET imaging. PET imaging with [^{11}C]IMA107 was used to assess *in vivo* the integrity of PDE10A enzyme in the Project 1, 2 and 3. PET imaging with [^{11}C]PE2I and SPECT imaging with [^{123}I]FP-CIT were used to assess *in vivo* the integrity of DAT in the Project 2. 3T MRI imaging was used in the Project 3 to assess *in vivo* markers of Parkinson's disease pathology such as changes in structural volumetric (assessed with Freesurfer MRI) and microstructural volumetric and connectivity (assessed with DTI MRI), neuromelanin loss (assessed with NM MRI) and iron depositions (assessed with SWI MRI).

2.1 Study planned

We aimed to investigate the role of PDE10A in the early stages of the Parkinson's disease with the main hypothesis that a reduction of PDE10A expression is an early phenomenon in the course of Parkinson's disease, and that PDE10A expression decreases further as Parkinson's disease progress (in term of duration and clinical severity).

In the Project 1, we used [^{11}C]IMA107 PET imaging to assess *in vivo* the integrity of PDE10A enzyme in early *de novo* and early levodopa-treated patients with Parkinson's disease compared to age- and sex-matched healthy control subjects. We also investigated the associations between PDE10A and non-motor symptoms considered pre-motor (sleep problems, autonomic dysfunction, mood disorders etc).

In the Project 2, we compared the expression of PDE10A, measured with [^{11}C]IMA107 PET imaging, with the best known molecular markers of dopaminergic dysfunction in Parkinson's patients, the [^{11}C]PE2I PET imaging, and the clinical validated [^{123}I]FP-CIT SPECT imaging in early *de novo* and early levodopa-treated patients with Parkinson's disease compared to age- and sex-matched healthy control subjects. In this Project, we also compared [^{11}C]PE2I PET versus [^{123}I]FP-CIT SPECT because the two tracers have a different affinity for the DAT ([^{11}C]PE2I is more specific of DAT where [^{123}I]FP-CIT binds both DAT and SERT).

In the Project 3, we compared the expression of PDE10A, measured with [^{11}C]IMA107 PET imaging, with MRI markers of Parkinson's pathology such as iron depositions (assessed with susceptibility-weighted MR imaging), neuromelanin loss (assessed with neuromelanin sensitive MR imaging) and changes in structural volumetric (assessed with T1 MR imaging) and microstructural connectivity (assessed with diffusion tensor MR imaging) in early *de novo* and early levodopa-treated patients with Parkinson's disease compared to age- and sex-matched healthy control subjects.

2.2 Population

A total of 54 subjects were included in these cross-sectional studies: 32 non-demented, non-depressed patients with idiopathic Parkinson's disease according to the UK Brain Bank criteria, and 22 age and sex-matched healthy controls. All subjects underwent to one 3T MRI (MPRAGE, DTI, NM, SWI) scan, one SPECT ([^{123}I]FP-CIT) scan, and two PET ([^{11}C]IMA107 and [^{11}C]PE2I) scans.

Group A: 17 early untreated Parkinson's disease patients (H&Y=1; disease duration <24 months; never treated with dopamine agonists or levodopa; MoCA>26 and BDI<13)

Group B: 15 early treated Parkinson's disease (H&Y=2-3; disease duration <60 months; treated dopamine agonists or levodopa for at least 12 months and maximum 24 months; with no motor complications; MoCA>26 and BDI<13).

Group C: 22 age- and sex-matched HCs (MoCA>26 and BDI<13).

2.2.1 Inclusion/Exclusion criteria

Inclusion criteria

For all groups:

- 40-80 years of age, male or female
- Able to give informed consent
- Adequate visual and auditory acuity to complete the psychological testing

Specific for Parkinson's disease patients Group A: early de novo

- Diagnosis of sporadic Parkinson's disease according to the U.K. Brain Bank Criteria
- H&Y=1
- Disease duration <24 months
- never treated with dopamine agonists or levodopa

- MoCA>26
- BDI<13

Specific for Parkinson's disease patients Group B: early treated

- Diagnosis of sporadic Parkinson's disease according to the U.K. Brain Bank Criteria
- H&Y=2-3
- Disease duration <60 months
- Treated with dopamine agonists or levodopa for at least 12 months and maximum 24 months
- No motor complications
- MoCA>26
- BDI<13

Exclusion criteria

For all groups:

- Presence or history of other neurological or psychiatric disorders
- Presence of cognitive impairment (MoCA>26)
- Presence of depressive symptoms (BDI<13)
- Current or a recent history of drug or alcohol abuse/dependence
- Presence of known intracranial co-morbidities such as stroke, hemorrhage, space-occupying lesions
- Pregnancy or breastfeeding
- Contraindication to MRI, such as the presence of metal devises or implants (e.g. pacemaker, vascular- or heart- valves, stents, clips), the metal deposited in the body (e.g. bullets or shells), or metal grains in the eyes
- History of cancer
- Claustrophobia and history of back pain that makes prolonged laying on the PET or MRI scanner intolerable
- Use of medications with known actions on PDEs (e.g. aminophylline, theophylline, papaverine).
- Participants participating in clinical trials investigating PDEs or with PDEs inhibitors

Specific for Parkinson's disease patients

- Presence of diagnostic criteria for Parkinson's disease mild cognitive impairment (MCI) (Litvan *et al.*, 2011) or dementia (Emre *et al.*, 2007) or depression (Marsh *et al.*, 2006)

2.2.2 Recruitment

A nationally unique collection of scientific groups and research facilities makes KCL an optimal place for study recruitment. The facilities KCL, Guy's and St Thomas' hospital, King's College Hospital and South London and Maudsley NHS Foundation Trusts are part of King's Health Partners and jointly have responsibility for delivering movement disorder services through an integrated service to 6 million people living in South London and surrounding areas. In the studies that comprise this thesis, 80% of the population of Parkinson's disease patients were recruited from the Movement Disorders clinics at King's Health Partners and 20% through the network of Parkinson's disease charities (Fox Finder tool of Michael J. Fox Foundation and Parkinson's UK mailing lists). Healthy volunteers were recruited through advertisement.

Screening and clinical assessments were performed by myself and took place at the National Institute of Health Research (NIHR)-Wellcome Trust KCL Clinical Research Facility (Visit 1). SPECT imaging assessments took place at KCH Nuclear Medicine (Visit 2). MRI and PET Imaging assessments took place at Imanova ltd. (now Invicro London Ltd, A Konica Minolta Company) (Visit 3). Data processing, data analysis and dissemination of findings were performed by myself and took place at the NIG Lab based at the Maurice Wohl Clinical Neuroscience Institute.

Ethical consideration

The study was approved by the institutional review boards and the research ethics committee (IRAS number: 1692665). Written informed consent was obtained from all study participants in accordance with the Declaration of Helsinki.

2.3 Clinical assessments

The screening/clinical assessments were performed during the Visit 1 as follows:

Taking informed consent

Screening assessments

- Detailed medical and family history

  Medical interview was conducted to collect: risk factors (coffee use, smoking habits, alcohol frequency, rural living, use of well water, history of head injuries, occupation associated with night shifts, exposure to pesticide), comorbidities (recent head injury with hospitalization, cardio-/cerebrovascular diseases, migraine, depression, hypertension, diabetes, dyslipidaemia, obesity, metabolic syndrome) and medications (antihypertensives, vitamins, analgesics, respiratory, gastrointestinal, urinary system, metabolic, antidiabetic, lipid-lowering, thyroid, osteoporosis, neuroleptics, anticonvulsants, anticoagulants/antiplatelets, antidepressants and daily levodopa equivalent dose*)
- General screening questions (including MRI safety questionnaire)
- Physical and neurological examination
- Structured Clinical Interview for DSM-IV (to exclude the presence of other neurological or psychiatric disorders)
- Montreal Cognitive Assessment (MoCA) (to exclude the presence of cognitive impairment)
- Beck Depression Inventory (BDI) (to exclude the presence of depressive symptoms)

Clinical assessments

- Motor scales
  - MDS-UPDRS
  - H&Y
  - Schwab and England

- Non-motor scales
    - PD Non-motor symptom assessment scale (NMSS)
    - Modified Constipation Assessment Scale
    - Parkinson's disease Sleeping Scale (PDSS)
    - Excessive Daytime Sleepiness Scale (ESS)
    - RBD Screening Questionnaire (RBDSQ)
    - PD Fatigue Scale
    - Scales for Outcomes in Parkinson's disease – Autonomic (SCOPA-AUT)
    - University of Pennsylvania Smell Identification Test (UPSIT)
- Quality of Life
    - PD Questionnaire (PDQ-39)
- Neuropsychological battery
    - Mini-Mental State Examination (MMSE)
    - Montreal Cognitive Assessment (MoCA)**
    - Beck Depression Inventory (BDI)**
    - Geriatric Depression Scale (GDS)

*Calculation of daily dopaminergic medication equivalent dose was based on the following theoretical equivalence to levodopa formula:

Daily LED (mg) = (1 X levodopa) + (0.77 X levodopa CR) + (1.43 X levodopa + Entacapone) + (1.11 X levodopa CR + Entacapone) + (20 X Ropinirole) + (20 X Ropinirole ER) + (100 X Pramipexole) + (30 X Rotigotine) + (10 X Bromocriptine) + (8 X Apomorphine) + (100 X Pergolide) + (67 X Cabergoline) (Niccolini *et al.*, 2015a)

**This scale was performed at screening

2.3.1 Motor scales

All subjects underwent MDS-UPDRS, H&Y and Schwab and England motor scales. Motor assessments have been performed OFF medication after overnight withdrawal of dopaminergic medications.

MDS-UPDRS: The MDS-UPDRS is a multimodal scale assessing both impairment and disability and is separated into 4 subscales (Parts I- IV) (Goetz, 2010). The MDS-UPDRS was performed by myself for all subjects throughout the course of the studies in each component: Part I: This assesses non-motor experiences of daily living and is comprised of two components (Part IA: This contains 6 questions that are assessed by the Investigator and focuses on complex behaviours and Part IB: This contains 7 questions that are part of the Patient Questionnaire completed by the subject); Part II: This assesses motor experiences of daily living. There are an additional 13 questions that are also part of the Patient Questionnaire completed by the subject; Part III: This assesses the motor signs of Parkinson's disease and is administered by the Investigator and Part IV: This assesses motor complications, dyskinesias and motor fluctuations using historical and objective information. The Investigator completed this assessment only for treated Parkinson's disease patients. Each item was rated 0–4 following the MDS-UPDRS scoring system. Based on the MDS-UPDRS part III items, motor subscores were calculated as follows (Niccolini *et al.*, 2017): *tremor subscore*: postural tremor of the hands (left and right), kinetic tremor of the hands (left and right), rest tremor amplitude (extremities and lip/jaw) and constancy of rest tremor; *bradykinesia subscore*: facial expression, finger tapping (left and right), hand movements (left and right), pronation-supination movements of hands (left and right), toe-tapping (left and right), leg agility (left and right), arising from chair, global spontaneity of movement (body bradykinesia); *rigidity subscore*: rigidity (extremities and neck) and *axial subscore*: speech, gait, freezing of gait, postural stability and posture.

H&Y: The H&Y is a commonly used system for describing how the symptoms of Parkinson's disease progress (Goetz *et al.*, 2004). The scale allocates stages from 0 to 5 to indicate the relative level of

disability. This scale is included within the MDS-UPDRS and have been completed for all subjects as follows: Stage zero: No symptoms; Stage one: Symptoms on one side of the body only; Stage two: Symptoms on both sides of the body. No impairment of balance; Stage three: Balance impairment. Mild to moderate disease. Physically independent; Stage four: Severe disability, but still able to walk or stand unassisted and Stage five: Wheelchair-bound or bedridden unless assisted.

Schwab and England: The Modified Schwab & England ADL scale reflects the speed, ease, and independence with which an individual performs daily activities, or personal chores, such as eating, toileting, and dressing (Schwab, 1969). This scale uses a rating scale from 0% to 100%, with 100% representing complete independence in performing daily activities and 0% representing a vegetative, bedridden state (Ramaker *et al.,* 2002; Harrison *et al.,* 2009; Shulman *et al.,* 2016). The Schwab and England scale has become a standard assessment tool in Parkinson's disease and has been used in hundreds of studies. The data available from studies with a primary aim to investigate characteristics of other rating scales suggest a moderate to substantial validity and good reliability (Martinez-Martin *et al.,* 1995; Stebbins and Goetz, 1998).

2.3.2 Non-motor scales

All subjects underwent NMSS, Modified Constipation Assessment Scale, PDSS, ESS, RBDSQ, PD Fatigue Scale, SCOPA-AUT and UPSIT.

NMSS: The NMSS is a 30-item self-rated questionnaire that captures the presence, frequency, and severity of non-motor symptoms attributed to Parkinson's disease (Chaudhuri *et al.,* 2007). Non-motor symptoms, such as autonomic dysfunction, depression, apathy, memory problems, sleep, and psychiatric problems, are present in the large majority of Parkinson's disease patients (Barone *et al.,* 2009) and profoundly affect the quality of life. It contains 30 items, each one rated for severity (from 0 to 3) and frequency (from 1 to 4) and scored through the multiplication of both figures (from 0 to

12). Items are grouped in 9 domains: cardiovascular, sleep/fatigue, mood/apathy, perceptual problems/hallucinations, attention/memory, autonomic, and miscellaneous. The maximum total score, indicative of higher severity and frequency of non-motor symptoms, is 360 (Martinez-Martin *et al.*, 2011). The scores obtained from items of this scale have recently been found to have a high correlation in Parkinson's disease patients with the MDS-UPDRS part I (Martinez-Martin *et al.*, 2015).

Modified Constipation Assessment Scale: The Modified Constipation Assessment Scale is an 8-item self-report measure designed to assess the presence and severity of constipation (McMillan and Williams, 1989). Characteristics included are: abdominal distention or bloating, change in the amount of gas passed rectally, less frequent bowel movements, oozing liquid stool, rectal fullness or pressure, rectal pain with bowel movements, a small volume of stool and inability to pass stool. For each item, there is a three-point summated rating scale (0=no problem, 1=some problem, 2=severe problem). A total score is calculated that can range from 0 (no constipation) to 16 (severe constipation). Each item is rated based on the patients' experience with each feature in the previous week. A score of >1 indicates constipation and higher scores indicate worse constipation.

PDSS: The PDSS is a self-report scale to assess the quality of sleep in patients specifically designed for Parkinson's disease patients (Chaudhuri *et al.*, 2002). It is composed of 15 questions tailored to commonly reported symptoms associated with sleep disturbance in Parkinson's disease, particularly: overall quality of night's sleep, sleep onset and maintenance insomnia, nocturnal restlessness, nocturnal psychosis nocturia, nocturnal motor symptoms, sleep refreshment, daytime dozing. For each item, there is a ten-point summated rating scale with lower scores indicated worse sleep problems.

ESS: The ESS is an 8-item self-report measure of daytime sleepiness developed as a brief tool to measure the general level of sleepiness at the bedside (Johns, 1991). Responders are required to rate

on a scale of 0-3 the chance of dozing off or falling asleep while engaged in 8 activities. The score ranges from 0 to 24 with higher scores indicate worse sleepiness. In comparison to the instrumental Multiple Sleep Latency Test, considered the gold standard for daytime sleepiness, the ESS has demonstrated higher sensitivity and specificity in the screening of patients with daytime sleepiness (Johns, 2000). Beside primary sleep disturbances, it has found application to characterize important levels of daytime sleepiness in Parkinson's disease. Also, the ESS has been used as an outcome measure for daytime sleepiness for randomized controlled trials in Parkinson's disease (Postuma *et al.*, 2012; Eggert *et al.*, 2014). An ESS score of greater than 10 has been validated as a cut-off for experiencing EDS (Johns, 1991).

RBDSQ: The RBDSQ is a 10-item self-report questionnaire used to gauge the presence of symptoms of RBD. The maximum total score that can be obtained on the RBDSQ is 13. RBD occurs during rapid eye movement sleep where patients primarily experience muscle atonia where muscles are not paralyzed as they normally are. As REM sleep involves vivid dreaming, a variety of resultant behaviors can occur. The RBDSQ captures notable components of RBD including vivid dreaming, limb movement during sleep, verbal expressions during sleep, night-time awakening dye to movements, and sleep disturbance. RBD has been shown to precede and also occur within the course of Parkinson's disease (Marion *et al.*, 2008). The RBDSQ has demonstrated a sensitivity of 0.96 and a specificity of 0.56 in differentiating RBD patients and controls considering a score of 5 as an indicator for RBD (Stiasny-Kolster *et al.*, 2007).

PD Fatigue Scale: The PD Fatigue Scale is a 16-item self-report questionnaire that measures the presence of fatigue (seven items, i.e. "I feel totally drained") and its impact on daily function (nine items, i.e. "I get more tired than other people I know") over the prior 2 weeks (Brown *et al.*, 2005). However, neither severity nor frequency of fatigue symptoms is specifically measured but the scale is designed to exclude the cognitive and emotional features of fatigue. Scoring options range from 1

("strongly disagree") to 5 ("strongly agree") and are usually scored as total ordinal (from 16 to 80 based on the sum of scores for the 16 individual items).

SCOPA-AUT: The SCOPA-AUT is a 26-item self-administered test developed to evaluate autonomic symptoms, such as gastrointestinal and urinary problems, in subjects with Parkinson's disease (Visser *et al.*, 2004). The assessment will measure whether subject's experience an increase in autonomic dysfunction as the disease severity progresses.

UPSIT: The UPSIT is a 40-item, multiple choice, scratch and sniff test used to evaluate odor identification. It is a forced-choice test in which subjects must identify an odor among four response alternatives. There are four booklets containing ten odorants each. The instructions have been explained to the subjects by the coordinator at the clinical site. The UPSIT have been scored by the coordinator reflecting the number of correct responses out of 40 items. Score >26 are considered normal and the cut-off of 18 and of 26 are used for the definition of anosmia and hyposmia, respectively.

2.3.3 Quality of Life

PDQ-39: This is a 39-item self-report questionnaire to assess the quality of life in Parkinson's Disease patients (Jenkinson *et al.*, 1997), and is meant to measure the degree of burden and constraint that the fact of being diagnosed with Parkinson's disease or its symptoms cause to the patient. It comprises 39 items grouped in 8 domains: mobility, ADL, emotional well-being, stigma, social support, cognition, communication, and body discomfort. Responses are scored on a scale from 0 (never) to 4 (always). Each subscale's scores are transformed into a 0–100 scale by summing the items' raw scores, divided by the maximum possible raw score, and then multiplying by 100. Higher scores mean poorer HRQoL.

2.3.4 Neuropsychological battery

All subjects underwent MMSE, MoCA, BDI, and GDS.

MMSE: The MMSE is a widely used screening test for cognition in community surveys and in research studies (Folstein *et al.*, 1975). It is recommended by the NINDCS-ADRDA to document the diagnosis of probable AD (McKhann *et al.*, 1984). It consists of a variety of questions, grouped into 7 categories spanning orientation in time and in space, registration of three words, attention and calculation, recall of three words, language and visual construction. The maximum score is 30 points and can be adjusted for age and years of education. Internal reliability and test-retest reliability of this test are excellent (Tombaugh and McIntyre, 1992).

MoCA: The MoCA is a widely used screening neuropsychological assessment to test cognitive performance and provides more precise data on cognitive impairment in patients with MCI or with memory issues, not to the extent of dementia (Smith *et al.*, 2007). Items are constituted by parts of other well-known neuropsychological tests (TMT-B, clock drawing, forward and backward digit span, immediate and delayed recall, sentence repetition) and tests orientation, memory, attention,

vigilance, verbal fluency, visuospatial and visuoconstructional skills. The cut-off used are as follows: 26-30: no cognitive impairment; 22-25: MCI; <22: moderate-severe cognitive impairment (Damian *et al.*, 2011).

BDI: The BDI is a scale for the assessment of the levels of depression and has been developed in 1996 as an update of the first BDI version to comply with the diagnostic criteria for major depressive disorder published by the DSM-IV. It contains 21 questions to which the patient should answer according to a score from 0 to 3. Higher total scores indicate more severe depressive symptoms. Items on this scale are related to symptoms of depression such as hopelessness, irritability, suicidal intentions, loss of interest, fatigue, weight loss and sense of guilt. The cut-off used are as follows: 0-13: minimal depression; 14-19: mild depression; 20-28: moderate depression; 29 or higher: severe depression. This scale is endorsed by the National Institute of Health and Clinical Excellence for use in primary care, to an adult audience, for baseline screening of depressive symptoms.

GDS: The GDS is a 30-item self-report measure to assess the presence and severity of depressive symptoms particularly in elderly individuals (Havins *et al.*, 2012). Responses on the GDS are presented in a simple yes/no format and scored according to a binary 0/1 format depending on how the question is keyed (positive or negative). Depressive symptoms covered by the GDS include life satisfaction, anhedonia, hopelessness, worrying, helplessness, sadness, lack of energy, difficulties concentrating, excessive sleep, withdrawal, and cognitive issues. Ranges of scores and associated clinical categorization are as follows: 0 to 9 is ‘normal’, 10 to 19 is ‘mildly depressed’, and 20 to 30 is ‘severely depressed’.

2.4 Molecular SPECT and PET imaging

All subjects underwent to one SPECT ([^{123}I]FP-CIT) scan (approximately 45 minutes – 4 hours uptake time), and two PET ([^{11}C]IMA107 and [^{11}C]PE2I) scans (approximately 90 minutes each). SPECT imaging was acquired on a 3-headed gamma camera system (Philips IRIX 3), and PET imaging on Siemens Biograph Hi-Rez 6 PET-CT scanner (Erlangen, Germany).

2.4.1 SPECT DAT Scan

[^{123}I]FP-CIT DAT SPECT scans were performed at KCH NHS Foundation Trust, London, UK – Nuclear Medicine Department; acquired on a 3-headed gamma camera system (Philips IRIX 3), equipped with a low-energy high-resolution collimator.

2.4.1.1 Scanning details

Patients were given an intravenous injection of approximately 185 MBq [^{123}I]FP-CIT, with images obtained 4 hours post-injection. Data were acquired in a 128 x 128 matrix, using a 20% energy window and magnification x 2. All SPECT images were reconstructed on a HERMES workstation, using the HERMES Hybrid Recon™ - Neurology software. Reconstruction was performed using the 3D ordered-subset expectation maximum (OSEM) method, using 5 iterations with attenuation correction. Finally, a 3D Gaussian postfilter was applied with a 0·90cm FWHM. All iteratively reconstructed SPECT images were then transferred to BRASS™ software to quantify striatal tracer uptake. Patients SPECT images were fitted against a pre-existing three-dimensional reference template, containing a number of VOIs. The caudate, putamen and striatum specific uptake ratios were calculated using the occipital cortex as a reference region.

2.4.1.2 Imaging analyses

[^{123}I]FP-CIT-SPECT was processed using Hybrid-Recon and Statistical Parametric Mapping 12 (SPM, Wellcome Trust Centre for Neuroimaging, London, UK) implemented in MATLAB (The Math-Works, Natick, MA, USA). [^{123}I]FP-CIT SPECT image volumes were spatially normalized to a FP-CIT template in MNI space. The eight most prominent axial slices containing the striatum were summed and a standardized VOI template was then applied to this image. VOI analyses were performed on the right and left caudate and putamen, employing the occipital region as the reference tissue. SBR was calculated as the ratio of the putamen or caudate VOI count density divided by the occipital cortex count density minus one. This measure approximates the binding potential, BP_{ND}, when the radioligand is in equilibrium at the target site and has previously been reported with [^{123}I]FP-CIT SPECT (Qamhawi *et al.*, 2015).

2.4.2 PET DAT Scan

[^{11}C]PE2I PET imaging was acquired on a Siemens Biograph Hi-Rez 6 PET-CT scanner (Erlangen, Germany).

2.4.2.1 Scanning details

Dynamic emission data [^{11}C]PE2I PET data were acquired continuously for 90 minutes after the injection of [^{11}C]PE2I at a target dose of 350 MBq administered intravenously as a slow bolus injection over 10 seconds, followed by the injection of 10 mL of saline flush over 10 seconds. Cerebellum was previously validated as a reference region devoid of specific DAT activity; therefore, arterial cannulation was not required for [^{11}C]PE2I PET (Jucaite *et al.*, 2006). The dynamic images were reconstructed into 26 frames (8 x 15s, 3 x 60s, 5 x 120s, 5 x 300s, and 5 x 600s), using a filtered back projections algorithm (direct inversion Fourier transform) with a 128 matrix, zoom of 2.6

producing images with isotropic voxel size of 2 x 2 x 2 mm^3, and smoothed with a transaxially Gaussian filter of 5mm.

2.4.2.2 Imaging analyses

The Molecular Imaging and Kinetic Analysis Toolbox software package (MIAKAT™: www.miakat.org) combines in-house code with wrappers for FMRIB Software Library (FSL, http://fsl.fmrib.ox.ac.uk/fsl/fslwiki/) and Statistical Parametric Mapping (SPM, http://www.fil.ion.ucl.ac.uk/spm/) commands in order to provide state-of-the-art functionality within a coherent analysis framework. This software includes a range of analytical procedures including image registration, brain extraction, segmentation, generation of time-activity curves and input functions, graphical analysis, kinetic modeling and parametric imaging. Individual PET frames were corrected for head motion using frame-by-frame rigid registration using a frame with high signal-to-noise ratio as a reference. The MIAKAT™ processing pipeline was followed, ensuring that all quality control steps were completed (Figure 4).

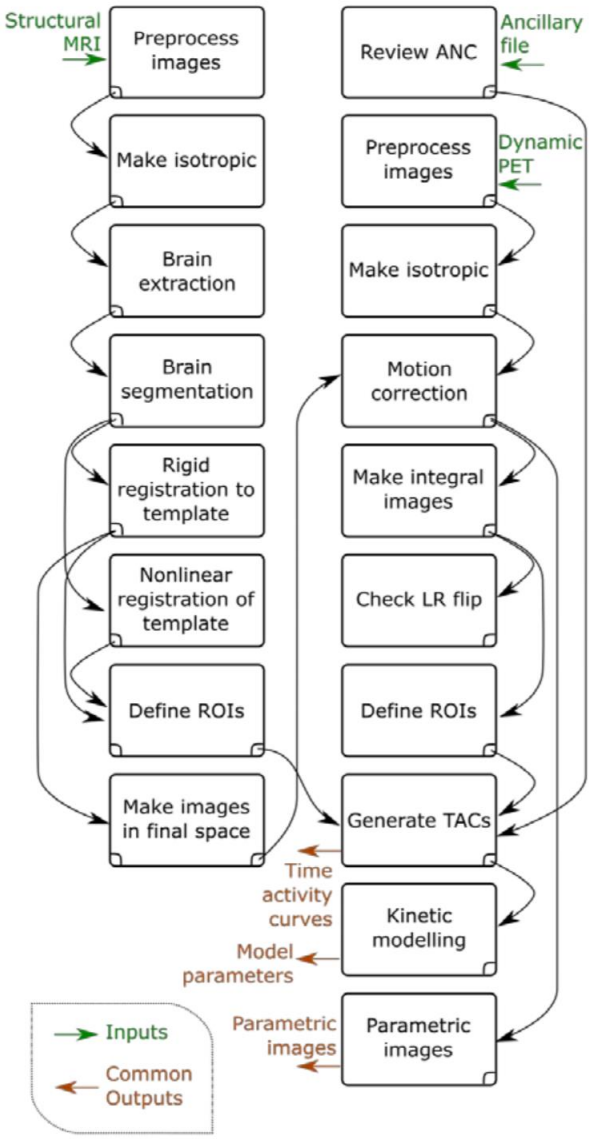

Figure 4. MIAKAT^{TM} Pipeline

A study with [^{11}C]PE2I PET has shown high signal in the striatum, lower in the midbrain and very low in the cerebellum, which may be interpreted by kinetic compartment models (Jucaite *et al.*, 2006). In addition, a comparison between the SRTM and 2-TCM showed a good agreement (Jucaite *et al.*, 2006). Therefore, parametric images of [^{11}C]PE2I BP_{ND} were generated from the dynamic [^{11}C]PE2I scans using the SRTM with the cerebellum as the reference tissue.

Region of interest-based and voxel-based analysis were carried out on [^{11}C]PE2I parametric images to quantify changes in DAT levels. For regions of interest-based analysis, parametric images was co-

registered to subjects' T1-weighted MRI to quantify DAT within manually delineated anatomical ROIs, including the caudate, putamen, ventral striatum, globus pallidus (external and internal segments), substantia nigra and thalamus, following published guidelines (Tziortzi *et al.*, 2011b).

2.4.3 PET PDE10A scan

[^{11}C]IMA107 PET imaging was acquired on a Siemens Biograph Hi-Rez 6 PET-CT scanner (Erlangen, Germany).

2.4.3.1 Scanning details

Dynamic emission data [^{11}C]IMA107 PET data were acquired continuously for 90 minutes after the injection of [^{11}C]IMA107 at a target dose of 350 MBq administered intravenously as a slow bolus injection over 20 seconds, no saline flush. All participants were scanned after withholding consumption of caffeinated beverages for 12 hours (Fredholm *et al.*, 1999b). A reference region devoid of specific PDE10A activity has been validated; therefore, arterial cannulation was not required for [^{11}C]IMA107 PET. The dynamic images were reconstructed into 26 frames (8 x 15s, 3 x 60s, 5 x 120s, 5 x 300s, and 5 x 600s), using a filtered back projections algorithm (direct inversion Fourier transform) with a 128 matrix, zoom of 2.6 producing images with isotropic voxel size of 2 x 2 x 2 mm3, and smoothed with a transaxially Gaussian filter of 5mm.

2.4.3.2 Imaging analyses

The Molecular Imaging and Kinetic Analysis Toolbox software package (MIAKAT^{TM}: www.miakat.org) combines in-house code with wrappers for FMRIB Software Library (FSL, http://fsl.fmrib.ox.ac.uk/fsl/fslwiki/) and Statistical Parametric Mapping (SPM, http://www.fil.ion.ucl.ac.uk/spm/) commands in order to provide state-of-the-art functionality within a coherent analysis framework. This software includes a range of analytical procedures including image registration, brain extraction, segmentation, generation of time-activity curves and input functions, graphical analysis, kinetic modeling and parametric imaging. Individual PET frames were corrected for head motion using frame-by-frame rigid registration using a frame with high signal-to-noise ratio as a reference. The MIAKAT^{TM} processing pipeline was followed, ensuring that all quality control steps were completed.

A human PDE10A inhibitor occupancy study with [^{11}C]IMA107 PET has shown up to 90% occupancy in striatal regions with no displacement in the cerebellum (Plisson *et al.*, 2014a). Moreover, comparisons between the SRTM; (Gunn *et al.*, 1997) and 2-TCM (Gunn *et al.*, 2001) values have shown good agreement. Therefore, parametric images of [^{11}C]IMA107 BP_{ND} were generated from the dynamic [^{11}C]IMA107 scans using the SRTM with the cerebellum as the reference tissue.

The region of interest-based and voxel-based analysis was carried out on [^{11}C]IMA107 parametric images to quantify changes in PDE10A levels. For regions of interest-based analysis, parametric images was co-registered to subjects' T1-weighted MRI to quantify PDE10A within manually delineated anatomical ROIs, including the caudate, putamen, ventral striatum, globus pallidus (external and internal segments), substantia nigra and thalamus, following published guidelines (Tziortzi *et al.*, 2011b).

2.5 MRI imaging

MRI imaging was performed at Imanova Ltd, London, UK; acquired with a 32-channel head coil on a Siemens Magnetom MAGNETOM TrioTim syngo MR B17 (Erlangen, Germany), 3T MRI scanner. MRI acquisition included a T1-weighted Magnetization Prepared Rapid Gradient Echo sequence (MPRAGE); Fast Grey Matter Acquisition T1 Inversion Recovery (FGATIR); diffusion tensor imaging (DTI); neuromelanin-sensitive (NM) MRI and susceptibility weighted imaging (SWI) MRI.

2.5.1 Structural volumetric T1

Structural T1-weighted MRI data were used to assess changes in cortical thickness and subcortical volumes. Analysis of T1-weighted structural MR data have been conducted using FreeSurfer image analysis suite (version 5.3.0 http://surfer. nmr.mgh.harvard.edu) processing pipeline to derive measures of subcortical volumes and cortical thickness. This procedure automatically assigns a neuroanatomical label to each voxel in an MRI volume based on probabilistic information automatically estimated from a manually labeled training set. This technique has previously been shown to be comparable in accuracy to manual labeling (Fischl *et al.*, 2002). Furthermore, T1-weighted MRI data have been used to define anatomical regions of interest.

2.5.1.1 Scanning details

Structural T1-weighted MPRAGE data was acquired with the following protocol: time repetition = 2300 ms, time echo = 2.98 ms, flip angle of 9°, time to inversion = 900 ms, matrix = 240 x 256. FGATIR data was acquired with the following protocol: time repetition = 3000 ms, time echo = 2.96 ms, flip angle of 8°, time to inversion = 409 ms, matrix = 240 x 256.

2.5.1.2 Imaging analyses

Anatomical borders were defined manually for the ROIs, including caudate, putamen, ventral striatum, globus pallidus, substantia nigra and thalamic motor nuclei in both hemispheres as follows:

Caudate: it was drawn on the axial plane. The anterior and medial borders were defined by the lateral ventricle, the posterior border was defined by the internal capsule, and the lateral border was defined by the external capsule.

Putamen: it was defined on the axial plane and traced on all slices where dense grey matter could be clearly observed and differentiated from surrounding structures. The anterior border was defined by the anterior limb of the internal capsule, the posterior border was defined by the posterior limb of the internal capsule, the lateral border was defined by the external capsule/claustrum, and the medial border was defined by the lamina medullaris lateralis.

Ventral striatum: it is drawn on the coronal plane. The boundaries between ventral and dorsal striatum are defined by a line connecting two points (Marker A and Point C) on the coronal plane. These two points are predefined by the placement of two markers (Markers A and B) on the sagittal plane. Marker A is a horizontal line intersecting the most ventral part of the splenium of the corpus callosum, which is placed on the most midsagittal slice. In coronal view, Marker A appears as a single voxel in each slice and this voxel is used for the definition of the dorsal boundary of the ventral striatum. Marker B is a rectangle placed on the head of caudate, which in coronal view appears as a column. The inferior intersection of this column with GM of putamen is defined as the point C. Ventral striatum tracing begins when point C comes into view, up to the slice where anterior commissure connects the two hemispheres.

Globus pallidus: it was performed on the coronal plane including external and internal pallidum and was defined up to the slice where anterior commissure connects the two hemispheres. The putamen served as the lateral border of the globus pallidus throughout its course. The superior border was

defined by the internal capsule. The temporal limb of the anterior commissure served as the inferior border. Using enhanced contrast FGATIR MRI sequences was possible to separate the external and internal segment of the globus pallidus. Globus pallidus internal is identifiable on the axial plane immediately caudal to the intercommissural line connecting the anterior and posterior commissures. Lamina pallida medialis separates the internal from the external segment of globus pallidus.

Substantia nigra: it is located in the midbrain, includes both pars reticulata and pars compacta and is a small region with no clear-cut boundaries. The substantia nigra is distinguishable from the surrounding tissues due to its hyperintensity in contrast to the adjacent cerebral peduncle in FGATIR MR images. The ROIs were drawn on five successive axial slices centered to the maximal signal in the substantia nigra.

Thalamus: they correspond to the motor function according to primates tracing studies and include the ventral anterior and ventral lateral thalamic nuclei. The thalamus was divided into three regions (anterior, lateral and medial subdivisions) that are anatomically defined by a "Y" shaped bundle of nerve fibers termed the internal medullary lamina. The ventral anterior and ventral lateral thalamic nuclei were defined on the axial plane and end just before the superior colliculi become visible. The posterior limb of internal capsule and the internal medullary lamina are the lateral and medial boundaries, respectively. The ventral anterior nucleus occupies the rostral part of the lateral nuclear mass. The ventral lateral nucleus lies immediately caudal to the ventral anterior nucleus in the ventral tier of the lateral nuclear complex. The ROIs were drawn on five successive axial slices.

PET images of each subject were co-registered to their respective structural MRI using SPM12 (Wellcome Trust Centre for Neuroimaging) in MATLAB (r2015a; The MathWorks). The quality of co-registration was checked visually for each subject.

MRI Analysis: FreeSurfer Subcortical Volumetric analysis

FreeSurfer image analysis suite (version 5·3·0 http://surfer. nmr.mgh.harvard.edu) was used to derive measures of deep grey matter nuclei volume. Reconstructed data sets were visually inspected to ensure the accuracy of registration, skull stripping, segmentation, and cortical surface reconstruction. Subcortical structure volumes were derived by automated procedures, which automatically assign a neuroanatomical label to each voxel in an MRI volume based on probabilistic information automatically estimated from a manually labeled training set (Fischl *et al.*, 2002). All individual nuclei volumes were normalized for total intracranial volume automatically generated by FreeSurfer (Buckner *et al.*, 2004).

2.5.2 Structural connectivity DTI

Structural connectivity DTI MRI data were used to assess microstructural changes in cortical and subcortical grey and white matter areas.

2.5.2.1 Scanning details

Diffusion-weighted data was acquired using echo planar imaging (EPI; TR = 3010 ms, TE = 88 ms, multi-band acceleration factor = 3, flip angle of 90° and voxel size of 2.0 x 2.0 x 2.0 mm^3). The diffusion weighting have been isotropically distributed along the 64 directions (b-value = 1500 s/mm2), and a 6 non-DWIs (B0) have been acquired at the beginning of each scan. The EPI acquisitions are prone to geometric distortions that can lead to errors in tractography. To minimize this, a second 6 non-DWI (B0) image sets have been acquired with the phase-encoded direction reversed—"blip-up" and "blip-down" (Chang and Fitzpatrick, 1992)— which resulted in images with geometric distortions of equal magnitude but in the opposite direction allowing for the calculation of a corrected image (Andersson *et al.*, 2003). Before correcting geometric distortions, each image set—blip-up and blip-down—have been corrected for motion and eddy-current-related distortions. The total duration of this scan have been approximately 15 minutes.

2.5.2.2 Imaging analyses

Diffusion data analysis was performed with FSL Diffusion Toolbox (FDT) (FMRIB Software Library (FSL), Centre Software Library, University of Oxford, Oxford, UK). Correction for head motion, artefacts, and eddy currents were performed using top-up (Andersson *et al.*, 2003) and eddy correct (Andersson *et al.*, 2016). DTIFit was used to fit diffusor tensor model at each voxel to generate maps of FA and MD.

T1 MPRAGE and FGATIR images were registered to subject's diffusion space, using FMRIB's Linear Image Registration Tool (FLIRT), and parameters applied to transform subcortical regions

(caudate, putamen and substantia nigra) into subject's diffusion space. With this technique, a quantification of FA and MD was performed for caudate, putamen and substantia nigra ROIs.

2.5.3 Neuromelanin

NM MRI data were used to assess structural changes in the substantia nigra and in the locus coeruleus by using NM density.

2.5.3.1 Scanning details

NM data was acquired with oblique-axial fast gradient-echo sequence [time repetition = 829 ms; time echo = 12 ms, matrix = 256 x 256 x 33; voxel size = 0.8×0.8×2.5 mm; slice thickness 2.5 mm; 12 slices].

2.5.3.2 Imaging analyses

For quantification of NM, substantia nigra and locus coeruleus were manually delineated on the neuromelanin-sensitive and T1-weighted image using Analyze 12.0 (Analyze Direct, Overland Park, KS, United States). On NM-space, each substantia nigra and locus coeruleus ROIs were manually drawn on both hemispheres on 3-4 (substantia nigra) and 1-2 (locus coeruleus) axial slices together with the reference regions of the superior peduncle (for substantia nigra) and rostral pontomesencephalic area (for locus coeruleus). To calculate the signal intensity in the substantia nigra and in the locus coeruleus area, the superior peduncle and the rostral pontomesencephalic area were used as a reference region, respectively for the substantia nigra and for the locus coeruleus, to normalize the intensity of the slices to remove the inter-slice and inter-subject variability (Figure 5).

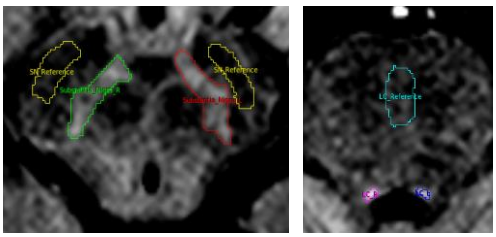

Figure 3. ROIs for substantia nigra and locus coeruleus were manually drawn on both hemispheres on 3-4 (substantia nigra) and 1-2 (locus coeruleus) axial slices together with the reference regions

Figure 5. ROIs for Substantia nigra and Locus coeruleus. *ROIs were manually drawn on both hemispheres on 3-4 (substantia nigra) and 1-2 (locus coeruleus) axial slices together with the reference regions*

Mean regional values, number of voxels, standard deviations and regional areas were then extracted for each ROIs on both hemispheres individually before averaging to obtain bilateral data for NM. The NM density for Substantia nigra and locus coeruleus have been calculated with the following formulas: Ratio 1 = Mean value of substantia nigra / mean substantia nigra reference; ratio 2 = mean value of substantia nigra – substantia nigra reference / substantia nigra reference SD and ratio 3 = mean value of substantia nigra – substantia nigra reference / substantia nigra reference.

2.5.4 Susceptibility weighted imaging

SWI MRI data were used to assess iron depositions in the striatum and in the substantia nigra.

2.5.4.1 Scanning details

SWI MRI data was acquired with the following protocol: time repetition = 60 ms; time echo = 30 ms; echo train length 5; flip angle 19°; voxel size = 0.55×0.55×0.7 mm; 70 slices.

2.5.4.2 Imaging analyses

Combined SWI images were reconstructed automatically on the Siemens workstation (Syngo MR B17 software, SWI version 1), which included the application of a 64*64 high-pass filter to the phase images in order to remove low spatial frequency effects that may otherwise result in false phase information. Manual delineation of the ROIs was performed on high-pass filtered phase images using Analyze 12.0 (AnalyzeDirect, Overland Park, KS, United States). Each ROI was hand drawn on both hemispheres on a single axial slice and included the caudate, putamen, and substantia nigra. The substantia nigra was delineated on the 3rd axial slice ventral to the most dorsal aspect of the red nucleus.

2.6 Statistical Analysis

Statistical analysis and graph illustration were performed with SPSS (version 20) and GraphPad Prism (version 6.0c), respectively. For all variables, variance homogeneity and Gaussianity were tested with Kolmogorov-Smirnov tests. Student t-test (parametric variables) and Mann-Whitney U test (non-parametric variables) were used for between-group comparisons, as appropriate. Categorical variables were compared using a $\chi 2$ test. Multivariate analysis of variance (MANCOVA) was used to assess the main effects of regional BP_{ND} between patients with Parkinson's disease and healthy controls, with Bonferroni *post-hoc* analysis for comparisons among subgroups (early *de novo*, early treated and controls). If the overall multivariate test was significant, *P*-values for each variable were calculated following Bonferroni's multiple comparisons test. Correlations between imaging and clinical data were performed using Pearson (r) or Spearman (rho) test, as appropriate, applying the Benjamini-Hochberg correction to reduce false discovery rate. False discovery rate cut-off was set at 0.05. All data are presented as the mean ± standard deviation (SD), and the level α was set for all comparisons at $P<0.05$, corrected. SPM voxel-by-voxel comparison was performed between controls and Parkinson's disease patients with a priori hypothesis restricted to the basal ganglia. This masking drastically reduces the number of voxel-by-voxel statistical comparisons, and a corrected threshold of $P<0.05$ used to test for statistically significant effects.

With regards to power calculations, previous and pilot data have shown that cross-sectional standardized differences (Cohen's d) between PD and HCs in PET biomarkers range between 1.48-1.57 ([^{11}C]IMA107 PET in the putamen and [^{11}C]PE2I PET in the striatum). Eighteen participants per group (54 in total), will provide 80% power to detect baseline differences between idiopathic-PD subgroups and healthy controls that correspond to a Cohen's d of 1.48 or larger with a one-sided test, 5% type I error rate.

Chapter 3. PDE10A in Parkinson's Disease

This chapter summarizes the clinical characteristics of the populations and the Project 1 on the *in vivo* evaluation of the integrity of PDE10A enzyme (with [^{11}C]IMA107 PET imaging) in early *de novo* Parkinson's disease patients compared to age- and sex-matched healthy control subjects. The integrity of PDE10A enzyme in early *de novo* Parkinson's disease patients was then compared to early levodopa-treated Parkinson's disease patients, evaluating how PDE10A changes are associated with disease duration and severity. Finally, the associations between the motor (tremor, rigidity, bradykinesia and postural instability) and non-motor symptoms (sleep problems, cognitive impairment, autonomic dysfunction, mood disorders etc) and the expression of PDE10A have been explored and described in detail.

3.1 Clinical characteristics of the populations

Between September 2015, and September 2016, a total of 54 subjects were recruited from specialist Movement Disorders clinics at King's College Hospital NHS Foundation Trust, 32 non-demented, non-depressed patients with idiopathic Parkinson's disease according to the UK Brain Bank criteria, and 22 age and sex-matched healthy controls. Among the 32 Parkinson's disease patients, 17 were early untreated (H&Y=1; disease duration <24 months; never treated with dopamine agonists or levodopa; MoCA>26 and BDI<13) and 15 early were treated with dopamine agonists or levodopa for at least 12 months (H&Y=2-3; disease duration <60 months; treated; with no motor complications; MoCA>26 and BDI<13).

The full demographics and clinical characteristics of the populations are shown in Table 1. As the cohorts were carefully matched for age, we found no effect of age in imaging biomarkers in all regions-of-interest across all cohorts (P>0.10).

Early *de novo* Parkinson's disease patients had worse NMSS (P<0.05), constipation (P<0.05), autonomic (SCOPA-AUT, P<0.05) and olfactory dysfunction (UPSIT, P<0.05), and worse quality of life (PDQ-39, P<0.05) scores compared to healthy controls.

Early treated Parkinson's disease patients had greater motor impairment than early *de novo* Parkinson's disease patients and healthy controls. Early treated Parkinson's disease patients had greater global non-motor symptoms impairment compared to healthy controls (MDS-UPDRS Part-I, Part-I quest, NMSS, P<0.05), with worse constipation (P<0.05), sleep (PDSS, ESS, RBQS, P<0.05) autonomic (SCOPA-AUT, P<0.05) and olfactory (UPSIT, P<0.05) dysfunction, and worse quality of life (PDQ-39, P<0.05). They also showed greater global non-motor symptoms impairment compared to early *de novo* Parkinson's patients (NMSS, P<0.05), with worse constipation (P<0.05), sleep (PDSS, P<0.05) and autonomic (SCOPA-AUT, P<0.05) dysfunction. Early treated Parkinson's

disease patients had worse depressive symptoms, although in the range of normality, compared to healthy controls (on both GDS and BDI-II, $P<0.05$) and to early *de novo* Parkinson's disease (on BDI-II, $P<0.05$).

Table 1. Demographic and clinical characteristics of cohorts of early *de novo* and early treated patients with idiopathic Parkinson's disease and healthy controls

	Healthy Controls (n=22)	Early *de novo* Parkinson's disease (n=17)	Early treated Parkinson's disease (n=15)
Demographic features			
Age, years	52.68 ± 14.97	58.97 ± 8.98	61.02 ± 5.49
Gender	16 M / 6 F	11 M / 6 F	8 M / 7 F
Disease duration, months	0 ± 0	12.74 ± 6.89	52.58 ± 11.73$^{\&}$
Year of Education	14.14 ± 1.83	13.12 ± 1.83	14.13 ± 1.77
Clinical characteristics			
LEDD	0 ± 0	0 ± 0	864.6 ± 435.59
Motor symptoms			
MDS-UPDRS Part-II	0 ± 0	7 ± 5.94*	14.93 ± 8.98*$^{\&}$
MDS-UPDRS Part-III	0 ± 0	23.29 ± 9.76*	47.47 ± 18.91*$^{\&}$
MDS-UPDRS Part-III Rigidity	0 ± 0	4.76 ± 1.64*	10.53 ± 5.87*$^{\&}$
MDS-UPDRS Part-III Bradykinesia	0 ± 0	11.06 ± 5.85*	25.27 ± 11.23*$^{\&}$
MDS-UPDRS Part-III Resting Tremor	0 ± 0	3.94 ± 2.95*	3.27 ± 3.88*
MDS-UPDRS Part-III Axial symptoms	0 ± 0	1.24 ± 1.48*	6.53 ± 3.85*
H&Y OFF	0 ± 0	1.12 ± 0.33*	2.47 ± 1.06*$^{\&}$
Schwab and England	100 ± 0	88.24 ± 14.57*	70 ± 6.55*$^{\&}$
Non-motor symptoms			
MDS-UPDRS Part-I	0.18 ± 0.39	1.47 ± 3.37	3.07 ± 2.46*
MDS-UPDRS Part-I questionnaire	1.41 ± 2.38	4.06 ± 4.31	8.47 ± 5.11*$^{\&}$
NMSS	3.95 ± 6.75	24.76 ± 26.53*	57.47 ± 34.61*$^{\&}$
Modified Constipation Assessment Scale	0.55 ± 1.18	4.06 ± 4.63*	6.87 ± 6.31*$^{\&}$
PDSS	130.09 ± 14.21	117.76 ± 16.77	102.33 ± 16.91*$^{\&}$
ESS	4.59 ± 2.61	5.65 ± 5.17	8.2 ± 4.8*
RBQS	0.82 ± 1.44	2.12 ± 1.96	2.67 ± 2.69*
Parkinson Fatigue Scale	5.77 ± 9.73	7.59 ± 18.19	12.93 ± 16.78
SCOPA-AUT	3.32 ± 2.46	8.12 ± 5.93*	13.93 ± 3.92*$^{\&}$
UPSIT	30.64 ± 5.46	18.41 ± 5.52*	17.8 ± 4.14*
Quality of Life			
PDQ-39	0.18 ± 0.59	20.06 ± 22.54*	27 ± 10.45*
Neuropsychological battery			
MMSE	29.27 ± 0.98	29.71 ± 0.69	29.47 ± 0.99
MoCA	28.59 ± 1.3	28.41 ± 2	27.53 ± 1.6
GDS	1.82 ± 1.76	4.35 ± 4.06	7.67 ± 6.07*
BDI-II	1.23 ± 1.54	6.47 ± 8.91*	8 ± 5.17*

Continuous variables are expressed as mean ± standard deviation. Abbreviations: F=Female: M=Male: LEDD=Levodopa Equivalent Daily Dosage; MDS-UPDRS=Movement Disorder Society-sponsored revision of the Unified Parkinson's Disease Rating Scale; H&Y=Hoehn and Yahr; NMSS=Non-motor Symptoms Scale; PDSS=Parkinson's Disease Sleep Scale; ESS=Epworth Sleepiness Scale; RBQS= REM Sleep Behaviour Sleep Disorder Questionnaire; SCOPA-AUT= Scales for Outcomes in PD-Autonomic dysfunction; UPSIT= University of Pennsylvania Smell Identification Test; PDQ-39=39-item Parkinson's Disease Questionnaire; MMSE=Mini Mental Status Examination; MoCA=Montreal Cognitive Assessment; GDS=Geriatric Depression Scale; BDI-II=Beck Depression Inventory-II. P value vs. healthy controls Bonferroni post-hoc corrected. *P <0.05 vs. healthy controls, $^{\&}$P <0.05 vs. early *de novo* Parkinson's disease patients.

3.2 PDE10A and early Parkinson's disease

3.2.1 Introduction

PDE10A is a striatal enzyme expressed in the axons of the medium spiny neurons, where it hydrolyses cAMP and cGMP (Fujishige *et al.*, 1999; Coskran *et al.*, 2006). In the striatal pathways, PDE10A plays a pivotal role in the regulation of dopaminergic signalling (Nishi *et al.*, 2008) and of several other brain functions, ranging from ion conductance to synaptic plasticity (Girault, 2012).

Preclinical studies have suggested an early role for PDE10A in the development of Parkinson's disease. A lesion of the nigrostriatal dopaminergic projections with 6-OHDA increased cAMP levels in the caudate and putamen of rats (Hossain and Weiner, 1993). In 6-OHDA lesioned rats, PDE10A protein levels and mRNA levels were reduced in the caudate-putamen and striatal projections (Giorgi *et al.*, 2011). In an another experimental model of Parkinson's disease, PDE10A inhibitors had an anti-cataleptic effect during a depletion of dopamine release induced by reserpine, which suggests a therapeutic perspective in Parkinson's disease (Megens *et al.*, 2014).

A recent imaging study has been performed in Parkinson's disease patients, investigating PDE10A expression by using [^{11}C]IMA107 PET imaging in 24 moderate-advanced Parkinson's disease patients (Niccolini *et al.*, 2015a). Parkinson's disease patients showed lower [^{11}C]IMA107 binding in the caudate, putamen and globus pallidus compared to healthy controls. Longer Parkinson's disease duration and higher Unified Parkinson's Disease Rating Scale part-III motor scores correlated with lower [^{11}C]IMA107 binding in the caudate, putamen, and globus pallidus. Higher Unified Dyskinesia Rating Scale scores in those Parkinson's disease with levodopa-induced dyskinesias correlated with lower [^{11}C]IMA107 binding in the caudate and putamen. This provides evidence for the role of PDE10A within the striatum in the development of cardinal motor symptoms in Parkinson's disease. Interestingly, a decline in PDE10A expression within the globus pallidus correlated with worse axial signs including the freezing of gait, falls and imbalance (Niccolini *et al.*, 2015a). Therefore, PDE10A,

as an enzyme regulating striatal output and dopaminergic signalling, shows promise to serve as a marker of disease burden in patients with early Parkinson's disease. However, it is unknown whether PDE10A is implicated at the earlier stages of the disease.

We hypothesized that the failure of dopamine to activate properly post-synaptic striatal neurons (which is associated with the development of motor symptoms in Parkinson's disease) might not be due only to a deficit of dopamine release (consequence of SNpc cell loss) but also due to a primary dysregulation of PDE10A expression, with a reduction below the physiological levels. This would be associated with an increased level of cAMP, which mimics the condition induced by the 6-OHDA in animal models of Parkinson's disease, and could potentially be a pathogenic mechanism fundamental to the dysfunction of second messenger signaling associated with the development of motor symptoms typical of Parkinson's disease. Thus, loss of PDE10A expression could be one of the earliest pathophysiological events in the course of Parkinson's disease, even earlier that DAT terminal loss.

Using molecular imaging, we aimed to investigate the role of PDE10A in the early stages of the Parkinson's disease with the main hypothesis that a reduction of PDE10A expression is an early phenomenon in the course of Parkinson's disease, and that PDE10A expression decreases further as Parkinson's disease progress (in term of duration and clinical severity). We have investigated this in the Project 1, in which, by using [^{11}C]IMA107 PET imaging, we assessed *in vivo* the integrity of PDE10A enzyme in early *de novo* and in a population of early levodopa-treated patients with three-year longer Parkinson's disease duration in relation to a group of age- and sex-matched healthy controls.

We also hypothesize that PDE10A expression might be affected earlier on in the course of the disease, investigating the associations between PDE10A and non-motor symptoms considered pre-motor (sleep problems, autonomic dysfunction, mood disorders etc).

Here, we used PET with [^{11}C]IMA107 to assess PDE10A expression and to explore for associations with clinical markers of disease burden in patients with early Parkinson's disease including those who have never been treated with dopaminergic medications.

3.2.2 Hypothesis

The main hypothesis that a reduction of PDE10A expression is an early phenomenon in the course of Parkinson's disease, and that PDE10A expression decreases further as Parkinson's disease progress (in term of duration and clinical severity). We have investigated this in the Project 1, in which, by using [^{11}C]IMA107 PET imaging, we assessed *in vivo* the integrity of PDE10A enzyme in early *de novo* and early levodopa-treated patients with Parkinson's disease compared to age- and sex-matched healthy control subjects.

We aim to test this hypothesis comparing the expression of PDE10A (measured by using [^{11}C]IMA107 PET imaging) in early *de novo* and early levodopa-treated patients with Parkinson's disease versus age- and sex-matched healthy control subjects (*Project 1 Aim*).

We also hypothesize that PDE10A expression might be affected earlier on in the course of the disease investigating the associations between PDE10A and non-motor symptoms considered pre-motor (sleep problems, autonomic dysfunction, mood disorders etc).

We aim to test this hypothesis checking for correlations between the expression of PDE10A and non-motor symptoms considered pre-motor (sleep problems, autonomic dysfunction, mood disorders etc).

3.2.3 Methods

We enrolled 60 participants recruited from specialist Movement Disorders clinics at King's College Hospital, and through public advertisement, of which 54 subjects completed the study and were

included in the analyses (Table 1). We included 32 patients with idiopathic Parkinson's disease according to the Queen Square Brain Bank criteria, and 22 age- and gender-matched healthy individuals with no history of neurological or psychiatric disorders, who served as the control group *(healthy controls)*. Parkinson's disease patients included 17 subjects with a recent diagnosis (duration of symptoms ≤24 months) who were naïve to treatment for Parkinson's symptoms *(de novo)*, and 15 subjects with early Parkinson's disease (duration of symptoms ≤60 months) who were recently treated with levodopa (duration of treatment ≤24 months) and had no motor complications *(early levodopa-treated)*. None of the Parkinson's disease patients fulfilled the diagnostic criteria for Parkinson's disease MCI (Litvan *et al.*, 2011) or dementia (Emre *et al.*, 2007) or depression (Marsh *et al.*, 2006), had any history of other neurological or psychiatric disorders, and were not under treatment with substances with known actions in PDEs (e.g. apremilast, cilomilast, luteolin, piclamilast, roflumilast and ibudilast).

Motor symptom severity was assessed with the MDS-UPDRS-III and staged with H&Y scale. MDS-UPDRS-III subscores for rigidity, bradykinesia, tremor and axial symptoms were calculated as previously described (Niccolini *et al.*, 2015a). Quality of life was measured with the PDQ-39. Neuropsychiatric symptoms were assessed with the Beck Depression Inventory second edition BDI-II. MMSE and MoCA were used to assess general cognitive status. Disability was assessed by Modified Schwab and England Activities of Daily Living Scale. NMSS for Parkinson's disease was used to assess non-motor symptoms (Pagano *et al.*, 2016a).

The study was approved by the institutional review boards and the research ethics committee. Written informed consent was obtained from all study participants in accordance with the Declaration of Helsinki.

Scanning procedures

All participants were screened successfully to undertake PET with [^{11}C]IMA107, and one 3-Tesla MRI scanning under standard criteria (http://www.mrisafety.com; https://www.gov.uk/government/publications/arsac-notes-for-guidance). PET and MR imaging have been performed at Imanova Ltd, London, UK. All participants were scanned on Siemens Biograph Hi-Rez 6 PET-CT scanner (Erlangen, Germany).

Dynamic emission data [^{11}C]IMA107 PET data were acquired continuously for 90 minutes after the injection of [^{11}C]IMA107 at a target dose of 350 MBq administered intravenously as a slow bolus injection over 20 seconds, no saline flush. All participants were scanned after withholding consumption of caffeinated beverages for 12 hours (Fredholm *et al.*, 1999b). A reference region devoid of specific PDE10A activity has been validated; therefore, arterial cannulation was not required for [^{11}C]IMA107 PET. The dynamic images were reconstructed into 26 frames (8 x 15s, 3 x 60s, 5 x 120s, 5 x 300s, and 5 x 600s), using a filtered back projections algorithm (direct inversion Fourier transform) with a 128 matrix, zoom of 2.6 producing images with isotropic voxel size of 2 x 2 x 2 mm3, and smoothed with a transaxially Gaussian filter of 5mm. MRI scans were acquired with a 32-channel head coil on a 3-Tesla MRI Siemens Magnetom TrioTim syngo MR B17 (Erlangen, Germany) scanner, and included a T1-weighted magnetization prepared rapid gradient echo sequence [MPRAGE; time repetition (TR) = 2300 ms, time echo (TE) = 2.98 ms, flip angle of 9°, time to inversion (TI) = 900 ms, matrix = 240 x 256] for co-registration with the PET images; fast grey matter T1 inversion recovery (FGATIR; repetition time = 3000 ms, echo time = 2.96 ms, flip angle of 8, time to inversion = 409 ms, matrix = 240 x 256) (Sudhyadhom *et al.*, 2009) sequences for delineation of regions-of-interest. All MRI sequences used a 1 mm^3 voxel size, anteroposterior phase encoding direction, and a symmetric echo.

Imaging data analysis

[^{11}C]IMA107 data analysis

The Molecular Imaging and Kinetic Analysis Toolbox software package (MIAKAT^{TM}: www.miakat.org), implemented in MATLAB® (The Mathworks, Natick, MA, USA) was used to carry out image processing and kinetic modelling. MIAKAT™ combines in-house code with wrappers for FMRIB Software Library (FSL, http://fsl.fmrib.ox.ac.uk/fsl/fslwiki/) and Statistical Parametric Mapping (SPM, http://www.fil.ion.ucl.ac.uk/spm/) commands in order to provide state-of-the-art functionality within a coherent analysis framework. The MIAKAT™ processing pipeline was followed, ensuring that all quality control steps were completed to generate parametric images and regional estimates of [^{11}C]IMA107 BP_{ND}. BP_{ND} were generated using a basis function implementation of the simplified reference tissue model, with the cerebellum as the reference tissue for non-specific binding. Individual PET frames were corrected for head motion using frame-by-frame rigid registration using a frame with high signal-to-noise ratio as reference. PET images were co-registered to the corresponding MPRAGE MRI.

Region of interest-based analysis

To facilitate anatomical delineation of regions of interest, PET images were anatomically co-registered and re-sliced to the corresponding volumetric structural T1-weighted MRI images in Statistical Parametric Mapping version12 (SPM12) software package implemented in Matlab 2015a. Regions of interest were delineated manually on the T1 co-registered FGATIR MRI sequence using ANALYZE version 12.0 (Mayo Foundation) medical imaging software package by two assessors who were blinded to groups allocation, using used a reliable, robust and repeatable technique for manual delineation of basal ganglia structures (Tziortzi *et al.*, 2011a). Regions of interest included caudate, putamen, ventral striatum, globus pallidus (external and internal segments), substantia nigra

and motor thalamic nuclei. These brain regions express PDE10A to a varying degree (Seeger *et al.*, 2003; Coskran *et al.*, 2006).

Statistical analysis

Statistical analysis and graph illustration were performed with SPSS (version 22) and GraphPad Prism (version 6.0c) for Windows 10, respectively. For all variables, Gaussianity was tested with Shapiro-Wilk test and we proceeded with parametric tests as our PET and clinical data were normally distributed. Multivariate analysis of variance (MANOVA) was used to assess the main effects of regional [^{11}C]IMA107 BP_{ND} among the groups. If the overall multivariate test was significant, *P*-values for each variable were calculated following Bonferroni's multiple comparisons test. We interrogated correlations between PET and clinical data using Spearman rho and we applied Benjamini-Hochberg correction to reduce false discovery rate(Benjamini and Cohen, 2017). We set the false discovery rate cut-off at 0.05. All data are presented as mean ± standard deviation, and the level α was set for all comparisons at $P<0.05$, corrected.

3.2.4 Results

A mean dose of 276.05 ± 48.35, 278.39 ± 33.51 and 310.43 ± 16.93 [^{11}C]IMA107 MBq was respectively administered in healthy controls, early *de novo* and early treated Parkinson's patients. The results of [^{11}C]IMA107 BP_{ND} in healthy controls, early *de novo* and treated Parkinson's disease patients are shown in Table 2.

Early *de novo* patients with Parkinson's disease had lower mean [^{11}C]IMA107 BP_{ND} values in caudate ($P<0.001$), putamen ($P<0.001$) and ventral striatum ($P<0.05$) compared to healthy controls. There were no differences in mean [^{11}C]IMA107 BP_{ND} values between early *de novo* Parkinson's disease

patients and healthy controls in globus pallidus internal (P>0.10), globus pallidus external (P>0.10), substantia nigra (P>0.10) and thalamus (P>0.10).

Table 2. [^{11}C]IMA107 BP_{ND} in early *de novo* and early treated patients with idiopathic Parkinson's disease compared to healthy controls

	Healthy Controls (n=22)	Early *de novo* Parkinson's disease (n=17)	Early treated Parkinson's disease (n=15)
[^{11}C]IMA107 BP_{ND}			
Dose injected (MBq)	276.05 ± 48.35	278.39 ± 33.51	310.43 ± 16.93
Caudate	1.43 ± 0.18	0.91 ± 0.13*	0.75 ± 0.08*$^{\&}$
Putamen	2.17 ± 0.24	1.91 ± 0.14*	1.73 ± 0.18*$^{\&}$
Ventral Striatum	1.79 ± 0.32	1.49 ± 0.27*	1.37 ± 0.25*
Globus Pallidus Internal	1.62 ± 0.2	1.54 ± 0.16	1.49 ± 0.22
Globus Pallidus External	1.99 ± 0.25	1.88 ± 0.21	1.83 ± 0.23
Substantia Nigra	0.59 ± 0.09	0.62 ± 0.07	0.66 ± 0.13
Thalamus	0.6 ± 0.06	0.57 ± 0.09	0.59 ± 0.09

Continuous variables are expressed as mean ± standard deviation. Abbreviations: BP_{ND}= Non-displaceble binding potential;. P value vs. healthy controls Bonferroni post-hoc corrected. *P <0.05 vs. healthy controls, $^{\&}$P <0.05 vs. early *de novo* Parkinson's disease patients.

Early treated patients with Parkinson's disease had lower mean [^{11}C]IMA107 BP_{ND} values in caudate (P<0.001), putamen (P<0.001) and ventral striatum (P<0.05) compared to healthy controls. There were no differences in mean [^{11}C]IMA107 BP_{ND} values between early treated Parkinson's disease patients and healthy controls in globus pallidus internal (P>0.10), globus pallidus external (P>0.10), substantia nigra (P>0.10) and thalamus (P>0.10) (Figure 6).

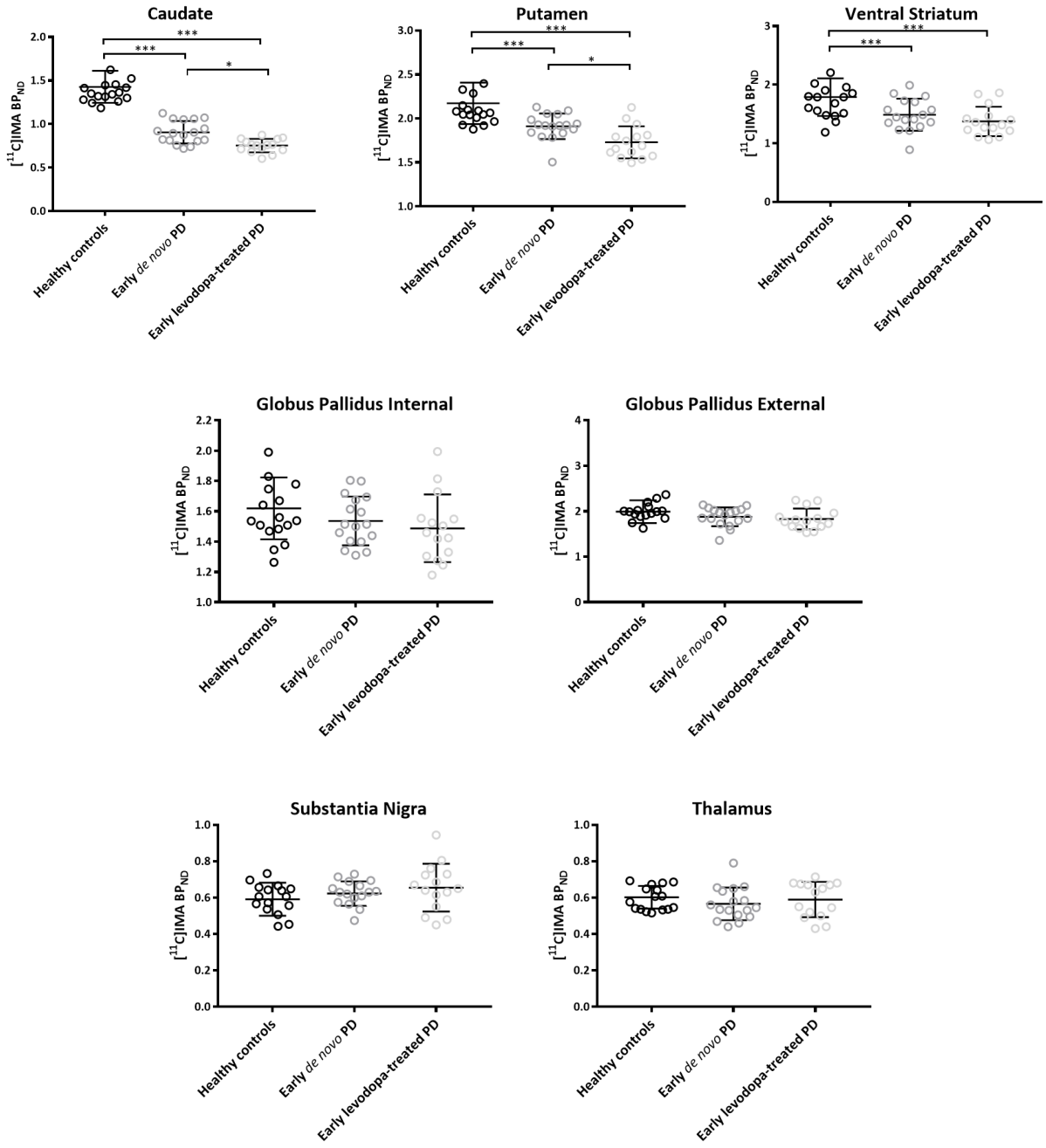

Figure 6. PDE10A expression in the groups of Parkinson's disease (PD) patients and healthy controls. *Dot plot graphs showing mean [^{11}C]IMA107 BP_{ND} ± standard deviation in subcortical brain regions in PD early de novo patients, PD early levodopa-treated patients and healthy controls. *P <0.05, **P <0.01, ***P <0.001 ANOVA with Bonferroni post-hoc correction*

Compared to early *de novo* Parkinson's disease patients, early levodopa-treated patients with Parkinson's disease showed additional [^{11}C]IMA107 BP_{ND} loss of 17.2% (SD: 8.4%) in the caudate

(*P*<0.001; reflecting a 5.7% mean annual decline) and 9.5% (SD: 9.6%) in the putamen (*P*<0.001; reflecting a 3.2% mean annual decline) (Figure 7).

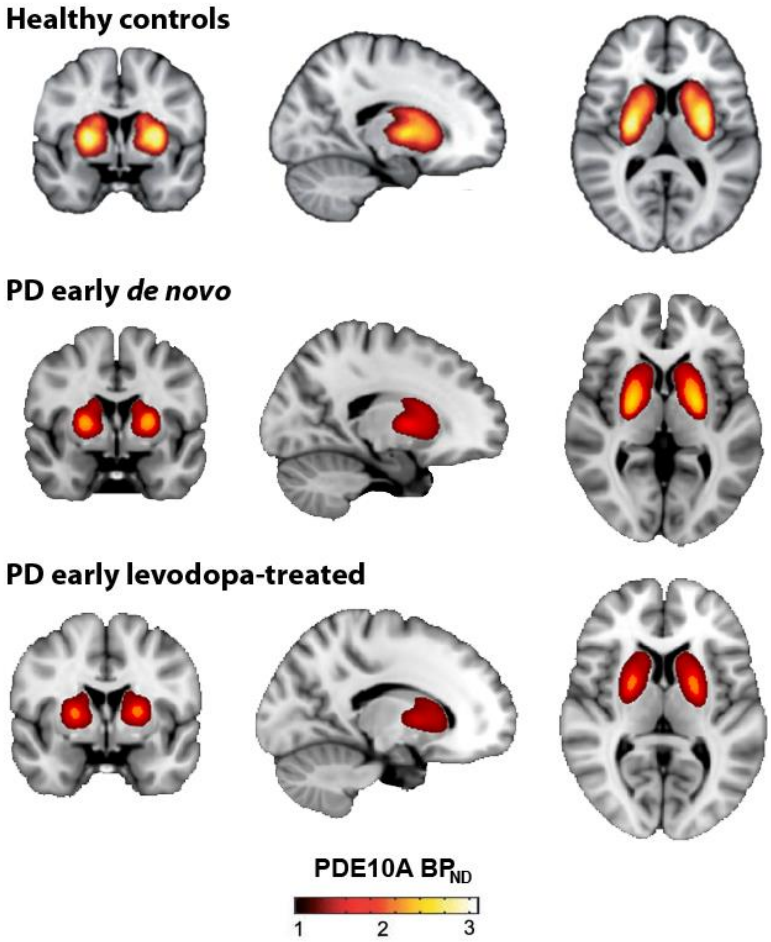

Figure 7. Altered PDE10A expression in anatomically defined brain regions of Parkinson's disease patients. *Axial, sagittal and coronal (MNI co-ordinates: x = 19, y = −8, z = 4) mean summed PET images derived from (top) 22 healthy controls, (middle) 17 Parkinson's disease early de novo and (bottom) Parkinson's disease early levodopa-treated patients in stereotaxic space showing progressive loss of [^{11}C]IMA107 BP_{ND} in PD. Colour bar reflects range of [^{11}C]IMA107 BP_{ND} intensity.*

Furthermore, longer Parkinson's disease duration correlated with lower [^{11}C]IMA107 BP_{ND} in the caudate (*rho*=-0.72; *P*<0.001) and putamen (*rho*=-0.48; *P*<0.01) (Figure 8).

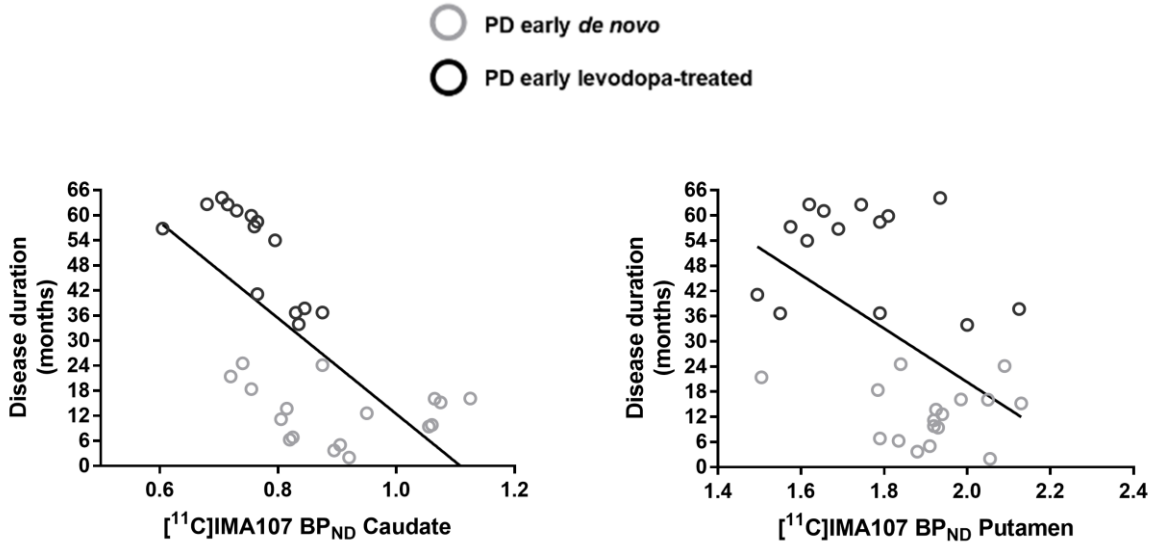

Figure 8. Correlations between PDE10A and disease duration in Parkinson's disease (PD) patients. *Spearman correlation between disease duration and [^{11}C]IMA107 (left) in the caudate (rho=-0.72; P<0.001) and (right) in the putamen (rho=-0.48; P<0.01). PD early de novo in black circles and PD early levodopa-treated in grey circles.*

Compared to early *de novo*, early treated Parkinson's patients showed greater rigidity and bradykinesia (higher scores in MDS-UPDRS Part-III Rigidity and Bradykinesia, P<0.05), but similar scores in resting tremor and axial symptoms.

In term of lateralization, in the group of early *de novo* patients with Parkinson's disease with unilateral motor symptoms, we assessed whether the clinically affected side of the body was associated with greater decreases in contralateral brain regions of interest [^{11}C]IMA107 BP_{ND} values. We found no differences in [^{11}C]IMA107 BP_{ND} values in any of the regions of interest between the most and less affected side.

When the group of early *de novo* and early treated Parkinson's patients were evaluated as a whole, higher MDS-UPDRS-III total scores correlated with lower [^{11}C]IMA107 BP_{ND} in the caudate (*rho*=-0.42; *P*<0.05) and putamen (*rho*=-0.41; *P*<0.05). Higher MDS-UPDRS-III rigidity scores correlated with lower [^{11}C]IMA107 BP_{ND} in the caudate (*rho*=-0.52; *P*<0.01) and putamen (*rho*=-0.43; *P*<0.05).

Higher MDS-UPDRS-III bradykinesia scores correlated with lower [^{11}C]IMA107 BP_{ND} in the caudate (*rho*=-0.45; *P*<0.01) and putamen (*rho*=-0.47; *P*<0.01). No correlations were found with MDS-UPDRS-III resting tremor or axial scores (Figure 9).

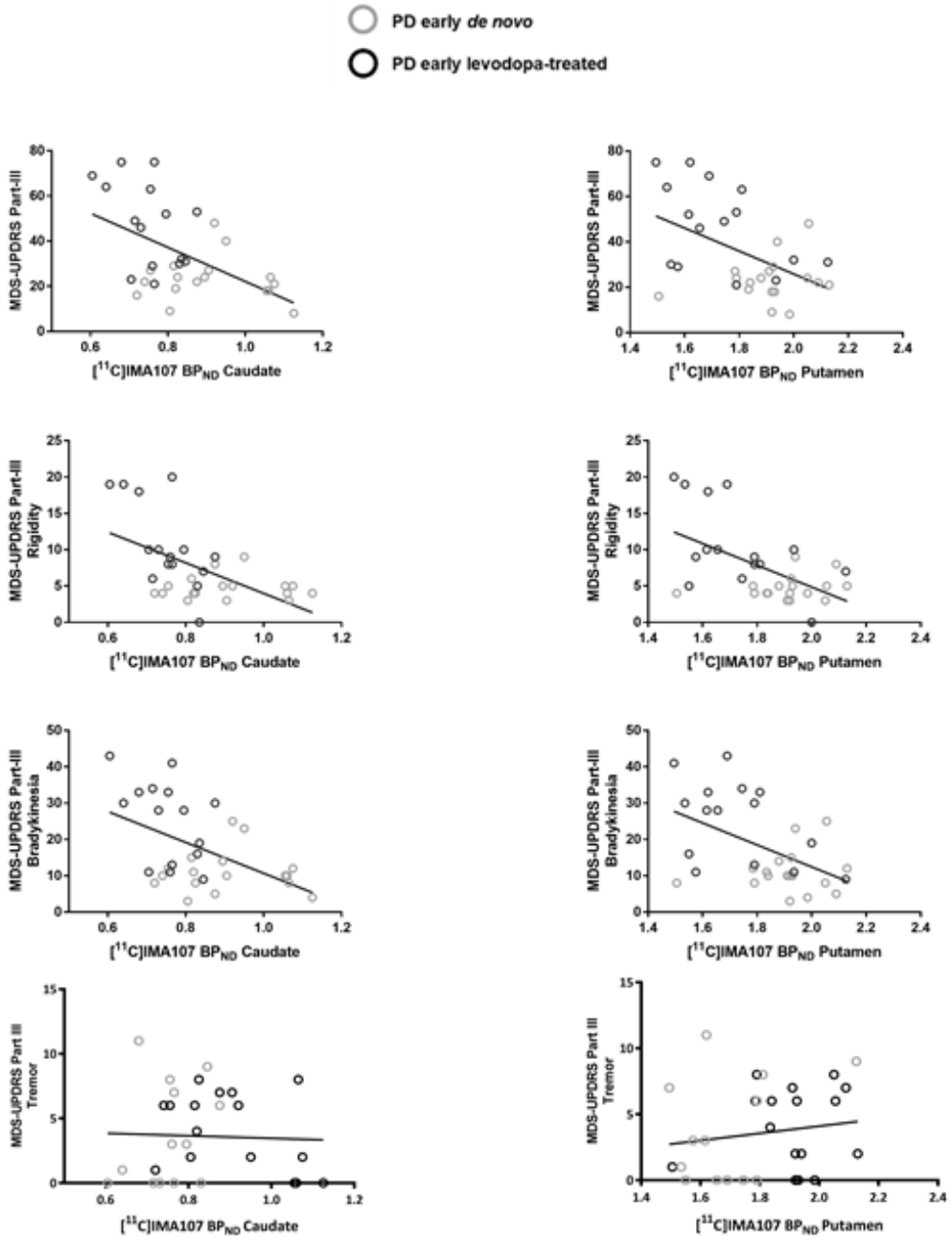

Figure 9. Correlations between PDE10A to motor symptoms in Parkinson's disease (PD) patients. *Spearman correlation between MDS-UPDRS-III motor scores (first line) and [^{11}C]IMA107 BP_{ND} in the caudate (rho=-0.42;*

P<0.05) and putamen (rho=-0.41; P<0.05). Correlation between MDS-UPDRS-III rigidity subscores (second line) and [^{11}C]IMA107 BP_{ND} in the caudate (rho=-0.515; P=0.003) and putamen (rho=-0.432; P=0.014). Correlation between MDS-UPDRS-III bradykinesia subscores (third line) and [^{11}C]IMA107 BP_{ND} in caudate (rho=-0.448; P=0.010) and putamen (rho=-0.467 ; P=0.007). No correlation between MDS-UPDRS-III tremor subscores (forth line) and [^{11}C]IMA107 BP_{ND} in caudate (rho=0.085; P>0.10) and putamen (rho=0.127 ; P>0.10). PD early de novo in black circles and PD early levodopa-treated in grey circles.

In the subgroup of early *de novo* patients with Parkinson's disease, higher MDS-UPDRS-III total scores correlated only with lower [^{11}C]IMA107 BP_{ND} in the ventral striatum (*rho*=-0.54; *P*<0.05), and no correlations were found with caudate (*P*>0.10), putamen (*P*>0.10), globus pallidus internal (*P*>0.10), globus pallidus external (*P*>0.10), substantia nigra (*P*>0.10) and thalamus (*P*>0.10). No correlations were found with MDS-UPDRS-III rigidity, bradykinesia, resting tremor or axial scores.

In the subgroup of early treated patients with Parkinson's disease, higher MDS-UPDRS-III total scores correlated only with lower [^{11}C]IMA107 BP_{ND} in the globus pallidus external (*rho*=-0.57; *P*<0.05) and in the substantia nigra (*rho*=-0.713; *P*<0.05), and no correlations were found with caudate (*P*>0.10), putamen (*P*>0.10), ventral striatum (*P*>0.10), globus pallidus internal (*P*>0.10) and thalamus (*P*>0.10). Higher MDS-UPDRS-III rigidity scores correlated with lower [^{11}C]IMA107 BP_{ND} in the caudate (*rho*=-0.57; *P*<0.01), putamen (*rho*=-0.54; *P*<0.05) and globus pallidus external (*rho*=-0.54; *P*<0.05). Higher MDS-UPDRS-III bradykinesia and axial scores correlated with lower [^{11}C]IMA107 BP_{ND} in the substantia nigra (bradykinesia: *rho*=-0.57; *P*<0.05; axial: *rho*=-0.52; *P*<0.05). No correlations were found with MDS-UPDRS-III resting tremor.

No correlations were found with global non-motor symptoms (MDS-UPDRS-I, MDS-UPDRS Part-I questionnaire or NMSS), constipation (Modified Constipation Assessment Scale), sleep (PDSS,

ESS, RBQS), fatigue (Parkinson Fatigue Scale), autonomic dysfunction (SCOPA-AUT), olfaction (UPSIT), quality of life (PDQ-39) when the group of early *de novo* and early treated Parkinson's patients were evaluated as a whole or when evaluated as subgroups.

No correlations were found with cognitive impairment (MMSE, MoCA) or depression (GDS, BDI-II) when the group of early *de novo* and early treated Parkinson's patients were evaluated as a whole or when evaluated as subgroups.

3.2.5 Discussion

Our hypothesis was that a reduction of PDE10A expression is an early phenomenon in the course of Parkinson's disease, and that PDE10A expression decreases further as Parkinson's disease progress (in term of duration and clinical severity).

We aimed to test this hypothesis comparing the expression of PDE10A (measured by using [^{11}C]IMA107 PET imaging) in early *de novo* and early levodopa-treated patients with Parkinson's disease versus age- and sex-matched healthy control subjects (*Project 1 Aim*).

We found that early *de novo* and early levodopa-treated patients with Parkinson's disease had lower mean [^{11}C]IMA107 BP_{ND} values in caudate, putamen and ventral striatum compared to healthy controls. Early levodopa-treated patients had lower striatal [^{11}C]IMA107 BP_{ND} values compared to early *de novo* patients, and striatal [^{11}C]IMA107 BP_{ND} values were correlated with disease duration and disease severity.

Our findings demonstrate our hypothesis that loss of striatal PDE10A expression is an early phenomenon in the course of Parkinson's disease and is associated with duration and severity of motor symptoms. Our study agrees with previous experimental work, which has demonstrated that

lesions of nigrostriatal projections with 6-OHDA, induce a downregulation of PDE10A expression in the striatum in rodent models of Parkinson's disease (Giorgi *et al.*, 2008; Giorgi *et al.*, 2011).

We also hypothesize that PDE10A expression might be affected earlier on in the course of the disease investigating the associations between PDE10A and non-motor symptoms considered pre-motor (sleep problems, autonomic dysfunction, mood disorders etc). We aimed to test this hypothesis checking for correlations between the expression of PDE10A and non-motor symptoms considered pre-motor (sleep problems, autonomic dysfunction, mood disorders etc). PDE10A expression did not correlate with non-motor symptoms considered pre-motor (sleep problems, autonomic dysfunction, mood disorders etc), which suggests that reduction of PDE10A might be concomitant and not earlier than DAT expression loss. Thus, we cannot accept this hypothesis.

We used PET molecular imaging to quantify PDE10A expression in the same cohorts of Parkinson's disease patients and healthy controls. In both early *de novo* and early levodopa-treated patients with Parkinson's disease PDE10A expression was decreased in the striatum. Our early *de novo* cohort of Parkinson's disease patients had less than two year of disease duration and the cohort of early levodopa-treated less than five year of Parkinson's symptoms and were taking levodopa for less than two years. Previously, we have reported loss of striatal PDE10A expression and correlations with the burden of motor symptoms and complications in middle-stage treated Parkinson's disease patients with a mean of seven years of disease duration and advanced treated Parkinson's disease patients with a mean of 13 years of disease duration (Niccolini *et al.*, 2015a). Collectively, our data suggest that loss of striatal PDE10A expression appears very early in the course of Parkinson's disease, might progresses over time, and is associated with the gradual increase of motor symptom burden in different disease stages. Our findings suggest that loss of PDE10A expression in globus pallidus is a phenomenon appearing later in the disease (Niccolini *et al.*, 2015a) as PDE10A expression in this

region was not affected in the earlier cohorts. Our findings were not affected by volumetric changes in the brain, age or gender.

3.2.6 Conclusion

Our findings demonstrate loss of PDE10A expression very early in the course of Parkinson's disease that might progresses over time and is associated with the gradual increase of motor symptom burden in different disease stages. However, we cannot draw any conclusion regarding the relationship between PDE10A and DAT expression, which represents the main pathological process underlying Parkinson's disease.

We aim to investigate the relationship between PDE10A and DAT expression in the Project 2.

Chapter 4. DAT SPECT and PET in Parkinson's Disease

This chapter summarizes the main results on the *in vivo* evaluation of the integrity of PDE10A expression in comparison to DAT (measured with [^{123}I]FP-CIT SPECT and [^{11}C]PE2I PET imaging) in early *de novo* Parkinson's disease patients compared to age- and sex-matched healthy control subjects. The integrity of DAT in early *de novo* Parkinson's disease patients was then compared to early levodopa-treated Parkinson's disease patients, evaluating how PET and SPECT measures of DAT changes are associated with disease duration and severity. Finally, the associations between the motor (tremor, rigidity, bradykinesia and postural instability) and non-motor symptoms (sleep problems, cognitive impairment, autonomic dysfunction, mood disorders etc) and the expression of DAT PET and SPECT have been explored and described in detail.

4.1.1 Introduction

Previous PET imaging studies have shown that changes in the molecular binding profile of selected brain targets may serve as promising markers of disease burden and progression, drug target identification and treatment response in therapeutic trials in patients with Parkinson's disease (Politis, 2014). Loss of DAT signal in Parkinson's disease patients reflects loss of nigrostriatal dopamine neurons and is typically associated with dopaminergic pathology in the putamen and the motor features of bradykinesia and rigidity (Pirker, 2003). However, molecular imaging of DAT cannot be considered an ideal biomarker for Parkinson's disease due to several limitations, including a lack of specificity for Parkinson's compared to atypical parkinsonism, and the fact that dopaminergic supplementation may modulate DAT levels, limiting its use as biomarker for clinical trials testing disease-modification drugs (Fahn *et al.*, 2004; Schapira, 2013). DAT expression can be measured with several tracers but [^{11}C]PE2I PET and [^{123}I]FP-CIT SPECT represents the most different ones because the two tracers have a different affinity for the DAT ([^{11}C]PE2I is more specific of DAT where [^{123}I]FP-CIT binds both DAT and SERT). This allows to investigate dopaminergic but also in part non-dopaminergic pathology.

PDE10A is a striatal enzyme expressed in the axons of the medium spiny neurons, where it hydrolyses cAMP and cGMP (Fujishige *et al.*, 1999; Coskran *et al.*, 2006). In the striatal pathways, PDE10A plays a pivotal role in the regulation of dopaminergic signalling (Nishi *et al.*, 2008) and of several other brain functions, ranging from ion conductance to synaptic plasticity (Girault, 2012). Recent work with PET molecular imaging has demonstrated loss of PDE10A expression in moderate to advanced levodopa-treated patients with Parkinson's disease, which was associated with motor symptoms and complications (Niccolini *et al.*, 2015a). Therefore, PDE10A, as an enzyme regulating striatal output and dopaminergic signalling, shows promise to serve as a marker of disease burden in

patients with early Parkinson's disease. However, it is unknown whether PDE10A is implicated at the earlier stages of the disease and how its biomarker value compares with the gold standard DAT molecular imaging.

Here, we used PET with [^{11}C]IMA107 to assess PDE10A expression in comparison with two DAT markers, the [^{11}C]PE2I PET imaging, and the clinical validated [^{123}I]FP-CIT SPECT imaging. We explored for associations with clinical markers of disease burden in patients with early Parkinson's disease including those who have never been treated with dopaminergic medications.

4.1.2 Hypothesis

We hypothesize that PDE10A expression was correlated with dopaminergic pathology, which can be measured either with PET or SPECT. We have investigated this in the Project 2, in which we compared the expression of PDE10A, measured with [^{11}C]IMA107 PET imaging, with the best known molecular markers of dopaminergic dysfunction in Parkinson's patients, the [^{11}C]PE2I PET imaging, and the clinical validated [^{123}I]FP-CIT SPECT imaging. We aim to test this hypothesis checking for correlations between the expression of PDE10A and the expression of dopamine transporters (measured by using [^{11}C]PE2I PET and [^{123}I]FP-CIT SPECT molecular imaging) (*Project 2 Aim*). In this Project, we also compared [^{11}C]PE2I PET versus [^{123}I]FP-CIT SPECT because the two tracers have a different affinity for the DAT ([^{11}C]PE2I is more specific of DAT where [^{123}I]FP-CIT binds both DAT and SERT). This would give us a greater understanding of the relationship between PDE10A expression and dopaminergic and non-dopaminergic pathology.

4.1.3 Methods

We enrolled 60 participants recruited from specialist Movement Disorders clinics at King's College Hospital, and through public advertisement, of which 54 subjects completed the study and were included in the analyses (Table 1). We included 32 patients with idiopathic Parkinson's disease according to the Queen Square Brain Bank criteria, and 22 age- and gender-matched healthy individuals with no history of neurological or psychiatric disorders, who served as the control group *(healthy controls)*. Parkinson's disease patients included 17 subjects with a recent diagnosis (duration of symptoms ≤24 months) who were naïve to treatment for Parkinson's symptoms *(de novo)*, and 15 subjects with early Parkinson's disease (duration of symptoms ≤60 months) who were recently treated with levodopa (duration of treatment ≤24 months) and had no motor complications *(early levodopa-treated)*. None of the Parkinson's disease patients fulfilled the diagnostic criteria for Parkinson's disease MCI (Litvan *et al.*, 2011) or dementia (Emre *et al.*, 2007) or depression (Marsh *et al.*, 2006), had any history of other neurological or psychiatric disorders, and were not under treatment with substances with known actions in PDEs (e.g. apremilast, cilomilast, luteolin, piclamilast, roflumilast and ibudilast).

Motor symptom severity was assessed with the MDS-UPDRS-III and staged with H&Y scale. MDS-UPDRS-III subscores for rigidity, bradykinesia, tremor and axial symptoms were calculated as previously described (Niccolini *et al.*, 2015a). Quality of life was measured with the PDQ-39. Neuropsychiatric symptoms were assessed with the Beck Depression Inventory second edition BDI-II. MMSE and MoCA were used to assess general cognitive status. Disability was assessed by Modified Schwab and England Activities of Daily Living Scale. NMSS for Parkinson's disease was used to assess non-motor symptoms (Pagano *et al.*, 2016a).

The study was approved by the institutional review boards and the research ethics committee. Written informed consent was obtained from all study participants in accordance with the Declaration of Helsinki.

Scanning procedures

All participants were screened successfully to undertake PET with [^{11}C]IMA107 and with [^{11}C]PE2I, one [^{123}I]FP-CIT DAT SPECT and one 3-Tesla MRI scanning under standard criteria(http://www.mrisafety.com; https://www.gov.uk/government/publications/arsac-notes-for-guidance). PET and MR imaging have been performed at Imanova Ltd, London, UK. All participants were scanned on Siemens Biograph Hi-Rez 6 PET-CT scanner (Erlangen, Germany). [^{11}C]IMA107 and [^{11}C]PE2I have been performed on the same day after withholding consumption of caffeinated beverages for 12 hours (Fredholm *et al.*, 1999a). [^{123}I]FP-CIT DAT SPECT scans were performed at KCH NHS Foundation Trust within 2 weeks from PET scans.

Dynamic emission data were acquired continuously for 90 minutes following the injection of [^{11}C]IMA107. The dynamic images were reconstructed into 26 frames (8 x 15 s, 3 x 60 s, 5 x 120 s, 5 x 300 s, and 5 x 600 s), using a filtered back projection algorithm (direct inversion Fourier transform) with a 128 matrix, zoom of 2.6 producing images with isotropic voxel size of 2 x 2 x 2 mm^3, and smoothed with a transaxial Gaussian filter of 5 mm. MRI scans were acquired with a 32-channel head coil on a 3-Tesla MRI Siemens Magnetom TrioTim syngo MR B17 (Erlangen, Germany) scanner, and included a T1-weighted magnetization prepared rapid gradient echo sequence [MPRAGE; time repetition (TR) = 2300 ms, time echo (TE) = 2.98 ms, flip angle of 9°, time to inversion (TI) = 900 ms, matrix = 240 x 256] for co-registration with the PET images; fast grey matter T1 inversion recovery (FGATIR; repetition time = 3000 ms, echo time = 2.96 ms, flip angle of 8, time to inversion = 409 ms, matrix = 240 x 256) (Sudhyadhom *et al.*, 2009) sequences for delineation

of regions-of-interest. All MRI sequences used a 1 mm^3 voxel size, anteroposterior phase encoding direction, and a symmetric echo.

Patients were given an intravenous injection of approximately 185 MBq [^{123}I]FP-CIT, with images obtained 4 hours post-injection. Data were acquired in a 128 x 128 matrix, using a 20% energy window and magnification x 2. All SPECT images were reconstructed on a HERMES workstation, using the HERMES Hybrid Recon™ - Neurology software. Reconstruction was performed using the 3D ordered-subset expectation maximum (OSEM) method, using 5 iterations with attenuation correction. Finally, a 3D Gaussian postfilter was applied with a 0·90cm FWHM. All iteratively reconstructed SPECT images were then transferred to BRASS™ software to quantify striatal tracer uptake. Patients SPECT images were fitted against a pre-existing three-dimensional reference template, containing a number of VOIs. The caudate, putamen and striatum specific uptake ratios were calculated using the occipital cortex as a reference region.

Imaging data analysis

[^{11}C]IMA107 and [^{11}C]PE2I PET data analysis

The Molecular Imaging and Kinetic Analysis Toolbox software package (MIAKAT^{TM}: www.miakat.org), implemented in MATLAB® (The Mathworks, Natick, MA, USA) was used to carry out image processing and kinetic modelling. MIAKAT™ combines in-house code with wrappers for FMRIB Software Library (FSL, http://fsl.fmrib.ox.ac.uk/fsl/fslwiki/) and Statistical Parametric Mapping (SPM, http://www.fil.ion.ucl.ac.uk/spm/) commands in order to provide state-of-the-art functionality within a coherent analysis framework. The MIAKAT™ processing pipeline was followed, ensuring that all quality control steps were completed to generate parametric images and regional estimates of [^{11}C]IMA107 and [^{11}C]PE2I BP_{ND}. BP_{ND} were generated using a basis function implementation of the simplified reference tissue model, with the cerebellum as the reference

tissue for non-specific binding. Individual PET frames were corrected for head motion using frame-by-frame rigid registration using a frame with high signal-to-noise ratio as reference. PET images were co-registered to the corresponding MPRAGE MRI.

[^{123}I]FP-CIT-SPECT Imaging analyses

[^{123}I]FP-CIT-SPECT was processed using Hybrid-Recon and Statistical Parametric Mapping 12 (SPM, Wellcome Trust Centre for Neuroimaging, London, UK) implemented in MATLAB (The Math-Works, Natick, MA, USA). [^{123}I]FP-CIT SPECT image volumes were spatially normalized to a FP-CIT template in MNI space. The eight most prominent axial slices containing the striatum were summed and a standardized VOI template was then applied to this image. VOI analyses were performed on the right and left caudate and putamen, employing the occipital region as the reference tissue. SBR was calculated as the ratio of the putamen or caudate VOI count density divided by the occipital cortex count density minus one. This measure approximates the binding potential, BP_{ND}, when the radioligand is in equilibrium at the target site and has previously been reported with [^{123}I]FP-CIT SPECT (Qamhawi *et al.*, 2015).

Region of interest-based analysis

To facilitate anatomical delineation of regions of interest, PET and SPECT images were anatomically co-registered and re-sliced to the corresponding volumetric structural T1-weighted MRI images in Statistical Parametric Mapping version12 (SPM12) software package implemented in Matlab 2015a. Regions of interest were delineated manually on the T1 co-registered FGATIR MRI sequence using ANALYZE version 12.0 (Mayo Foundation) medical imaging software package by two assessors who were blinded to groups allocation, using used a reliable, robust and repeatable technique for

manual delineation of basal ganglia structures (Tziortzi *et al.*, 2011a). Regions of interest included caudate, putamen, ventral striatum, globus pallidus (external and internal segments), substantia nigra and motor thalamic nuclei.

Statistical analysis

Statistical analysis and graph illustration were performed with SPSS (version 22) and GraphPad Prism (version 6.0c) for Windows 10, respectively. For all variables, Gaussianity was tested with Shapiro-Wilk test and we proceeded with parametric tests as our imaging and clinical data were normally distributed. Multivariate analysis of variance (MANOVA) was used to assess the main effects of regional BP_{ND} among the groups. If the overall multivariate test was significant, *P*-values for each variable were calculated following Bonferroni's multiple comparisons test. We interrogated correlations between imaging and clinical data using Spearman rho and we applied Benjamini-Hochberg correction to reduce false discovery rate (Benjamini and Cohen, 2017). We set the false discovery rate cut-off at 0.05. All data are presented as mean ± standard deviation, and the level α was set for all comparisons at $P<0.05$, corrected.

4.1.4 Results

A mean dose of 180.26 ± 3.62, 179.52 ± 3.27 and 179.5 ± 3.2 [^{123}I]FP-CIT MBq was respectively administered in healthy controls, early *de novo* and early treated Parkinson's patients, whereas for [^{11}C]PE2I MBq was administered a mean dose of 328.99 ± 10.46, 309.31 ± 35.4 and 312.44 ± 22.91. The results of [^{123}I]FP-CIT SBR and [^{11}C]PE2I BP_{ND} in healthy controls, early *de novo* and treated Parkinson's disease patients are shown in Table 3.

Table 3. [^{11}C]PE2I BP_{ND} and [^{123}IFP-CIT SBR in early *de novo* and early treated patients with idiopathic Parkinson's disease compared to healthy controls

	Healthy Controls (n=22)	Early *de novo* Parkinson's disease (n=17)	Early treated Parkinson's disease (n=15)
[^{11}C]PE2I BP_{ND}			
Dose injected (MBq)	328.99 ± 10.46	309.31 ± 35.4	312.44 ± 22.91
Caudate	2.58 ± 0.42	1.87 ± 0.38*	1.74 ± 0.44*
Putamen	3.16 ± 0.33	1.75 ± 0.44*	1.14 ± 0.3*$^{\&}$
Ventral Striatum	2.09 ± 0.8	2.03 ± 0.44	1.63 ± 0.39
Globus Pallidus Internal	1.22 ± 0.24	0.85 ± 0.24*	0.6 ± 0.23*$^{\&}$
Globus Pallidus External	2.03 ± 0.37	1.27 ± 0.31*	1 ± 0.36*
Substantia Nigra	0.7 ± 0.2	0.61 ± 0.09	0.62 ± 0.08
Thalamus	0.45 ± 0.07	0.49 ± 0.05	0.28 ± 0.08*$^{\&}$
[^{123}I]FP-CIT SBR			
Dose injected (MBq)	180.26 ± 3.62	179.52 ± 3.27	179.5 ± 3.2
Caudate	3.72 ± 0.47	2.88 ± 0.62*	2.33 ± 0.36*$^{\&}$
Putamen	3.67 ± 0.41	2.44 ± 0.51*	2.01 ± 0.26*$^{\&}$
Ventral Striatum	2.13 ± 0.37	1.7 ± 0.46*	1.55 ± 0.2*
Globus Pallidus Internal	2.46 ± 0.31	1.97 ± 0.38*	1.88 ± 0.2*
Globus Pallidus External	3.08 ± 0.39	2.26 ± 0.45*	2.1 ± 0.26*
Substantia Nigra	1.55 ± 0.24	1.53 ± 0.34	1.45 ± 0.15
Thalamus	1.76 ± 0.18	1.63 ± 0.32	1.58 ± 0.14

Continuous variables are expressed as mean ± standard deviation. Abbreviations: BP_{ND}= Non-displaceble binding potential; SBR=Signal-Binding-Ratio. P value vs. healthy controls Bonferroni post-hoc corrected. *P <0.05 vs. healthy controls, $^{\&}$P <0.05 vs. early *de novo* Parkinson's disease patients.

Early *de novo* patients with Parkinson's disease had lower mean [^{123}I]FP-CIT SBR values in caudate (P<0.001), putamen (P<0.001), ventral striatum (P<0.05), globus pallidus internal (P<0.05) and globus pallidus external (P<0.05) compared to healthy controls (Figure 10A and 11A). They had lower mean [^{11}C]PE2I BP_{ND} values in caudate (P<0.001), putamen (P<0.001), globus pallidus internal (P<0.05) and globus pallidus external (P<0.05) compared to healthy controls (Figure 10B and 11B).

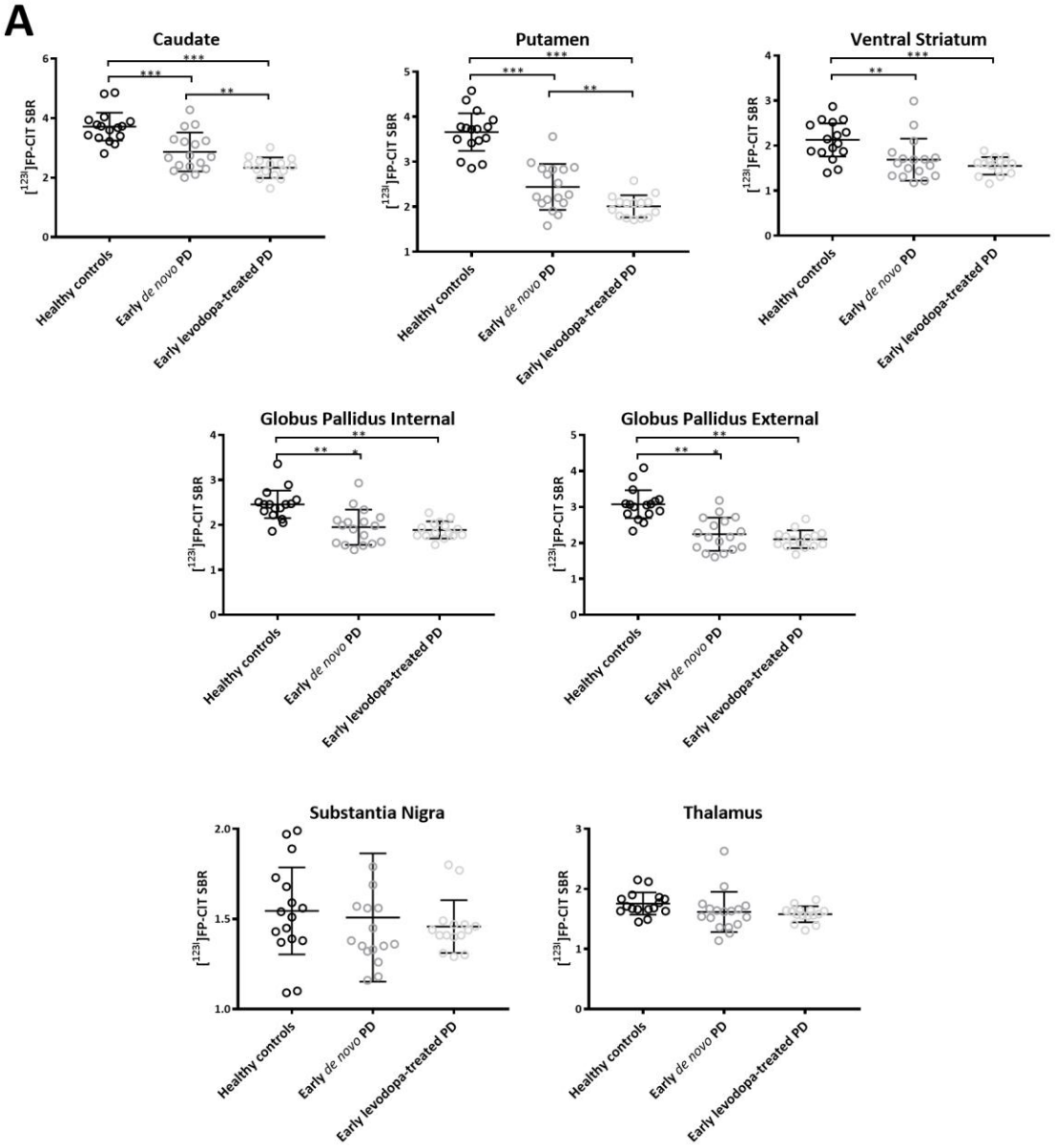
A
Caudate
Putamen
Ventral Striatum
Globus Pallidus Internal
Globus Pallidus External
Substantia Nigra
Thalamus
[123]FP-CIT SBR
Healthy controls
Early de novo PD
Early levodopa-treated PD

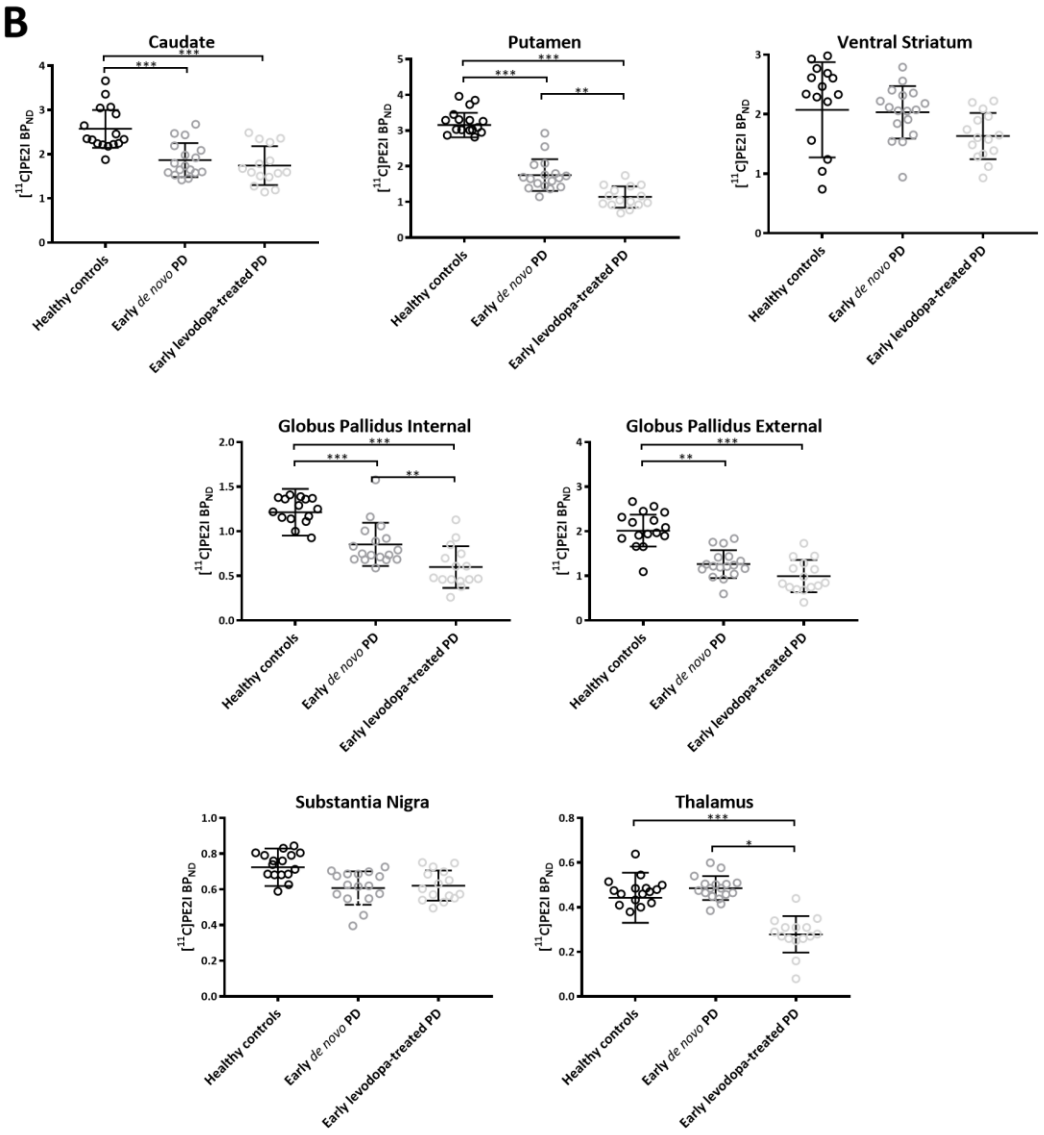

Figure 10. DAT SPECT (A) and PET (B) expression in the groups of Parkinson's disease (PD) patients and healthy controls. *Dot plot graphs showing mean [^{123}I]FP-CIT SBR (A) and [^{11}C]PE2I BP_{ND} (B) ± standard deviation in subcortical brain regions in PD early de novo patients, PD early levodopa-treated patients and healthy controls. *P <0.05, **P <0.01, ***P <0.001 ANOVA with Bonferroni post-hoc correction*

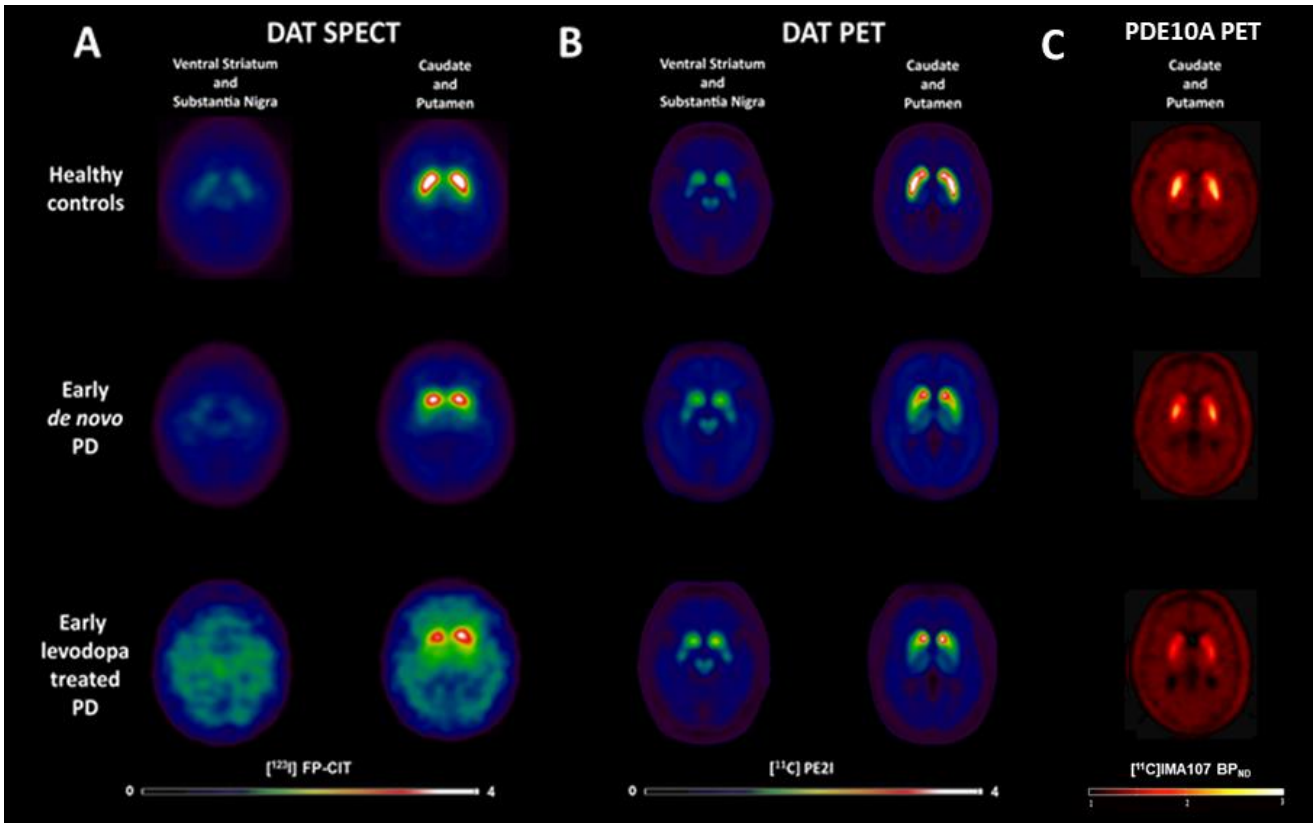

Figure 11. Altered DAT and PDE10A expression in anatomically defined brain regions of Parkinson's disease patients. *Axial PET images derived from (top) a healthy control, (middle) a Parkinson's disease early de novo and (bottom) a Parkinson's disease early levodopa-treated patient in stereotaxic space showing progressive loss of [^{123}I]FP-CIT SBR (A), [^{11}C]PE2I BP_{ND} (B) and [^{11}C]IMA107 BP_{ND} (C). Colour bar reflects range of SBR or BP_{ND} intensity.*

Early treated patients with Parkinson's disease had lower mean [^{123}I]FP-CIT SBR values in caudate (P<0.001), putamen (P<0.001), ventral striatum (P<0.05), globus pallidus internal (P<0.05) and globus pallidus external (P<0.05) compared to healthy controls (Figure 10A and 11A). They had lower mean [^{11}C]PE2I BP_{ND} values in caudate (P<0.001), putamen (P<0.001), globus pallidus internal (P<0.05), globus pallidus external (P<0.05) and thalamus (P<0.05) compared to healthy controls (Figure 10B and 11B). Compared to early *de novo* Parkinson's disease patients, early levodopa-treated patients with Parkinson's disease showed additional [^{123}I]FP-CIT SPECT loss of 21% (SD: 7.4%) in the caudate (P<0.001; reflecting a 7% mean annual decline) and 17% (SD: 7.6%) in the putamen (P<0.001; reflecting a 5.6% mean annual decline) (Figure 10A and 11A). Early levodopa-treated Parkinson's disease patients showed additional [^{11}C]PE2I BP_{ND} loss of was 34.7%

(SD: 17%) in the putamen (P<0.001; reflecting an 11.6% mean annual decline), whereas changes were not significant in the caudate, compared to early *de novo* Parkinson's disease patients (Figure 10A and 11A).

Longer Parkinson's disease duration correlated with lower [^{11}C]PE2I BP_{ND} in the putamen (*rho*=-0.65; P<0.001). No correlations were found between Parkinson's disease duration and [^{123}I]FP-CIT SPECT SBR in any brain areas (Figure 12).

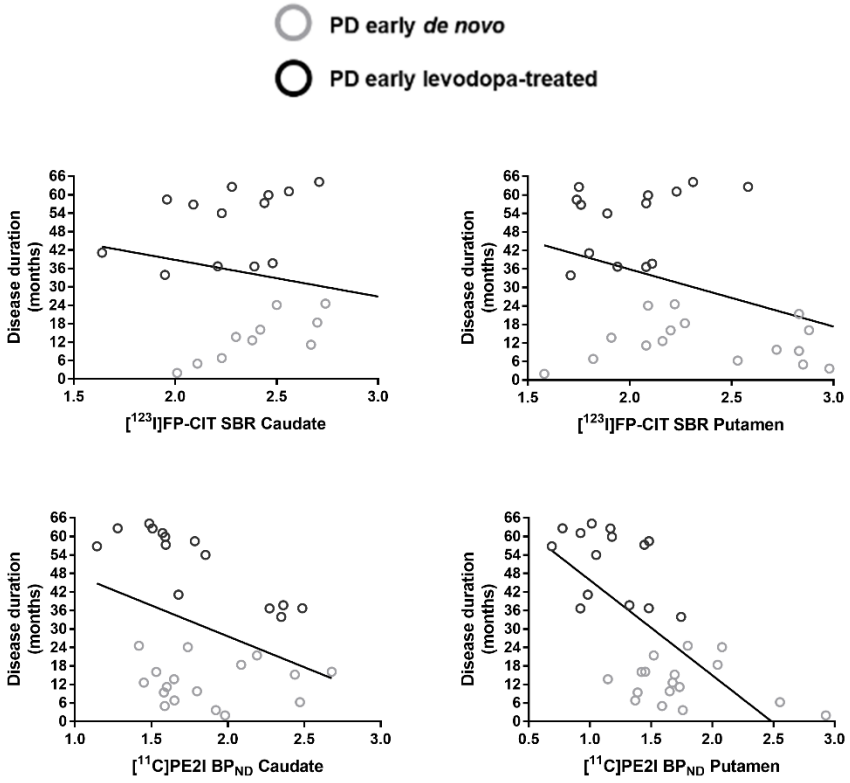

Figure 12. Correlations between DAT and disease duration in Parkinson's disease (PD) patients. *Spearman orrelation between disease duration and [^{11}C]PE2I (down - right) in the putamen (rho=-0.65; P<0.001). No correlations with [^{123}I]FP-CIT SBR (top) in the caudate (rho=-0.253; P>0.10) or putamen (rho=-0.258; P>0.10) and [^{11}C]PE2I BP_{ND} (down - left) in the caudate (rho=-0.267; P>0.10). PD early de novo in black circles and PD early levodopa-treated in grey circles*

In term of lateralization, in the group of early *de novo* patients with Parkinson's disease with unilateral motor symptoms, we assessed whether the clinically affected side of the body was associated with greater decreases in contralateral brain regions of interest [^{11}C]PE2I BP_{ND} values. We found that

[^{11}C]PE2I BP_{ND} values in caudate (P<0.001), putamen (P<0.001), ventral striatum (P<0.001), globus pallidus internal (P<0.001), globus pallidus external (P<0.001) and substantia nigra (P<0.001) were decreased in the contralateral to most affected compared to the less affected side of the body. Equivalent results were found for [^{123}I]FP-CIT SPECT SBR values .

When the group of early *de novo* and early treated Parkinson's patients were evaluated as a whole, higher MDS-UPDRS-III total scores correlated with lower [^{123}I]FP-CIT SPECT SBR in the caudate (*rho*=-0.59; P<0.001), putamen (*rho*=-0.50; P<0.001), globus pallidus internal (*rho*=-0.36; P<0.05) and globus pallidus external (*rho*=-0.43; P<0.05) and with lower [^{11}C]PE2I BP_{ND} in the putamen (*rho*=-0.54; P<0.001), ventral striatum (*rho*=-0.50; P<0.05) and thalamus (*rho*=-0.51; P<0.05). Higher MDS-UPDRS-III rigidity scores correlated with lower [^{11}C]PE2I BP_{ND} in the caudate (*rho*=-0.37; P<0.001), putamen (*rho*=-0.61; P<0.001), ventral striatum (*rho*=-0.45; P<0.05) and thalamus (*rho*=-0.48; P<0.05); whereas no correlations were found with [^{123}I]FP-CIT SPECT SBR. Higher MDS-UPDRS-III bradykinesia scores correlated with lower [^{123}I]FP-CIT SPECT SBR in the caudate (*rho*=-0.45; P<0.05) in the putamen (*rho*=-0.42; P<0.05) and with lower [^{11}C]PE2I BP_{ND} in the putamen (*rho*=-0.47; P<0.001), ventral striatum (*rho*=-0.39; P<0.05) and thalamus (*rho*=-0.42; P<0.05). No correlations were found with MDS-UPDRS-III resting tremor and [^{123}I]FP-CIT SPECT SBR or [^{11}C]PE2I BP_{ND}. No correlations were found with MDS-UPDRS-III axial symptoms and [^{123}I]FP-CIT SPECT SBR. Higher MDS-UPDRS-III axial symptoms also correlated with lower [^{11}C]PE2I BP_{ND} in the putamen (*rho*=-0.55; P<0.001), ventral striatum (*rho*=-0.40; P<0.001), and thalamus (*rho*=-0.57; P<0.05, Figure 13).

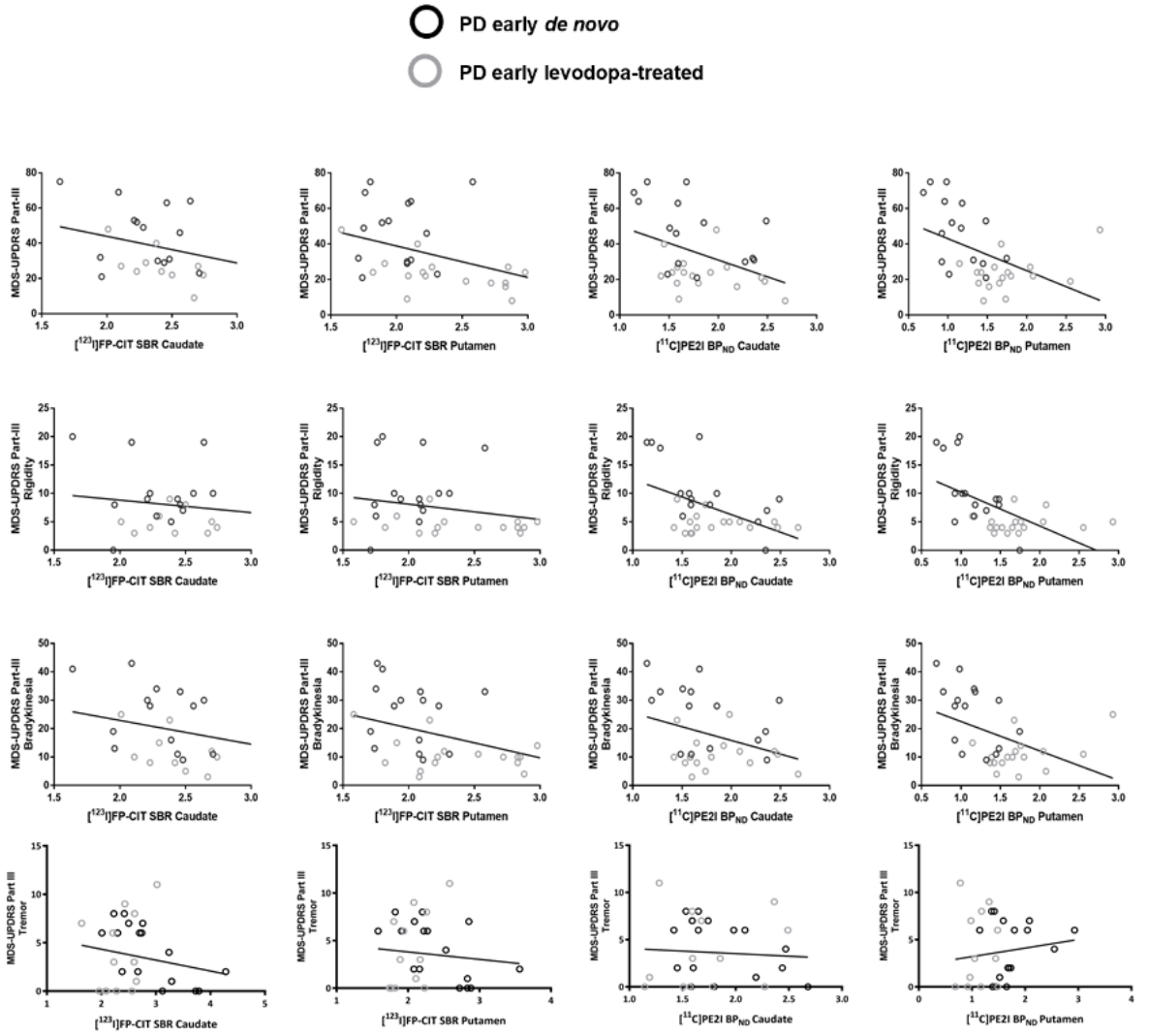

Figure 13. Correlations between DAT and motor symptoms in Parkinson's disease (PD) patients. *Spearman correlation between MDS-UPDRS-III motor scores (first line) and [^{123}I]FP-CIT SBR in the caudate (rho=-0.59; P<0.001) and putamen (rho=-0.50; P<0.001) and [^{11}C]PE2I BP_{ND} in the putamen rho=-0.54; P<0.001). No correlations between MDS-UPDRS-III motor scores and [^{11}C]PE2I BP_{ND} in the caudate (rho=-0.328; P>0.10). Correlations between MDS-UPDRS-III rigidity subscores (second line) and [^{11}C]PE2I BP_{ND} in the caudate (rho=-0.37; P<0.001) and putamen (rho=-0.61; P<0.001). No correlations between rigidity and [^{123}I]FP-CIT SBR. Correlation between MDS-UPDRS-III bradykinesia subscores (third line) and [^{123}I]FP-CIT SBR in the caudate (rho=-0.45; P<0.05) and putamen (rho=-0.42; P<0.05) and [^{11}C]PE2I BP_{ND} in the putamen (rho=-0.47; P<0.001). No correlation between bradykinesia and [^{11}C]PE2I BP_{ND} in the caudate (rho=-0.263; P>0.10). No correlation between MDS-UPDRS-III tremor subscores (forth line) and [^{123}I]FP-CIT SBR in caudate (rho=0.089; P>0.10) and putamen (rho=0.022 ; P>0.10) and [^{11}C]PE2I BP_{ND} in caudate (rho=0.019; P>0.10) and putamen (rho=0.141 ; P>0.10). PD early de novo in black circles and PD early levodopa-treated in grey circles.*

On [^{123}I]FP-CIT SPECT scan, in the subgroup of early *de novo* patients with Parkinson's disease, higher MDS-UPDRS-III total scores correlated with lower [^{123}I]FP-CIT SPECT SBR in the caudate (*rho*=-0.76; *P*<0.05), putamen (*rho*=-0.44; *P*<0.05), ventral striatum (*rho*=-0.72; *P*<0.05), globus pallidus internal (*rho*=-0.70; *P*<0.05), globus pallidus external (*rho*=-0.72; *P*<0.05), substantia nigra (*rho*=-0.60; *P*<0.05) and thalamus (*rho*=-0.66; *P*<0.05). Higher MDS-UPDRS-III resting tremor correlated with lower [^{123}I]FP-CIT SPECT SBR in the caudate (*rho*=-0.73; *P*<0.05), putamen (*rho*=-0.54; *P*<0.05), ventral striatum (*rho*=-0.67; *P*<0.05), globus pallidus internal (*rho*=-0.68; *P*<0.05), globus pallidus external (*rho*=-0.72; *P*<0.05), substantia nigra (*rho*=-0.54; *P*<0.05) and thalamus (*rho*=-0.64; *P*<0.05). No correlations were found with MDS-UPDRS-III rigidity, bradykinesia, axial scores and [^{123}I]FP-CIT SPECT SBR.

In the subgroup of early treated patients with Parkinson's disease, no correlations were found with MDS-UPDRS-III total, rigidity, bradykinesia, resting tremor, axial scores and [^{123}I]FP-CIT SPECT SBR.

On [^{11}C]PE2I PET scan, in the subgroup of early *de novo* patients with Parkinson's disease, no correlations were found with MDS-UPDRS-III total, rigidity, bradykinesia, resting tremor or axial scores and [^{11}C]PE2I BP_{ND}.

In the subgroup of early treated patients with Parkinson's disease, higher MDS-UPDRS-III total scores correlated with lower [^{11}C]PE2I BP_{ND} in the substantia nigra (*rho*=-0.53; *P*<0.05). Higher MDS-UPDRS-III rigidity scores correlated with lower [^{11}C]PE2I BP_{ND} in the caudate (*rho*=-0.59; *P*<0.05), putamen (*rho*=-0.59; *P*<0.05) and substantia nigra (*rho*=-0.74; *P*<0.05). No correlations were found with MDS-UPDRS-III bradykinesia, resting tremor or axial scores and [^{11}C]PE2I BP_{ND}.

No correlations were found with global non-motor symptoms (higher MDS-UPDRS-I, MDS-UPDRS Part-I questionnaire or NMSS), constipation, sleep (PDSS, ESS, RBQS), fatigue (Parkinson Fatigue Scale), autonomic dysfunction (SCOPA-AUT), olfaction (UPSIT) and quality of life (PDQ-39) when the group of early *de novo* and early treated Parkinson's patients were evaluated as a whole or as subgroups.

No correlations were found with global non-motor symptoms (MDS-UPDRS-I, MDS-UPDRS Part-I questionnaire or NMSS), constipation (Modified Constipation Assessment Scale), sleep (PDSS, ESS, RBQS), fatigue (Parkinson Fatigue Scale), autonomic dysfunction (SCOPA-AUT), olfaction (UPSIT), quality of life (PDQ-39) and [^{11}C]PE2I BP_{ND} when the group of early *de novo* and early treated Parkinson's patients were evaluated as a whole or in the subgroup of early *de novo* patients with Parkinson's disease.

In the subgroup of early treated patients with Parkinson's disease, worse global non-motor symptoms (higher NMSS) correlated with lower [^{11}C]PE2I BP_{ND} in the thalamus (NMSS: *rho*=-0.54; $P<0.05$). No correlations were found with constipation, fatigue, sleep (PDSS, ESS, RBQS), autonomic dysfunction (SCOPA-AUT), olfaction (UPSIT), quality of life (PDQ-39) and [^{11}C]PE2I BP_{ND}.

On [^{123}I]FP-CIT SPECT scan, when the group of early *de novo* and early treated Parkinson's patients were evaluated as a whole, greater cognitive impairment (lower MoCA) correlated with lower [^{123}I]FP-CIT SPECT SBR in the caudate (MoCA: *rho*=0.49; $P<0.05$), putamen (MoCA: *rho*=0.41; $P<0.05$), ventral striatum (MoCA: *rho*=0.43; $P<0.05$), globus pallidus external (MoCA: *rho*=0.56; $P<0.05$) and thalamus (MoCA: *rho*=0.43; $P<0.05$). No correlations were found with depressive symptoms (GDS, BDI-II) and [^{123}I]FP-CIT SPECT SBR.

In the subgroup of early *de novo* patients with Parkinson's disease, greater cognitive impairment (lower MoCA) correlated with lower [^{123}I]FP-CIT SPECT SBR in the caudate (MoCA: *rho*=0.53; *P*<0.05), ventral striatum (MMSE: *rho*=0.49; *P*<0.05; MoCA: *rho*=0.62; *P*<0.05), globus pallidus internal (MMSE: *rho*=0.59; *P*<0.05;MoCA: *rho*=0.56; *P*<0.05), globus pallidus external (MMSE: *rho*=0.56; *P*<0.05; MoCA: *rho*=0.64; *P*<0.05), thalamus (MMSE: *rho*=0.56; *P*<0.05; MoCA: *rho*=0.59; *P*<0.05) and substantia nigra (MoCA: *rho*=0.49; *P*<0.05). No correlations were found with depressive symptoms (GDS, BDI-II) and [^{123}I]FP-CIT SPECT SBR.

In the subgroup of early treated patients with Parkinson's disease, no correlations were found with cognitive impairment (MMSE, MoCA) or depressive symptoms (GDS, BDI-II) and [^{123}I]FP-CIT SPECT SBR.

On [^{11}C]PE2I PET scan, when the group of early *de novo* and early treated Parkinson's patients were evaluated as a whole, greater cognitive impairment (lower MMSE) correlated with lower [^{11}C]PE2I BP_{ND} in the globus pallidus external (MMSE: *rho*=-0.41; *P*<0.05) and worse depressive symptoms (higher GDS) correlated with lower [^{11}C]PE2I BP_{ND} in the thalamus (GDS: *rho*=-0.38; *P*<0.05).

No correlations were found with cognitive impairment (MMSE, MoCA) or depression (GDS, BDI-II) and [^{11}C]PE2I BP_{ND} in the subgroup of patients early *de novo* or treated with Parkinson's disease.

Comparison between PDE10A and DAT PET and SPECT

We evaluated whether PDE10A and DAT levels were correlated in the subcortical nuclei. We found that lower individual [^{11}C]IMA107 BP_{ND} values correlated with lower individual [^{11}C]PE2I BP_{ND} values in the caudate (*rho*=0.51; *P*<0.01) and putamen (*rho*=0.53; *P*<0.01), but not in ventral striatum (*rho*=0.013; *P*>0.10), globus pallidus internal (*rho*=0.21; *P*>0.10), globus pallidus external (*rho*=0.46; *P*>0.05), substantia nigra (*rho*=0.15; *P*>0.10) or thalamus (*rho*=0.15; *P*>0.10) in Parkinson's disease patients. We found that lower individual [^{11}C]IMA107 BP_{ND} values were not correlated with lower individual [^{123}I]FP-CIT SBR values in the caudate (*rho*=0.11; *P*>0.10) or putamen (*rho*=0.19; *P*>0.10) in Parkinson's disease patients (Figure 14).

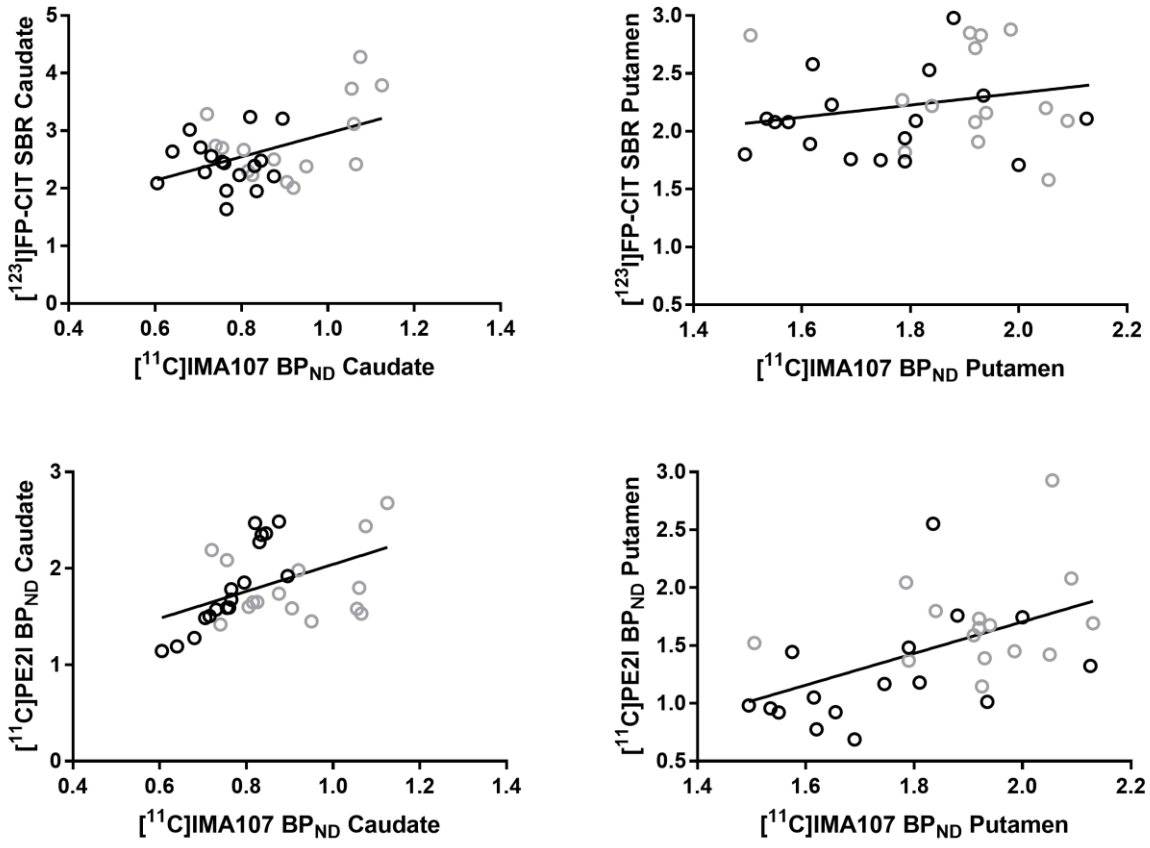

Figure 14. Correlations between PDE10A and DAT imaging in Parkinson's disease (PD) patients. *Spearman correlation between [^{11}C]IMA107 BP_{ND} and [^{11}C]PE2I BP_{ND} (down) in the caudate (rho=0.51; P<0.01) and putamen (rho=0.53; P<0.01). No correlations between [^{11}C]IMA107 BP_{ND} and [^{123}I]FP-CIT SBR (top) in the caudate (rho=0.11; P>0.10) or putamen (rho=0.19; P>0.10). PD early de novo in black circles and PD early levodopa-treated in grey circles.*

Then. we compared the loss of [^{11}C]IMA107 BP_{ND} with loss of [^{11}C]PE2I BP_{ND} in each region of interest in Parkinson's disease patients relative to normality data from the group of healthy controls. We found that loss of [^{11}C]IMA107 BP_{ND} was greater than loss of [^{11}C]PE2I BP_{ND} in the caudate (P<0.01) but lower in the putamen (P<0.001), globus pallidus internal (P<0.01), globus pallidus external (P<0.001) and substantia nigra (P<0.01), and no different in ventral striatum (P>0.10) and thalamus (P>0.10) in early *de novo* Parkinson's disease patients. Similarly, we found that loss of [^{11}C]IMA107 BP_{ND} was greater than loss of [^{11}C]PE2I BP_{ND} in the caudate (P<0.01) but lower in the putamen (P<0.001), globus pallidus internal (P<0.05), globus pallidus external (P<0.01) and substantia nigra (P<0.05), and no different in ventral striatum (P>0.10) and thalamus (P>0.10) in early levodopa-treated Parkinson's disease patients.

We also evaluated the coefficient of variance (COV% = SD/mean *100) for [^{11}C]IMA107 and [^{11}C]PE2I BP_{ND}. In early *de novo* Parkinson's disease patients: (a) [^{11}C]IMA107 BP_{ND} COV% was 9% in the whole striatum, 14% in the caudate, 8% in the putamen, 18% in the ventral striatum, 10% in the globus pallidus internal, 11% in the globus pallidus external, 11% in substantia nigra, and 16% in the thalamus; (b) [^{11}C]PE2I BP_{ND} COV% was 19% in the whole striatum, 21% in the caudate, 26% in the putamen, 22% in the ventral striatum, 29% in the globus pallidus internal, 26% in the globus pallidus external, 16% in the substantia nigra, and 11% in the thalamus.

In early levodopa-treated Parkinson's disease patients: (a) [^{11}C]IMA107 BP_{ND} COV% was 9% in the whole striatum, 10% in the caudate, 11% in the putamen, 18% in the ventral striatum, 15% in the globus pallidus internal, 13% in the globus pallidus external, 20% in substantia nigra, and 17% in the thalamus; (b) [^{11}C]PE2I BP_{ND} COV% was 21% in the whole striatum, 25% in the caudate, 26% in the putamen, 24% in the ventral striatum, 30% in the globus pallidus internal, 27% in the globus pallidus external, 14% in the substantia nigra, and 12% in the thalamus.

Comparison between DAT PET and DAT SPECT

We evaluated whether DAT levels measured with PET and with SPECT were correlated in the subcortical nuclei. We found that lower individual [^{123}I]FP-CIT-SPECT SBR values correlated with lower individual [^{11}C]PE2I BP_{ND} values in the caudate (r = 0.44; *P*=0.011) and putamen (*rho* = 0.36; *P*=0.044), but not in ventral striatum, globus pallidus external, globus pallidus internal, thalamus or substantia nigra (all *P*>0.10) in Parkinson's patients.

Then, we compared the loss of [^{123}I]FP-CIT-SPECT SBR with loss of [^{11}C]PE2I-PET BP_{ND} in each region-of-interest in Parkinson's patients relative to normality data from the group of healthy controls. We found that loss of [^{11}C]PE2I-PET BP_{ND} was greater than loss of [^{123}I]FP-CIT-SPECT SBR in the putamen (–11%, *P*<0.01), globus pallidus external (–14%, *P*<0.01), globus pallidus internal (–16%, *P*<0.001) and no different in caudate (+1%, *P*>0.10), ventral striatum (+8%, *P*>0.10) and thalamus (-1%, *P*>0.10), and substantia nigra (–2%, *P*>0.10) in early *de novo* Parkinson's patients. Similarly, we found in early levodopa-treated Parkinson's patients that loss of [^{11}C]PE2I-PET BP_{ND} was greater than loss of [^{123}I]FP-CIT-SPECT SBR in the putamen (–16%, *P*<0.01), globus pallidus external (–14%, *P*<0.01), globus pallidus internal (–17%, *P*<0.001), thalamus (–11%, *P*<0.001), but lower in the caudate (+10%, *P*<0.001) and ventral striatum (+17%, *P*<0.001).

5.1.1 Discussion

Our hypothesis was that a PDE10A expression was correlated with dopaminergic pathology, which can be measured either with PET or SPECT.

We aimed to test this hypothesis checking for correlations between the expression of PDE10A and the expression of dopamine transporters (measured by using [^{11}C]PE2I PET and [^{123}I]FP-CIT SPECT molecular imaging) (*Project 2 Aim*).

We found that striatal [^{11}C]IMA107 BP_{ND} values were correlated with striatal using [^{11}C]PE2I PET and [^{123}I]FP-CIT SPECT values.

Our findings demonstrate our hypothesis that loss of PDE10A correlated with loss of DAT in the striatum in early *de novo* and early levodopa-treated patients with Parkinson's disease, suggesting an association between PDE10A and dopaminergic function. PDE10A plays a key role in the regulation of dopaminergic signalling and is essential for dopamine neurotransmission through the interaction with cAMP and the activation of PKA/DARPP-32 downstream cascade in striatal pathways (Greengard *et al.*, 1999; Nishi *et al.*, 2008; Girault, 2012).

We attempted to understand how informative PET molecular imaging of PDE10A and DAT could be for monitoring the disease progression. Our levodopa-treated patients with Parkinson's disease had three years longer disease duration compared to early *de novo* Parkinson's disease patients. PDE10A expression showed further decline in both the caudate and putamen, whereas DAT expression was further reduced only in the putamen in early levodopa-treated compared to early *de novo* Parkinson's disease patients. Specifically, the loss of PDE10A in the caudate reflected a 5.7% and in the putamen a 3.2% mean annual decline, whereas loss of DAT in the putamen reflected a 11.6% mean annual decline. PDE10A showed also a lower variability over the time, with a SD of 8.4% in the caudate and 9.6% in the putamen, whereas DAT showed a 17% SD in the putamen. In our study we have shown that standardized differences (Cohen's d) between early *de novo* and levodopa-treated with three-year longer disease duration are 1.48 for caudate measured with [^{11}C]IMA107, and 1.57 for putamen measured with [^{11}C]PE2I. Assuming in detecting a 50% reduction in these differences in a potential 18-month clinical trial testing a disease modifying drug that reduces disease progression by 50%, we

will have a 0.7412 Cohen's d for caudate PDE10A and a 0.7851 for putamen DAT. These figures are greater than [^{18}F]FDOPA, a validated biomarker of Parkinson's progression, that showed Cohen's d of 0.7993 at three-year follow-up in early *de novo* patients with Parkinson's (Bruck *et al.*, 2009), thus having a 0.3996 Cohen's d in this hypothetical trial. Providing a 80% power with a two-sided test using 5% type I error rate, we may need 60 participants if we use as endpoint the changes in the caudate [^{11}C]IMA107 levels, 54 subjects if we use as endpoint the changes in the putamen [^{11}C]PE2I levels and 200 subjects if we use as endpoint the changes in the putamen [^{11}F]FDOPA levels.

We performed head-to-head comparisons between loss of PDE10A and DAT in Parkinson's disease patients relative to normality data from the group of healthy controls. We found that loss of PDE10A was greater than loss of DAT in the caudate, but lower in the putamen, globus pallidus and substantia nigra in both early *de novo* and early levodopa-treated patients with Parkinson's disease. In early *de novo* and levodopa-treated patients with Parkinson's disease, PDE10A tracer showed a 10% lower COV variability in the striatum, caudate and putamen compared to DAT. This suggests that PDE10A might be a more stable biomarker. Loss of PDE10A in both the caudate and putamen, and loss of DAT only in the putamen correlated with longer Parkinson's duration, total burden of motor symptoms, and with increased rigidity and bradykinesia. The level of correlations between PDE10A and DAT and clinical scales were similar.

Considering the underlying pathophysiology of Parkinson's disease includes progressive deposition of α-synuclein, the ideal neuroimaging biomarker to monitor disease progression should be able to quantify regional deposition of abnormal α-synuclein accumulation. Development of such a molecular imaging radiotracer has been the focus of much research but is not yet forthcoming and assessment of DAT represents the most direct approach able to quantify presynaptic nigrostriatal dopaminergic neurons. Loss of striatal DAT signal is currently considered the gold standard in the differential diagnosis between degenerative *vs*. non-degenerative parkinsonism. However, this approach has some shortcomings. For example, DAT levels have a floor effect that limit its use to the

initial stages of the disease and may be modulated by dopaminergic supplementation, with levodopa inducing a decline proportional to the dose used (Fahn *et al.*, 2004). Clinical trials that used DAT as a marker of Parkinson's disease pathology showed controversial results, with imaging studies appearing to contradict the clinical findings (Whone *et al.*, 2003; Fahn *et al.*, 2004; Parkinson Study Group, 2009). In CALM-PD (Parkinson Study Group, 2009) and REAL-PET (Whone *et al.*, 2003), subjects randomized to dopamine agonists showed worse clinical symptoms but lower DAT decline than subjects randomized to levodopa. In ELLEDOPA trial (Fahn *et al.*, 2004), subjects randomized to levodopa showed better clinical symptoms but greater DAT decline than subjects on placebo. However, it is not clear whether dopaminergic treatment hasten disease progression or it was a simple down-regulation of DAT due to the use of levodopa.

5.1.2 Conclusion

PDE10A imaging could be a robust alternative to DAT imaging regarding diagnosis and for evaluating disease burden and progression. Collectively in our studies, we found a gradual progressive decline of PDE10A in Parkinson's from very early to advanced stages, which was independent of levodopa treatment (Niccolini *et al.*, 2015a) and had no floor effect. This makes PDE10A imaging potentially attractive to explore its clinical use further. It is important to note that both [^{11}C]IMA107 and [^{11}C]PE2I are kinetically well-behaved tracers with good-to-very good reproducibility, and the differences in their binding in the striatum are probably related to the pathological processes underlying Parkinson's disease, more than characteristics of the tracers. Despite all these potential advantages of PDE10A imaging, only PET ligands are currently available for PDE10A whereas DAT levels can be measured with SPECT imaging. This limitation reduces the cost-effective use of this novel molecular imaging technique until a SPECT PDE10A tracer becomes available. Neither DAT or PDE10A are good biomarkers for other Parkinson's symptoms, like tremor

or depression, where other mechanisms, such as serotonergic transporter deficit, seems to have a prominent role (Politis *et al.*, 2010b; Politis *et al.*, 2011; Loane *et al.*, 2013; Pagano *et al.*, 2017).

However, no conclusion can be drawn regarding the relationship between PDE10A expression and other markers of Parkinson's disease pathology, such as iron depositions, neuromelanin loss, and changes in structural and microstructural changes in the substantia nigra and in the striatum. We have investigated this in the Project 3, in which we compared the expression of PDE10A, measured with [^{11}C]IMA107 PET imaging, with MRI markers of Parkinson's pathology such as iron depositions (assessed with susceptibility-weighted MR imaging), neuromelanin loss (assessed with neuromelanin sensitive MR imaging) and changes in structural volumetric (assessed with T1 MR imaging) and microstructural connectivity (assessed with diffusion tensor MR imaging).

Chapter 5. MRI markers in Parkinson's Disease

This chapter summarizes the main results on the *in vivo* evaluation of the relationship between PDE10A expression and MRI markers of Parkinson's pathology such as iron depositions (assessed with susceptibility-weighted MR imaging), neuromelanin loss (assessed with neuromelanin sensitive MR imaging) and changes in structural volumetric (assessed with T1 MR imaging) and connectivity (assessed with diffusion tensor MR imaging) in early *de novo* Parkinson's disease patients compared to age- and sex-matched healthy control subjects, as potential novel tool for Parkinson's disease diagnosis. MRI markers in early *de novo* Parkinson's disease patients were then compared to early levodopa-treated Parkinson's disease patients, evaluating whether they are associated with disease duration and severity. Finally, the associations between the motor (tremor, rigidity, bradykinesia and postural instability) and non-motor symptoms (sleep problems, cognitive impairment, autonomic dysfunction, mood disorders etc) and the MRI markers have been explored and described in detail.

5.1.3 Introduction

PDE10A is a striatal enzyme expressed in the axons of the medium spiny neurons, where it hydrolyses cAMP and cGMP (Fujishige *et al.*, 1999; Coskran *et al.*, 2006). In the striatal pathways, PDE10A plays a pivotal role in the regulation of dopaminergic signalling (Nishi *et al.*, 2008) and of several other brain functions, ranging from ion conductance to synaptic plasticity (Girault, 2012). Recent work with PET molecular imaging has demonstrated loss of PDE10A expression in moderate to advanced levodopa-treated patients with Parkinson's disease, which was associated with motor symptoms and complications (Niccolini *et al.*, 2015a). Therefore, PDE10A, as an enzyme regulating striatal output and dopaminergic signalling, shows promise to serve as a marker of disease burden in patients with early Parkinson's disease. However, it is unknown whether PDE10A is implicated at the earlier stages of the disease and how PDE10A biomarker value compares with the other markers of Parkinson's disease pathology.

Molecular imaging of DAT expression is currently considered the gold standard tool for the diagnosis of Parkinson's disease. DAT expression can be measured with PET or SPECT imaging to quantify dopaminergic terminals and recognise the presence of striatal dysfunction in neurodegenerative parkinsonism (Pirker, 2003; Politis, 2014). Subclinical pathological processes in dopaminergic terminals may be detected also in subjects at higher risk of developing Parkinson's disease, such as susceptibility gene mutation carriers, or patients with idiopathic REM sleep behaviour disorder (Politis, 2014). DAT expression, however, is mainly indicative of dopamine nerve terminals loss, which could also be induced by compensatory mechanisms, and only subsequent to the death of dopaminergic neurons within substantia nigra (Stoessl *et al.*, 2014). Molecular imaging of DAT has shown also other limitations, including mild to moderate affinity for serotonin transporter (Laruelle *et al.*, 1994; de Win *et al.*, 2005) and lack of specificity and sensitivity in differential diagnosis of

neurodegenerative parkinsonisms (Schapira, 2013). In addition, the use of levodopa (Fahn *et al.*, 2004) or antidepressants (de Win *et al.*, 2005; Booij *et al.*, 2007), may hinder the accuracy of its measurements and limiting its use as a biomarker for clinical trials monitoring the efficacy of disease-modification drugs (Schapira, 2013)

Deficit of dopaminergic terminals in the striatum has been associated with loss of NM containing neurons in the substantia nigra (Ehringer and Hornykiewicz, 1998) and with increased iron deposition (Dexter *et al.*, 1987). A neurodegeneration of at least 60% of SN neurons is expected before the onset of motor symptoms, and a tool able to measure directly the substantia nigra cells is ideal to quantify dopaminergic pathology in Parkinson's disease (Fearnley and Lees, 1991).

Several novel MRI techniques have been developed in the last decade to measure NM (Sasaki *et al.*, 2006; Kitao *et al.*, 2013; Ogisu *et al.*, 2013; Nakamura and Sugaya, 2014; Ohtsuka *et al.*, 2014; Hashido and Saito, 2016; Matsuura *et al.*, 2016; Kuya *et al.*, 2017; Xiang *et al.*, 2017) and iron depositions, (Martin *et al.*, 2008; Baudrexel *et al.*, 2010; Lotfipour *et al.*, 2012; Ulla *et al.*, 2013) and have provided evidence of substantia nigra degeneration with potential applications as biomarkers of Parkinson's disease (Schwarz *et al.*, 2011; Castellanos *et al.*, 2015). However, the accuracy of this novel techniques has not been compared with a validated quantification of DAT expression, such [^{11}C]PE2I PET imaging or in relationship with the novel PDE10A [^{11}C]IMA107 PET imaging.

Here, we aimed to compare Parkinson's disease pathology in the substantia nigra by using PET with [^{11}C]IMA107, [^{11}C]PE2I and MRI with NM-sensitive, SWI and DTI, to quantify NM-SN loss, iron depositions and connectivity changes in relation to DAT and PDE10A expression. We also explored for associations with clinical markers of disease burden in Parkinson's disease.

5.1.4 Hypothesis

We hypothesize that PDE10A expression was correlated with other markers of Parkinson's disease pathology, such as iron depositions, neuromelanin loss, and changes in structural and microstructural changes in the substantia nigra and in the striatum. We have investigated this in the Project 3, in which we compared the expression of PDE10A, measured with [^{11}C]IMA107 PET imaging, with MRI markers of Parkinson's pathology such as iron depositions (assessed with susceptibility-weighted MR imaging), neuromelanin loss (assessed with neuromelanin sensitive MR imaging) and changes in structural volumetric (assessed with T1 MR imaging) and microstructural connectivity (assessed with diffusion tensor MR imaging).

We aim to test this hypothesis checking for correlations between the expression of PDE10A and MRI markers of Parkinson's pathology such as iron depositions (assessed with susceptibility-weighted MR imaging), neuromelanin loss (assessed with neuromelanin sensitive MR imaging) and changes in structural volumetric (assessed with T1 MR imaging) and microstructural connectivity (assessed with diffusion tensor MR imaging) (*Project 3 Aim*).

5.1.5 Methods

We enrolled 60 participants recruited from specialist Movement Disorders clinics at King's College Hospital, and through public advertisement, of which 54 subjects completed the study and were included in the analyses (Table 1). We included 32 patients with idiopathic Parkinson's disease according to the Queen Square Brain Bank criteria, and 22 age- and gender-matched healthy individuals with no history of neurological or psychiatric disorders, who served as the control group *(healthy controls)*. Parkinson's disease patients included 17 subjects with a recent diagnosis (duration of symptoms ≤24 months) who were naïve to treatment for Parkinson's symptoms *(de novo)*, and 15 subjects with early Parkinson's disease (duration of symptoms ≤60 months) who were recently treated

with levodopa (duration of treatment ≤24 months) and had no motor complications *(early levodopa-treated)*. None of the Parkinson's disease patients fulfilled the diagnostic criteria for Parkinson's disease MCI (Litvan *et al.*, 2011) or dementia (Emre *et al.*, 2007) or depression (Marsh *et al.*, 2006), had any history of other neurological or psychiatric disorders, and were not under treatment with substances with known actions in PDEs (e.g. apremilast, cilomilast, luteolin, piclamilast, roflumilast and ibudilast).

Motor symptom severity was assessed with the MDS-UPDRS-III and staged with H&Y scale. MDS-UPDRS-III subscores for rigidity, bradykinesia, tremor and axial symptoms were calculated as previously described (Niccolini *et al.*, 2015a). Quality of life was measured with the PDQ-39. Neuropsychiatric symptoms were assessed with the Beck Depression Inventory second edition BDI-II. MMSE and MoCA were used to assess general cognitive status. Disability was assessed by Modified Schwab and England Activities of Daily Living Scale. NMSS for Parkinson's disease was used to assess non-motor symptoms (Pagano *et al.*, 2016a).

The study was approved by the institutional review boards and the research ethics committee. Written informed consent was obtained from all study participants in accordance with the Declaration of Helsinki.

Scanning procedures

All participants were screened successfully to undertake PET with [^{11}C]IMA107 and with [^{11}C]PE2I, and one 3-Tesla MRI scanning under standard criteria(http://www.mrisafety.com; https://www.gov.uk/government/publications/arsac-notes-for-guidance). PET and MR imaging have been performed at Imanova Ltd, London, UK. All participants were scanned on Siemens Biograph Hi-Rez 6 PET-CT scanner (Erlangen, Germany). [^{11}C]IMA107 and [^{11}C]PE2I have been performed

on the same day after withholding consumption of caffeinated beverages for 12 hours (Fredholm *et al.*, 1999a).

Dynamic emission data were acquired continuously for 90 minutes following the injection of [^{11}C]IMA107 or [^{11}C]PE2I. The dynamic images were reconstructed into 26 frames (8 x 15 s, 3 x 60 s, 5 x 120 s, 5 x 300 s, and 5 x 600 s), using a filtered back projection algorithm (direct inversion Fourier transform) with a 128 matrix, zoom of 2.6 producing images with isotropic voxel size of 2 x 2 x 2 mm^3, and smoothed with a transaxial Gaussian filter of 5 mm. MRI scans were acquired with a 32-channel head coil on a 3-Tesla MRI Siemens Magnetom TrioTim syngo MR B17 (Erlangen, Germany) scanner, and included a T1-weighted magnetization prepared rapid gradient echo sequence [MPRAGE; time repetition (TR) = 2300 ms, time echo (TE) = 2.98 ms, flip angle of 9°, time to inversion (TI) = 900 ms, matrix = 240 x 256] for co-registration with the PET images; fast grey matter T1 inversion recovery (FGATIR; repetition time = 3000 ms, echo time = 2.96 ms, flip angle of 8, time to inversion = 409 ms, matrix = 240 x 256) (Sudhyadhom *et al.*, 2009) sequences for delineation of regions-of-interest. All MRI sequences used a 1 mm^3 voxel size, anteroposterior phase encoding direction, and a symmetric echo.

Imaging data analysis

[^{11}C]IMA107 and [^{11}C]PE2I data analysis

The Molecular Imaging and Kinetic Analysis Toolbox software package (MIAKAT^{TM}: www.miakat.org), implemented in MATLAB® (The Mathworks, Natick, MA, USA) was used to carry out image processing and kinetic modelling. MIAKAT™ combines in-house code with wrappers for FMRIB Software Library (FSL, http://fsl.fmrib.ox.ac.uk/fsl/fslwiki/) and Statistical

Parametric Mapping (SPM, http://www.fil.ion.ucl.ac.uk/spm/) commands in order to provide state-of-the-art functionality within a coherent analysis framework. The MIAKAT™ processing pipeline was followed, ensuring that all quality control steps were completed to generate parametric images and regional estimates of [^{11}C]IMA107 and [^{11}C]PE2I BP_{ND}. BP_{ND} were generated using a basis function implementation of the simplified reference tissue model, with the cerebellum as the reference tissue for non-specific binding. Individual PET frames were corrected for head motion using frame-by-frame rigid registration using a frame with high signal-to-noise ratio as reference. PET images were co-registered to the corresponding MPRAGE MRI.

MRI-based analysis

FreeSurfer image analysis suite (version 5·3·0 http://surfer. nmr.mgh.harvard.edu) was used to derive measures of deep grey matter nuclei volume. Reconstructed data sets were visually inspected to ensure the accuracy of registration, skull stripping, segmentation, and cortical surface reconstruction. Subcortical structure volumes were derived by automated procedures, which automatically assign a neuroanatomical label to each voxel in an MRI volume based on probabilistic information automatically estimated from a manually labeled training set (Fischl *et al.,* 2002). All individual nuclei volumes were normalized for total intracranial volume automatically generated by FreeSurfer (Buckner *et al.*, 2004).

For iron quantification, manual delineation of the region-of-interests was performed on SWI high-pass filtered combined images using Analyze 12.0 (AnalyzeDirect, Overland Park, KS, United States). Each region-of-interest was hand drawn on both hemispheres on a single axial slice and included the following: caudate, putamen and substantia nigra. The substantia nigra was delineated on the 3rd axial slice ventral to the most dorsal aspect of the red nucleus. For quantification of NM, SN was manually delineated on neuromelanin-sensitive T1-weighted image using Analyze 12.0

(AnalyzeDirect, Overland Park, KS, United States). Each region-of-interest was hand drawn on both hemispheres on 3-4 axial slices. Mean regional values, number of voxels, standard deviations and regional areas was then extracted for each region-of-interest on both hemispheres individually before averaging to obtain bilateral data for SWI.

For quantification of NM, substantia nigra and locus coeruleus were manually delineated on the neuromelanin-sensitive and T1-weighted image using Analyze 12.0 (Analyze Direct, Overland Park, KS, United States). On NM-space, each substantia nigra and locus coeruleus ROIs were manually drawn on both hemispheres on 3-4 (substantia nigra) and 1-2 (locus coeruleus) axial slices together with the reference regions of the superior peduncle (for substantia nigra) and rostral pontomesencephalic area (for locus coeruleus). To calculate the signal intensity in the substantia nigra and in the locus coeruleus area, the superior peduncle and the rostral pontomesencephalic area were used as a reference region, respectively for the substantia nigra and for the locus coeruleus, to normalize the intensity of the slices to remove the inter-slice and inter-subject variability (Figure 5).

Diffusion data were analysed using the FMRIB's FSL Diffusion Tool box (FDT) including pre-processing steps, to correct for susceptibility-induced and current-induced distortions and head movements. For local diffusion modelling, fractional anisotropy (FA) and mean diffusivity (MD) maps were generated using DTIFit within FDT.

Region of interest-based analysis

To facilitate anatomical delineation of regions of interest, PET and MRI images were anatomically co-registered and re-sliced to the corresponding volumetric structural T1-weighted MRI images in Statistical Parametric Mapping version12 (SPM12) software package implemented in Matlab 2015a. Regions of interest were delineated manually on the T1 co-registered FGATIR MRI sequence using ANALYZE version 12.0 (Mayo Foundation) medical imaging software package by two assessors

who were blinded to groups allocation, using used a reliable, robust and repeatable technique for manual delineation of basal ganglia structures (Tziortzi *et al.*, 2011a). Regions of interest included caudate, putamen, ventral striatum, globus pallidus (external and internal segments), substantia nigra and motor thalamic nuclei.

Statistical analysis

Statistical analysis and graph illustration were performed with SPSS (version 22) and GraphPad Prism (version 6.0c) for Windows 10, respectively. For all variables, Gaussianity was tested with Shapiro-Wilk test and we proceeded with parametric tests as our imaging and clinical data were normally distributed. Multivariate analysis of variance (MANOVA) was used to assess the main effects of regional BP_{ND} among the groups. If the overall multivariate test was significant, *P*-values for each variable were calculated following Bonferroni's multiple comparisons test. We interrogated correlations between imaging and clinical data using Spearman rho and we applied Benjamini-Hochberg correction to reduce false discovery rate (Benjamini and Cohen, 2017). We set the false discovery rate cut-off at 0.05. All data are presented as mean ± standard deviation, and the level α was set for all comparisons at $P<0.05$, corrected.

5.1.6 Results

The results of MRI markers in healthy controls, early *de novo* and treated Parkinson's disease patients are shown in Table 4.

Table 4. Freesurfer volumes, microstructural DTI, SWI iron depositions and NM changes in subcortical areas and substantia nigra in early *de novo* and early treated patients with idiopathic Parkinson's disease compared to healthy controls

	Healthy Controls (n=22)	Early *de novo* Parkinson's disease (n=17)	Early treated Parkinson's disease (n=15)
Freesurfer Volumes			
Caudate	2.42 ± 0.22	2.39 ± 0.23	2.32 ± 0.31
Putamen	3.5 ± 0.32	3.34 ± 0.28	3.2 ± 0.31
Ventral Striatum	0.34 ± 0.07	0.32 ± 0.05	0.28 ± 0.07
Globus Pallidus	0.94 ± 0.13	0.97 ± 0.13	0.99 ± 0.12
Thalamus	4.86 ± 0.65	4.68 ± 0.44	4.22 ± 0.39
Microstructural DTI changes			
Caudate MD	0.00094 ± 0.00011	0.00104 ± 0.00013	0.00232 ± 0.00042*&
Putamen MD	0.00071 ± 0.00007	0.00073 ± 0.00002	0.00228 ± 0.00046*&
Substantia Nigra MD	0.0007 ± 0.00008	0.00075 ± 0.00008	0.00233 ± 0.00051*&
Caudate FA	0.19 ± 0.02	0.205 ± 0.02	0.151 ± 0.03*&
Putamen FA	0.209 ± 0.02	0.215 ± 0.02	0.155 ± 0.03*&
Substantia Nigra FA	0.433 ± 0.04	0.43 ± 0.08	0.154 ± 0.04*&
SWI iron depositions			
Caudate	148.68 ± 18.46	189.83 ± 23.18*	207.7 ± 47.44*
Putamen	149.96 ± 19.78	191.74 ± 19.96*	213.36 ± 55.42*
Substantia Nigra	154.89 ± 25.88	186.12 ± 17.31*	211.72 ± 45.37*
NM changes			
Substantia Nigra volume	358.02 ± 95.26	128.85 ± 33.84*	106.12 ± 24.83*
Locus coeruleus volume	20 ± 10.56	9.44 ± 3.32*	6.63 ± 1.55*
Substantia Nigra - Ratio 1	1.11 ± 0.05	1.15 ± 0.03	1 ± 0.23*&
Substantia Nigra - Ratio 2	0.91 ± 0.41	1.22 ± 0.25*	1.62 ± 0.38*&
Substantia Nigra - Ratio 3	0.11 ± 0.05	0.15 ± 0.03*	0.14 ± 0.03
Locus coeruleus - Ratio 1	1.15 ± 0.04	1.16 ± 0.03	1.01 ± 0.24*&
Locus coeruleus - Ratio 2	1.36 ± 0.41	1.46 ± 0.36	1.85 ± 0.43*&
Locus coeruleus - Ratio 3	0.15 ± 0.04	0.16 ± 0.03	0.15 ± 0.04

Continuous variables are expressed as mean ± standard deviation. Freesurfer volumes are corrected for total intracranial volume. Abbreviations: DTI= Diffusion tensor imaging; MD= Mean diffusivity; FA= fractional anisotropy; SWI= Susceptibility-weighted imaging; NM= Neuromelanin. P value vs. healthy controls Bonferroni post-hoc corrected. *P <0.05 vs. healthy controls, $^{\&}$P <0.05 vs. early *de novo* Parkinson's disease patients.

There were no differences in structural or microstructural volumetric MRI between early *de novo* patients and healthy controls (Table 4).

In term of iron depositions SWI MRI, early *de novo* Parkinson's disease patients had increased iron in caudate (P<0.05), putamen (P<0.05), and substantia nigra (P<0.05) compared to healthy controls (Figure 15).

In term of neuromelanin density NM MRI, early *de novo* Parkinson's disease patients had lower volume in the substantia nigra and locus coeruleus compared to healthy controls (Figure 16).

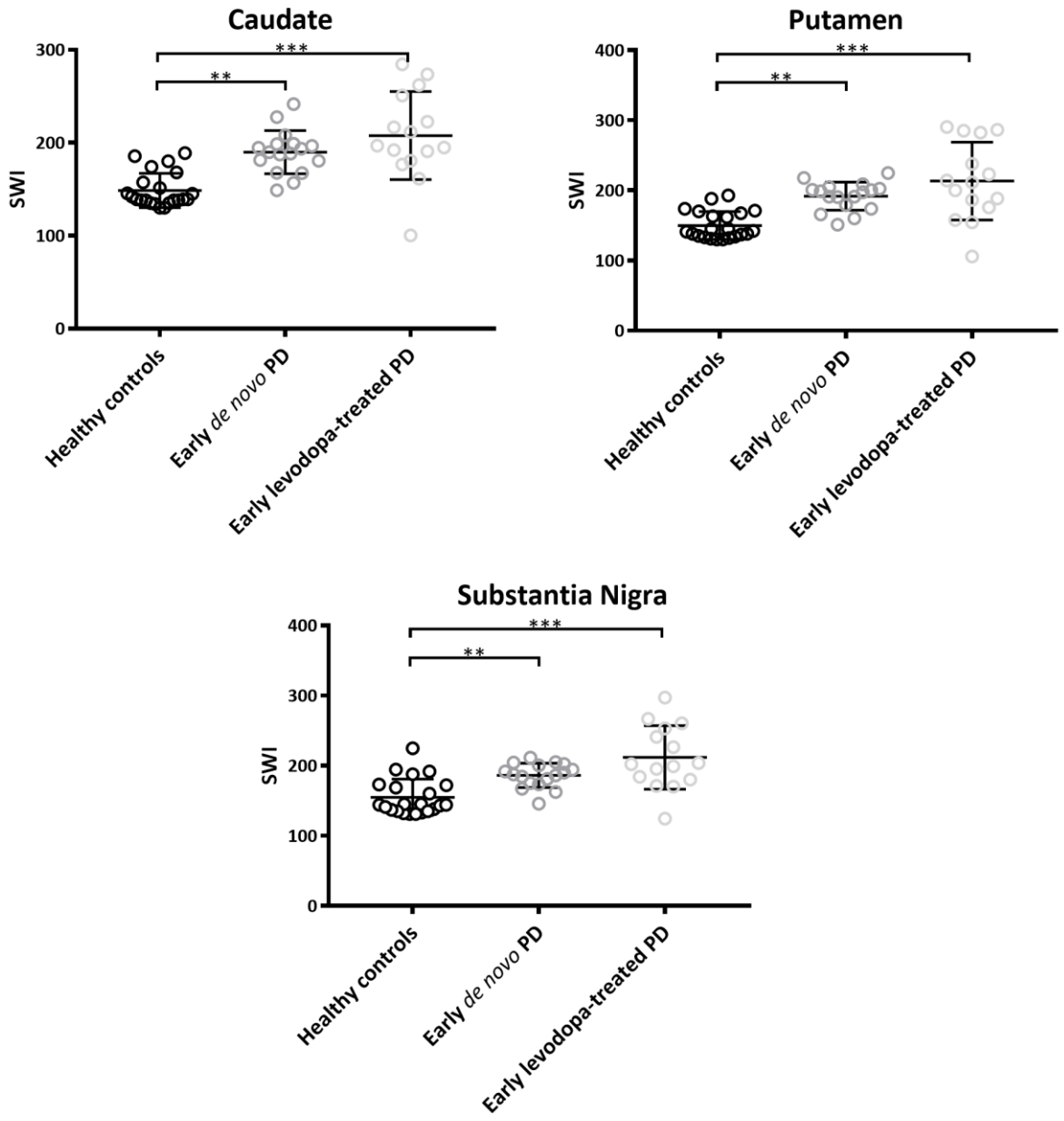

Figure 15. SWI MRI markers in the groups of Parkinson's disease (PD) patients and healthy controls. *Dot plot graphs showing mean SWI values ± standard deviation in subcortical brain regions in PD early de novo patients, PD early levodopa-treated patients and healthy controls. *P <0.05, **P <0.01, ***P <0.001 ANOVA with Bonferroni post-hoc correction*

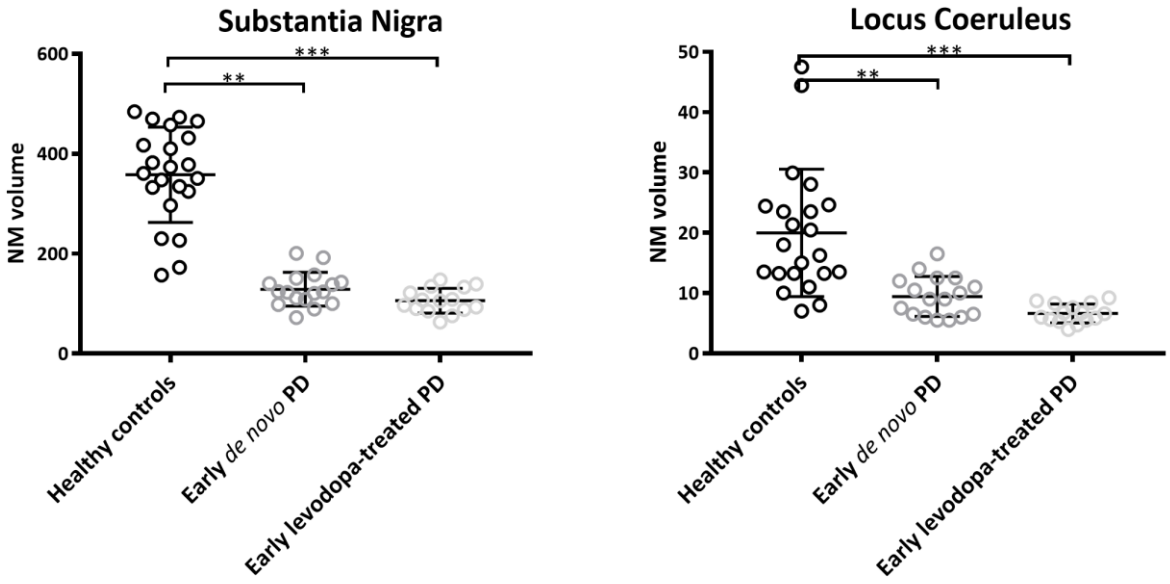

Figure 16. NM MRI markers in the groups of Parkinson's disease (PD) patients and healthy controls. *Dot plot graphs showing mean NM values ± standard deviation in subcortical brain regions in PD early de novo patients, PD early levodopa-treated patients and healthy controls. *P <0.05, **P <0.01, ***P <0.001 ANOVA with Bonferroni post-hoc correction*

In term of structural MRI, early treated Parkinson's disease patients had no changes in Freesurfer volumes compared to healthy controls or early *de novo* patients.

In term of iron depositions SWI MRI, early treated Parkinson's disease patients had increased iron in caudate, putamen, and substantia nigra compared to healthy controls, but similar values to early *de novo* patients (Figure 15).

In term of neuromelanin density NM MRI, early treated Parkinson's disease patients had lower volume in the substantia nigra and locus coeruleus, compared to healthy controls, but similar values to early *de novo* patients (Figure 16).

In term of structural Microstructural DTI MRI, early treated Parkinson's disease patients had increased MD and reduced FA in caudate, putamen, and substantia nigra compared to early *de novo* patients and healthy controls (Figure 17).

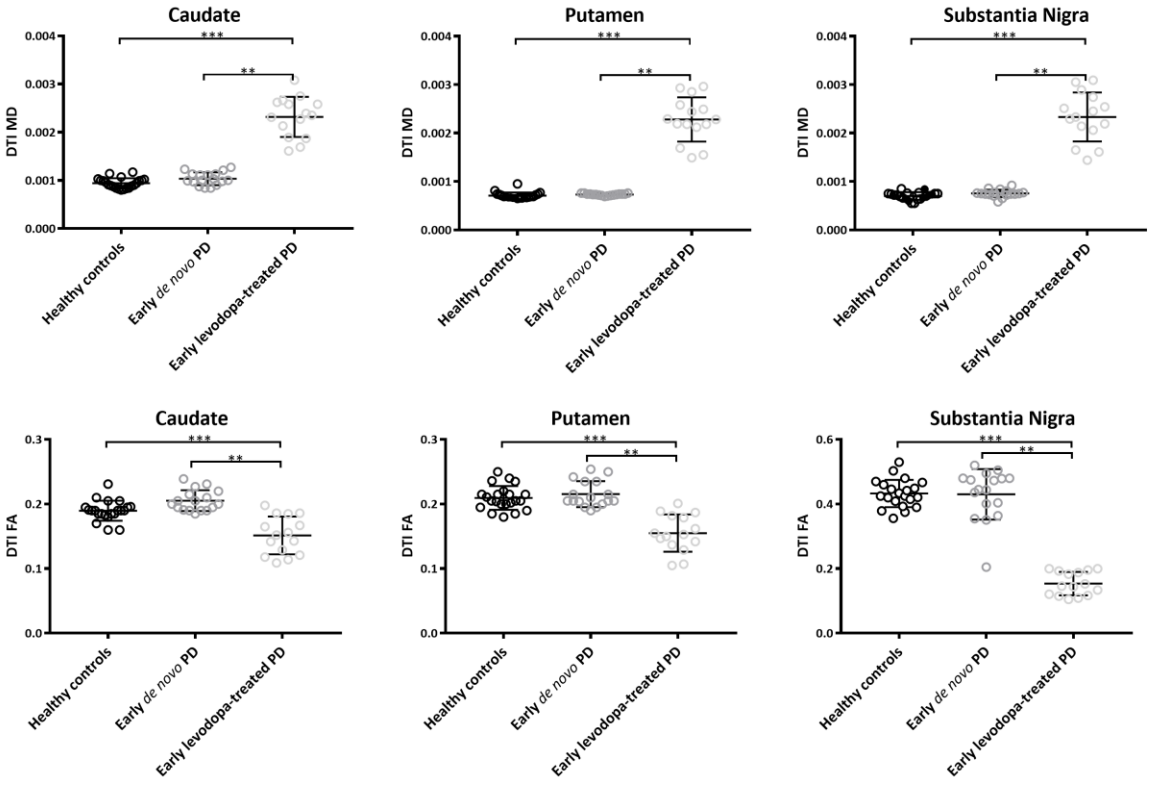

Figure 17. DTI MRI markers in the groups of Parkinson's disease (PD) patients and healthy controls. *Dot plot graphs showing mean DTI MD (top) and DTI FA (down) ± standard deviation in subcortical brain regions in PD early de novo patients, PD early levodopa-treated patients and healthy controls. *P <0.05, **P <0.01, ***P <0.001 ANOVA with Bonferroni post-hoc correction*

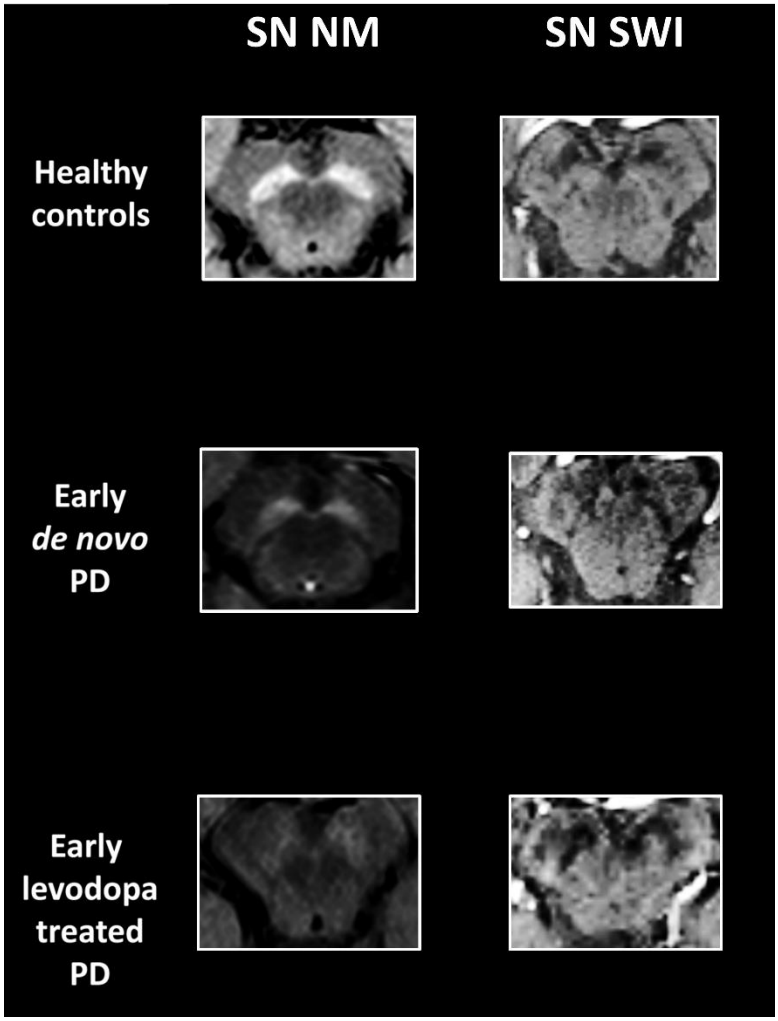

Figure 18. Altered SWI and NM markers in the substantia nigra of Parkinson's disease patients. *Axial images derived from (top) a healthy control, (middle) a Parkinson's disease early de novo and (bottom) a Parkinson's disease early levodopa-treated patient in stereotaxic space showing increased SWI iron deposition (left) and NM volume loss (right) in the substantia nigra.*

Older age was associated with smaller FreeSurfer volumes in the thalamus (*rho*=-0.61; *P*<0.05). Longer Parkinson's disease duration and was associated with smaller Freesurfer volumes in the thalamus (*rho*=-0.45; *P*<0.05), with increased DTI MD in the caudate (*rho*=0.67; *P*<0.05), putamen (*rho*=0.76; *P*<0.05) and substantia nigra (*rho*=0.77; *P*<0.05), reduced DTI FA in the caudate (*rho*=-0.72; *P*<0.05), putamen (*rho*=-0.74; *P*<0.05) and substantia nigra (*rho*=-0.78; *P*<0.05), and smaller

NM locus coeruleus volume (*rho*=-0.39; *P*<0.05). No correlations were found between Parkinson's disease duration and iron depositions SWI MRI (Figure 18).

In term of lateralization, in the group of early *de novo* patients with Parkinson's disease with unilateral motor symptoms, we assessed whether the clinically affected side of the body was associated with greater decreases in contralateral brain regions of interest DTI values. We found that DTI FA values in caudate (*P*<0.05) were decreased in the contralateral to most affected compared to the less affected side of the body. No differences were found for DTI MD, SWI or NM values.

When the group of early *de novo* and early treated Parkinson's patients were evaluated as a whole, higher MDS-UPDRS-III total scores, rigidity, bradykinesia and axial symptoms correlated with increased DTI MD in the caudate (total: *rho*=0.75; *P*<0.05; rigidity: *rho*=0.57; *P*<0.05; bradykinesia: *rho*=0.71; *P*<0.05; axial: *rho*=0.72; *P*<0.05), putamen (total: *rho*=0.71; *P*<0.05; rigidity: *rho*=0.69; *P*<0.05; bradykinesia: *rho*=0.67; *P*<0.05; axial: *rho*=0.61; *P*<0.05) and substantia nigra (total: *rho*=0.59; *P*<0.05; rigidity: *rho*=0.57; *P*<0.05; bradykinesia: *rho*=0.47; *P*<0.05; axial: *rho*=0.61; *P*<0.05), reduced DTI FA in the caudate (total: *rho*=-0.39; *P*<0.05; rigidity: *rho*=-0.53; *P*<0.05; bradykinesia: *rho*=-0.37; *P*<0.05; axial: *rho*=-0.46; *P*<0.05), putamen (total: *rho*=-0.48; *P*<0.05; rigidity: *rho*=-0.47; *P*<0.05; bradykinesia: *rho*=-0.42; *P*<0.05; axial: *rho*=-0.55; *P*<0.05) and substantia nigra (total: *rho*=-0.61; *P*<0.05; rigidity: *rho*=-0.52; *P*<0.05; bradykinesia: *rho*=-0.58; *P*<0.05; axial: *rho*=-0.60; *P*<0.05). No correlations were found with MDS-UPDRS-III resting tremor and DTI MD or FA.

In the subgroup of early *de novo* patients with Parkinson's disease, higher MDS-UPDRS-III total and bradykinesia scores correlated with increased DTI MD in the caudate (total: *rho*=0.59; *P*<0.05) and putamen (total: *rho*=0.72; *P*<0.05; *P*<0.05), reduced DTI FA in the caudate (total: *rho*=-0.51; *P*<0.05; bradykinesia: *rho*=-0.64; *P*<0.05), and putamen (total: *rho*=-0.60; *P*<0.05; bradykinesia: *rho*=-0.64;

P<0.05). No correlations were found with MDS-UPDRS-III rigidity, resting tremor or axial scores and DTI MD or FA.

In the subgroup of early treated patients with Parkinson's disease, no correlations were found with MDS-UPDRS-III total, rigidity, bradykinesia, resting tremor, axial scores and DTI MD or FA.

When the group of early *de novo* and early treated Parkinson's patients were evaluated as a whole, higher MDS-UPDRS-III total, rigidity, bradykinesia and axial symptoms scores correlated with smaller NM substantia nigra volume (total: *rho*=-0.47; *P*<0.05; rigidity: *rho*=-0.41; *P*<0.05; bradykinesia: *rho*=-0.49; *P*<0.05, Figure 19), locus coeruleus volume (total: *rho*=-0.50; *P*<0.05; rigidity: *rho*=-0.48; *P*<0.05; bradykinesia: *rho*=-0.54; *P*<0.05; axial: *rho*=-0.472; *P*<0.05). No correlations were found with MDS-UPDRS-III resting tremor and NM values.

In the subgroup of early *de novo* patients with Parkinson's disease, no correlations were found with MDS-UPDRS-III total, rigidity, bradykinesia, resting tremor, axial scores and NM values.

In the subgroup of early treated patients with Parkinson's disease, higher MDS-UPDRS-III total, rigidity and bradykinesia scores correlated with smaller NM substantia nigra volume (rigidity: *rho*=-0.79; *P*<0.05) and locus coeruleus volume (total: *rho*=-0.59; *P*<0.05; rigidity: *rho*=-0.59; *P*<0.05; bradykinesia: *rho*=-0.54; *P*<0.05). No correlations were found with MDS-UPDRS-III resting tremor or axial scores and NM values.

When the group of early *de novo* and early treated Parkinson's patients were evaluated as a whole, and in the two subgroups, no correlations were found with motor symptoms and Freesurfer volumes or SWI values.

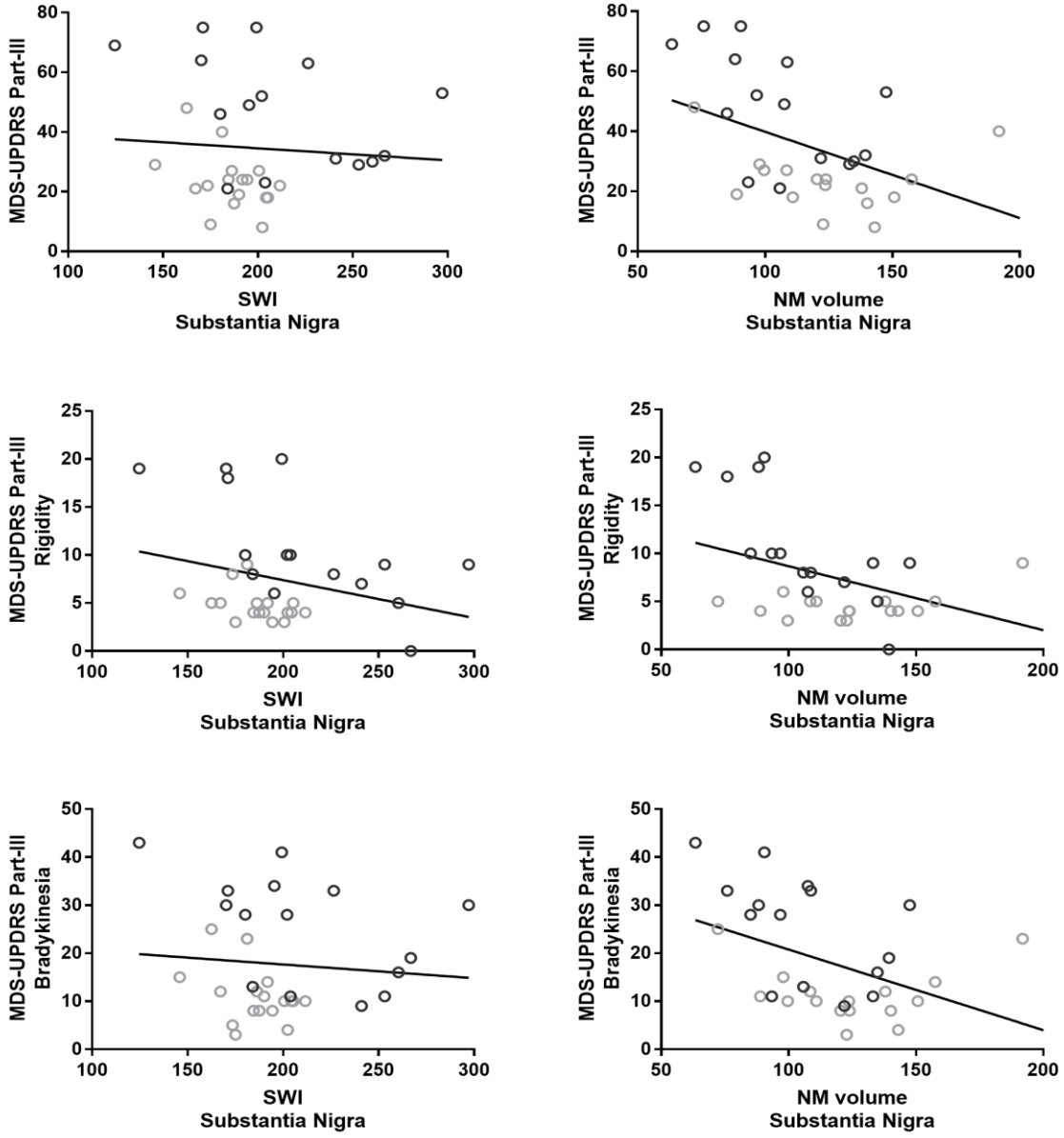

Figure 19. Correlations between MRI and motor symptoms in Parkinson's disease (PD) patients. *Spearman correlations between MDS-UPDRS-III total, rigidity and bradykinesia, and NM substantia nigra (left) volume (total: rho=-0.47; P<0.05; rigidity: rho=-0.41; P<0.05; bradykinesia: rho=-0.49; P<0.05). No correlations between MDS-UPDRS-III total, rigidity and bradykinesia, and SWI iron deposition in the substantia nigra (right) (total: rho=-0.053; P>0.10; rigidity: rho=-0.201; P>0.10; bradykinesia: rho=-0.031; P>0.10). PD early de novo in black circles and PD early levodopa-treated in grey circles.*

On T1 MRI scan, when the group of early *de novo* and early treated Parkinson's patients were evaluated as a whole, worse global non-motor symptoms impairment (higher MDS-UPDRS-I, MDS-UPDRS Part-I questionnaire or NMSS), correlated with lower Freesurfer volume in the thalamus

(MDS-UPDRS-I: *rho*=-0.39; *P*<0.05; MDS-UPDRS Part-I questionnaire: *rho*=-0.37; *P*<0.05; NMSS: *rho*=-0.42; *P*<0.05), putamen (MDS-UPDRS Part-I questionnaire: *rho*=-0.42; *P*<0.05), worse olfaction (lower UPSIT) correlated with Freesurfer volume in the caudate (*rho*=0.39; *P*<0.05). No correlations were found with constipation (Modified Constipation Assessment Scale), sleep (PDSS, ESS, RBQS), fatigue (Parkinson Fatigue Scale), autonomic dysfunction (SCOPA-AUT), and Freesurfer values.

No correlations were found with global non-motor symptoms (MDS-UPDRS-I, MDS-UPDRS Part-I questionnaire or NMSS), constipation (Modified Constipation Assessment Scale), sleep (PDSS, ESS, RBQS), fatigue (Parkinson Fatigue Scale), autonomic dysfunction (SCOPA-AUT), olfaction (UPSIT), quality of life (PDQ-39) and DTI or SWI values when the group of early *de novo* and early treated Parkinson's patients were evaluated as a whole or as subgroups.

When the group of early *de novo* and early treated Parkinson's patients were evaluated as a whole, worse global non-motor symptoms impairment (higher MDS-UPDRS-I, MDS-UPDRS Part-I questionnaire or NMSS) and worse sleep (higher ESS and RBQS) correlated with smaller NM locus coeruleus volume (MDS-UPDRS-I: *rho*=-0.42; *P*<0.05; NMSS: *rho*=-0.51; *P*<0.05; ESS: *rho*=-0.47; *P*<0.05, *rho*=-0.54; *P*<0.05) and worse autonomic dysfunction (higher SCOPA-AUT) correlated with smaller NM substantia nigra volume (*rho*=-0.56; *P*<0.05) and smaller NM locus coeruleus volume (*rho*=-0.44; *P*<0.05). No correlations were found with constipation (Modified Constipation Assessment Scale), global sleep (PDSS), fatigue (Parkinson Fatigue Scale) and NM values.

In the subgroup of early *de novo* patients with Parkinson's disease, worse autonomic dysfunction (higher SCOPA-AUT) correlated with smaller NM substantia nigra volume (*rho*=-0.51; *P*<0.05). No

correlations were found with constipation (Modified Constipation Assessment Scale), sleep (PDSS, ESS, RBQS), fatigue (Parkinson Fatigue Scale), olfaction (UPSIT), quality of life (PDQ-39) and NM values.

No correlations were found with constipation (Modified Constipation Assessment Scale), sleep (PDSS, ESS, RBQS), fatigue (Parkinson Fatigue Scale), autonomic dysfunction (SCOPA-AUT), olfaction (UPSIT), quality of life (PDQ-39) and NM values in the subgroup of early treated patients with Parkinson's disease.

On T1 MRI scan, when the group of early *de novo* and early treated Parkinson's patients were evaluated as a whole, worse global cognitive function (lower MSSE and MoCA) correlated with lower Freesurfer volume in the caudate (MoCA: *rho*=0.39; $P<0.05$), and putamen (MoCA: *rho*=0.36; $P<0.05$) and worse depressive symptoms (higher GDS, BDI-II) correlated with lower Freesurfer volume in the thalamus (GDS: *rho*=-0.45; $P<0.05$; BDI-II: *rho*=-0.39; $P<0.05$).

No correlations were found with cognitive impairment (MMSE, MoCA) or depressive symptoms (GDS, BDI-II) and Freesurfer values in the subgroups of early *de novo* or early treated patients with Parkinson's disease.

No correlations were found with cognitive impairment (MMSE, MoCA) or depressive symptoms (GDS, BDI-II) and DTI or SWI or NM values when the group of early *de novo* and early treated Parkinson's patients were evaluated as a whole on as subgroups.

Comparison between PDE10A PET and MRI markers of Parkinson's disease pathology

Lower individual [^{11}C]IMA107 BP_{ND} values in the caudate correlated with higher DTI MD values in the caudate (*rho*=-0.53; *P*<0.01), putamen (*rho*=-0.55; *P*<0.01) and substantia nigra (*rho*=-0.41; *P*<0.01), lower DTI FA values in the caudate (*rho*=0.37; *P*<0.01), putamen (*rho*=0.36; *P*<0.01) and substantia nigra (*rho*=0.49; *P*<0.01) and lower NM volume in the substantia nigra (*rho*=0.55; *P*<0.01) and locus coeruleus (*rho*=0.39; *P*<0.01) (Figure 20). No correlations were found [^{11}C]IMA107 BP_{ND} values and Freesurfer volumes, SWI or NM values in any other areas. We found that lower individual [^{11}C]IMA107 BP_{ND} values in the putamen correlated with higher DTI MD values in the caudate (*rho*=-0.49; *P*<0.01) and putamen (*rho*=-0.46; *P*<0.01) and lower DTI FA values in the caudate (*rho*=0.35; *P*<0.01) and substantia nigra (*rho*=0.38; *P*<0.01, Figure 20). No correlations were found [^{11}C]IMA107 BP_{ND} values and Freesurfer volumes, SWI or NM values in any other areas.

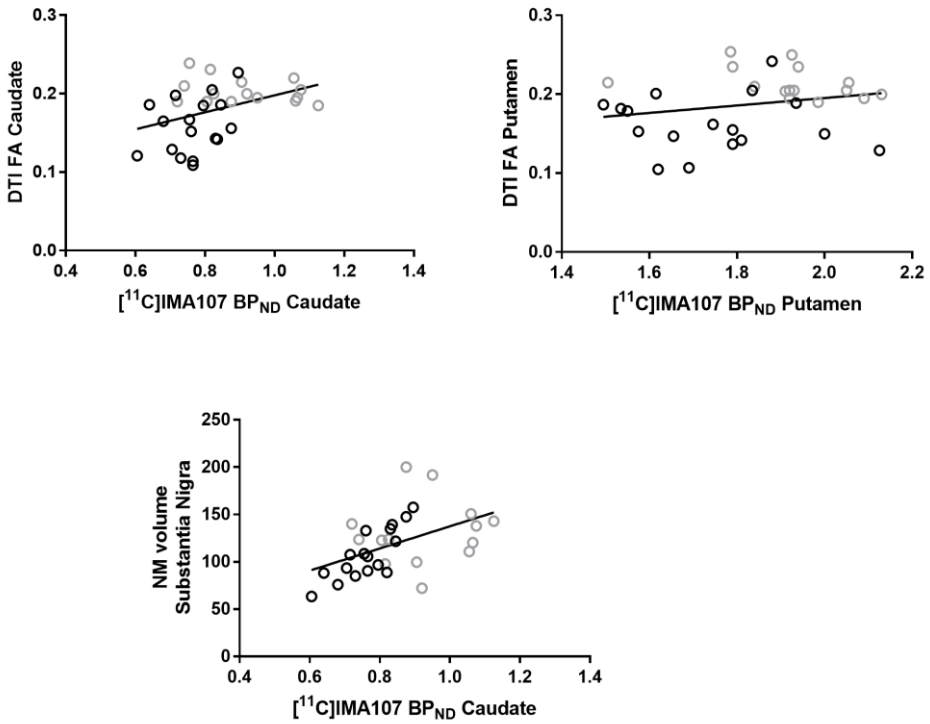

Figure 20. Correlations between PDE10A and MRI imaging in Parkinson's disease (PD) patients. *Spearman correlation between DTI and [^{11}C]IMA107 BP_{ND} (top) in the caudate (rho=0.37; P<0.01) and between NM substantia nigra volume and [^{11}C]IMA107 BP_{ND} (down) in the caudate (rho=0.554; P<0.001). No correlation between DTI and [^{11}C]IMA107 BP_{ND} (top) in the putamen (rho=0.227; P>0.10) PD early de novo in black circles and PD early levodopa-treated in grey circles.*

Comparison between DAT PET and MRI markers of Parkinson's disease pathology

Lower NM volume in the substantia nigra correlated with lower individual [^{11}C]PE2I BP_{ND} in the substantia nigra (rho = 0.545; P<0.0001), in the caudate (rho = 0.516; P<0.0001), in the putamen (rho = 0.720; P<0.0001) but not with SWI iron depositions. Early *de novo* and treated Parkinson's disease patients had significantly loss of [^{11}C]PE2I BP_{ND} and increased SWI iron depositions in the caudate (*P*<0.0001), putamen (*P*<0.0001) and substantia nigra (*P*<0.0001) and loss of NM in the substantia nigra (*P*<0.0001) compared to healthy controls (Table 4). No differences were found for DTI MD and FA maps in the *de novo*, while early levodopa-treated had significantly greater DTI MD in the caudate (*P*<0.0001), putamen (*P*<0.0001) and substantia nigra (*P*<0.0001) and lower DTI FA in the substantia nigra (*P*<0.0001) compared to healthy controls (Table 4).

We compared the loss of NM and increased SWI iron with loss of [^{11}C]PE2I BP_{ND} in each region-of-interest in Parkinson's disease patients relative to normality data from the group of healthy controls. We found that loss of NM was greater than the loss of [^{11}C]PE2I BP_{ND} in the substantia nigra (*P*<0.005). Increased SWI iron was greater than the loss of [^{11}C]PE2I BP_{ND} in the substantia nigra but lower in the putamen (*P*<0.0001). No differences were found in the caudate between increased SWI iron and loss of [^{11}C]PE2I BP_{ND}.

Early levodopa-treated showed loss of [^{11}C]PE2I BP_{ND} in the putamen (P<0.05), with additional loss of DAT in the putamen of 34% (decline per year = 10%) compared to early *de novo*, but not in the caudate (*P*>0.10) or in the substantia nigra (*P*>0.10), and loss of NM in the substantia nigra of 19.3% (decline per year = 3.58%). Early levodopa-treated patients had significantly higher DTI MD in the caudate (*P*<0.0001), putamen (*P*<0.0001) and substantia nigra (*P*<0.0001) and lower DTI FA in the caudate (*P*<0.0001), putamen (*P*<0.0001) and substantia nigra (*P*<0.0001) compared to early *de novo*

patients (Table 4). No differences were found for SWI iron depositions between early *de novo* and levodopa-treated Parkinson's disease patients.

5.1.7 Discussion

Our hypothesis was that a PDE10A expression was correlated with other markers of Parkinson's disease pathology, such as iron depositions, neuromelanin loss, and changes in structural and microstructural changes in the substantia nigra and in the striatum.

We aimed to test this hypothesis checking for correlations between the expression of PDE10A and MRI markers of Parkinson's pathology such as iron depositions (assessed with susceptibility-weighted MR imaging), neuromelanin loss (assessed with neuromelanin sensitive MR imaging) and changes in structural volumetric (assessed with T1 MR imaging) and microstructural connectivity (assessed with diffusion tensor MR imaging) (*Project 3 Aim*).

We have demonstrated that PDE10A expression in the caudate and putamen correlated with microstructural damage of substantia nigra (as measured by higher DTI MD values and lower NM volume) and of striatal terminals (as measured by lower DTI FA values). We found no correlations between PDE10A and brain atrophy (Freesurfer volumes) or SWI iron depositions.

Our findings demonstrate our hypothesis that loss of PDE10A correlated with neuromelanin loss and microstructural changes in the striatum, but we have to reject the hypothesis that loss of PDE10A correlated iron depositions or structural changes in the striatum.

This is a further confirmation of the value of PDE10A but also that Parkinson's disease pathology can be measured with advanced MRI techniques, since the earliest stages of the disease, through the quantification of NM-containing neurons of the SN. Our early PD patients have loss of NM in the SN and increased SWI iron in the SN and in the striatum. Loss of NM in the SN is correlated with the loss of DAT terminals and with loss of PDE10A expression in the striatum but not with the increased iron depositions. Levels of iron were not correlated with the duration of the disease or the severity of

motor symptoms, suggesting that this might be a trigger of neurodegeneration, since it was present since the earliest stages of the disease, but it is not specific of PD pathology, since is not correlated with other measures of Parkinson's disease pathology, such as DAT expression, and do not progress as the disease advances. We established that loss of NM in the SN is a pathological feature of Parkinson's disease since the early stage of the disease, independently of levodopa treatment, and correlated with the duration burden. Our results support the ability of NM-MRI to differentiate PD patients from healthy subjects as indicated in previous reports (Sasaki *et al.*, 2006; Ohtsuka *et al.*, 2014).

Our results confirm the concept that NM and DAT should be positively correlated with the dopaminergic neuronal density in the SN. A loss of NM has been previously demonstrated with MRI in Parkinson's disease patients as a stage-dependent phenomenon (Schwarz *et al.*, 2011; Nakamura and Sugaya, 2014) and correlated *post-mortem* with the number of NM-containing neurons in Parkinson's disease patients (Kitao *et al.*, 2013). This raises the panorama of NM-sensitive MRI being a potential biomarker of Parkinson's disease.

Imaging DAT with PET or SPECT imaging is currently considered the main biomarker for PD diagnosis and for evaluation of the progression of the disease. However, the availability of nuclear medicine evaluations in common clinical practice is still limited. MRI has been becoming a suitable and attractive alternative to radiotracer methods, when possible, due to its non-invasive nature, lower cost, good availability, and the fact that is not using ionizing radiation, contribute to its attractiveness for large cohorts of patients when longitudinal assessments are needed.

Here, we investigated the correlations between MRI markers of Parkinson's disease pathology in the SN and the corresponding nigro-striatal dopaminergic innervation loss as measured with [^{11}C]PE2I

PET imaging. Loss of NM is correlated with dopaminergic striatal innervation loss, with the duration of the disease and with the severity of motor symptoms. This loss was greater than DAT in the SN, but not in the putamen. This suggests that both biomarkers should be used and integrated for the evaluation of different brain structures.

We found that iron was higher in Parkinson's disease compared to controls but did not increase over the time in more advanced patients. Disease duration and motor symptoms were not correlated with iron levels, neither in the striatum or the SN. The process of iron accumulation in SN of PD patients is also not completely understood. Iron concentrations in dissected SN pars compacta and pars reticulata measured with accurate spectroscopic methods have shown that iron concentrations in these regions increase with disease severity,(Dexter *et al.*, 1987; Hirsch *et al.*, 1991) and it has been proposed that high iron content in the SN makes this region susceptible to neurodegeneration (Zecca *et al.*, 2004; Ward *et al.*, 2014). In the literature however, iron imaging results are mixed. Several reports have described an increase iron concentration in the SN of PD patients (Martin *et al.*, 2008; Baudrexel *et al.*, 2010), as we found in our study, but equally, others did not find significant differences in iron concentration between PD and controls (Zecca *et al.*, 2004; Ward *et al.*, 2014). Moreover, across the available MRI studies a rather large range of iron concentration and confidence intervals has been reported both in PD patients and controls.[9,11,12] These observations lead us to suspect that subtle differences in patient characteristics and measurement technique may be responsible for the inconsistency of results obtained with iron imaging by MRI, such that better standardization of technique is needed if the limitations of MRI for accurate measurement of iron in brain tissue are to be overcome and it is to have a role as a biomarker for PD (Martin *et al.*, 2008).

We did not attempt nigral subdivision into pars compacta and pars reticulata, such as can be performed at higher magnetic field (Lotfipour *et al.*, 2012; Lehericy *et al.*, 2014). The region of

interest definitions we have used are however strongly tied to the contrast in the images. Differences in location and morphology of the SN are apparent in the region-of-interests defined for our NM- and SWI MRI. Langley et al. have recently found NM and SWI contrasts to be selectively sensitive to caudal and rostral compartments of the SN respectively (Langley *et al.*, 2015). They proposed that the two histologically subregions of the SN, the SN pars compacta and the SN pars reticulata, are delineated by NM and SWI MRI, respectively. Considering this complementary role in their respective sensitivities to neuronal death, such that study of the progression of neurodegeneration in the SN is likely to benefit from their combined use. This confirms also why NM and iron were not correlated in the SN in our study.

We did not find any differences in DTI FA and MD values in early *de novo* patients compared to healthy controls, which is in line with a recent meta-analysis that questioned the stability and validity of this measure as a PD biomarker (Schwarz *et al.*, 2013). Whereas at baseline PD patients and controls did not consistently differ from controls with regards to diffusion measures, as the disease progresses a significant decrease of nigral FA and an increase of nigral MD become apparent, both in comparison with the controls and longitudinally (PD baseline vs PD follow up) (Loane *et al.*, 2016). In our study, early levodopa-treated PD had four years longer disease duration and showed lower MD and increased FA in the striatum and SN, in line with this finding. However, DTI reports of striatal diffusion over time in PD are not concordant (Loane, Politis et al. 2016), and we do not suggest using this technique as biomarker of PD pathology.

5.1.8 Conclusion

In summary, PDE10A expression in the caudate and putamen correlates with microstructural damage of substantia nigra and of striatal terminals but not with brain atrophy or iron depositions. This is a further confirmation of the value of PDE10A but also that Parkinson's disease pathology can be

measured with advanced MRI techniques, since the earliest stages of the disease, through the quantification of NM-containing neurons of the SN.

NM-MRI is a reliable tool to quantify PD pathology in the SN, strictly correlated with loss of strital DAT expression over the time and with worsening of motor symptoms. Further studies with a longitudinal multi-imaging design are needed to validate this novel imaging marker of PD for clinical practice and trials.

Chapter 6. Discussion

In Project 1, our hypothesis was that a reduction of PDE10A expression is an early phenomenon in the course of Parkinson's disease, and that PDE10A expression decreases further as Parkinson's disease progress (in term of duration and clinical severity).

We aimed to test this hypothesis comparing the expression of PDE10A (measured by using [^{11}C]IMA107 PET imaging) in early *de novo* and early levodopa-treated patients with Parkinson's disease versus age- and sex-matched healthy control subjects (*Project 1 Aim*).

We found that early *de novo* and early levodopa-treated patients with Parkinson's disease had lower mean [^{11}C]IMA107 BP_{ND} values in caudate, putamen and ventral striatum compared to healthy controls. Early levodopa-treated patients had lower striatal [^{11}C]IMA107 BP_{ND} values compared to early *de novo* patients, and striatal [^{11}C]IMA107 BP_{ND} values were correlated with disease duration and disease severity.

Our findings demonstrate our hypothesis that loss of striatal PDE10A expression is an early phenomenon in the course of Parkinson's disease and is associated with duration and severity of motor symptoms. Our study agrees with previous experimental work, which has demonstrated that lesions of nigrostriatal projections with 6-OHDA, induce a downregulation of PDE10A expression in the striatum in rodent models of Parkinson's disease (Giorgi *et al.*, 2008; Giorgi *et al.*, 2011).

We also hypothesize that PDE10A expression might be affected earlier on in the course of the disease investigating the associations between PDE10A and non-motor symptoms considered pre-motor (sleep problems, autonomic dysfunction, mood disorders etc). We aimed to test this hypothesis checking for correlations between the expression of PDE10A and non-motor symptoms considered pre-motor (sleep problems, autonomic dysfunction, mood disorders etc). PDE10A expression did not correlate with non-motor symptoms considered pre-motor (sleep problems, autonomic dysfunction,

mood disorders etc), which suggests that reduction of PDE10A might be concomitant and not earlier than DAT expression loss. Thus, we cannot accept this hypothesis.

In Project 2, our hypothesis was that a PDE10A expression was correlated with dopaminergic pathology, which can be measured either with PET or SPECT.

We aimed to test this hypothesis checking for correlations between the expression of PDE10A and the expression of dopamine transporters (measured by using [^{11}C]PE2I PET and [^{123}I]FP-CIT SPECT molecular imaging) (*Project 2 Aim*).

We found that striatal [^{11}C]IMA107 BP_{ND} values were correlated with striatal using [^{11}C]PE2I PET and [^{123}I]FP-CIT SPECT values.

Our findings demonstrate our hypothesis that loss of PDE10A correlated with loss of DAT in the striatum in early *de novo* and early levodopa-treated patients with Parkinson's disease, suggesting an association between PDE10A and dopaminergic function Both PDE10A and DAT expression were decreased in the striatum, and DAT also decreased in globus pallidus and thalamus. Our early *de novo* cohort of Parkinson's disease patients had less than two years of disease duration and the cohort of early levodopa-treated less than five years of Parkinson's symptoms and was taking levodopa for less than two years. Previously, it has been reported that the loss of striatal PDE10A expression was correlated with the burden of motor symptoms and complications in middle-stage treated Parkinson's disease patients with a mean of seven years of disease duration and advanced treated Parkinson's disease patients with a mean of 13 years of disease duration (Niccolini *et al.*, 2015a). Collectively, our findings and previous data suggest that loss of striatal PDE10A expression appears very early in the course of Parkinson's disease and progresses over time and is associated with the gradual increase of motor symptom burden in different disease stages. Our findings suggest that loss of PDE10A expression in globus pallidus is a phenomenon appearing later in the disease (Niccolini *et al.*, 2015a)

as PDE10A expression in this region was not affected in our earlier cohorts. Our findings were not affected by volumetric changes in the brain, age or gender.

Loss of PDE10A correlated with loss of DAT in the striatum in early *de novo* and early levodopa-treated patients with Parkinson's disease, suggesting an association between PDE10A and dopaminergic function. PDE10A plays a key role in the regulation of dopaminergic signaling and is essential for dopamine neurotransmission through the interaction with cAMP and the activation of PKA/DARPP-32 downstream cascade in striatal pathways (Greengard *et al.*, 1999; Nishi *et al.*, 2008; Girault, 2012).

In Project 3, our hypothesis was that a PDE10A expression was correlated with other markers of Parkinson's disease pathology, such as iron depositions, neuromelanin loss, and changes in structural and microstructural changes in the substantia nigra and in the striatum.

We aimed to test this hypothesis checking for correlations between the expression of PDE10A and MRI markers of Parkinson's pathology such as iron depositions (assessed with susceptibility-weighted MR imaging), neuromelanin loss (assessed with neuromelanin sensitive MR imaging) and changes in structural volumetric (assessed with T1 MR imaging) and microstructural connectivity (assessed with diffusion tensor MR imaging) (*Project 3 Aim*).

We have demonstrated that PDE10A expression in the caudate and putamen correlated with microstructural damage of substantia nigra (as measured by higher DTI MD values and lower NM volume) and of striatal terminals (as measured by lower DTI FA values). We found no correlations between PDE10A and brain atrophy (Freesurfer volumes) or SWI iron depositions.

Our findings demonstrate our hypothesis that loss of PDE10A correlated with neuromelanin loss and microstructural changes in the striatum, but we have to reject the hypothesis that loss of PDE10A correlated iron depositions or structural changes in the striatum.

This is a further confirmation of the value of PDE10A but also that Parkinson's disease pathology can be measured with advanced MRI techniques, since the earliest stages of the disease, through the

quantification of NM-containing neurons of the SN. Our early PD patients have loss of NM in the SN and increased SWI iron in the SN and in the striatum. Loss of NM in the SN is correlated with the loss of DAT terminals and with loss of PDE10A expression in the striatum but not with the increased iron depositions. Levels of iron were not correlated with the duration of the disease or the severity of motor symptoms, suggesting that this might be a trigger of neurodegeneration, since it was present since the earliest stages of the disease, but it is not specific of Parkinson's disease pathology, since is not correlated with other measures of Parkinson's disease pathology, such as DAT expression, and do not progress as the disease advances. We established that loss of NM in the substantia nigra is a pathological feature of Parkinson's disease since the early stage of the disease, independently of levodopa treatment, and correlated with the duration burden.

Comparison between PDE10A and DAT expression

We attempted to understand how informative PET molecular imaging of PDE10A and DAT could be used for monitoring the disease progression. Our levodopa-treated patients with Parkinson's disease had three years longer disease duration compared to early *de novo* Parkinson's disease patients. PDE10A expression showed a further decline in both the caudate and putamen, whereas DAT expression was further reduced only in the putamen in early levodopa-treated compared to early *de novo* Parkinson's disease patients. Specifically, the loss of PDE10A in the caudate reflected a 5.7% and in the putamen a 3.2% mean annual decline, whereas loss of DAT in the putamen reflected an 11.6% mean annual decline. PDE10A showed also a lower variability over the time, with an SD of 8.4% in the caudate and 9.6% in the putamen, whereas DAT showed a 17% SD in the putamen. In our study, we have shown that standardized differences (Cohen's d) between early *de novo* and levodopa-treated with three-year longer disease duration are 1.48 for caudate measured with [^{11}C]IMA107, and 1.57 for putamen measured with [^{11}C]PE2I. Assuming in detecting a 50% reduction in these differences in a potential 18-month clinical trial testing a disease-modifying drug

that reduces disease progression by 50%, we will have a 0.7412 Cohen's d for caudate PDE10A and a 0.7851 for putamen DAT. These figures are greater than [^{18}F]FDOPA, a validated biomarker of Parkinson's progression, that showed Cohen's d of 0.7993 at three-year follow-up in early *de novo* patients with Parkinson's (Bruck *et al.*, 2009), thus having a 0.3996 Cohen's d in this hypothetical trial. Providing an 80% power with a two-sided test using 5% type I error rate, we may need 60 participants if we use as endpoint the changes in the caudate [^{11}C]IMA107 levels, 54 subjects if we use as endpoint the changes in the putamen [^{11}C]PE2I levels and 200 subjects if we use as endpoint the changes in the putamen [^{11}F]FDOPA levels.

A recent study has compared [^{18}F]FDOPA and [^{11}C]PE2I in thirty-three patients with mild-moderate Parkinson's disease at baseline and at 18-month follow-up (Li *et al.*, 2018). They found that that [^{11}C]PE2I, but not [^{18}F]FDOPA, was able to predict changes in motor scores (UPDRS-III and bradykinesia-rigidity scores). These results were confirmed at voxel-wise analysis showing that lower [^{11}C]PE2I BP_{ND} in the striatum was correlated with higher motor severity. In addition, only the striatal changes in [^{11}C]PE2I BP_{ND} , but not in [^{18}F]FDOPA, were correlated with the progression of motor symptoms (changes in UPDRS-III and bradykinesia-rigidity scores) (Li *et al.*, 2018). This is a further confirmation that striatal [^{11}C]PE2I has a greater sensitivity for detecting differences in motor severity than [^{18}F]FDOPA and [^{11}C]PE2I should be used in clinical trials because more effective for evaluating the efficacy of neuroprotective treatments in Parkinson's disease.

We performed head-to-head comparisons between loss of PDE10A and DAT in Parkinson's disease patients relative to normality data from the group of healthy controls. We found that loss of PDE10A was greater than the loss of DAT in the caudate, but lower in the putamen, globus

pallidus and substantia nigra in both early *de novo* and early levodopa-treated patients with Parkinson's disease. In early *de novo* and levodopa-treated patients with Parkinson's disease, PDE10A tracer showed a 10% lower COV variability in the striatum, caudate and putamen compared to DAT. This suggests that PDE10A might be a more stable biomarker. Loss of PDE10A in both the caudate and putamen, and loss of DAT only in the putamen correlated with longer Parkinson's duration, the total burden of motor symptoms, and with increased rigidity and bradykinesia. The level of correlations between PDE10A and DAT and clinical scales were similar.

Considering the underlying pathophysiology of Parkinson's disease includes progressive deposition of α-synuclein, the ideal neuroimaging biomarker to monitor disease progression should be able to quantify regional deposition of abnormal α-synuclein accumulation. Development of such a molecular imaging radiotracer has been the focus of much research but is not yet forthcoming and assessment of DAT represents the most direct approach able to quantify presynaptic nigrostriatal dopaminergic neurons. Loss of striatal DAT signal is currently considered the gold standard in the differential diagnosis between degenerative *vs*. non-degenerative parkinsonism. However, this approach has some shortcomings. For example, DAT levels have a floor effect that limits its use to the initial stages of the disease and may be modulated by dopaminergic supplementation, with levodopa inducing a decline proportional to the dose used (Fahn *et al.*, 2004). Clinical trials that used DAT as a marker of Parkinson's disease pathology showed controversial results, with imaging studies appearing to contradict the clinical findings (Whone *et al.*, 2003; Fahn *et al.*, 2004; Parkinson Study Group, 2009). In CALM-PD (Parkinson Study Group, 2009) and REAL-PET (Whone *et al.*, 2003), subjects randomized to dopamine agonists showed worse clinical symptoms but lower DAT decline than subjects randomized to levodopa. In ELLEDOPA trial (Fahn *et al.*, 2004), subjects randomized to levodopa showed better

clinical symptoms but greater DAT decline than subjects on placebo. However, it is not clear whether dopaminergic treatment hastens disease progression, or it was a simple down-regulation of DAT due to the use of levodopa.

PDE10A imaging could be a robust alternative to DAT imaging regarding diagnosis and for evaluating disease burden and progression. Collectively in our studies, we found a gradual progressive decline of PDE10A in Parkinson's from very early to advanced stages, which was independent of levodopa treatment (Niccolini *et al.*, 2015a) and had no floor effect. This makes PDE10A imaging potentially attractive to explore its clinical use further. It is important to note that both [^{11}C]IMA107 and [^{11}C]PE2I are kinetically well-behaved tracers with good-to-very good reproducibility, and the differences in their binding in the striatum are probably related to the pathological processes underlying Parkinson's disease, more than characteristics of the tracers. Despite all these potential advantages of PDE10A imaging, only PET ligands are currently available for PDE10A whereas DAT levels can be measured with SPECT imaging. This limitation reduces the cost-effective use of this novel molecular imaging technique until a SPECT PDE10A tracer becomes available. Neither DAT or PDE10A are good biomarkers for other Parkinson's symptoms, like tremor or depression, where other mechanisms, such as serotonergic transporter deficit, seems to have a prominent role (Politis *et al.*, 2010b; Politis *et al.*, 2011; Loane *et al.*, 2013; Pagano *et al.*, 2017).

Comparison between DAT PET and DAT SPECT markers of Parkinson's disease pathology

Secondly, we used [^{123}I]FP-CIT-SPECT molecular imaging to quantify DAT expression in the same cohorts of Parkinson's patients and healthy controls. DAT [^{11}C]PE2I-PET and [^{123}I]FP-CIT-SPECT were decreased in the striatum and globus pallidus of early *de novo* and early levodopa-

treated patients with Parkinson's disease. Our findings demonstrate that loss of striatal DAT expression in Parkinson's disease can be effectively measured both with [^{123}I]FP-CIT-SPECT and [^{11}C]PE2I-PET, which were also associated with duration of the disease and severity of motor symptoms. Loss of [^{11}C]PE2I-PET correlated with loss of [^{123}I]FP-CIT-SPECT in the striatum in early *de novo* and early levodopa-treated patients with Parkinson's disease, which is a further confirmation that both tracers were good at measuring loss of dopaminergic terminals and can be used in clinical practice for confirmation of Parkinson's disease diagnosis. To note, disease duration correlated with lower DAT [^{11}C]PE2I-PET in the putamen, but not with DAT [^{123}I]FP-CIT-SPECT (probably due to the small size of our sample), which confirms the greater power of PET compared to SPECT imaging.

[^{11}C]PE2I-PET showed a higher accuracy than [^{123}I]FP-CIT-SPECT in measuring DAT expression in levodopa-treated patients. Our early *de novo* cohort of Parkinson's patients had less than 2 years of disease duration and the cohort of early levodopa-treated less than 5 years of Parkinson's symptoms and was in levodopa for less than 2 years. Our findings were not affected by volumetric changes in the brain, age or gender effect and were confirmed at a voxel level.

It has been demonstrated that the use of levodopa (Fahn *et al.*, 2004) and serotonin transporter inhibitors (de Win *et al.*, 2005; Booij *et al.*, 2007) interfere with [^{123}I]FP-CIT-SPECT signal. These drugs directly (SERT) or indirectly (levodopa) bind the peripheral serotonin transporter in circulating cells, which is associated with changes in the relative fraction of [^{123}I]FP-CIT ligand available within the brain. Clinical trials that used [^{123}I]FP-CIT-SPECT as a marker of Parkinson's disease pathology have shown controversial results, with imaging appeared to contradict the clinical results. In CALM-PD (Parkinson Study Group, 2009) and REAL-PET (Whone *et al.*, 2003), subjects randomized to dopamine agonists showed worse clinical symptoms but lower [^{123}I]FP-CIT-SPECT decline than subjects randomized to levodopa. In ELLEDOPA trial (Fahn *et al.*, 2004), subjects randomized to levodopa showed better clinical symptoms but greater [^{123}I]FP-

CIT-SPECT decline than subjects on placebo. However, it is not clear whether dopaminergic treatment hastens disease progression, or it was a simply a pharmacological interference on [^{123}I]FP-CIT-SPECT signal. This currently represents one of the main limitations for the use of [^{123}I]FP-CIT-SPECT in the evaluation of the efficacy of neuroprotective drugs on dopaminergic pathology, which [^{11}C]PE2I-PET might be able to overcome.

We attempted to understand how informative [^{11}C]PE2I-PET molecular imaging could be for monitoring the progression of the disease. Our levodopa-treated patients with Parkinson's disease had three years longer disease duration compared to early *de novo* Parkinson's patients. We found here that [^{123}I]FP-CIT-SPECT was equally good as [^{11}C]PE2I-PET in discriminating *de novo* untreated patients from healthy controls but showed lower accuracy in levodopa-treated. Compared to healthy controls, early levodopa-treated Parkinson's patients showed a loss of 30% in the putamen [^{11}C]PE2I-PET BP_{ND} but of only 17% in the putamen [^{123}I]FP-CIT-SPECT SBR. We also found within the early levodopa-treated Parkinson's patients that loss of [^{11}C]PE2I-PET BP_{ND} was 16% greater than the loss of [^{123}I]FP-CIT-SPECT SBR. This might be explained by the fact that [^{11}C]PE2I-PET BP_{ND} is independent of the use of levodopa, dopamine agonists or antidepressants (Bang *et al.*, 2016), where clearly [^{123}I]FP-CIT-SPECT SBR is not, which is another confirmation that [^{11}C]PE2I-PET might be better than [^{123}I]FP-CIT-SPECT in the quantification of DAT expression in treated patients.

[^{11}C]PE2I has also high specificity for DAT where [^{123}I]FP-CIT binds both DAT and serotonin transporter (Hall *et al.*, 1999; Emond *et al.*, 2008). Progressive loss of serotonin transporter has been demonstrated in Parkinson's disease, which is prominent in the putamen and is directly related to the duration of the disease (Politis *et al.*, 2010a; Pagano *et al.*, 2017). Lack of specificity for DAT in [^{123}I]FP-CIT signal might be then associated with lower accuracy in the determination

of dopaminergic terminals pathology. Lower DAT [^{123}I]FP-CIT-SPECT binding, but not DAT [^{11}C]PE2I-PET, is associated with greater cognitive impairment (lower MoCA) in the limbic pathway (ventral striatum, thalamus, caudate and putamen). This is a further confirmation of fact that [^{11}C]PE2I is more specific for DAT compared to [^{123}I]FP-CIT that binds also SERT. Recent evidence has shown that serotonergic dysfunction is associated with β-amyloid pathology and might underline the development of cognitive impairment in Parkinson's disease (Kotagal *et al.*, 2018).

Clinical trials aimed to show neuroprotective effect on dopaminergic terminals need to use a biomarker that is specific for DAT expression. Identification of molecular biomarkers characterising the pathological processes in Parkinson's disease could also help monitor disease burden and progression, and drug target identification. So far, markers of presynaptic dopaminergic system such as quantification of striatal DAT have been extensively used for aiding diagnostics between neurodegenerative and non-neurodegenerative forms of parkinsonism and as correlates with motor symptoms. Our findings demonstrate that quantification of [^{11}C]PE2I-PET has potential as a molecular imaging biomarker for Parkinson's disease progression and, taking all these evidence into account, the use of [^{11}C]PE2I-PET should be suggested rather than [^{123}I]FP-CIT-SPECT in future clinical trials.

[^{11}C]PE2I-PET seems to be a more stable biomarker for diagnosis of Parkinson's disease. [^{11}C]PE2I-PET have shown higher specificity than [^{123}I]FP-CIT-SPECT for the differential diagnosis between Parkinson's disease and other neurodegenerative parkinsonism (Appel *et al.*, 2015). In line with our study, they found a high consistency between [^{11}C]PE2I-PET and [^{123}I]FP-CIT-SPECT images. [^{11}C]PE2I-PET has several advantages over [^{123}I]FP-CIT-SPECT in the differential diagnosis of parkinsonian disorders with respect to data quality, radiation dose, and

scanning logistics. One advantage is that PET images have a higher resolution than SPECT images. The data quality is further improved by the use of established kinetic models for generation of parametric images, which allow valid voxel-wise analysis. In addition, as indicated above, the radioligand [^{11}C]PE2I binds highly selectively to DAT, whereas [^{123}I]FP-CIT-SPECT also has high affinity for serotonin transporters and moderate affinity for norepinephrine transporters, causing an overestimation of DAT availability. When using solely a single [^{11}C]PE2I-PET scan, the radiation dose is reduced by 50% from about 5 mSv for the [^{123}I]FP-CIT-SPECT (Darcourt *et al.*, 2010) to about 2.5 mSv for [^{11}C]PE2I-PET (Ribeiro *et al.*, 2007). From a patient perspective, the preparation time before scanning can be up to 6 h for a [^{123}I]FP-CIT-SPECT scan but less than 30 min for an [^{11}C]PE2I-PET scan.

[^{11}C]PE2I-PET has also potential limitations in quantifying DAT expression. First, the relatively slow kinetics of [^{11}C]PE2I-PET requires imaging acquisitions 90 min long, which certainly increases the risk for significant movement or for the patient's being unable to complete the scan. Second, a radiometabolite of [^{11}C]PE2I-PET has been found to cross the blood-brain barrier of the rat brain, and to accumulate in the striatum, which limited the kinetic analysis (Hirvonen *et al.*, 2008). Also, relatively short half-life is an impediment of the 11C-labeled compound for clinical application. In contrast to [^{18}F]-ligands, [^{11}C]PE2I can therefore not be transported over long distances. Then, the [^{11}C]PE2I ligand has to be produced in-house at the PET facility with its own production capacity because of the limited half-life of [^{11}C]. This limitation tremendously reduces the possible widespread use of [^{11}C]PE2I (but also of [^{11}C]IMA107) in clinical settings, limiting its use to clinical trials.

In conclusion, our findings demonstrate that [^{123}I]FP-CIT-SPECT and [^{11}C]PE2I-PET are both good biomarkers in differentiate Parkinson's disease from healthy controls. However, [^{11}C]PE2I-PET showed a higher accuracy for DAT expression, particularly in the levodopa-treated subjects, which suggests its potential use in clinical trials testing drugs on disease progression.

Comparison between DAT PET and MRI markers of Parkinson's disease pathology

Lastly, we demonstrate that Parkinson's disease pathology can be measured with advanced MRI techniques, since the earliest stages of the disease, through the quantification of NM-containing neurons of the substantia nigra. Our early Parkinson's disease patients have loss of NM in the substantia nigra and increased SWI iron in the substantia nigra and in the striatum. Loss of NM in the substantia nigra is correlated with the loss of dopaminergic terminals in the striatum but not with the increased iron depositions. Levels of iron were not correlated with the duration of the disease or the severity of motor symptoms, suggesting that this might be a trigger of neurodegeneration, since it was present since the earliest stages of the disease, but it is not specific of Parkinson's disease pathology, since is not correlated with other measures of Parkinson's disease pathology, such as DAT expression, and do not progress as the disease advances. We established that loss of NM in the substantia nigra is a pathological feature of Parkinson's disease since the early stage of the disease, independently of levodopa treatment, and correlated with the duration burden. Our results support the ability of NM-MRI to differentiate Parkinson's disease patients from healthy subjects as indicated in previous reports (Sasaki *et al.*, 2006; Ohtsuka *et al.*, 2014).

Our results confirm the concept that NM and DAT should be positively correlated with the dopaminergic neuronal density in the substantia nigra. This finding can also be extended to PDE10A, which closely correlates with DAT and NM. A loss of NM has been previously demonstrated with MRI in Parkinson's disease patients as a stage-dependent phenomenon (Schwarz *et al.*, 2011; Nakamura and Sugaya, 2014) and correlated *post-mortem* with the number of NM-containing neurons in Parkinson's disease patients (Kitao *et al.*, 2013). This raises the panorama of NM-sensitive MRI being a potential biomarker of Parkinson's disease.

Imaging DAT with PET or SPECT imaging is currently considered the main biomarker for Parkinson's disease diagnosis and for evaluation of the progression of the disease. However, the availability of nuclear medicine evaluations in common clinical practice is still limited. MRI has been becoming a suitable and attractive alternative to radiotracer methods, when possible, due to its non-invasive nature, lower cost, good availability, and the fact that is not using ionizing radiation, contribute to its attractiveness for large cohorts of patients when longitudinal assessments are needed.

Here, we investigated the correlations between MRI markers of Parkinson's disease pathology in the substantia nigra and the corresponding nigro-striatal dopaminergic innervation loss as measured with [^{11}C]PE2I PET imaging. Loss of NM is correlated with dopaminergic striatal innervation loss, with the duration of the disease and with the severity of motor symptoms. This loss was greater than DAT in the substantia nigra, but not in the putamen. This suggests that both biomarkers should be used and integrated for the evaluation of different brain structures.

We found that iron was higher in Parkinson's disease compared to controls but did not increase over the time in more advanced patients. Disease duration and motor symptoms were not correlated with iron levels, neither in the striatum or the substantia nigra. The process of iron accumulation in substantia nigra of Parkinson's disease patients is also not completely understood. Iron concentrations in dissected SNpc and substantia nigra pars reticulata measured with accurate spectroscopic methods have shown that iron concentrations in these regions increase with disease severity (Dexter *et al.*, 1987; Hirsch *et al.*, 1991), and it has been proposed that high iron content in the substantia nigra makes this region susceptible to neurodegeneration (Zecca *et al.*, 2004; Ward *et al.*, 2014). In the literature however, iron imaging results are mixed. Several reports have

described an increase iron concentration in the substantia nigra of Parkinson's disease patients (Martin *et al.*, 2008; Baudrexel *et al.*, 2010), as we found in our study, but equally, others did not find significant differences in iron concentration between Parkinson's disease and controls (Zecca *et al.*, 2004; Ward *et al.*, 2014). Moreover, across the available MRI studies a rather broad range of iron concentration and confidence intervals has been reported both in Parkinson's disease patients and controls. These observations lead us to suspect that subtle differences in patient characteristics and measurement technique may be responsible for the inconsistency of results obtained with iron imaging by MRI, such that better standardization of technique is needed if the limitations of MRI for accurate measurement of iron in brain tissue are to be overcome and it is to have a role as a biomarker for Parkinson's disease (Martin *et al.*, 2008). A seminal paper on brain MRI iron measurement has been recently published (Martin-Bastida *et al.*, 2017). They studied seventy patients with mild to moderate Parkinson's disease and twenty age- and gender-matched healthy volunteers and found an increased iron accumulation in the putamen, globus pallidus and substantia nigra at SWI-MRI in Parkinson's disease patients, which appeared to be stratified according to disease motor severity and correlated with UPDRS-III and bradykinesia-rigidity subscores, but not with tremor subscores. This study suggests that a semi-quantitative *in vivo* iron assessment with SWI-MRI could prove useful for objectively monitoring Parkinson's disease progression, especially in clinical trials concerning iron chelation therapies (Martin-Bastida *et al.*, 2017).

We did not attempt nigral subdivision into pars compacta and pars reticulata, such as can be performed at higher magnetic field (Lotfipour *et al.*, 2012; Lehericy *et al.*, 2014). The region of interest definitions we have used are however strongly tied to the contrast in the images. Differences in location and morphology of the substantia nigra are apparent in the region-of-interests defined for our NM- and SWI MRI. Langley et al. have recently found NM and SWI

contrasts to be selectively sensitive to caudal and rostral compartments of the substantia nigra respectively (Langley *et al.*, 2015). They proposed that the two histologically sub-regions of the substantia nigra, the SNpc and the substantia nigra pars reticulata, are delineated by NM and SWI MRI, respectively. Considering this complementary role in their respective sensitivities to neuronal death, such that study of the progression of neurodegeneration in the substantia nigra is likely to benefit from their combined use. This confirms also why NM and iron were not correlated in the substantia nigra in our study.

We did not find any differences in DTI FA and MD values in early *de novo* patients compared to healthy controls, which is in line with a recent meta-analysis that questioned the stability and validity of this measure as a Parkinson's disease biomarker (Schwarz *et al.*, 2013). Whereas at baseline Parkinson's disease patients and controls did not consistently differ from controls with regards to diffusion measures, as the disease progresses a significant decrease of nigral FA and an increase of nigral MD become apparent, both in comparison with the controls and longitudinally (Parkinson's disease baseline vs Parkinson's disease follow up) (Loane *et al.*, 2016). In our study, early levodopa-treated Parkinson's disease had four years longer disease duration and showed lower MD and increased FA in the striatum and substantia nigra, in line with this finding. However, DTI reports of striatal diffusion over time in Parkinson's disease are not concordant (Loane, Politis et al. 2016), and we do not suggest using this technique as biomarker of Parkinson's disease pathology.

Imaging of Parkinson's disease pathology and non-motor symptoms

Our findings indicate that PDE10A does not correlate with non-motor or premotor symptoms. Thalamic atrophy is associated with greater non-motor symptoms burden, substantia nigra atrophy

is associated with depressive symptoms, autonomic dysfunction and olfactory dysfunction and locus coeruleus atrophy is associated with excessive daytime sleepiness, RBD symptoms and autonomic dysfunction in Parkinson's disease patients. However, further studies, investigating morphological brain changes and non-motor symptoms burden in a larger cohort of Parkinson's disease patients are needed to confirm our findings.

In summary, NM-MRI is a reliable tool to quantify Parkinson's disease pathology in the substantia nigra, strictly correlated with loss of striatal DAT and PDE10A expression over the time and with worsening of motor symptoms. Further studies with a longitudinal multi-imaging design are needed to validate this novel imaging marker of Parkinson's disease for clinical practice and trials.

Chapter 7. Future directions

This chapter summarizes the future directions based on the results of this thesis, which includes the potential use in clinical practice of PDE10A PET, the development of PDE10A SPECT tracers, the potential use in clinical practice of PE2I PET, the development of PE2I SPECT tracers, the potential use in clinical practice of novel MRI techniques for diagnosis of Parkinson's disease, and the potential use in clinical trials of these novel biomarkers (PDE10A, DAT PET, NM or SWI MRI) stronger than the ones currently used (DAT SPECT or FDOPA).

PDE10A PET imaging might be used in clinical practice to aid in the diagnosis of Parkinson's disease. Our study confirms that patients with Parkinson's disease have a loss of both DAT and PDE10A in the striatum. This will open avenues to investigate PDE10A in Parkinsonism with unaffected DAT levels, the so-called Scan Without Evidence of Dopaminergic Deficit (SWEDD). This population represents about 10% of patients enrolled in clinical trials and having a second independent measure of Parkinson's disease pathology might be fundamental for a better identification of the candidate of neuroprotective drugs. PDE10A PET imaging can be used to monitor disease progression, independently of the use of dopaminergic supplementation or antidepressants. In this instance, also DAT-PET with [^{11}C]PE2I showed a greater power and specificity compared to DAT-SPECT with [^{123}I]FP-CIT, which suggests that DAT-PET (over DAT-SPECT) should be used in Parkinson's disease clinical trials. PDE10A might also be investigated in atypical parkinsonism, where an overlap with DAT imaging is currently present. Further studies using both PDE10A and DAT PET imaging should be performed in patients with multiple system atrophy, progressive supranuclear palsy and corticobasal syndrome. As previously indicated in Huntington's disease, we expected a profound loss of PDE10A that can be diagnostic in the earliest phase of these conditions, complex to diagnosis in clinical practice. Another area to investigate further is the relationship between PDE10A expression

and the development of cognitive decline. Our and experimental data suggests that the PDE10A system is a dynamic player within large-scale brain networks and more local neurotransmitter circuits. Limbic loss of PDE10A might be an important determinant of neuropsychiatric changes and the presence of more severe neuropsychiatric symptoms may serve as a risk factor for dementia in Parkinson's disease. Great loss of PDE10A might be also associated with falls, slow gait speed, freezing of gait, sensory processing during postural control and dyskinesias in PD. The development of motor complications and its relationship with PDE10A is another area to investigate further. Several drug acting directly or indirectly on PDE10A activity might be tested in Parkinson's disease patients to improve not only motor symptoms but also motor complications. A diffuse use of molecular imaging of the PDE10A system is poised to guide and evaluate future drug development in Parkinson's disease.

Currently only PET ligands are available for the *in vivo* assessment of PDE10A whereas DAT levels can be measured with SPECT imaging. Future studies might focus on the development of a SPECT PDE10A tracer, which will facilitate the extension of the use of PDE10A in clinical practice. Having a PDE10A SPECT tracer will reduce the cost-effective use of this novel molecular imaging technique. There are however several technical constrains in the development of reliable SPECT tracers. Several attempts have been performed to finally obtain a reliable PET tracer for PDE10A, thus, the costs of implementation and development of novel SPECT tracer might be higher than the actual clinical benefit gained afterwards.

Another interesting topic suggested by the results of this thesis is that DAT-PET with [^{11}C]PE2I might be implement in clinical practice. Although the cost are currenlty about 3-4 times higher than DAT-SPECT with [^{123}I]FP-CIT, the main advantage will be a lower exposure to ionizing radiation with

[^{11}C]PE2I (about 1.5 mSv) compared to [^{123}I]FP-CIT (about 4.5 mSv). DAT-PET with [^{11}C]PE2I might be useful in the patients that take antidepressants or high dose of levodopa. The greater power of DAT-PET with [^{11}C]PE2I might also be useful in the identification of atypical Parkinsonism. Although a DAT-SPECT with [^{123}I]PE2I is currently possible, as the tracer already used in the past, this exam is not licenced or available in clinical practice.

Our findings corroborate the recent evidence that advanced MRI might be useful in clinical practice for diagnosis of Parkinson's disease. Brain MRI is widely available and do not involve the use of ionizing radiation. The identification of a reliable MRI biomarker to monitor disease progression would be the cornerstone in the neuroimaging research on Parkinson's disease. However, the ones we identified are more useful for diagnosis in the early (NM and SWI) or more advanced (DTI, Freesurfer) stages and did not show a linear progressive loss, as instead shown by PDE10A or DAT expression. Brain MRI in Parkinson's disease can became crucial in supporting the pathophysiological pathways underlying the specific symptoms developed by the Parkinson's disease patients. Abnormalities of structural and microstructural may be indeed detected in the earlier stages of the disease, even before the onset of motor symptoms and may used to track development and progression of complications over the disease course. At this stage, divergent and sometimes conflicting results are probably due to different methodological approaches, thus, the development of international validated approach is a necessary condition to move forward with the brain MRI imaging. Further studies are needed to be performed with multicentre desing in order to standardize the research protocols and improve the current techniques. Finally, our findings increase the potential array of biomarkers available for use in clinical trials. We anticipate that PDE10A-PET, DAT-PET, NM and SWI-MRI are powerful and specific biomarkers of Parkinson's disease pathology and should be used over current ones, such as DAT-SPECT or [^{18}F]FDOPA-PET.

Chapter 8. References

Ahmad R, Bourgeois S, Postnov A, Schmidt ME, Bormans G, Van Laere K, *et al.* PET imaging shows loss of striatal PDE10A in patients with Huntington disease. Neurology 2014; 82(3): 279-81.

Andersson JL, Skare S, Ashburner J. How to correct susceptibility distortions in spin-echo echo-planar images: application to diffusion tensor imaging. Neuroimage 2003; 20(2): 870-88.

Andersson JLR, Graham MS, Zsoldos E, Sotiropoulos SN. Incorporating outlier detection and replacement into a non-parametric framework for movement and distortion correction of diffusion MR images. Neuroimage 2016; 141: 556-72.

Andre VM, Cepeda C, Levine MS. Dopamine and glutamate in Huntington's disease: A balancing act. CNS Neurosci Ther 2010; 16(3): 163-78.

Antonini A, Vitale C, Barone P, Cilia R, Righini A, Bonuccelli U, *et al.* The relationship between cerebral vascular disease and parkinsonism: The VADO study. Parkinsonism & related disorders 2012; 18(6): 775-80.

Appel L, Jonasson M, Danfors T, Nyholm D, Askmark H, Lubberink M, *et al.* Use of 11C-PE2I PET in differential diagnosis of parkinsonian disorders. Journal of nuclear medicine : official publication, Society of Nuclear Medicine 2015; 56(2): 234-42.

Ashburner J, Friston KJ. Voxel-based morphometry--the methods. Neuroimage 2000; 11(6 Pt 1): 805-21.

Asikainen S, Rudgalvyte M, Heikkinen L, Louhiranta K, Lakso M, Wong G, *et al.* Global microRNA expression profiling of Caenorhabditis elegans Parkinson's disease models. J Mol Neurosci 2010; 41(1): 210-8.

Atkinson-Clement C, Pinto S, Eusebio A, Coulon O. Diffusion tensor imaging in Parkinson's disease: Review and meta-analysis. Neuroimage Clin 2017; 16: 98-110.

Bang JI, Jung IS, Song YS, Park HS, Moon BS, Lee BC, *et al.* PET imaging of dopamine transporters with [(18)F]FE-PE2I: Effects of anti-Parkinsonian drugs. Nucl Med Biol 2016; 43(2): 158-64.

Barbosa JH, Santos AC, Tumas V, Liu M, Zheng W, Haacke EM, *et al.* Quantifying brain iron deposition in patients with Parkinson's disease using quantitative susceptibility mapping, R2 and R2. Magn Reson Imaging 2015; 33(5): 559-65.

Barone P, Antonini A, Colosimo C, Marconi R, Morgante L, Avarello TP, *et al.* The PRIAMO study: A multicenter assessment of nonmotor symptoms and their impact on quality of life in Parkinson's disease. Movement disorders : official journal of the Movement Disorder Society 2009; 24(11): 1641-9.

Barret O, Thomae D, Tavares A, Alagille D, Papin C, Waterhouse R, *et al.* In vivo assessment and dosimetry of 2 novel PDE10A PET radiotracers in humans: 18F-MNI-659 and 18F-MNI-654. Journal of nuclear medicine : official publication, Society of Nuclear Medicine 2014; 55(8): 1297-304.

Baudrexel S, Nurnberger L, Rub U, Seifried C, Klein JC, Deller T, *et al.* Quantitative mapping of T1 and T2* discloses nigral and brainstem pathology in early Parkinson's disease. Neuroimage 2010; 51(2): 512-20.

Benitez-Rivero S, Marin-Oyaga VA, Garcia-Solis D, Huertas-Fernandez I, Garcia-Gomez FJ, Jesus S, *et al.* Clinical features and 123I-FP-CIT SPECT imaging in vascular parkinsonism and Parkinson's disease. Journal of neurology, neurosurgery, and psychiatry 2013; 84(2): 122-9.

Benjamini Y, Cohen R. Weighted false discovery rate controlling procedures for clinical trials. Biostatistics 2017; 18(1): 91-104.

Booij J, de Jong J, de Bruin K, Knol R, de Win MM, van Eck-Smit BL. Quantification of striatal dopamine transporters with 123I-FP-CIT SPECT is influenced by the selective serotonin reuptake inhibitor paroxetine: a double-blind, placebo-controlled, crossover study in healthy control subjects. Journal of nuclear medicine : official publication, Society of Nuclear Medicine 2007; 48(3): 359-66.

Boscutti G, E AR, Plisson C. PET Radioligands for imaging of the PDE10A in human: current status. Neurosci Lett 2018.

Braak H, Del Tredici K, Rub U, de Vos RA, Jansen Steur EN, Braak E. Staging of brain pathology related to sporadic Parkinson's disease. Neurobiol Aging 2003; 24(2): 197-211.

Braak H, Sastre M, Bohl JR, de Vos RA, Del Tredici K. Parkinson's disease: lesions in dorsal horn layer I, involvement of parasympathetic and sympathetic pre- and postganglionic neurons. Acta Neuropathol 2007; 113(4): 421-9.

Brooks DJ, Pavese N. Imaging biomarkers in Parkinson's disease. Prog Neurobiol 2011; 95(4): 614-28.

Brown RG, Dittner A, Findley L, Wessely SC. The Parkinson fatigue scale. Parkinsonism & related disorders 2005; 11(1): 49-55.

Bruck A, Aalto S, Rauhala E, Bergman J, Marttila R, Rinne JO. A follow-up study on 6-[18F]fluoro-L-dopa uptake in early Parkinson's disease shows nonlinear progression in the putamen. Movement disorders : official journal of the Movement Disorder Society 2009; 24(7): 1009-15.

Buckner RL, Head D, Parker J, Fotenos AF, Marcus D, Morris JC, *et al.* A unified approach for morphometric and functional data analysis in young, old, and demented adults using automated atlas-based head size normalization: reliability and validation against manual measurement of total intracranial volume. Neuroimage 2004; 23(2): 724-38.

Castellanos G, Fernandez-Seara MA, Lorenzo-Betancor O, Ortega-Cubero S, Puigvert M, Uranga J, *et al.* Automated neuromelanin imaging as a diagnostic biomarker for Parkinson's disease. Mov Disord 2015; 30(7): 945-52.

Celen S, Koole M, Ooms M, De Angelis M, Sannen I, Cornelis J, *et al.* Preclinical evaluation of [(18)F]JNJ42259152 as a PET tracer for PDE10A. Neuroimage 2013; 82: 13-22.

Chang H, Fitzpatrick JM. A technique for accurate magnetic resonance imaging in the presence of field inhomogeneities. IEEE transactions on medical imaging 1992; 11(3): 319-29.

Chaudhuri KR, Martinez-Martin P, Brown RG, Sethi K, Stocchi F, Odin P, *et al.* The metric properties of a novel non-motor symptoms scale for Parkinson's disease: Results from an international pilot study. Movement Disord 2007; 22(13): 1901-11.

Chaudhuri KR, Pal S, DiMarco A, Whately-Smith C, Bridgman K, Mathew R, *et al.* The Parkinson's disease sleep scale: a new instrument for assessing sleep and nocturnal disability in Parkinson's disease. J Neurol Neurosur Ps 2002; 73(6): 629-35.

Chen X, Guo C, Kong J. Oxidative stress in neurodegenerative diseases. Neural Regen Res 2012; 7(5): 376-85.

Chou KL, Hurtig HI, Stern MB, Colcher A, Ravina B, Newberg A, *et al.* Diagnostic accuracy of [99mTc]TRODAT-1 SPECT imaging in early Parkinson's disease. Parkinsonism & related disorders 2004; 10(6): 375-9.

Colloby SJ, Williams ED, Burn DJ, Lloyd JJ, McKeith IG, O'Brien JT. Progression of dopaminergic degeneration in dementia with Lewy bodies and Parkinson's disease with and without dementia assessed using 123I-FP-CIT SPECT. Eur J Nucl Med Mol Imaging 2005; 32(10): 1176-85.

Coskran TM, Morton D, Menniti FS, Adamowicz WO, Kleiman RJ, Ryan AM, *et al.* Immunohistochemical localization of phosphodiesterase 10A in multiple mammalian species. J Histochem Cytochem 2006; 54(11): 1205-13.

Cox CD, Hostetler ED, Flores BA, Evelhoch JL, Fan H, Gantert L, *et al.* Discovery of [(1)(1)C]MK-8193 as a PET tracer to measure target engagement of phosphodiesterase 10A (PDE10A) inhibitors. Bioorg Med Chem Lett 2015; 25(21): 4893-8.

Crosiers D, Theuns J, Cras P, Van Broeckhoven C. Parkinson disease: insights in clinical, genetic and pathological features of monogenic disease subtypes. J Chem Neuroanat 2011; 42(2): 131-41.

Damian AM, Jacobson SA, Hentz JG, Belden CM, Shill HA, Sabbagh MN, *et al.* The Montreal Cognitive Assessment and the mini-mental state examination as screening instruments for cognitive impairment: item analyses and threshold scores. Dement Geriatr Cogn Disord 2011; 31(2): 126-31.

Darcourt J, Booij J, Tatsch K, Varrone A, Vander Borght T, Kapucu OL, *et al.* EANM procedure guidelines for brain neurotransmission SPECT using (123)I-labelled dopamine transporter ligands, version 2. Eur J Nucl Med Mol Imaging 2010; 37(2): 443-50.

Davie CA. A review of Parkinson's disease. Br Med Bull 2008; 86: 109-27.

de la Fuente-Fernandez R, Lu JQ, Sossi V, Jivan S, Schulzer M, Holden JE, *et al.* Biochemical variations in the synaptic level of dopamine precede motor fluctuations in Parkinson's disease: PET evidence of increased dopamine turnover. Annals of neurology 2001; 49(3): 298-303.

de Win MM, Habraken JB, Reneman L, van den Brink W, den Heeten GJ, Booij J. Validation of [(123)I]beta-CIT SPECT to assess serotonin transporters in vivo in humans: a double-blind, placebo-controlled, crossover study with the selective serotonin reuptake inhibitor citalopram. Neuropsychopharmacology 2005; 30(5): 996-1005.

Dexter DT, Wells FR, Agid F, Agid Y, Lees AJ, Jenner P, *et al.* Increased nigral iron content in postmortem parkinsonian brain. Lancet 1987; 2(8569): 1219-20.

Dickson DW. Parkinson's disease and parkinsonism: neuropathology. Cold Spring Harbor perspectives in medicine 2012; 2(8).

Diggle CP, Sukoff Rizzo SJ, Popiolek M, Hinttala R, Schulke JP, Kurian MA, *et al.* Biallelic Mutations in PDE10A Lead to Loss of Striatal PDE10A and a Hyperkinetic Movement Disorder with Onset in Infancy. Am J Hum Genet 2016; 98(4): 735-43.

Djaldetti R, Lorberboym M, Karmon Y, Treves TA, Ziv I, Melamed E. Residual striatal dopaminergic nerve terminals in very long-standing Parkinson's disease: a single photon emission computed tomography imaging study. Movement disorders : official journal of the Movement Disorder Society 2011; 26(2): 327-30.

Eggert K, Ohlwein C, Kassubek J, Wolz M, Kupsch A, Ceballos-Baumann A, *et al.* Influence of the nonergot dopamine agonist piribedil on vigilance in patients With Parkinson Disease and excessive

daytime sleepiness (PiViCog-PD): an 11-week randomized comparison trial against pramipexole and ropinirole. Clin Neuropharmacol 2014; 37(4): 116-22.

Ehringer H, Hornykiewicz O. Distribution of noradrenaline and dopamine (3-hydroxytyramine) in the human brain and their behavior in diseases of the extrapyramidal system. Parkinsonism Relat Disord 1998; 4(2): 53-7.

Ehrminger M, Latimier A, Pyatigorskaya N, Garcia-Lorenzo D, Leu-Semenescu S, Vidailhet M, *et al.* The coeruleus/subcoeruleus complex in idiopathic rapid eye movement sleep behaviour disorder. Brain 2016; 139(Pt 4): 1180-8.

Emond P, Garreau L, Chalon S, Boazi M, Caillet M, Bricard J, *et al.* Synthesis and Ligand Binding of Nortropane Derivatives: N-Substituted 2β-Carbomethoxy-3β-(4‘-iodophenyl)nortropane and N-(3-Iodoprop-(2E)-enyl)-2β-carbomethoxy-3β-(3‘,4‘-disubstituted phenyl)nortropane. New High-Affinity and Selective Compounds for the Dopamine Transporter. Journal of Medicinal Chemistry 1997; 40(9): 1366-72.

Emond P, Guilloteau D, Chalon S. PE2I: a radiopharmaceutical for in vivo exploration of the dopamine transporter. CNS Neurosci Ther 2008; 14(1): 47-64.

Emre M, Aarsland D, Brown R, Burn DJ, Duyckaerts C, Mizuno Y, *et al.* Clinical diagnostic criteria for dementia associated with Parkinson's disease. Movement disorders : official journal of the Movement Disorder Society 2007; 22(12): 1689-707; quiz 837.

Eshuis SA, Jager PL, Maguire RP, Jonkman S, Dierckx RA, Leenders KL. Direct comparison of FP-CIT SPECT and F-DOPA PET in patients with Parkinson's disease and healthy controls. Eur J Nucl Med Mol Imaging 2009; 36(3): 454-62.

Fahn S, Oakes D, Shoulson I, Kieburtz K, Rudolph A, Lang A, *et al.* Levodopa and the progression of Parkinson's disease. N Engl J Med 2004; 351(24): 2498-508.

Fan J, Zhang X, Li J, Jin H, Padakanti PK, Jones LA, *et al.* Radiosyntheses and in vivo evaluation of carbon-11 PET tracers for PDE10A in the brain of rodent and nonhuman primate. Bioorg Med Chem 2014; 22(9): 2648-54.

Fazio P, Schain M, Mrzljak L, Amini N, Nag S, Al-Tawil N, *et al.* Patterns of age related changes for phosphodiesterase type-10A in comparison with dopamine D2/3 receptors and sub-cortical volumes in the human basal ganglia: A PET study with (18)F-MNI-659 and (11)C-raclopride with correction for partial volume effect. Neuroimage 2017; 152: 330-9.

Fearnley JM, Lees AJ. Ageing and Parkinson's disease: substantia nigra regional selectivity. Brain 1991; 114 (Pt 5): 2283-301.

Felicio AC, Godeiro-Junior C, Shih MC, Borges V, Silva SM, Aguiar Pde C, *et al.* Evaluation of patients with Clinically Unclear Parkinsonian Syndromes submitted to brain SPECT imaging using the technetium-99m labeled tracer TRODAT-1. Journal of the neurological sciences 2010; 291(1-2): 64-8.

Fienberg AA, Hiroi N, Mermelstein PG, Song W, Snyder GL, Nishi A, *et al.* DARPP-32: regulator of the efficacy of dopaminergic neurotransmission. Science 1998; 281(5378): 838-42.

Filippi L, Manni C, Pierantozzi M, Brusa L, Danieli R, Stanzione P, *et al.* 123I-FP-CIT semi-quantitative SPECT detects preclinical bilateral dopaminergic deficit in early Parkinson's disease with unilateral symptoms. Nuclear medicine communications 2005; 26(5): 421-6.

Fischl B, Salat DH, Busa E, Albert M, Dieterich M, Haselgrove C, *et al.* Whole brain segmentation: automated labeling of neuroanatomical structures in the human brain. Neuron 2002; 33(3): 341-55.

Folstein MF, Folstein SE, McHugh PR. "Mini-mental state". A practical method for grading the cognitive state of patients for the clinician. J Psychiatr Res 1975; 12(3): 189-98.

Fredholm BB, Battig K, Holmen J, Nehlig A, Zvartau EE. Actions of caffeine in the brain with special reference to factors that contribute to its widespread use. Pharmacol Rev 1999a; 51(1): 83-133.

Fredholm BB, Battig K, Holmen J, Nehlig A, Zvartau EE. Actions of caffeine in the brain with special reference to factors that contribute to its widespread use. Pharmacol Rev 1999b; 51(1): 83-133.

Fujishige K, Kotera J, Omori K. Striatum- and testis-specific phosphodiesterase PDE10A isolation and characterization of a rat PDE10A. Eur J Biochem 1999; 266(3): 1118-27.

Gagnon JF, Postuma RB, Mazza S, Doyon J, Montplaisir J. Rapid-eye-movement sleep behaviour disorder and neurodegenerative diseases. Lancet Neurol 2006; 5(5): 424-32.

Garau L, Govoni S, Stefanini E, Trabucchi M, Spano PF. Dopamine receptors: pharmacological and anatomical evidences indicate that two distinct dopamine receptor populations are present in rat striatum. Life Sci 1978; 23(17-18): 1745-50.

Garcia-Lorenzo D, Longo-Dos Santos C, Ewenczyk C, Leu-Semenescu S, Gallea C, Quattrocchi G, *et al.* The coeruleus/subcoeruleus complex in rapid eye movement sleep behaviour disorders in Parkinson's disease. Brain 2013; 136(Pt 7): 2120-9.

Gasser T. Genetics of Parkinson's disease. J Neurol 2001; 248(10): 833-40.

Gelb DJ, Oliver E, Gilman S. Diagnostic criteria for Parkinson disease. Archives of neurology 1999; 56(1): 33-9.

Giorgi M, D'Angelo V, Esposito Z, Nuccetelli V, Sorge R, Martorana A, *et al.* Lowered cAMP and cGMP signalling in the brain during levodopa-induced dyskinesias in hemiparkinsonian rats: new aspects in the pathogenetic mechanisms. Eur J Neurosci 2008; 28(5): 941-50.

Giorgi M, Melchiorri G, Nuccetelli V, D'Angelo V, Martorana A, Sorge R, *et al.* PDE10A and PDE10A-dependent cAMP catabolism are dysregulated oppositely in striatum and nucleus accumbens after lesion of midbrain dopamine neurons in rat: a key step in parkinsonism physiopathology. Neurobiology of disease 2011; 43(1): 293-303.

Girault JA. Integrating neurotransmission in striatal medium spiny neurons. Adv Exp Med Biol 2012; 970: 407-29.

Goetz CG. [Movement Disorder Society-Unified Parkinson's Disease Rating Scale (MDS-UPDRS): a new scale for the evaluation of Parkinson's disease]. Rev Neurol (Paris) 2010; 166(1): 1-4.

Goetz CG, Poewe W, Rascol O, Sampaio C, Stebbins GT, Counsell C, *et al.* Movement Disorder Society Task Force report on the Hoehn and Yahr staging scale: status and recommendations. Movement disorders : official journal of the Movement Disorder Society 2004; 19(9): 1020-8.

Greengard P, Allen PB, Nairn AC. Beyond the dopamine receptor: the DARPP-32/protein phosphatase-1 cascade. Neuron 1999; 23(3): 435-47.

Gunn RN, Gunn SR, Cunningham VJ. Positron emission tomography compartmental models. J Cereb Blood Flow Metab 2001; 21(6): 635-52.

Gunn RN, Lammertsma AA, Hume SP, Cunningham VJ. Parametric imaging of ligand-receptor binding in PET using a simplified reference region model. Neuroimage 1997; 6(4): 279-87.

Guttman M, Burkholder J, Kish SJ, Hussey D, Wilson A, DaSilva J, *et al.* [11C]RTI-32 PET studies of the dopamine transporter in early dopa-naive Parkinson's disease: implications for the symptomatic threshold. Neurology 1997; 48(6): 1578-83.

Hall H, Halldin C, Guilloteau D, Chalon S, Emond P, Besnard J, *et al.* Visualization of the dopamine transporter in the human brain postmortem with the new selective ligand [125I]PE2I. Neuroimage 1999; 9(1): 108-16.

Hallett PJ, Dunah AW, Ravenscroft P, Zhou S, Bezard E, Crossman AR, *et al.* Alterations of striatal NMDA receptor subunits associated with the development of dyskinesia in the MPTP-lesioned primate model of Parkinson's disease. Neuropharmacology 2005; 48(4): 503-16.

Harrison MB, Wylie SA, Frysinger RC, Patrie JT, Huss DS, Currie LJ, *et al.* UPDRS activity of daily living score as a marker of Parkinson's disease progression. Movement disorders : official journal of the Movement Disorder Society 2009; 24(2): 224-30.

Hashido T, Saito S. Quantitative T1, T2, and T2* Mapping and Semi-Quantitative Neuromelanin-Sensitive Magnetic Resonance Imaging of the Human Midbrain. PLoS One 2016; 11(10): e0165160.

Hattori T, Orimo S, Aoki S, Ito K, Abe O, Amano A, *et al.* Cognitive status correlates with white matter alteration in Parkinson's disease. Hum Brain Mapp 2012; 33(3): 727-39.

Havins WN, Massman PJ, Doody R. Factor structure of the Geriatric Depression Scale and relationships with cognition and function in Alzheimer's disease. Dement Geriatr Cogn Disord 2012; 34(5-6): 360-72.

Helms G, Dathe H, Kallenberg K, Dechent P. High-resolution maps of magnetization transfer with inherent correction for RF inhomogeneity and T1 relaxation obtained from 3D FLASH MRI. Magn Reson Med 2008; 60(6): 1396-407.

Hely MA, Morris JG, Reid WG, Trafficante R. Sydney Multicenter Study of Parkinson's disease: non-L-dopa-responsive problems dominate at 15 years. Movement disorders : official journal of the Movement Disorder Society 2005; 20(2): 190-9.

Hely MA, Reid WG, Adena MA, Halliday GM, Morris JG. The Sydney multicenter study of Parkinson's disease: the inevitability of dementia at 20 years. Movement disorders : official journal of the Movement Disorder Society 2008; 23(6): 837-44.

Herve D, Le Moine C, Corvol JC, Belluscio L, Ledent C, Fienberg AA, *et al.* Galpha(olf) levels are regulated by receptor usage and control dopamine and adenosine action in the striatum. J Neurosci 2001; 21(12): 4390-9.

Hirsch EC, Brandel JP, Galle P, Javoy-Agid F, Agid Y. Iron and aluminum increase in the substantia nigra of patients with Parkinson's disease: an X-ray microanalysis. J Neurochem 1991; 56(2): 446-51.

Hirvonen J, Johansson J, Teras M, Oikonen V, Lumme V, Virsu P, *et al.* Measurement of striatal and extrastriatal dopamine transporter binding with high-resolution PET and [11C]PE2I: quantitative modeling and test-retest reproducibility. J Cereb Blood Flow Metab 2008; 28(5): 1059-69.

Hossain MA, Weiner N. Dopaminergic functional supersensitivity: effects of chronic L-dopa and carbidopa treatment in an animal model of Parkinson's disease. J Pharmacol Exp Ther 1993; 267(3): 1105-11.

Hostetler ED, Fan H, Joshi AD, Zeng Z, Eng W, Gantert L, *et al.* Preclinical Characterization of the Phosphodiesterase 10A PET Tracer [(11)C]MK-8193. Mol Imaging Biol 2016; 18(4): 579-87.

Hotter A, Esterhammer R, Schocke MF, Seppi K. Potential of advanced MR imaging techniques in the differential diagnosis of parkinsonism. Movement disorders : official journal of the Movement Disorder Society 2009; 24 Suppl 2: S711-20.

Houslay MD, Milligan G. Tailoring cAMP-signalling responses through isoform multiplicity. Trends Biochem Sci 1997; 22(6): 217-24.

Hu E, Chen N, Kunz RK, Hwang DR, Michelsen K, Davis C, *et al.* Discovery of Phosphodiesterase 10A (PDE10A) PET Tracer AMG 580 to Support Clinical Studies. ACS Med Chem Lett 2016; 7(7): 719-23.

Huang WS, Lin SZ, Lin JC, Wey SP, Ting G, Liu RS. Evaluation of early-stage Parkinson's disease with 99mTc-TRODAT-1 imaging. Journal of nuclear medicine : official publication, Society of Nuclear Medicine 2001; 42(9): 1303-8.

Huertas-Fernandez I, Garcia-Gomez FJ, Garcia-Solis D, Benitez-Rivero S, Marin-Oyaga VA, Jesus S, *et al.* Machine learning models for the differential diagnosis of vascular parkinsonism and Parkinson's disease using [(123)I]FP-CIT SPECT. Eur J Nucl Med Mol Imaging 2015; 42(1): 112-9.

Hwang AB, Franc BL, Gullberg GT, Hasegawa BH. Assessment of the sources of error affecting the quantitative accuracy of SPECT imaging in small animals. Phys Med Biol 2008; 53(9): 2233-52.

Hwang DR, Hu E, Rumfelt S, Easwaramoorthy B, Castrillon J, Davis C, *et al.* Initial characterization of a PDE10A selective positron emission tomography tracer [11C]AMG 7980 in non-human primates. Nucl Med Biol 2014; 41(4): 343-9.

Hwang KS, Beyer MK, Green AE, Chung C, Thompson PM, Janvin C, *et al.* Mapping cortical atrophy in Parkinson's disease patients with dementia. Journal of Parkinson's disease 2013; 3(1): 69-76.

Ibarretxe-Bilbao N, Junque C, Marti MJ, Valldeoriola F, Vendrell P, Bargallo N, *et al.* Olfactory impairment in Parkinson's disease and white matter abnormalities in central olfactory areas: A voxel-based diffusion tensor imaging study. Movement disorders : official journal of the Movement Disorder Society 2010; 25(12): 1888-94.

Ibarretxe-Bilbao N, Junque C, Segura B, Baggio HC, Marti MJ, Valldeoriola F, *et al.* Progression of cortical thinning in early Parkinson's disease. Movement disorders : official journal of the Movement Disorder Society 2012; 27(14): 1746-53.

Im JH, Chung SJ, Kim JS, Lee MC. Differential patterns of dopamine transporter loss in the basal ganglia of progressive supranuclear palsy and Parkinson's disease: analysis with [(123)I]IPT single photon emission computed tomography. Journal of the neurological sciences 2006; 244(1-2): 103-9.

Insel PA, Zhang L, Murray F, Yokouchi H, Zambon AC. Cyclic AMP is both a pro-apoptotic and anti-apoptotic second messenger. Acta Physiol (Oxf) 2012; 204(2): 277-87.

Isaias IU, Trujillo P, Summers P, Marotta G, Mainardi L, Pezzoli G, *et al.* Neuromelanin Imaging and Dopaminergic Loss in Parkinson's Disease. Front Aging Neurosci 2016; 8: 196.

Jenkinson C, Fitzpatrick R, Peto V, Greenhall R, Hyman N. The Parkinson's Disease Questionnaire (PDQ-39): development and validation of a Parkinson's disease summary index score. Age Ageing 1997; 26(5): 353-7.

Johns MW. A new method for measuring daytime sleepiness: the Epworth sleepiness scale. Sleep 1991; 14(6): 540-5.

Johns MW. Sensitivity and specificity of the multiple sleep latency test (MSLT), the maintenance of wakefulness test and the epworth sleepiness scale: failure of the MSLT as a gold standard. J Sleep Res 2000; 9(1): 5-11.

Jones PG, Hewitt MC, Campbell JE, Quinton MS, Engel S, Lew R, *et al.* Pharmacological evaluation of a novel phosphodiesterase 10A inhibitor in models of antipsychotic activity and cognition. Pharmacol Biochem Behav 2015; 135: 46-52.

Jubault T, Gagnon JF, Karama S, Ptito A, Lafontaine AL, Evans AC, *et al.* Patterns of cortical thickness and surface area in early Parkinson's disease. Neuroimage 2011; 55(2): 462-7.

Jucaite A, Odano I, Olsson H, Pauli S, Halldin C, Farde L. Quantitative analyses of regional [11C]PE2I binding to the dopamine transporter in the human brain: a PET study. Eur J Nucl Med Mol Imaging 2006; 33(6): 657-68.

Kaasinen V, Joutsa J, Noponen T, Johansson J, Seppanen M. Effects of aging and gender on striatal and extrastriatal [123I]FP-CIT binding in Parkinson's disease. Neurobiol Aging 2015; 36(4): 1757-63.

Kalia LV, Lang AE. Parkinson's disease. Lancet 2015; 386(9996): 896-912.

Kebabian JW. Multiple classes of dopamine receptors in mammalian central nervous system: the involvement of dopamine-sensitive adenylyl cyclase. Life Sci 1978; 23(5): 479-83.

Kehler J, Kilburn JP, Estrada S, Christensen SR, Wall A, Thibblin A, *et al.* Discovery and development of 11C-Lu AE92686 as a radioligand for PET imaging of phosphodiesterase10A in the brain. Journal of nuclear medicine : official publication, Society of Nuclear Medicine 2014; 55(9): 1513-8.

Khalil MM, Tremoleda JL, Bayomy TB, Gsell W. Molecular SPECT Imaging: An Overview. Int J Mol Imaging 2011; 2011: 796025.

Kim YJ, Ichise M, Ballinger JR, Vines D, Erami SS, Tatschida T, *et al.* Combination of dopamine transporter and D2 receptor SPECT in the diagnostic evaluation of PD, MSA, and PSP. Movement disorders : official journal of the Movement Disorder Society 2002; 17(2): 303-12.

Kitao S, Matsusue E, Fujii S, Miyoshi F, Kaminou T, Kato S, *et al.* Correlation between pathology and neuromelanin MR imaging in Parkinson's disease and dementia with Lewy bodies. Neuroradiology 2013; 55(8): 947-53.

Knudsen GM, Karlsborg M, Thomsen G, Krabbe K, Regeur L, Nygaard T, *et al.* Imaging of dopamine transporters and D2 receptors in patients with Parkinson's disease and multiple system atrophy. Eur J Nucl Med Mol Imaging 2004; 31(12): 1631-8.

Korczyn AD, Gurevich T. Parkinson's disease: before the motor symptoms and beyond. Journal of the neurological sciences 2010; 289(1-2): 2-6.

Koshibu K, Graff J, Beullens M, Heitz FD, Berchtold D, Russig H, *et al.* Protein phosphatase 1 regulates the histone code for long-term memory. J Neurosci 2009; 29(41): 13079-89.

Kotagal V, Spino C, Bohnen NI, Koeppe R, Albin RL. Serotonin, beta-amyloid, and cognition in Parkinson disease. Annals of neurology 2018.

Kuya K, Ogawa T, Shinohara Y, Ishibashi M, Fujii S, Mukuda N, *et al.* Evaluation of Parkinson's disease by neuromelanin-sensitive magnetic resonance imaging and 123I-FP-CIT SPECT. Acta Radiol 2017: 284185117722812.

Lakics V, Karran EH, Boess FG. Quantitative comparison of phosphodiesterase mRNA distribution in human brain and peripheral tissues. Neuropharmacology 2010; 59(6): 367-74.

Langley J, Huddleston DE, Chen X, Sedlacik J, Zachariah N, Hu X. A multicontrast approach for comprehensive imaging of substantia nigra. Neuroimage 2015; 112: 7-13.

Laruelle M, Wallace E, Seibyl JP, Baldwin RM, Zea-Ponce Y, Zoghbi SS, *et al.* Graphical, kinetic, and equilibrium analyses of in vivo [123I] beta-CIT binding to dopamine transporters in healthy human subjects. J Cereb Blood Flow Metab 1994; 14(6): 982-94.

Lees AJ, Hardy J, Revesz T. Parkinson's disease. Lancet 2009; 373(9680): 2055-66.

Lehericy S, Bardinet E, Poupon C, Vidailhet M, Francois C. 7 Tesla magnetic resonance imaging: a closer look at substantia nigra anatomy in Parkinson's disease. Movement disorders : official journal of the Movement Disorder Society 2014; 29(13): 1574-81.

Li J, Jin H, Zhou H, Rothfuss J, Tu Z. Synthesis and in vitro biological evaluation of pyrazole group-containing analogues for PDE10A. Medchemcomm 2013; 4(2): 443-9.

Li J, Zhang X, Jin H, Fan J, Flores H, Perlmutter JS, *et al.* Synthesis of Fluorine-Containing Phosphodiesterase 10A (PDE10A) Inhibitors and the In Vivo Evaluation of F-18 Labeled PDE10A PET Tracers in Rodent and Nonhuman Primate. J Med Chem 2015; 58(21): 8584-600.

Li W, Lao-Kaim NP, Roussakis AA, Martin-Bastida A, Valle-Guzman N, Paul G, *et al.* (11) C-PE2I and (18) F-Dopa PET for assessing progression rate in Parkinson's: A longitudinal study. Movement disorders : official journal of the Movement Disorder Society 2018; 33(1): 117-27.

Lin SF, Labaree D, Chen MK, Holden D, Gallezot JD, Kapinos M, *et al.* Further evaluation of [11C]MP-10 as a radiotracer for phosphodiesterase 10A: PET imaging study in rhesus monkeys and brain tissue metabolite analysis. Synapse (New York, NY) 2015; 69(2): 86-95.

Litvan I, Aarsland D, Adler CH, Goldman JG, Kulisevsky J, Mollenhauer B, *et al.* MDS Task Force on mild cognitive impairment in Parkinson's disease: critical review of PD-MCI. Movement disorders : official journal of the Movement Disorder Society 2011; 26(10): 1814-24.

Liu C, Li W, Tong KA, Yeom KW, Kuzminski S. Susceptibility-weighted imaging and quantitative susceptibility mapping in the brain. J Magn Reson Imaging 2015; 42(1): 23-41.

Liu H, Jin H, Yue X, Han J, Yang H, Flores H, *et al.* Comparison of [(11)C]TZ1964B and [(18)F]MNI659 for PET imaging brain PDE10A in nonhuman primates. Pharmacol Res Perspect 2016; 4(5): e00253.

Loane C, Politis M, Kefalopoulou Z, Valle-Guzman N, Paul G, Widner H, *et al.* Aberrant nigral diffusion in Parkinson's disease: A longitudinal diffusion tensor imaging study. Mov Disord 2016; 31(7): 1020-6.

Loane C, Wu K, Bain P, Brooks DJ, Piccini P, Politis M. Serotonergic loss in motor circuitries correlates with severity of action-postural tremor in PD. Neurology 2013; 80(20): 1850-5.

Lotfipour AK, Wharton S, Schwarz ST, Gontu V, Schafer A, Peters AM, *et al.* High resolution magnetic susceptibility mapping of the substantia nigra in Parkinson's disease. J Magn Reson Imaging 2012; 35(1): 48-55.

Lyoo CH, Ryu YH, Lee MS. Cerebral cortical areas in which thickness correlates with severity of motor deficits of Parkinson's disease. J Neurol 2011; 258(10): 1871-6.

Marek K, Innis R, van Dyck C, Fussell B, Early M, Eberly S, *et al.* [123I]beta-CIT SPECT imaging assessment of the rate of Parkinson's disease progression. Neurology 2001; 57(11): 2089-94.

Marek KL, Seibyl JP, Zoghbi SS, Zea-Ponce Y, Baldwin RM, Fussell B, *et al.* [123I] beta-CIT/SPECT imaging demonstrates bilateral loss of dopamine transporters in hemi-Parkinson's disease. Neurology 1996; 46(1): 231-7.

Marion MH, Qurashi M, Marshall G, Foster O. Is REM sleep behaviour disorder (RBD) a risk factor of dementia in idiopathic Parkinson's disease? J Neurol 2008; 255(2): 192-6.

Marsden CD. Basal ganglia disease. Lancet 1982; 2(8308): 1141-7.

Marsh L, McDonald WM, Cummings J, Ravina B, Depression NNWGo, Parkinson's D. Provisional diagnostic criteria for depression in Parkinson's disease: report of an NINDS/NIMH Work Group. Movement disorders : official journal of the Movement Disorder Society 2006; 21(2): 148-58.

Martin-Bastida A, Lao-Kaim NP, Loane C, Politis M, Roussakis AA, Valle-Guzman N, *et al.* Motor associations of iron accumulation in deep grey matter nuclei in Parkinson's disease: a cross-sectional study of iron-related magnetic resonance imaging susceptibility. European journal of neurology 2017; 24(2): 357-65.

Martin WR, Wieler M, Gee M. Midbrain iron content in early Parkinson disease: a potential biomarker of disease status. Neurology 2008; 70(16 Pt 2): 1411-7.

Martinez-Martin P, Chaudhuri KR, Rojo-Abuin JM, Rodriguez-Blazquez C, Alvarez-Sanchez M, Arakaki T, *et al.* Assessing the non-motor symptoms of Parkinson's disease: MDS-UPDRS and NMS Scale. European journal of neurology 2015; 22(1): 37-43.

Martinez-Martin P, Gil-Nagel A, Morlan Gracia L, Balseiro Gomez J, Martinez-Sarries FJ, Bermejo F, *et al.* Intermediate scale for assessment of Parkinson's disease. Characteristics and structure. Parkinsonism & related disorders 1995; 1(2): 97-102.

Martinez-Martin P, Rodriguez-Blazquez C, Kurtis MM, Chaudhuri KR. The impact of non-motor symptoms on health-related quality of life of patients with Parkinson's disease. Movement disorders : official journal of the Movement Disorder Society 2011; 26(3): 399-406.

Masliah E, Dumaop W, Galasko D, Desplats P. Distinctive patterns of DNA methylation associated with Parkinson disease: identification of concordant epigenetic changes in brain and peripheral blood leukocytes. Epigenetics 2013; 8(10): 1030-8.

Matsumine H, Saito M, Shimoda-Matsubayashi S, Tanaka H, Ishikawa A, Nakagawa-Hattori Y, *et al.* Localization of a gene for an autosomal recessive form of juvenile Parkinsonism to chromosome 6q25.2-27. Am J Hum Genet 1997; 60(3): 588-96.

Matsuura K, Maeda M, Tabei KI, Umino M, Kajikawa H, Satoh M, *et al.* A longitudinal study of neuromelanin-sensitive magnetic resonance imaging in Parkinson's disease. Neurosci Lett 2016; 633: 112-7.

McKhann G, Drachman D, Folstein M, Katzman R, Price D, Stadlan EM. Clinical diagnosis of Alzheimer's disease: report of the NINCDS-ADRDA Work Group under the auspices of Department of Health and Human Services Task Force on Alzheimer's Disease. Neurology 1984; 34(7): 939-44.

McMillan SC, Williams FA. Validity and reliability of the Constipation Assessment Scale. Cancer Nurs 1989; 12(3): 183-8.

Megens AA, Hendrickx HM, Mahieu MM, Wellens AL, de Boer P, Vanhoof G. PDE10A inhibitors stimulate or suppress motor behavior dependent on the relative activation state of the direct and indirect striatal output pathways. Pharmacol Res Perspect 2014; 2(4): e00057.

Meinkoth JL, Alberts AS, Went W, Fantozzi D, Taylor SS, Hagiwara M, *et al.* Signal transduction through the cAMP-dependent protein kinase. Mol Cell Biochem 1993; 127-128: 179-86.

Mencacci NE, Kamsteeg EJ, Nakashima K, R'Bibo L, Lynch DS, Balint B, *et al.* De Novo Mutations in PDE10A Cause Childhood-Onset Chorea with Bilateral Striatal Lesions. Am J Hum Genet 2016; 98(4): 763-71.

Mesulam MM, Mufson EJ, Levey AI, Wainer BH. Cholinergic innervation of cortex by the basal forebrain: cytochemistry and cortical connections of the septal area, diagonal band nuclei, nucleus basalis (substantia innominata), and hypothalamus in the rhesus monkey. J Comp Neurol 1983; 214(2): 170-97.

Miyoshi F, Ogawa T, Kitao SI, Kitayama M, Shinohara Y, Takasugi M, *et al.* Evaluation of Parkinson disease and Alzheimer disease with the use of neuromelanin MR imaging and (123)I-metaiodobenzylguanidine scintigraphy. AJNR Am J Neuroradiol 2013; 34(11): 2113-8.

Moccia M, Pappata S, Picillo M, Erro R, Coda AR, Longo K, *et al.* Dopamine transporter availability in motor subtypes of de novo drug-naive Parkinson's disease. J Neurol 2014; 261(11): 2112-8.

Mozley PD, Schneider JS, Acton PD, Plossl K, Stern MB, Siderowf A, *et al.* Binding of [99mTc]TRODAT-1 to dopamine transporters in patients with Parkinson's disease and in healthy volunteers. Journal of nuclear medicine : official publication, Society of Nuclear Medicine 2000; 41(4): 584-9.

Nakamura K, Sugaya K. Neuromelanin-sensitive magnetic resonance imaging: a promising technique for depicting tissue characteristics containing neuromelanin. Neural Regen Res 2014; 9(7): 759-60.

Nakane T, Nihashi T, Kawai H, Naganawa S. Visualization of neuromelanin in the Substantia nigra and locus ceruleus at 1.5T using a 3D-gradient echo sequence with magnetization transfer contrast. Magn Reson Med Sci 2008; 7(4): 205-10.

Nalls MA, Pankratz N, Lill CM, Do CB, Hernandez DG, Saad M, *et al.* Large-scale meta-analysis of genome-wide association data identifies six new risk loci for Parkinson's disease. Nature genetics 2014; 46(9): 989-93.

Niccolini F, Foltynie T, Reis Marques T, Muhlert N, Tziortzi AC, Searle GE, *et al.* Loss of phosphodiesterase 10A expression is associated with progression and severity in Parkinson's disease. Brain 2015a; 138(Pt 10): 3003-15.

Niccolini F, Haider S, Reis Marques T, Muhlert N, Tziortzi AC, Searle GE, *et al.* Altered PDE10A expression detectable early before symptomatic onset in Huntington's disease. Brain 2015b; 138(Pt 10): 3016-29.

Niccolini F, Mencacci NE, Yousaf T, Rabiner EA, Salpietro V, Pagano G, *et al.* PDE10A and ADCY5 mutations linked to molecular and microstructural basal ganglia pathology. Movement disorders : official journal of the Movement Disorder Society 2018.

Niccolini F, Wilson H, Pagano G, Coello C, Mehta MA, Searle GE, *et al.* Loss of phosphodiesterase 4 in Parkinson disease: Relevance to cognitive deficits. Neurology 2017; 89(6): 586-93.

Nishi A, Kuroiwa M, Miller DB, O'Callaghan JP, Bateup HS, Shuto T, *et al.* Distinct roles of PDE4 and PDE10A in the regulation of cAMP/PKA signaling in the striatum. J Neurosci 2008; 28(42): 10460-71.

Nishi A, Kuroiwa M, Shuto T. Mechanisms for the modulation of dopamine d(1) receptor signaling in striatal neurons. Front Neuroanat 2011; 5: 43.

Noyce AJ, Bestwick JP, Silveira-Moriyama L, Hawkes CH, Giovannoni G, Lees AJ, *et al.* Meta-analysis of early nonmotor features and risk factors for Parkinson disease. Annals of neurology 2012; 72(6): 893-901.

Nurmi E, Ruottinen HM, Kaasinen V, Bergman J, Haaparanta M, Solin O, *et al.* Progression in Parkinson's disease: a positron emission tomography study with a dopamine transporter ligand [18F]CFT. Annals of neurology 2000; 47(6): 804-8.

Ogisu K, Kudo K, Sasaki M, Sakushima K, Yabe I, Sasaki H, *et al.* 3D neuromelanin-sensitive magnetic resonance imaging with semi-automated volume measurement of the substantia nigra pars compacta for diagnosis of Parkinson's disease. Neuroradiology 2013; 55(6): 719-24.

Ohtsuka C, Sasaki M, Konno K, Kato K, Takahashi J, Yamashita F, *et al.* Differentiation of early-stage parkinsonisms using neuromelanin-sensitive magnetic resonance imaging. Parkinsonism Relat Disord 2014; 20(7): 755-60.

Pagano G, Ferrara N, Brooks DJ, Pavese N. Age at onset and Parkinson disease phenotype. Neurology 2016a; 86(15): 1400-7.

Pagano G, Niccolini F, Fusar-Poli P, Politis M. Serotonin transporter in Parkinson's disease: A meta-analysis of positron emission tomography studies. Annals of neurology 2017; 81(2): 171-80.

Pagano G, Niccolini F, Politis M. Imaging in Parkinson's disease. Clin Med (Lond) 2016b; 16(4): 371-5.

Pagonabarraga J, Corcuera-Solano I, Vives-Gilabert Y, Llebaria G, Garcia-Sanchez C, Pascual-Sedano B, *et al.* Pattern of regional cortical thinning associated with cognitive deterioration in Parkinson's disease. PloS one 2013; 8(1): e54980.

Parkinson J. An essay on the shaking palsy. 1817. The Journal of neuropsychiatry and clinical neurosciences 2002; 14(2): 223-36; discussion 2.

Parkinson Study Group CCI. Long-term effect of initiating pramipexole vs levodopa in early Parkinson disease. Archives of neurology 2009; 66(5): 563-70.

Paul S, Nairn AC, Wang P, Lombroso PJ. NMDA-mediated activation of the tyrosine phosphatase STEP regulates the duration of ERK signaling. Nat Neurosci 2003; 6(1): 34-42.

Pavese N, Brooks DJ. Imaging neurodegeneration in Parkinson's disease. Biochimica et biophysica acta 2009; 1792(7): 722-9.

Pereira JB, Svenningsson P, Weintraub D, Bronnick K, Lebedev A, Westman E, *et al.* Initial cognitive decline is associated with cortical thinning in early Parkinson disease. Neurology 2014; 82(22): 2017-25.

Pirker W. Correlation of dopamine transporter imaging with parkinsonian motor handicap: how close is it? Mov Disord 2003; 18 Suppl 7: S43-51.

Pirker W, Holler I, Gerschlager W, Asenbaum S, Zettinig G, Brucke T. Measuring the rate of progression of Parkinson's disease over a 5-year period with beta-CIT SPECT. Movement disorders : official journal of the Movement Disorder Society 2003; 18(11): 1266-72.

Plisson C, Weinzimmer D, Jakobsen S, Natesan S, Salinas C, Lin S-F, *et al.* Phosphodiesterase 10A PET radioligand development program: from pig to human. Journal of Nuclear Medicine 2014a; 55(4): 595-601.

Plisson C, Weinzimmer D, Jakobsen S, Natesan S, Salinas C, Lin SF, *et al.* Phosphodiesterase 10A PET radioligand development program: from pig to human. Journal of nuclear medicine : official publication, Society of Nuclear Medicine 2014b; 55(4): 595-601.

Politis M. Neuroimaging in Parkinson disease: from research setting to clinical practice. Nat Rev Neurol 2014; 10(12): 708-22.

Politis M, Loane C, Wu K, Brooks DJ, Piccini P. Serotonergic mediated body mass index changes in Parkinson's disease. Neurobiology of disease 2011; 43(3): 609-15.

Politis M, Wu K, Loane C, Kiferle L, Molloy S, Brooks DJ, *et al.* Staging of serotonergic dysfunction in Parkinson's disease: an in vivo 11C-DASB PET study. Neurobiology of disease 2010a; 40(1): 216-21.

Politis M, Wu K, Loane C, Turkheimer FE, Molloy S, Brooks DJ, *et al.* Depressive symptoms in PD correlate with higher 5-HTT binding in raphe and limbic structures. Neurology 2010b; 75(21): 1920-7.

Postuma RB, Lang AE, Munhoz RP, Charland K, Pelletier A, Moscovich M, *et al.* Caffeine for treatment of Parkinson disease: a randomized controlled trial. Neurology 2012; 79(7): 651-8.

Price S, Paviour D, Scahill R, Stevens J, Rossor M, Lees A, *et al.* Voxel-based morphometry detects patterns of atrophy that help differentiate progressive supranuclear palsy and Parkinson's disease. Neuroimage 2004; 23(2): 663-9.

Pringsheim T, Jette N, Frolkis A, Steeves TD. The prevalence of Parkinson's disease: a systematic review and meta-analysis. Movement disorders : official journal of the Movement Disorder Society 2014; 29(13): 1583-90.

Qamhawi Z, Towey D, Shah B, Pagano G, Seibyl J, Marek K, *et al.* Clinical correlates of raphe serotonergic dysfunction in early Parkinson's disease. Brain 2015; 138(Pt 10): 2964-73.

Ramaker C, Marinus J, Stiggelbout AM, Van Hilten BJ. Systematic evaluation of rating scales for impairment and disability in Parkinson's disease. Movement disorders : official journal of the Movement Disorder Society 2002; 17(5): 867-76.

Ravina B, Marek K, Eberly S, Oakes D, Kurlan R, Ascherio A, *et al.* Dopamine transporter imaging is associated with long-term outcomes in Parkinson's disease. Movement disorders : official journal of the Movement Disorder Society 2012; 27(11): 1392-7.

Reimao S, Ferreira S, Nunes RG, Pita Lobo P, Neutel D, Abreu D, *et al.* Magnetic resonance correlation of iron content with neuromelanin in the substantia nigra of early-stage Parkinson's disease. European journal of neurology 2016; 23(2): 368-74.

Reimao S, Pita Lobo P, Neutel D, Guedes LC, Coelho M, Rosa MM, *et al.* Quantitative Analysis Versus Visual Assessment of Neuromelanin MR Imaging for the Diagnosis of Parkinson's disease. Journal of Parkinson's disease 2015; 5(3): 561-7.

Ribeiro MJ, Ricard M, Lievre MA, Bourgeois S, Emond P, Gervais P, *et al.* Whole-body distribution and radiation dosimetry of the dopamine transporter radioligand [(11)C]PE2I in healthy volunteers. Nucl Med Biol 2007; 34(4): 465-70.

Richards JS. New signaling pathways for hormones and cyclic adenosine 3',5'-monophosphate action in endocrine cells. Mol Endocrinol 2001; 15(2): 209-18.

Richter W. 3',5' Cyclic nucleotide phosphodiesterases class III: members, structure, and catalytic mechanism. Proteins 2002; 46(3): 278-86.

Rinne JO, Bergman J, Ruottinen H, Haaparanta M, Eronen E, Oikonen V, *et al.* Striatal uptake of a novel PET ligand, [18F]beta-CFT, is reduced in early Parkinson's disease. Synapse (New York, NY) 1999a; 31(2): 119-24.

Rinne JO, Ruottinen H, Bergman J, Haaparanta M, Sonninen P, Solin O. Usefulness of a dopamine transporter PET ligand [(18)F]beta-CFT in assessing disability in Parkinson's disease. Journal of neurology, neurosurgery, and psychiatry 1999b; 67(6): 737-41.

Rossi ME, Ruottinen H, Saunamaki T, Elovaara I, Dastidar P. Imaging brain iron and diffusion patterns: a follow-up study of Parkinson's disease in the initial stages. Acad Radiol 2014; 21(1): 64-71.

Russell DS, Barret O, Jennings DL, Friedman JH, Tamagnan GD, Thomae D, *et al.* The phosphodiesterase 10 positron emission tomography tracer, [18F]MNI-659, as a novel biomarker for early Huntington disease. JAMA Neurol 2014; 71(12): 1520-8.

Russell DS, Jennings DL, Barret O, Tamagnan GD, Carroll VM, Caille F, *et al.* Change in PDE10 across early Huntington disease assessed by [18F]MNI-659 and PET imaging. Neurology 2016; 86(8): 748-54.

Sammut S, Bray KE, West AR. Dopamine D2 receptor-dependent modulation of striatal NO synthase activity. Psychopharmacology (Berl) 2007; 191(3): 793-803.

Sancesario G, Giorgi M, D'Angelo V, Modica A, Martorana A, Morello M, *et al.* Down-regulation of nitrergic transmission in the rat striatum after chronic nigrostriatal deafferentation. Eur J Neurosci 2004; 20(4): 989-1000.

Sancesario G, Morrone LA, D'Angelo V, Castelli V, Ferrazzoli D, Sica F, *et al.* Levodopa-induced dyskinesias are associated with transient down-regulation of cAMP and cGMP in the caudate-putamen of hemiparkinsonian rats: reduced synthesis or increased catabolism? Neurochem Int 2014; 79: 44-56.

Sanchez-Crespo A, Andreo P, Larsson SA. Positron flight in human tissues and its influence on PET image spatial resolution. Eur J Nucl Med Mol Imaging 2004; 31(1): 44-51.

Santin MD, Didier M, Valabregue R, Yahia Cherif L, Garcia-Lorenzo D, Loureiro de Sousa P, *et al.* Reproducibility of R2 * and quantitative susceptibility mapping (QSM) reconstruction methods in the basal ganglia of healthy subjects. NMR Biomed 2017; 30(4).

Sasaki M, Shibata E, Tohyama K, Takahashi J, Otsuka K, Tsuchiya K, *et al.* Neuromelanin magnetic resonance imaging of locus ceruleus and substantia nigra in Parkinson's disease. Neuroreport 2006; 17(11): 1215-8.

Schapira AH. Recent developments in biomarkers in Parkinson disease. Curr Opin Neurol 2013; 26(4): 395-400.

Scherfler C, Schwarz J, Antonini A, Grosset D, Valldeoriola F, Marek K, *et al.* Role of DAT-SPECT in the diagnostic work up of parkinsonism. Movement disorders : official journal of the Movement Disorder Society 2007; 22(9): 1229-38.

Schulz J, Pagano G, Fernandez Bonfante JA, Wilson H, Politis M. Nucleus basalis of Meynert degeneration precedes and predicts cognitive impairment in Parkinson's disease. Brain 2018; 141(5): 1501-16.

Schwab RS. Projection technique for evaluating surgery in Parkinson's disease. Third symposium on Parkinson's disease; 1969: E&S Livingstone; 1969. p. 152-7.

Schwarz J, Linke R, Kerner M, Mozley PD, Trenkwalder C, Gasser T, *et al.* Striatal dopamine transporter binding assessed by [I-123]IPT and single photon emission computed tomography in patients with early Parkinson's disease: implications for a preclinical diagnosis. Archives of neurology 2000; 57(2): 205-8.

Schwarz ST, Abaei M, Gontu V, Morgan PS, Bajaj N, Auer DP. Diffusion tensor imaging of nigral degeneration in Parkinson's disease: A region-of-interest and voxel-based study at 3 T and systematic review with meta-analysis. Neuroimage Clin 2013; 3: 481-8.

Schwarz ST, Rittman T, Gontu V, Morgan PS, Bajaj N, Auer DP. T1-weighted MRI shows stage-dependent substantia nigra signal loss in Parkinson's disease. Movement disorders : official journal of the Movement Disorder Society 2011; 26(9): 1633-8.

Schweser F, Deistung A, Lehr BW, Reichenbach JR. Quantitative imaging of intrinsic magnetic tissue properties using MRI signal phase: an approach to in vivo brain iron metabolism? Neuroimage 2011; 54(4): 2789-807.

Seeger TF, Bartlett B, Coskran TM, Culp JS, James LC, Krull DL, *et al.* Immunohistochemical localization of PDE10A in the rat brain. Brain research 2003; 985(2): 113-26.

Segura B, Baggio HC, Marti MJ, Valldeoriola F, Compta Y, Garcia-Diaz AI, *et al.* Cortical thinning associated with mild cognitive impairment in Parkinson's disease. Movement disorders : official journal of the Movement Disorder Society 2014; 29(12): 1495-503.

Seppi K, Poewe W. Brain magnetic resonance imaging techniques in the diagnosis of parkinsonian syndromes. Neuroimaging Clin N Am 2010; 20(1): 29-55.

Shaulsky G, Fuller D, Loomis WF. A cAMP-phosphodiesterase controls PKA-dependent differentiation. Development 1998; 125(4): 691-9.

Shulman LM, Armstrong M, Ellis T, Gruber-Baldini A, Horak F, Nieuwboer A, *et al.* Disability Rating Scales in Parkinson's Disease: Critique and Recommendations. Movement disorders : official journal of the Movement Disorder Society 2016; 31(10): 1455-65.

Siuciak JA, Chapin DS, Harms JF, Lebel LA, McCarthy SA, Chambers L, *et al.* Inhibition of the striatum-enriched phosphodiesterase PDE10A: a novel approach to the treatment of psychosis. Neuropharmacology 2006; 51(2): 386-96.

Smith T, Gildeh N, Holmes C. The Montreal Cognitive Assessment: validity and utility in a memory clinic setting. Can J Psychiatry 2007; 52(5): 329-32.

Soderling SH, Beavo JA. Regulation of cAMP and cGMP signaling: new phosphodiesterases and new functions. Curr Opin Cell Biol 2000; 12(2): 174-9.

Stebbins GT, Goetz CG. Factor structure of the Unified Parkinson's Disease Rating Scale: Motor Examination section. Movement disorders : official journal of the Movement Disorder Society 1998; 13(4): 633-6.

Stiasny-Kolster K, Mayer G, Schafer S, Moller JC, Heinzel-Gutenbrunner M, Oertel WH. The REM sleep behavior disorder screening questionnaire--a new diagnostic instrument. Movement disorders : official journal of the Movement Disorder Society 2007; 22(16): 2386-93.

Stipanovich A, Valjent E, Matamales M, Nishi A, Ahn JH, Maroteaux M, *et al.* A phosphatase cascade by which rewarding stimuli control nucleosomal response. Nature 2008; 453(7197): 879-84.

Stoessl AJ, Lehericy S, Strafella AP. Imaging insights into basal ganglia function, Parkinson's disease, and dystonia. Lancet 2014; 384(9942): 532-44.

Stoof JC, Kebabian JW. Opposing roles for D-1 and D-2 dopamine receptors in efflux of cyclic AMP from rat neostriatum. Nature 1981; 294(5839): 366-8.

Strick CA, James LC, Fox CB, Seeger TF, Menniti FS, Schmidt CJ. Alterations in gene regulation following inhibition of the striatum-enriched phosphodiesterase, PDE10A. Neuropharmacology 2010; 58(2): 444-51.

Sudhyadhom A, Haq IU, Foote KD, Okun MS, Bova FJ. A high resolution and high contrast MRI for differentiation of subcortical structures for DBS targeting: the Fast Gray Matter Acquisition T1 Inversion Recovery (FGATIR). Neuroimage 2009; 47 Suppl 2: T44-52.

Svenningsson P, Lindskog M, Rognoni F, Fredholm BB, Greengard P, Fisone G. Activation of adenosine A2A and dopamine D1 receptors stimulates cyclic AMP-dependent phosphorylation of DARPP-32 in distinct populations of striatal projection neurons. Neuroscience 1998; 84(1): 223-8.

Svenningsson P, Nishi A, Fisone G, Girault JA, Nairn AC, Greengard P. DARPP-32: an integrator of neurotransmission. Annu Rev Pharmacol Toxicol 2004; 44: 269-96.

Tanner M, Gambarota G, Kober T, Krueger G, Erritzoe D, Marques JP, *et al.* Fluid and white matter suppression with the MP2RAGE sequence. J Magn Reson Imaging 2012; 35(5): 1063-70.

Tessitore A, Giordano A, Russo A, Tedeschi G. Structural connectivity in Parkinson's disease. Parkinsonism & related disorders 2016; 22 Suppl 1: S56-9.

Thanvi BR, Lo TC. Long term motor complications of levodopa: clinical features, mechanisms, and management strategies. Postgrad Med J 2004; 80(946): 452-8.

Threlfell S, Sammut S, Menniti FS, Schmidt CJ, West AR. Inhibition of Phosphodiesterase 10A Increases the Responsiveness of Striatal Projection Neurons to Cortical Stimulation. J Pharmacol Exp Ther 2009; 328(3): 785-95.

Tombaugh TN, McIntyre NJ. The mini-mental state examination: a comprehensive review. Journal of the American Geriatrics Society 1992; 40(9): 922-35.

Tu Z, Fan J, Li S, Jones LA, Cui J, Padakanti PK, *et al.* Radiosynthesis and in vivo evaluation of [11C]MP-10 as a PET probe for imaging PDE10A in rodent and non-human primate brain. Bioorg Med Chem 2011; 19(5): 1666-73.

Tuite P. Brain Magnetic Resonance Imaging (MRI) as a Potential Biomarker for Parkinson's Disease (PD). Brain Sci 2017; 7(6).

Tziortzi AC, Searle GE, Tzimopoulou S, Salinas C, Beaver JD, Jenkinson M, *et al.* Imaging dopamine receptors in humans with [11C]-(+)-PHNO: dissection of D3 signal and anatomy. Neuroimage 2011a; 54(1): 264-77.

Tziortzi AC, Searle GE, Tzimopoulou S, Salinas C, Beaver JD, Jenkinson M, *et al.* Imaging dopamine receptors in humans with C-11 -(+)-PHNO: Dissection of D3 signal and anatomy. Neuroimage 2011b; 54(1): 264-77.

Ulla M, Bonny JM, Ouchchane L, Rieu I, Claise B, Durif F. Is R2* a new MRI biomarker for the progression of Parkinson's disease? A longitudinal follow-up. PLoS One 2013; 8(3): e57904.

Urdinguio RG, Sanchez-Mut JV, Esteller M. Epigenetic mechanisms in neurological diseases: genes, syndromes, and therapies. Lancet Neurol 2009; 8(11): 1056-72.

Vaillancourt DE, Spraker MB, Prodoehl J, Abraham I, Corcos DM, Zhou XJ, *et al.* High-resolution diffusion tensor imaging in the substantia nigra of de novo Parkinson disease. Neurology 2009; 72(16): 1378-84.

van Dyck CH, Seibyl JP, Malison RT, Laruelle M, Zoghbi SS, Baldwin RM, *et al.* Age-related decline in dopamine transporters: analysis of striatal subregions, nonlinear effects, and hemispheric asymmetries. The American journal of geriatric psychiatry : official journal of the American Association for Geriatric Psychiatry 2002; 10(1): 36-43.

Van Laere K, Ahmad RU, Hudyana H, Celen S, Dubois K, Schmidt ME, *et al.* Human biodistribution and dosimetry of 18F-JNJ42259152, a radioligand for phosphodiesterase 10A imaging. Eur J Nucl Med Mol Imaging 2013a; 40(2): 254-61.

Van Laere K, Ahmad RU, Hudyana H, Dubois K, Schmidt ME, Celen S, *et al.* Quantification of 18F-JNJ-42259152, a novel phosphodiesterase 10A PET tracer: kinetic modeling and test-retest study in human brain. Journal of nuclear medicine : official publication, Society of Nuclear Medicine 2013b; 54(8): 1285-93.

Van Laere K, De Ceuninck L, Dom R, Van den Eynden J, Vanbilloen H, Cleynhens J, *et al.* Dopamine transporter SPECT using fast kinetic ligands: 123I-FP-beta-CIT versus 99mTc-TRODAT-1. Eur J Nucl Med Mol Imaging 2004; 31(8): 1119-27.

Visser M, Marinus J, Stiggelbout AM, Van Hilten JJ. Assessment of autonomic dysfunction in Parkinson's disease: the SCOPA-AUT. Movement disorders : official journal of the Movement Disorder Society 2004; 19(11): 1306-12.

Wang JY, Zhuang QQ, Zhu LB, Zhu H, Li T, Li R, *et al.* Meta-analysis of brain iron levels of Parkinson's disease patients determined by postmortem and MRI measurements. Sci Rep 2016; 6: 36669.

Wang Y, Butros SR, Shuai X, Dai Y, Chen C, Liu M, *et al.* Different iron-deposition patterns of multiple system atrophy with predominant parkinsonism and idiopathetic Parkinson diseases demonstrated by phase-corrected susceptibility-weighted imaging. AJNR Am J Neuroradiol 2012; 33(2): 266-73.

Ward RJ, Zucca FA, Duyn JH, Crichton RR, Zecca L. The role of iron in brain ageing and neurodegenerative disorders. Lancet Neurol 2014; 13(10): 1045-60.

Weng YH, Yen TC, Chen MC, Kao PF, Tzen KY, Chen RS, *et al.* Sensitivity and specificity of 99mTc-TRODAT-1 SPECT imaging in differentiating patients with idiopathic Parkinson's disease from healthy subjects. Journal of nuclear medicine : official publication, Society of Nuclear Medicine 2004; 45(3): 393-401.

Whone AL, Watts RL, Stoessl AJ, Davis M, Reske S, Nahmias C, *et al.* Slower progression of Parkinson's disease with ropinirole versus levodopa: The REAL-PET study. Annals of neurology 2003; 54(1): 93-101.

Xiang Y, Gong T, Wu J, Li J, Chen Y, Wang Y, *et al.* Subtypes evaluation of motor dysfunction in Parkinson's disease using neuromelanin-sensitive magnetic resonance imaging. Neurosci Lett 2017; 638: 145-50.

Xie Z, Adamowicz WO, Eldred WD, Jakowski AB, Kleiman RJ, Morton DG, *et al.* Cellular and subcellular localization of PDE10A, a striatum-enriched phosphodiesterase. Neuroscience 2006; 139(2): 597-607.

Zarei M, Ibarretxe-Bilbao N, Compta Y, Hough M, Junque C, Bargallo N, *et al.* Cortical thinning is associated with disease stages and dementia in Parkinson's disease. Journal of neurology, neurosurgery, and psychiatry 2013; 84(8): 875-81.

Zecca L, Stroppolo A, Gatti A, Tampellini D, Toscani M, Gallorini M, *et al.* The role of iron and copper molecules in the neuronal vulnerability of locus coeruleus and substantia nigra during aging. Proc Natl Acad Sci U S A 2004; 101(26): 9843-8.

Zhang J, Zhang Y, Wang J, Cai P, Luo C, Qian Z, *et al.* Characterizing iron deposition in Parkinson's disease using susceptibility-weighted imaging: an in vivo MR study. Brain research 2010; 1330: 124-30.

Zhang L, Wang M, Sterling N, Lee E, Eslinger P, Wagner D, *et al.* Cortical Thinning and Cognitive Impairment in Parkinson's Disease Without Dementia. Computational Biology and Bioinformatics, IEEE/ACM Transactions on 2015; PP(99): 1-.

Zhang Y, Wu IW, Tosun D, Foster E, Schuff N, Parkinson's Progression Markers I. Progression of Regional Microstructural Degeneration in Parkinson's Disease: A Multicenter Diffusion Tensor Imaging Study. PloS one 2016; 11(10): e0165540.

Zheng LF, Wang ZY, Li XF, Song J, Hong F, Lian H, *et al.* Reduced expression of choline acetyltransferase in vagal motoneurons and gastric motor dysfunction in a 6-OHDA rat model of Parkinson's disease. Brain research 2011; 1420: 59-67.